ISTANBUL TECHNICAL UNIVERSITY ★ INSTITUTE OF SCIENCE AND TECHNOLOGY

CFD MODELING OF EMISSIONS FORMATION AND REDUCTION IN HEAVY DUTY DIESEL ENGINES

Ph.D. Thesis by

Alper T. ÇALIK, M.Sc.

Department : Mechanical Engineering

Programme: Automotive Department

SEPTEMBER 2007

ISTANBUL TECHNICAL UNIVERSITY ★ INSTITUTE OF SCIENCE AND TECHNOLOGY

CFD MODELING OF EMISSIONS FORMATION AND REDUCTION IN HEAVY DUTY DIESEL ENGINES

Ph.D. Thesis by

Alper T. ÇALIK, M.Sc.

(503992012)

Date of submission : 28 December 2006

Date of defence examination: 14 September 2007

Supervisor (Chairman): Prof. Dr. A. Metin ERGENEMAN

Co-supervisor : Doc. Dr. Valeri I. GOLOVITCHEV (CTH.)

Members of the Examining Committee Prof. Dr. Cem SORUSBAY

Prof. Dr. Ertugrul ARSLAN

Prof. Dr. Turgut ÖZAKTAS

Prof. Dr. Orhan DENIZ (YTU.)

Prof. Dr. Irfan YAVASLIOL (YTU.)

SEPTEMBER 2007

ISTANBUL TEKNIK ÜNIVERSITESI ★ FEN BILIMLERI ENSTITÜSÜ

HESAPLAMALI AKISKANLAR DINAMIGI (CFD) ILE AGIR VASITA DIZEL MOTORLARINDA EMISYON OLUSUMU ve AZALTILMASININ MODELLENMESI

DOKTORA TEZI

Y. Müh. Alper T. ÇALIK

(503992012)

Tezin Enstitüye Verildigi Tarih : 28 Aralik 2006

Tezin Savunuldugu Tarih: 14 Eylül 2007

Tez Danismani : Prof. Dr. A. Metin ERGENEMAN

Tez Es Danismani : Doç. Dr. Valeri I. GOLOVITCHEV (CTH.)

Diger Juri Üyeleri Prof. Dr. Cem SORUSBAY

Prof. Dr. Ertugrul ARSLAN

Prof. Dr. Turgut ÖZAKTAS

Prof. Dr. Orhan DENIZ (YTÜ.)

Prof. Dr. Irfan YAVASLIOL (YTÜ.)

EYLÜL 2007

PREFACE

This study is made at the Automotive Division of Mechanical Engineering Faculty of İstanbul Technical University (ITU). The field of study was defined in ITU by my supervisor Prof. Dr. A. Metin ERGENEMAN, and the specific subjects were clarified together with my co-supervisor Doc. Dr. Valeri I. GOLOVITCHEV at Combustion Divison of Applied Mechanics Department of Chalmers University of Technology (CTH). The final stage of the study was mostly finished at CTH. I would like to express my gratitude to Prof. Ingemar DENBRATT for accepting me at CTH and giving me the opportunity to complete this work.

First of all I would like to thank to; my supervisor Prof. Dr. A. Metin ERGENEMAN, for giving me an opportunity to work with him on this subject and for all of his supervising, valuable discussions, help, and support and to my co-supervisor Doc. Dr. Valeri I. GOLOVITCHEV, for accepting me and for great supervising with many discussions, his teaching how to use KIVA-3V RELEASE 2 (KIVA-3VR2) and CHEMKIN II^{TM} (CHEMKIN) codes and tough work, for his sincere advices and interest in my future.

My gratitude is also addressed to Dr. Orhan ATABAY, for your patience to deal with me and for everything which I cannot put into this limited space, sharing the same room is pleasure for me; Dr. O. Akın KUTLAR who encouraged and adviced me to be a researcher in ITU, and, of course, with Dr. Hikmet ARSLAN, for their endless, invaluable co-operation, moral support, teaching, guidance in a huge ocean of the internal combustion engines (ICE) and for many other special things, in which this study definitely this study would not appear without you and it is honor for me to meet and work with both of you; Prof. Dr. Rafig MEHDIYEV, for all his supervising, continues support, encouragement, and especially for his great tolerance and guidance; Prof. Dr. Orhan DENİZ and Prof. Dr. Cem SORUŞBAY for their guidance and advices; Prof. Orhan DALDAL, for his kind interest and advices; ITU, Tinçel Kültür Foundation and Vehbi Koç Foundation, for their financial support; my friends: Eng. Kürşat GÜLER, ace coder of all (architect), for all your software, discussions, invaluable advices about coding; MSc Eng. A. Barış SARI, the master, for every single word; MSc Cengiz İRFANOĞLU, atom ant, for conversations, global and continues support, all kind of extreme activities; Msc Eng. Özgür CENGİZ, the doctor, for technical and social discussions, conversations, your encouragement and for all kind of support; Doc. Dr. Filiz KARAOSMANOĞLU, for her advices, co-operation and continues moral support; Tech. Bedri B. DOĞRUL, the best driver I ever met, it is every time my pleasure to be in some vehicle which you drive, for all your moral support and conversations; Eng. Mustafa KAVİTAŞ, for valuable technical discussions and guidance; Tech. Faruk ARSLAN, for his kindness and immediately solving all our technical problems; Eng. Hami ÇEBİ, for his all kind of support and advices, Eng. Mustafa ÖZCAN, Tech. Ali HARPUT and Salim ÖZCAN (rest in peace) for their kind help; Dr. Savo GIRJA, for many discussions, advices and kind interest and support, MSc Eng. Mustafa YÜCEİL, for valuable

discussions and support on engine tests; MSc Eng. Michael V. JENSEN, for your good work and contribution during your training at ITU; Doc. Dr. Vedat TEMİZ, by chance who started the story for me, for his encouragement and unique teaching; MSc Eng. Ergün GÜRASLAN, who unawares clarified my decision to continue studying on ICEs when I first met him while testing at the engine dynamometer in FORD-OTOSAN, for his kind interest and support when we needed; MSc Eng. Özgür TAŞKIRAN, who first started CFD combustion modeling with KIVA-3VR2 in ITU, for your help and advices, MSc Eng. Abdurrahman İMREN for your support, especially for KIVA-3VR2 code, Dr. Cüneyt UYKUR, who gave me the basic computer knowledge and netiquette, for his encouragement and continues support; MSc Eng. Mehmet MUTLU, for your valuable discussions and help; MSc Eng. Özgür GÜNELSU and Msc Eng. Emrah ÖZGÜMÜŞ for their help; Ms. Yaşar SUNAR, Monika ORRBACKE and Sandra ARVIDSSON, for their very kind help and interest; Dr. Pratap SATHIAH, for your advices and help in programming in FORTRAN and for friendship during my stay in CTH, Dr. Luca MONTORSI, for your help, co-operation and friendship; Dr. Feng TAO, for your interest and kindness, Dr. Murat TUTKUN for your friendship, valuable scientific conversations and many other things during my stay in Göteborg; all friends in CTH, for their kindness and help; Ergül ÜSTÜNTAŞ and all staff of Institute of Science and Technology of ITU; all my students, for their help.

And my mother Ferihan ÇALIK, my father Haydar ÇALIK, my sister Eng. Gökhangül ÇALIK, my brother Oğuzhan ÇALIK and my uncle Prof. Dr. Adnan ÇALIK, thank you very much for your patience, tolerance and endless love.

Last but not least, to my love, Aysen. Thank you …

Without doubt, this study is appearing with all of your contributions. Then, what did I do myself? Not so much.

İstanbul, September 2007 Alper T. ÇALIK

CONTENTS

NOMENCLATURE

ATDC : After Top Dead Centre
ALE : Arbitrary Lagrangian Eulerian
BDF : Backward Differentiation Formula
BMEP : Break Mean Effective Pressure
BSFC : Break Specific Fuel Consumption
BTDC : Before Top Dead Centre
CA : Crank Angle
CAD : Crank Angle Degree
CDM : Continuum Droplet Model
CFD : Computational Fluid Dynamics
CI : Compression Ignition (diesel) engine
CN : Cetane Number
DASAC : Differential Algebraic Sensitivity Analysis Code
DASSL : Differential Algebraic System Solver
DDM : Discrete Droplet Model
DI : Direct Injection
DISI : Direct Injection Spark Ignition
DME : Dimethyl Ether
DNS : Direct Numerical Simulation
DOS : Diesel Oil Surrogate
EBU : Eddy-Break-Up
EDC : Eddy Dissipation Concept
EGR : Exhaust Gas Recirculation
EOC : End of Combustion
EVC : Exhaust Valve Closing
EVO : Exhaust Valve Opening
FP : Free Piston
HCCI : Homogeneous Charge Compression Ignition
HDDE : Heavy Duty Diesel Engine
HSDI : High Speed Direct Injection
ICE : Internal Combustion Engine
ID : Ignition Delay
IMEP : Indicated Mean Effective Pressure
ISFC : Indicated Specific Fuel Consumption
IVC : Intake Valve Closing
IVC : Intake Valve Opening
JSR : Jet-Stirred-Reactor
KHRT : Kelvin-Helmholtz/Rayleigh-Taylor
LES : Large Eddy Simulation
LHV : Lower Heating Value
LHS : Left Hand Side
LPC : Lean Premixed Combustion
LSODE : Livermore Solver for Ordinary Differential Equations

LTC : Low Temperature Combustion
MK : Modulated Kinetics
NLM : Number of Elements
NMHC : Non-methane hydrocarbon
NTC : Negative Temperature Coefficient
Nu : Nusselt Number
ON : Octane Number
ODE : Ordinary Differential Equation
PAH : Poly Aromatic Hydrocarbons
PaSR : Partially Stirred Reactor
PSR : Perfectly Stirred Reactor
PCCI : Premixed Charged Compression Ignition
PDF : Probably Density Function
RANS : Reynolds-Averaged Navier-Stokes equations
RHS : Right Hand Side
RGF : Residual Gas Fraction
RON : Research Octane Number
RQL : Rich Quick Lean
Sc : Schmidt Number
Sh : Sherwood Number
SI : Spark Ignition Engine
SMD : Sauter Mean Diameter
SOC : Start of Combustion
SOI : Start of Ignition
SSPs : Saturated Stoichimetric Products
St : Stokes Number
TDC : Top Dead Centre
TST : Transition State Theory
We : Weber Number
Z : Ohnesorge Number

TABLE LIST

Page No

FIGURE LIST

Page No

SYMBOLS

ε	Compression ratio	[-]
ϕ	Fuel/air equivalence ratio	[-]
λ	Air/fuel equivalence ratio (=1/ϕ)	[-]
ρ	Mass density	[kg m^{-3}]
τ	Residence time	[s]
ω	Angular velocity	[rad s^{-1}]
ω_i	Molar production rate of *i*-th species	[mol s^{-1}]
A, A′	Pre-exponential factor	[-]
A1	Benzene	[-]
A1-	Phenyl radical	[-]
$\mathbf{A_2R_5}$	acenaphthylene	[-]
c	Concentration	[mol m^{-3}]
c_p	Constant pressure specific heat capacity	[J mol^{-1} K^{-1}]
c_v	Constant volume specific heat capacity	[J mol^{-1} K^{-1}]
c_s	Specification of s- chemical species	[-]
C	Carbon atom	[-]
$\mathbf{CH_4}$	Methane	[-]
$\mathbf{C_nH_{2n}}$		[-]
$\mathbf{C_xH_y}$	Fuel	[-]
$\mathbf{C_2H_2}$	Acetylene	[-]
$\mathbf{C_2H_4}$	Ethylene	[-]
$\mathbf{C_2H_6}$	Ethane	[-]
$\mathbf{C_3H_3}$	Propargyl	[-]
$\mathbf{C_3H_4}$	1,2-Propadiene	[-]
$\mathbf{C_3H_6}$	Cyclopropane	[-]
$\mathbf{C_6H_2}$	Long-chain acetylene	[-]
$\mathbf{C_6H_6}$	Benzene	[-]
$\mathbf{C_7H_{16}}$	n-heptane	[-]
$\mathbf{C_7H_8}$	Toluene	[-]
$\mathbf{C_{11}H_{10}}$	α-methyl naphthalene	[-]
$\mathbf{C_{16}H_{34}}$	n-hexadecane	[-]
CO	Carbon monoxide	[-]
$\mathbf{CO_2}$	Carbon dioxide	[-]
e	Specific internal energy	[J kg^{-1}]
E	Potential energy	[J]
$\mathbf{E_a}$	Activation energy of the reaction	[kJ mol^{-1}]
G	Gibbs free energy	[J]
i	Species designation	[-]
H	Hydrogen atom	[-]
HC	Unburned hydrocarbon	[-]
$\mathbf{HO_2}$	Hydroperoxy radical	[-]
$\mathbf{H_2}$	Hydrogen	[-]

H_2O	Water	[-]
k	Reaction rate coefficient	[-]
n	Engine speed	[rpm]
n	Mole number	[mol]
N	Nitrogen atom	[-]
N_A	Avogadro number	[mol^{-1}]
NH	Imidogen	[-]
$(NH_2)_2CO$	Urea	[-]
NH_3	Ammonia	[-]
NMHC	Ammonia	[-]
NO	Nitric oxide	[-]
NO_x	Nitrogen oxide	[-]
NO_2	Nitrogen dioxide	[-]
N_2	Nitrogen	[-]
N_2O	Nitrous oxide	[-]
m	Mass	[kg]
M	Third body	[-]
M_i	Molecular weight	[g mol^{-1}]
$\overline{M}$	Mixture mean molar mass	[g mol^{-1}]
O	Oxygen atom	[-]
OH	Hydroxyl radical	[-]
O_2	Oxygen	[-]
P	Pressure	[bar]
Q	Heat loss	[J]
r	Reaction designation	[-]
R	Universal gas constant	[J mol^{-1} K^{-1}]
S	Number of species	[-]
SO_2	Sulfur dioxide	[-]
SPM or C(s)	Suspended particulate matter (soot)	[-]
T	Temperature	[K]
T_{cool}	Engine coolant temperature	[°C]
v	Specific volume	[m^3 kg^{-1}]
v_s'	Stoichiometric coefficient of the reactants	[-]
v_s''	Stoichiometric coefficient of the products	[-]
V	Volume	[m^3]
Y_i	Mass fraction	[-]
x_i	Mole fraction	[-]

CFD MODELING OF EMISSIONS FORMATION AND REDUCTION IN HEAVY DUTY DIESEL ENGINES

SUMMARY

The main emission problem for conventional diesel combustion is the NO_x-soot tradeoff (Diesel dilemma) which could not be completely eliminated with the in-cylinder combustion techniques until now, hence, after-treatment is still necessary to meet the present emission legislations. Also with the development of the new engines which have different combustion regimes such as Homogeneous Charge Compression Ignition (HCCI), Modulated Kinetics (MK), Premixed Charge Compression Ignition (PCCI), Low Temperature Combustion (LTC), other emissions such as HC and CO became significant for compression ignition (CI) engines. This study investigates mainly formation/reduction of NO_x and soot emissions in diesel engine combustion, especially in Heavy Duty Diesel (HDD) engines with the help of CFD engine modeling of the engine. The KIVA-3VR2 and CHEMKIN packages were used for the modeling purposes. CHALMERS diesel oil surrogate (DOS) model represented by a blend of aliphatic (n-heptane, 70%) and aromatic (toluene, 30%) components, turbulence/chemistry interaction approach, Partially Stirred Reactor (PaSR) model, applied with the detailed chemical mechanism and modified spray models were implemented into the KIVA-3VR2 for the modeling tasks. Diesel surrogate oil and detailed chemical mechanism were validated with shock-tube experiments on ignition delays for different pressures, temperatures and air/fuel ratios. Then modeling results for Volvo D12C engine for two compression ratios (18.0 and 14.0) and two different combustion regimes, MK and LTC, were compared with the experimental data. The reaction mechanism is modified in order to improve its NO_x-soot emissions behavior which was not accurate enough. Different fuel injection times, loads, and both EGR-free and EGR cases were studied to extend the modeling capabilities. For all cases presented modeling approach is used to predict in-cylinder pressure, temperature, Rate of Heat Release (RoHR), combustion efficiency, NO_x and soot emissions. Although tendency of the predicted emissions is in a good agreement with the experiments, a quantitative improvement of emission predictions is still required. Accurate modeling based on the detailed chemistry approach requires a proper balance between NO_x formation, soot and CO oxidations in the chemical mechanism which is not easy to achieve.

Also a new scientific tool, parametric ϕ-T dynamic map analysis, to evaluate engine combustion and emission formation based on the detailed chemical model of the diesel oil surrogate fuel. Emission formation and combustion efficiency can be predicted with the usage of this new type of analysis. The consistency of the map technique is mature enough to use it as a common tool, to analyze the engine combustion and emission formation processes.

HESAPLAMALI AKIŞKANLAR DİNAMİĞİ (CFD) İLE AĞIR VASITA DİZEL MOTORLARINDA EMİSYON OLUŞUMU ve AZALTILMASININ MODELLENMESİ

ÖZET

Klasik dizel yanma işleminde temel emisyon problemi olan NO_x-is ikilemi hala güncelliğini korumaktadır. Silindir içi yanma teknikleri günümüz emisyon standartlarını sağlamak için yeterli değildir ve ikincil önlemler olarak katalizatör kullanımı gereklidir. Ayrıca, homojen karışımlı sıkıştırma ateşlemeli (HCCI), kimyasal kinetik kontrollü (MK), ön-karışımlı sıkıştırma ateşlemeli (PCCI) gibi farklı yanma rejimlerine sahip yeni tip içten yanmalı motorların geliştirilmesiyle birlikte HC ve CO emisyonları da artık önem kazanmış olup sorun teşkil etmektedirler. Bu çalışma özellikle ağır vasıta dizel motorunda NO_x ve is emisyonlarının oluşumunu ve azaltılmasını, Sayısal Akışkanlar Dinamiği (CFD) modellemesi yardımıyla incelemektedir. Modelleme çalışmaları için KIVA-3VR2 ve CHEMKIN paketi kullanılmıştır. Chalmers University of Technology (CHALMERS)'da geliştirilen n-heptan (70%) ve toluen (30%) karışımından oluşan dizel yakıt modeli, türbülans/yanma etkileşimi için geliştirilen kısmi karışımlı reaktör modeli, detaylı reaksiyon mekanizması ve iyileştirilmiş yakıt püskürtme modeli KIVA-3VR2'ye uyarlanmış ve hesaplamalar gerçekleştirilmiştir. Dizel yakıt modeli ve reaksiyon mekanizması sabit hacimli bomba deneylerinde değişik sıcaklık, basınç, hava/yakıt oranları için, tutuşma gecikmesi esas alınarak doğrulanmıştır. Sonraki aşamada Volvo D12C ağır vasıta motorunda 18.0 ve 14.0 sıkıştırma oranları, farklı yük, püskürtme zamanı ve egzoz gazı geri dönüşü (EGR) oranları için modelleme çalışmaları yapılarak deney verileri ile karşılaştırılmıştır. Çalışılan durumlar için, silindir basıncı, sıcaklığı, ısı açığa çıkış karakteristiği, yanma verimi ve NO_x emisyonları oldukça iyi, is emisyonları ise nicelik olarak iyi modellenebilmiştir. Hesaplanan emisyon sonuçlarının eğilimi ve deney sonuçlarıyla uyumluluğu iyi olmakla birlikte, özellikle is emisyonları açısından hala geliştirmeye ihtiyaç vardır. Emisyon modellenmesi için kullanılan detaylı reaksiyon mekanizmasında karşılaşılan en büyük sorun, isin yanması, NO_x ve CO oluşumu reaksiyonları arasındaki çok hassas ve birbirini etkileyen dengenin bulunması olmuştur.

Ayrıca, içten yanmalı motorlarda yanma verimi ve emisyonlarının nitelik olarak önceden tahmin edilebilmesine yarayan yeni bir analiz yöntemi, parametrik dinamik ϕ-T haritası, geliştirilmiştir. Geliştirilen bu yeni analiz yöntemiyle üç boyutlu yanma modellemesinin karmaşık analizi iki boyutlu bir ortamda daha anlaşılır bir şekle dönüştürülmekte ve yüksek yanma verimi ile düşük emisyonlar için uygun bir yol önerilmektedir. Bu yeni yöntemin emisyonlarla ilgili nitel tahmin yeteneği oldukça iyidir ve gelecekte yanma analizi konusunda sürekli kullanılabilecek olgunluktadır.

1 INTRODUCTION

Combustion is the oldest technology of mankind; it has been used for more than one million years. At present, about 90% of worldwide energy support (e.g., in traffic, electrical power generation, heating) is provided by combustion [1]. Use of fossil fuels in combustion is one of the major well-known and extensively studied application fields of energy production. Despite of this immense research and background knowledge, there are still a lot of sub-fields in combustion which could not be wholly clarified and need further research and understanding. Hence, this study focuses on a specific part, i.e., combustion and emission formation, in Internal Combustion Engine (ICE) which are widely used as a power source in transportation and other power generation units, in particular diesel combustion and emission formation processes. With the increasing number of such applications, air pollution caused by exhaust emissions has become of primary significance due to its environmental impact. During the past forty years, with the pressure of governmental policies and research activity in this area, the emission (nitrogen oxides (NO_x), carbon monoxide (CO), suspended particulate matter (SPM) and unburned hydrocarbons (HC)) levels have been decreased significantly. In the future, a considerable decrease in emission levels due to further improvement in engine technology is expected [2, 3, 4]. On the other hand, for the next 40 years, it is not expected that any new energy source will replace the fossil fuels in an economical manner and oil remains the largest single source of energy in most parts of the world. The exceptions are the Former Soviet Union Republics, where natural gas dominates, and Asian Pacific countries, whether coal is the dominant fuel [5, 6].

1.1 Environment and Pollution

The atmosphere of the earth is composed of 21% oxygen (O_2) and 78% nitrogen (N_2), as well as water vapor (H_2O) and trace gases. Components that change the natural composition of the atmosphere are considered as air polluting substances. From Figure 1.1 one can schematically see main trace gases and their classification.

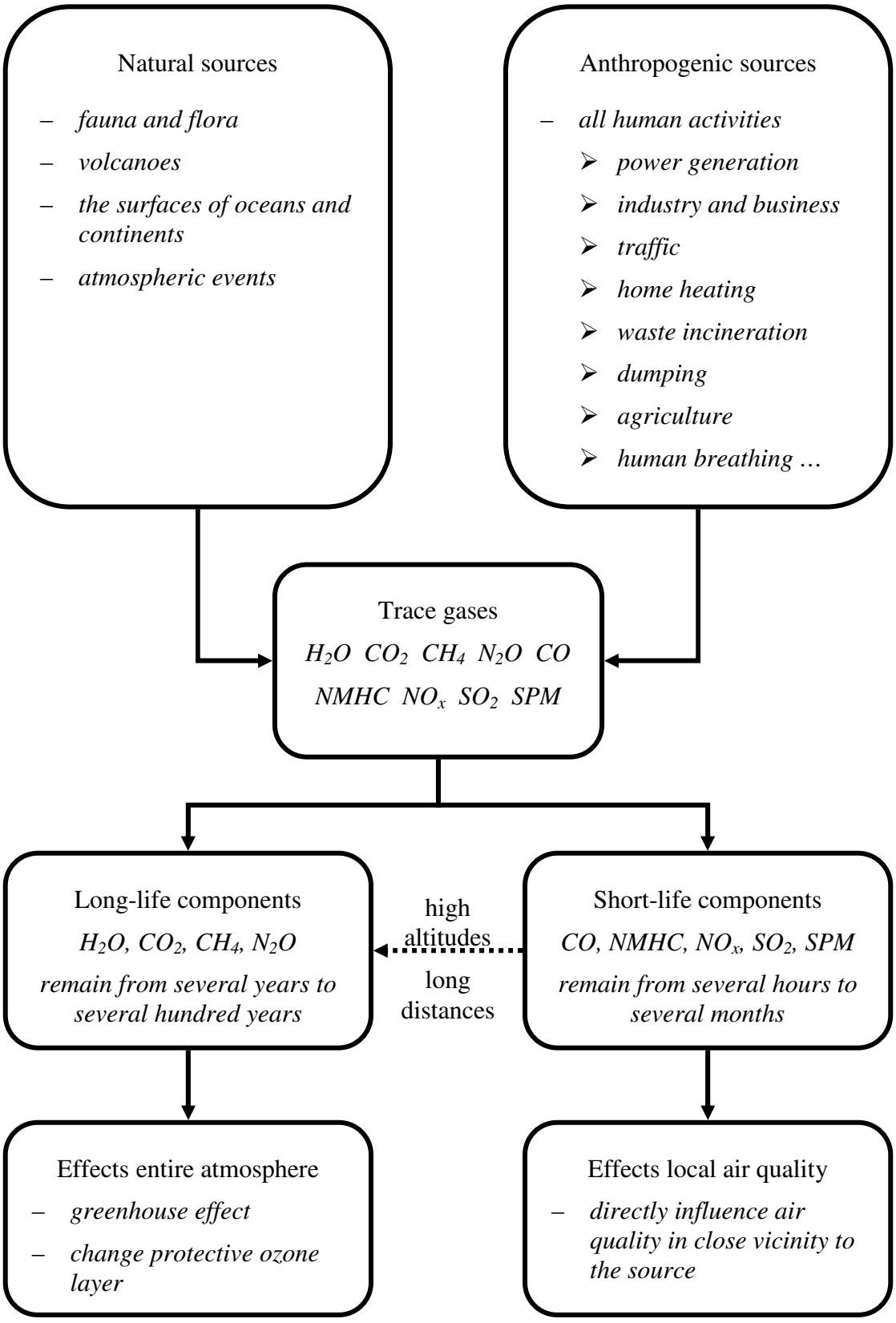

Figure 1.1 A preview of trace gases from source to the end effects on atmosphere and air pollution, reviewed from [2]

Here, while long-life components with global effects are well mixed and are distributed homogenously throughout the atmosphere, short-life components with local effects differ widely and depend largely on the geographic location of the source from which they are emitted. If we consider diesel-like combustion a long-life component, CO_2 which is a measure of fuel consumption and short-life components; NO_x and SPM will be the important ones amongst the others. In the complete combustion of hydrocarbon C_xH_y fuel consisting only of C and H atoms, the product gases contain the components CO_2, H_2O, O_2, and N_2, which obey the global complete combustion equation as below

$$C_xH_y + \left(x + \frac{y}{4}\right)(O_2 + 3.773N_2) = xCO_2 + \frac{y}{2}H_2O + 3.773\left(x + \frac{y}{4}\right)N_2 \qquad (1.1)$$

where we assume that the products are in low temperature, hence N_2 is not significantly affected by the reaction (1.1) [7]. However in real, incomplete combustion, CO, HC, NO_x and SPM (soot) also appear in addition to the above components. Incomplete (real) and complete combustion products are shown in Figure 1.2 for diesel engine with a fresh intake charge. While NO_x and SPM (soot) are hazardous for human health, CO_2, which is partially responsible for the greenhouse effect, is not considered as pollutant, since it does not effects human health directly and appears as a final product of every complete oxidation of HCs.

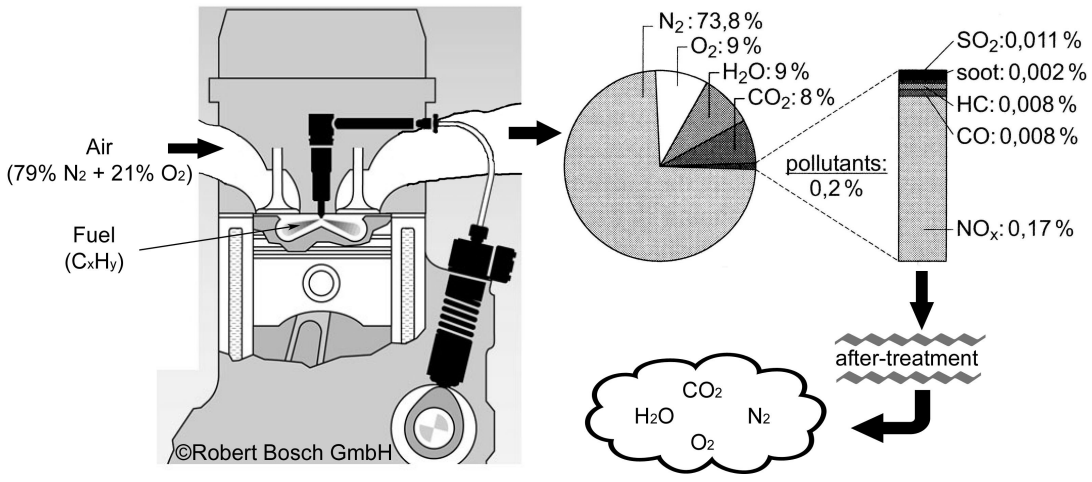

Figure 1.2 Raw emissions (without catalyst) in percent by volume and main emissions with after-treatment for a diesel engine combustion with fresh intake charge [8]

Volume percentages of these products will change for the combustion with Exhaust Gas Recirculation (EGR). In nearly all major ICE applications, the use of exhaust gas after-treatment systems is necessary in order to meet the present strict emission

legislations. Naturally, most of the incomplete combustion products are converted to the complete combustion products with the help of complicated and high-tech after-treatment systems which have a considerable production and maintenance cost in standalone ICE or whole vehicle [9]. Even if only complete combustion products considered, still CO_2 emissions will have an effect on global warming. In conclusion we can classify present research efforts on emissions of ICE into two main groups:

- to reduce fuel consumption, hence CO_2 emissions, and decrease the contribution of ICE applications to the global warming
- to extremely minimize raw exhaust emissions, even lower than the limits of the standards, in order to eliminate or decrease the use of highly complicated and expensive after-treatment systems

To clarify and to understand the role of ICE in air pollution, further quantitative data is given below. At first in Figure 1.3, we can see the effect of anthropogenic greenhouse gases on global warming. Although assumptions vary widely on the contribution of the anthropogenic greenhouse effect (0.5 to 1.5%) to the global greenhouse effect, it is evident that CO_2 has the largest effect.

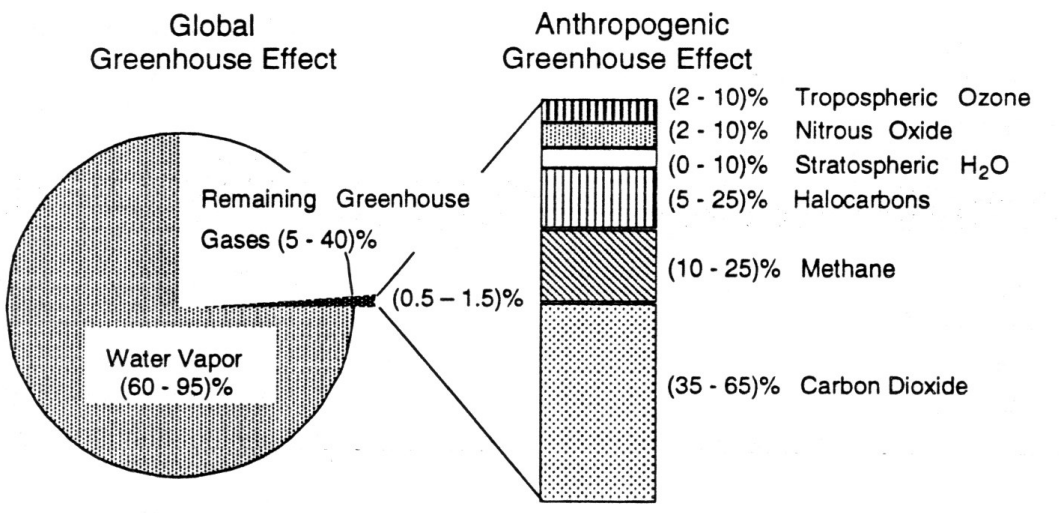

Figure 1.3 Volumetric distributions of anthropogenic greenhouse gases and contribution of anthropogenic greenhouse gases to the global greenhouse effect [2]

If we look the contribution of various sources to anthropogenic CO_2 emissions which is given in Figure 1.4 (reference year 1996), it can be concluded that approximately 15% contribution to the anthropogenic CO_2 emissions comes from ICE applications.

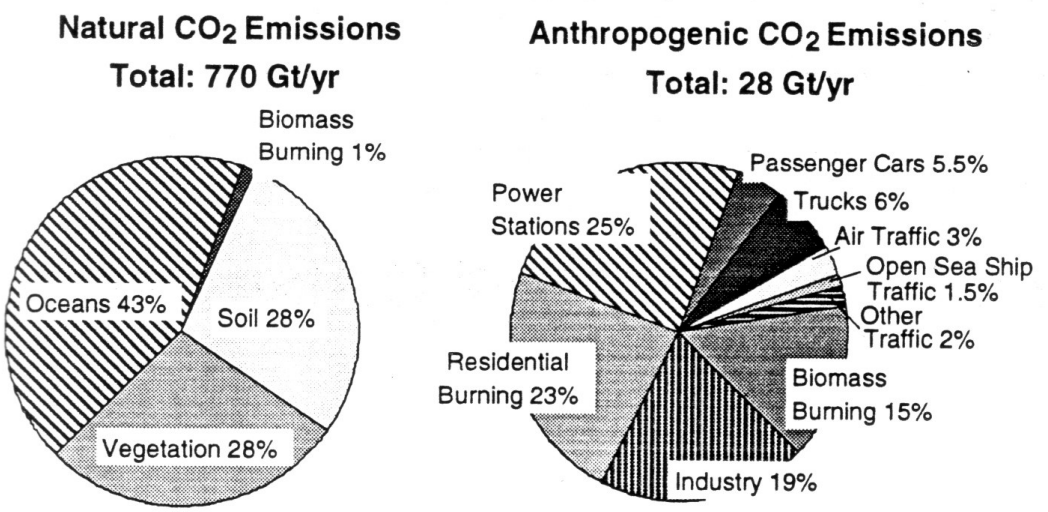

Figure 1.4 Contribution of various sources to global CO_2 emissions [2]

According to the data given in Figure 1.3 and Figure 1.4 we can calculate contribution of worldwide passenger car and commercial vehicle traffic to the global greenhouse effect as 0.2%. Although relatively small, this share of anthropogenic CO_2 emissions is nevertheless considered as additional emissions that may adversely affect the natural CO_2 equilibrium and thus, global climate [2].

From Figure 1.5 it is seen the effect of one of the real combustion products nitrogen oxides, NO_x, to total anthropogenic emissions worldwide.

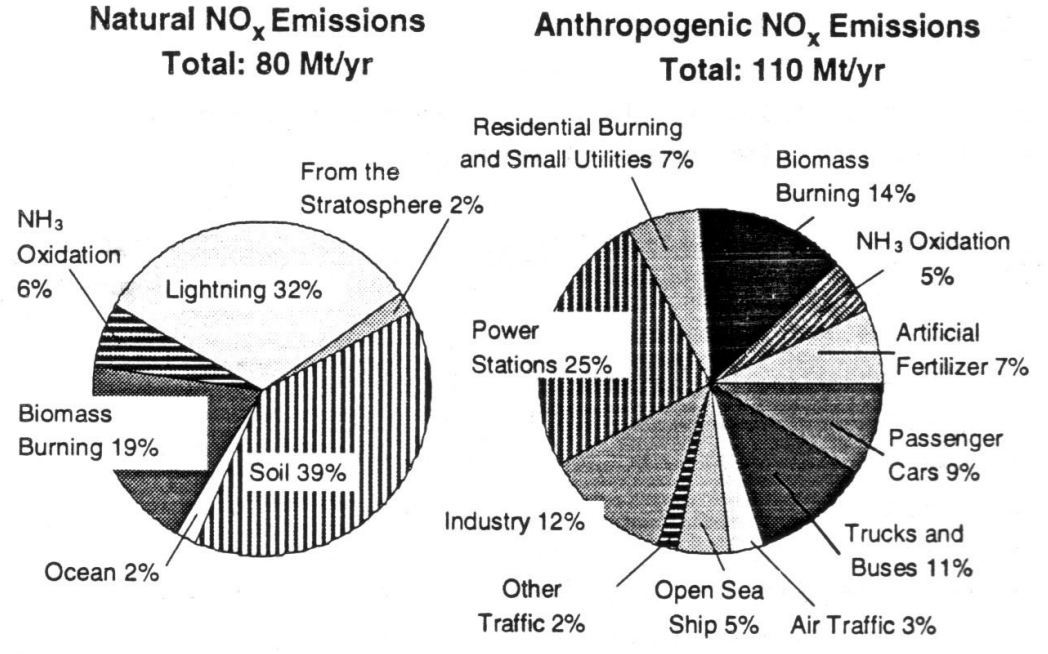

Figure 1.5 Contribution of various sources to global NO_x emissions [2]

NO_x is mainly formed from N_2 in air during the combustion process at high temperatures. Above, it can be seen that passenger cars and heavy duty vehicle traffic contribute 20% to total anthropogenic emissions worldwide. This ratio increases up to 50% in Europe. If the combustion process is efficient in ICE, then CO_2 and SPM (soot) emissions will be lower, but NO_x emissions will be higher. This opposite behavior is the main problem of diesel combustion and known as NO_x/soot tradeoff (Diesel diemma) and will be explained in detail in the next chapters.

SPM emissions or PM_{10} particles are the particles less than 10 micrometers (μm) in diameter that include both fine and coarse dust particles. These particles pose the greatest health concern because they can pass through the nose and throat and get into the lungs. For ICE, exhaust gas particles can vary in size between 0.01-10 μm. In Figure 1.6, estimation about the contribution of various sources to PM_{10} is given for the Europe (reference year 1993). Approximately 30% contribution comes from passenger cars and heavy-duty vehicles.

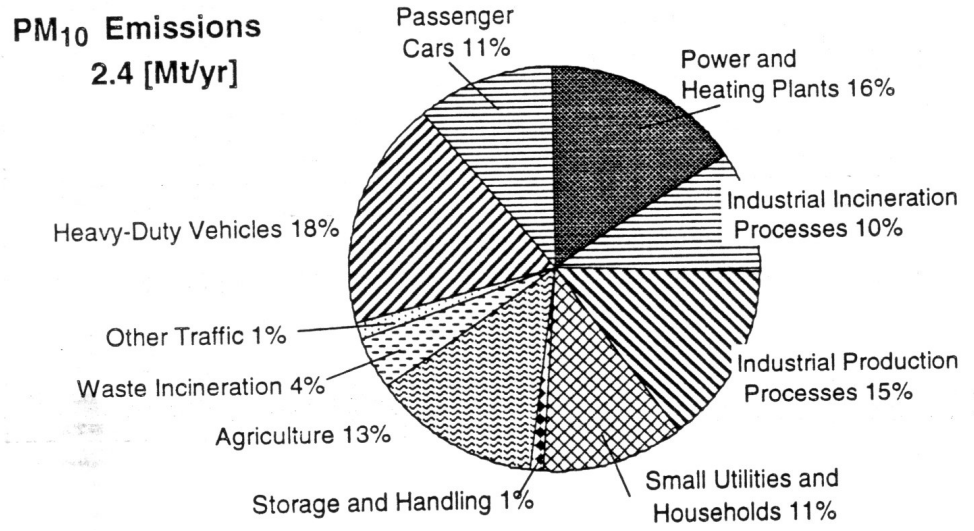

Figure 1.6 Contribution of various sources to PM_{10} emissions in the European Union [2]

It should be noted that the trend of SPM emissions decreases for the developed countries because of the improvement of the efficiency of existing filtering units in power and heating plants, also for the developing countries it is proper to say that SPM emissions will decrease because of adding new filtering units which have not used till now. To conclude this global overview about the diesel engine emissions and their affects, in Figure 1.7, continuum of exhaust emission standard for commercial vehicles (mass > 3.5 tons, engine power > 85 kW) is given. Naturally, emission limits decrease for newer standards.

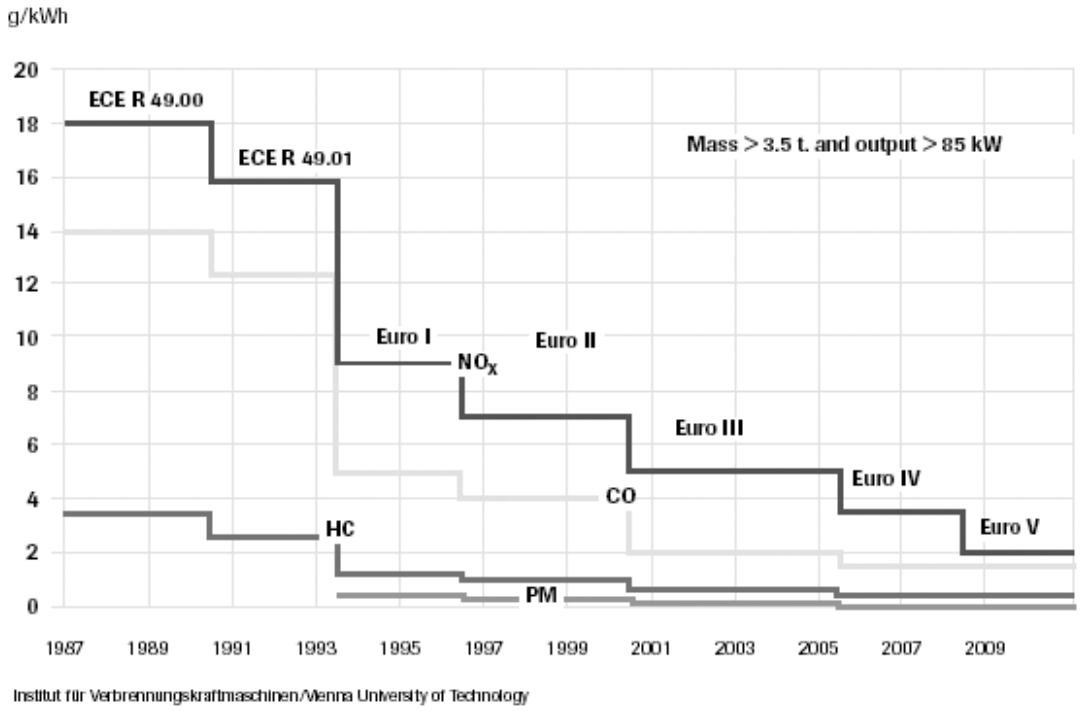

Figure 1.7 European exhaust emission standards for commercial vehicles with a vehicle mass of > 3.5 tons and engine power of > 85 kW

For the latest standards, Euro IV and Euro V, while NO_x limit value is decreased, other pollutant levels remain at the same level. After this global view to the trace gases and emissions sourced from ICEs, in the next chapter emission characteristics and actual problems for diesel engine will be given.

1.2 Hydrocarbon (HC) Fuels and Problems with Their Use

The world's most prominent natural liquid fuel resources are found within crude oil. Although petroleum reserves contain a variety of compounds which, depending on the reserve location, can range from heavy components to gases, most petroleum, on a mass basis, consists mainly of the following elements in Table 1.1 [10].

Table 1.1 Mass fraction of crude oil components

Element	Mass fraction, %
C	84-87
H	11-14
S	0-2
N	0-0.2

Only a small percentage of crude oil can be directly used as natural liquid fuels, hence after further chemical processing or refining crude petroleum are converted to useful fuels as well as several non-fuel products. Spark ignition (SI) or diesel engine

(DI) fuels such as natural gas, gasoline, kerosene and diesel oil are complex mixtures of hydrocarbons (Figure 1.8). These components differ with reference to molecular size and structure and as a result have sometimes strongly varying physical and chemical properties [8]. Hence many liquid fuel chemical and combustion characteristics are a direct result of a particular structure of those hydrocarbon components [10].

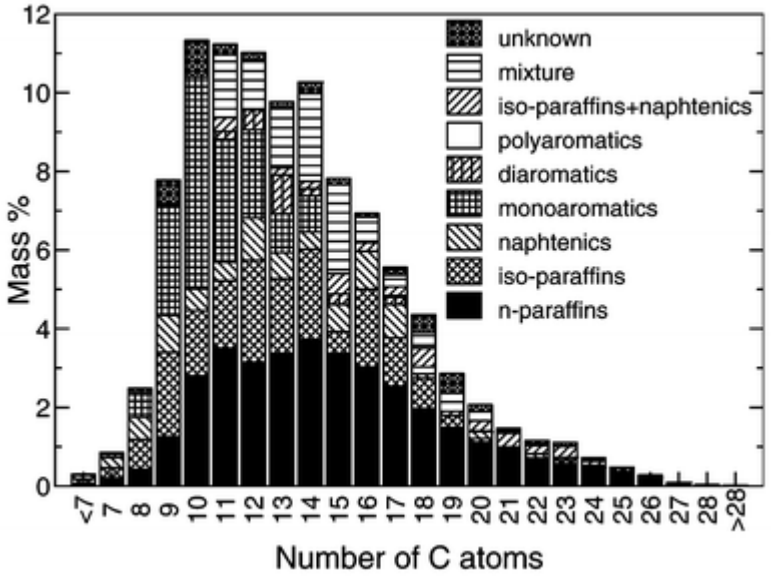

Figure 1.8 Composition of a commercial diesel fuel [11]

1.2.1 Chemical Structure

Before discussing HC oxidation it becomes necessary to identify components whose structure and nomenclature may seem complicated. Cathonnet [12] listed liquid fuel groups, which are also valid for diesel oil, as below

- linear or branched alkanes (paraffins)
- cycloalkanes with one or two rings (naphtenes)
- alkenes
- aromatics with one or several rings
- oxygenates (additives in gasoline and diesel fuel).

Below, elementary knowledge and chemical structure of the most important hydrocarbon components C_xH_y (including partially oxidized ones) will be described regarding to diesel fuel and diesel combustion.

1.2.1.1 Alkanes C_nH_{2n+2} (formerly: parrafins)

An alkane is a long chain of carbon linked together by single bonds and all are saturated (i.e., no more hydrogen can be added to any of the compounds [13]). The general formula for alkanes is C_nH_{2n+2}; the simplest possible alkane is therefore methane, CH_4 (Figure 1.9a). The next simplest is ethane, C_2H_6; the series continues indefinitely [14], i.e., n-heptane (Figure 1.9b). We can distinguish among them [8]:

- n-alkanes, with straight chain structures (higher autoignition tendency, hence not suitable for SI engines) and
- isoalkanes, with branched chain structures (lower autoignition tendency, hence suitable for SI engines)

(a) (b)

Figure 1.9 Examples of alkanes: a) Chemical structure and schematic view of methane (CH_4) and b) Chemical structure of n-heptane (C_7H_{16})

Nearly all alkanes are combustible and are the main components of practical fuels; this is why a good prediction of their combustion properties is crucial. There is a very large experimental and modeling database available for the combustion of lower alkanes, methane and ethane, (the major components of natural gas), and higher alkanes, n-hexadecane (the reference fuel for the cetane index). And also combustion mechanisms of HCs, those for alkanes are relatively more reliable among the others. However, even for the simpler and most studied one, methane, the accuracy of computed flame velocities for lean to rich mixtures lies in the 10-20% range and the situation is worse for higher HCs. This is because of the present uncertainties in both thermodynamic, transport and kinetic parameters of their combustion mechanisms. Although there is considerable progress in the modeling of C_7 and C_8 hydrocarbons in a wide range of temperatures and pressures using semi-detailed or detailed mechanisms, further detailed experimental and theoretical studies are necessary for the accurate prediction of ignition characteristics of branched alkanes, which is of practical importance for the prediction of fuel properties in ICEs.

General thermochemical characteristics of alkanes [10, 15]:

- maximum H/C ratio
- highest heating values per unit mass of liquid hydrocarbon fuels
- lowest densities (620-770 kg/m^3)
- lowest heating values per unit volume of liquid hydrocarbon fuels
- clean burning
- stable when stored

1.2.1.2 Alkenes C_nH_{2n} (formerly: olefins)

Alkenes (olefin or olefine) are hydrocarbon compounds having open unsaturated carbon chain structures with both single and double carbon atom bounds [10]. The compounds are unsaturated since C_nH_{2n} can be saturated to C_nH_{2n+2} [13]. The simplest alkenes, with only one double bond and no other functional groups, form a homologous series of hydrocarbons with the general formula C_nH_{2n} (i.e., ethylene in Figure 1.10a). For compounds having more than one double bond, diolefins, the chemical structure is C_nH_{2n-2} (i.e., allene in Figure 1.10b).

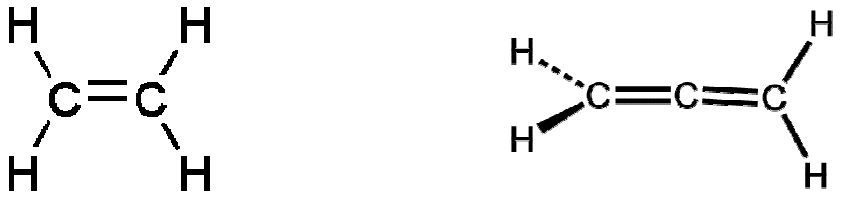

(a) (b)

Figure 1.10 Chemical structure of example alkenes: a) Ethylene (C_2H_4), the simplest alkyne hydrocarbon and b) Allene (C_3H_4)

Alkenes are formed predominantly by cracking heavy alkane compounds. They are relatively stable compounds, but are more reactive than alkanes [16]. Although they are only very minor components of diesel fuel, they are the major primary intermediates in the combustion sequence of hydrocarbons, and for this reason, their oxidation mechanism is a sub-set of the combustion mechanism of alkanes. And the combustion mechanism of alkenes is important for diesel fuel combustion because they have an important role in the formation of Polyaromatic Hydrocarbons (PAH) and soot.

General thermochemical characteristics of alkenes [10]:

- fewer H/C ratio than alkanes
- unstable when formed
- can form residue or gum with exposed O_2
- fairly clean-burning fuel

1.2.1.3 Alkines C_nH_{2n-2} (formerly: acetylenes)

Alkines are hydrocarbon compounds having open unsaturated carbon chain structures with at least one triple bond between two carbon atoms They have the same formula, C_nH_{2n-2}, with the diolefins and are traditionally known as acetylenes (Figure 1.11). Unlike alkanes, alkines are unstable and very reactive [10,17].

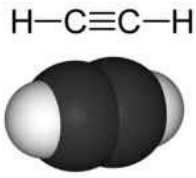

Figure 1.11 Chemical structure and schematic view of the simplest alkine, acetylene (C_2H_2)

1.2.1.4 Cycloalkane C_nH_{2n} (formerly: naphtene)

Cycloalkanes are single bond ring hydrocarbons having unsaturated one or more carbon rings to which hydrogen atoms are attached according to the formula C_nH_{2n}. The compounds are unsaturated since ring can be broken and additional hydrogen added (C_nH_{2n} can be saturated to C_nH_{2n+2}). In Figure 1.12a cyclopropane and in Figure 1.12b illustration of a PAH (source: NASA) are shown respectively.

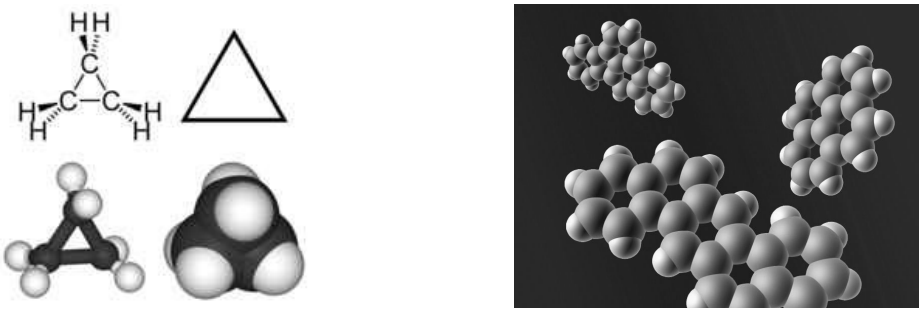

(a) (b)

Figure 1.12 a) Chemical structure and schematic view of cyclopropane (C_3H_6), the simplest cycloalkane hydrocarbon and b) Illustration of typical PAH (source NASA)

While the simple and the bigger cycloalkanes are very stable, like alkanes, the small cycloalkanes - particularly cyclopropane - have a lower stability [18]. They constitute an important fraction of diesel fuel and are suspected to increase PAH and soot emissions in CI engines.

1.2.1.5 Aromatic Compounds

Polycyclic aromatic hydrocarbons (PAHs) are chemical compounds that consist of fused aromatic rings and do not contain heteroatoms or carry substituents. They are formed by incomplete combustion of carbon-containing fuels such as wood, coal, diesel, fat, or tobacco [19]. Building block for aromatic hydrocarbons is then benzene, C_6H_6, ring structure which is shown in (Figure 1.13a). The ring structure is very stable and accommodates additional $–CH_2$ groups in side chains and not by ring expansion, i.e., toluene, C_7H_8, (Figure 1.13b).

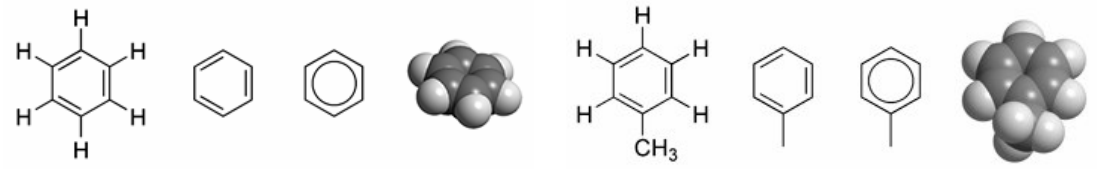

(a) (b)

Figure 1.13 a) Chemical structure and schematic view of a) Benzene (C_6H_6), building block of aromatic hydrocarbons and b) Toluene (C_7H_8)

Diesel fuel includes a significant proportion of polycyclic aromatics (~ 10% by mass). Most kinetic studies on the combustion of aromatics have been devoted to benzene and toluene. Concerning polycyclic aromatics, too many uncertainties remain on the important reaction paths and rate expressions of their combustion, to build comprehensive mechanisms. But because of the key role of aromatic hydrocarbons in the process of auto-ignition and in the formation of soot and other pollutants, a better description of their combustion mechanism, over the wide range of temperatures and pressures existing in ICEs, is of primary importance [12].

General thermochemical characteristics of aromatic compounds [10]:

- compact molecular structure
- stable when stored
- smoky combustion process

– highest fuel distillate densities

– highest heating values per unit volume of liquid hydrocarbon fuels

– lowest heating values per unit mass of liquid hydrocarbon fuels

1.2.1.6 Oxygenated Hydrocarbons

Any fuel substance containing oxygen (includes oxygen-bearing compounds such as ethanol and methanol) is named as oxygenated hydrocarbon and they tend to give a more complete combustion of its carbon into carbon dioxide (rather than monoxide), thereby reducing air pollution from exhaust emissions [20]. Oxygenated hydrocarbons are chain compounds, by among which we distinguish [8]:

– alcohols; contain a hydroxyl group (R-OH) and the simplest alcohols are methanol, CH_3OH, and ethanol, C_2H_5OH, (Figure 1.14).

– ethers; HC chains connected together over an oxygen bridge (R_1-O-R_2)

– ketones; HC remains connected together over a carbonyl group (R_1-CO-R_2)

– aldehydes; contain a CHO group, e.g. formaldehyde, HCHO

Concerning oxygenated compounds which are formed as intermediates in the combustion of hydrocarbons, their nature depends on the temperature regime where oxidation takes place. The more complex situation is at temperature lower than about 850 K, where the reactions of alkyl-peroxy radicals lead to high initial yields of oxygenates such as aldehydes, ketones, alcohols and O-heterocyclic compounds. Among oxygenated molecules used as fuels or additives, only some of them (methanol, ethanol, methyl- and ethyl- tertio butyl ethers, and dimethylether) have been widely studied for the validation of detailed comprehensive oxidation mechanisms, but the variety of oxygenated compounds in biofuels will enlarge the field of investigations [12].

(a) (b)

Figure 1.14 Chemical structure of a) Methanol (CH_3OH) and b) Ethanol (C_2H_5OH)

1.2.2 Physical and Chemical Properties of Diesel Fuel

The boiling temperature of hydrocarbons rises with the number of carbon atoms, whereby the structure of the molecule itself is of a lesser importance (Figure 1.15). Diesel fuels are distillate fractions that boil in the range 240-370 °C. Depending on engine size, speed and load, diesel engines can burn fuels that fall between kerosenes and heavy residuals.

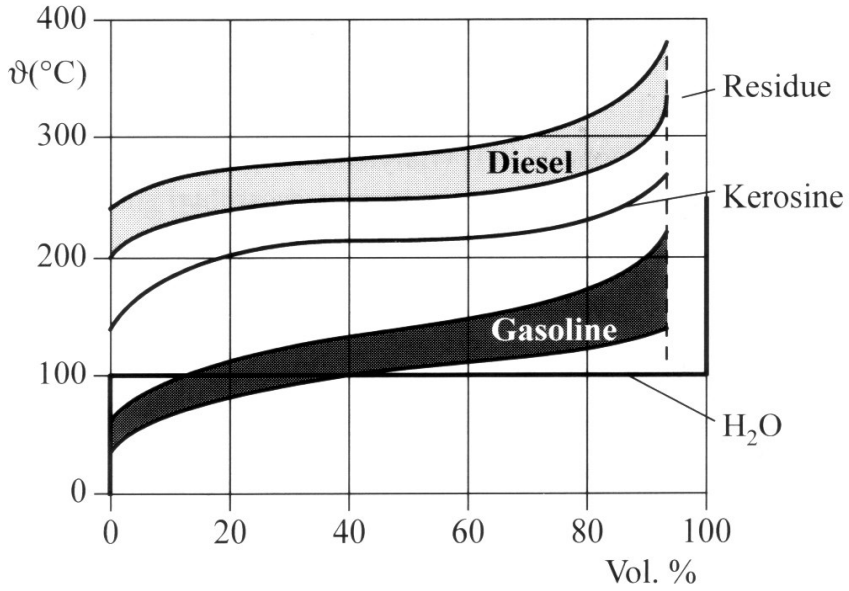

Figure 1.15 Boiling graph for diesel, gasoline, kerosene and water [8]

The lower heating value (LHV) of these components lies in the region:

40.200 kJ/kg (benzene) < LHV < 45.400 kJ/kg (n-pentane)

The density also increases with the number of carbon atoms and lies in the region:

600 kg/m^3 < ρ < 900 kg/m^3

The viscosity also rises with the number of carbon atoms.

In general, high-speed automotive type diesel engines require light kerosene type distillates, medium-speed diesels engines use fuel oil grade distillate, while low speed marine engines can burn heavy residual fuels [10].

Although these physical and chemical properties of diesel fuel such as volatility, density and heat capacity affects ignition and combustion processes, their effects will be insignificant when one considers fully or partially warmed-up engines [7]. The most important property of diesel fuel is the autoignition performance which is characterized by cetane number (CN).

1.2.3 Fuel Ignition Quality

The ignition delay in a diesel engine can be defined as the time (or crank angle) interval between the start of injection (SOI) and the start of combustion. Ignition delay is one of the most important characters of diesel fuel and affects all combustion process, emission formation and as well combustion efficiency. Hence ignition quality of a diesel fuel is very important and is characterized by cetane number. Cetane number scale is defined by blends of two pure hydrocarbon reference fuels (Figure 1.16):

- α-methyl naphthaline ($C_{11}H_{10}$) which has a very low ignition quality, represents the bottom of the scale with CN = 0 and
- n-hexadecane ($C_{16}H_{34}$, cetane) which has a very high ignition quality, represents the top of the scale with CN = 100

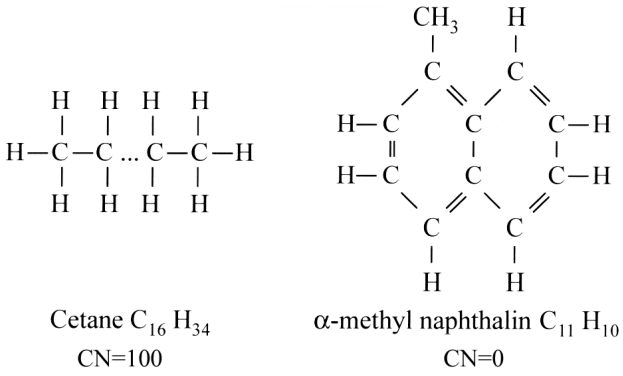

Figure 1.16 Components of the reference fuels for the determination of the cetane number: Left: n-hexadecane ($C_{16}H_{34}$, cetane), CN = 100 and Right: α-methyl naphthaline ($C_{11}H_{10}$), CN = 0

The engine used for cetane number determination is a standardized single-cylinder, variable compression ratio engine with special loading and accessory equipment and instrumentation. Main engine specifications and operating conditions for CN measurement process are: engine displacement volume, V_d = 0.613 dm^3; engine speed, n=900 rpm; SOI = 13 °CA BTDC; coolant temperature, T_{cool} = 100 °C, where compression ratio, ε, varied in the region $7 < \varepsilon < 28$. Details of engine, operating conditions and test procedure are specified by ASTM Method D613 [21]. In order to define CN, two groups of engine tests are done to get the same ignition delay duration (13 °CA) at the same compression ratio for both investigated diesel fuel and the reference fuel blend which its volumetric cetane ratio will give the CN.

This two step process is briefly defined below:

- At first step the engine is operated with the diesel fuel under investigation and start of combustion is adjusted at TDC through altering the compression ratio.
- Then, while compression ratio is kept same as the first run, engine is operated with the varied mixture of reference fuel blends (α-methyl naphthaline and cetane mixture) and cetane ratio in the blend is altered until combustion starts at TDC same as the first step (diesel fuel case). For this condition, the volumetric cetane ratio (percentage) of the blend is determined as the CN of the investigated diesel fuel.

Properties of selected two diesel fuels, Swedish Class 1 diesel (EC1), MK1 and United Kingdom ultra low sulfur diesel (UK ULSD), EN590/2005, are shown in Table 1.2 below. Swedish Class 1 diesel is the fuel used at the experimental work which results are reproduced in this study.

Table 1.2 Properties of selected diesel fuels [22, 23]

Fuel Name		**Swedish Class 1 MK1**	**UK ULSD EN590/2005**
Cetane Number	[-]	51	~ 53
Density (15 °C)	[kg/m^3]	800 ... 820	~ 835
Distillation °C – T10	[°C]	~ 210	~ 200
Distillation °C – T90	[°C]	~ 275	~ 350
Cloud point	[°C]	-22 … -36	~ -5
Heating value (lower)	[MJ/kg]	~ 44	~ 43
Sulphur	[ppm]	< 10	< 10
Polyaromatic content	[%vol]	0.02	~ 4
Aromatic content	[%vol]	< 5	~ 4
Viscosity (40 °C)	[mm^2/s]	1.5 … 4.0	~ 3.5

1.2.4 Future Fuel for Advanced ICEs

Although diesel fuel and diesel-like combustion are the subject of this study, it is worth to glance at the question; “What can be the main characteristics of HC fuel for the future advanced ICEs?” We define diesel fuels as those with CN > ~ 30 and gasoline fuels as those with CN < ~ 30 or Research Octane Number (RON) > ~ 60. Autoignition is determined by chemical kinetics, which depends on the pressure and temperature development, mixture strength and chemical composition of the fuel. Typical, practical diesel fuels have CN > ~ 40 and are very prone to auto-ignition; they will autoignite very quickly before the fuel and air are mixed sufficiently [24].

With the pressure of environmental and economic considerations, it is clear that higher efficiency and lesser emissions are the two main lasting expectations from ICEs. Combustion regimes and applications of both SI and CI engines are changing and new regimes and techniques such as, downsizing, throttles operation, variable compression ratio [25, 26], stratification [27, 28], MR-Process [9, 29], skip-cycle operation [30], etc, for SI engines and Low Temperature Combustion (LTC), Modulated Kinetics (MK), HCCI, etc, for CI engines are in use. Continues improvement of these two type SI and CI engines is getting their advantageous parts together in an applicable form. So this evolution of ICEs brings the need of new kind of fuel(s) which can be different from conventional gasoline or diesel fuels.

Until now, main idea for conventional CI engine (with diffusion combustion) was to increase injection pressures (to reduce soot, C(s), emissions) and the use of EGR (to reduce NO_x emissions) and these were supported by additional various concepts and technological applications such as different injection strategies, EGR, turbocharging, complicated and expensive injection and aftertreatment systems. Also this trend demands a fuel prone to autoignition (e.g., CN > 40). But, this extreme pressurizing brings some additional problems and considerable cost which makes it more questionable. Hence, new tendency arises switching from diffusion combustion to HCCI combustion which still has many unsolved problems. For this reason, now it becomes more important to properly understand fuel requirements for this incoming engine [31, 32, 33]. Because of present problems of HCCI engine, an alternative way may be promoting premixing of fuel and air before combustion, i.e., partially premixed engine.

Thus if the aim is to promote premixed combustion i.e. increase engine ignition delay in CI engines in order to control smoke and NO_x, the fuel needs to be as much like gasoline as possible. It was demonstrated that it is possible to run a CI engine on gasoline at high load and low smoke, low NO_x and low Indicated Fuel Specific Consumption (ISFC). The combustion mode is partially pre-mixed – "pre-mixed enough" – autoignition [34]. So at the moment, the practical debate on fuel autoignition quality in CI engines is about whether future engines will require higher cetane in the 40 to 60 range, not whether diesel fuel should be replaced by gasoline. If these future engines want to promote premixed combustion, higher fuel CN will certainly not help; it might hinder such operation. On the other hand if the strategy

used to control smoke and NO_x at high loads is to promote (low temperature) diffusion combustion and use exhaust aftertreatment, the fuel would need to have low resistance to autoignition – high CN. These will eventually have to be agreed by the different stakeholders such as the auto and oil industries, governments and regulatory bodies and environmental interests. In general the prospect of more premixed combustion in future CI engines is likely to reduce the pressure on the cetane requirement but might increase, to a lesser extent, the pressure on the volatility requirement of fuels for such engines [35, 36].

2 CONSTRUCTION OF A DIESEL OIL SURROGATE (DOS) MODEL

Conventional diesel fuel consists of a complex, ill-defined mixture of hundreds of hydrocarbon species (aliphatic, cyclic and aromatic compounds), many of them including more than 10-15 carbon atoms (see Figure 1.8). Furthermore, the exact composition of commercially available diesel fuel varies from day-to-day and from one fuel supply to another. Hence, their combustion chemistry is too complex to be modeled using detailed chemical mechanisms for all components. For careful modeling studies, it is necessary to identify a well-characterized fuel such as simple mixture of HCs called diesel oil surrogate (DOS) model. DOS models are used in numerical simulations and DOS models must have reproducible combustion characteristics that are similar to those of diesel fuel [37].

2.1 CHALMERS Diesel Oil Surrogate Model

Pure n-heptane, C_7H_{16}, is routinely used as a single component fuel to approximate the oxidation paths of real diesel fuel. Because aliphatic components can be represented by long chain HCs such as n-heptane due to its ignition properties and CN of ~ 56, which is similar to the CN of conventional diesel oil (Table 1.2). But, the amounts of soot produced from n-heptane alone are considerably less than those of real diesel oil because n-heptane has no aromatic characteristics. Therefore, an aromatic component, toluene, $C_7H_{8,}$ which ignite more slowly than n-heptane and significantly contributes to soot formation, should be added to the model. So, DOS model which can sufficiently represent the CN as well as the other properties of a real fuel, is assumed to be a 70/30 % mixture of n-heptane and toluene [38, 39].

If the physical properties of the model fuel are represented by properties of real diesel oil, the difference in combustion models seems not critical [40]. DOS model consists of two parts, describing the thermal and transport properties of the liquid fuel and its vapor and chemical (ignition) properties of vapor constituents. Diesel fuel as it is described in the KIVA-3VR2 [41] code is a compilation of properties of real diesel oil with a proposed chemical formula $C_{13}H_{23}$. Since n-heptane and toluene

are components of a similar volatility, the one-component fuel representation predicts reasonably well the spatial distribution and the local composition of the fuel vapor as it was demonstrated in [42], where multi-component fuel evaporation model based on the NIST HC thermo-physical properties database [43] has been used. To achieve a consistency with a proposed proportion of the vapor constituents, the fuel formula has been changed to $C_{14}H_{28}$. Then, detailed reaction mechanisms for n-heptane and toluene oxidation have been developed and validated using shock-tube auto-ignition experimental data [44, ANNEX 1].

3 CHEMICAL KINETIC ANALYSIS OF COMPLEX CHEMICAL MECHANISMS

3.1 Chemical Kinetics

Chemical kinetics is a branch of physical chemistry devoted to the analysis of reaction dynamics in time [45]. Before describing basic knowledge of chemical kinetics analysis which can be useful for an ICE engineer, the fundamental definitions are given according to [1].

3.1.1 Fundamental Definitions

A chemical reaction is the exchange and/or rearrangement of atoms and energy between colliding molecules. In the course of chemical reaction, e.g.,

$$\mathrm{HCN} + \mathrm{OH} \rightarrow \mathrm{CN} + \mathrm{H_2O} \tag{3.1}$$

the atoms (C, H, O and N) are conserved; i.e., they are not created or destroyed. On the other hand in (3.1), relevant molecules (HCN, OH, CN and H_2O) are not conserved. Reactant molecules are rearranged to become product molecules, with simultaneous release of heat. Also product molecules can be rearranged to become reactant molecules if the reactions are reversible (in two ways).

Atoms and molecules are conveniently counted in terms of amount of substance mass (unit: g) or mole numbers (unit: mol).

- 1 mol of a compound corresponds to $6.023 \cdot 10^{23}$ particles (atoms, molecules, etc.). This is Avogadro constant (Avogadro number), $N_A = 6.023 \cdot 10^{23}$ mol^{-1}.
- The mole fraction x_i of the species i denotes the ratio of the mole number n_i of the species i to the total mole number $n = \sum n_i$ of the mixture ($x_i = n_i / n$).
- The mass m is a fundamental property of matter (unit: kg). The mass fraction Y_i is the ratio of the mass m_i of the species i to the total mass $m = \sum m_i$ of the mixture ($Y_i = m_i / m$).

– The molar mass (molecular weight) M_i (unit: g/mol) of species *i* is the mass of 1 mol of this species. Some examples (for atomic carbon, molecular hydrogen, molecular oxygen, and methane) are M_C = 12 g/mol, M_{H_2} = 2 g/mol, M_{O_2} = 32 g/mol, M_{CH_4} = 16 g/mol. The mixture mean molar mass $\overline{M}$ (unit: g/mol) denotes an average molar mass, using the mole fractions as weighting ($\overline{M} = \sum x_i M_i$).

From above it is possible to obtain (2.1) and (2.2) relations (*S* is the number of different species):

$$Y_i = \frac{M_i n_i}{\sum_{j=1}^{S} M_j n_j} = \frac{M_i x_i}{\sum_{j=1}^{S} M_j x_j} = \frac{M_i x_i}{\overline{M}} \tag{3.2}$$

$$x_i = \frac{Y_i / M_i}{\sum_{j=1}^{S} Y_j / M_j} = \frac{Y_i}{M_i}\overline{M} \tag{3.3}$$

Variables that do not depend on the size (extent) of the system are called intensive properties and they are defined as the ratio of the corresponding extensive properties (which depend on the size of the system) and system volume *V*. Examples of intensive properties are

mass density (density)	$\rho = m/V$	kg/m^3
molar density (concentration)	$c = n/V$	mol/m^3

We can rewrite mean molar mass with density and concentration:

$$\frac{\rho}{c} = \frac{m}{n} = \overline{M} \tag{3.4}$$

Note that concentrations *c* of chemical species defined in this way (2.3) are usually denoted by species symbols in square brackets, e.g., c_{H_2O} = [H_2O].

For the gases and gas mixtures in combustion processes, the thermal equation of state relates temperature, pressure and density of the gas. For many conditions it is satisfactory to use the ideal gas equation of state,

$$pV = nRT \tag{3.5}$$

where,

p : pressure Pa

V : volume m^3

n : mole number mol

T : temperature K

R : universal gas constant $= 8.314\ J \cdot mol^{-1} \cdot K^{-1}$.

From relations (3.4)-(3.5), it follows that

$$c = \frac{p}{RT} \quad \text{and} \quad \rho = \frac{p\overline{M}}{RT} = \frac{p}{RT\sum_{i=1}^{S}\frac{Y_i}{M_i}} \tag{3.6}$$

When temperatures are close or below than the critical temperature, or when pressures are close or above critical pressures, the concentration or density is inadequately predicted using the ideal gas equation of state (3.6). The system is better approximated as a real gas.

3.1.2 Reaction Mass Balance Equation

Consider a one-step chemical reaction of arbitrary complexity, reaction equation for stoichiometric condition can be written in general form as (3.7) below:

$$\sum_{s=1}^{S} v_s^{'} c_s = \sum_{s=1}^{S} v_s^{''} c_s \tag{3.7}$$

where,

$v_s^{'}$: stoichiometric coefficient of the reactants

$v_s^{''}$: stoichiometric coefficient of the products

c_s : specification of s- chemical species

S : total number of species involved.

We can give an example reaction such as $H + H + H \longrightarrow H_2 + H$ to clarify this notation,

where,

$S = 2$

$c_1 = H \qquad c_2 = H_2$

$v_1^{'} = 3 \qquad v_1^{''} = 1$

$v_2^{'} = 0 \qquad v_2^{''} = 1.$

Then from (3.7) we can write a mass balance equation as (3.8) of this reaction. If a species represented by c_s does not occur as a reactant or product, its stoichiometric coefficient, v_s, will be equal to zero (in our example there is no H_2 as reactant, hence $v_2^{'} = 0$).

$$3 \cdot \mathrm{H} + 0 \cdot \mathrm{H_2} \longrightarrow 1 \cdot \mathrm{H} + 1 \cdot \mathrm{H_2} \tag{3.8}$$

3.1.3 Rate of a Chemical Reaction

If we consider that chemical reactions are fast compared to the other processes like diffusion, heat conduction and convection, thermodynamics alone is enough to describe the system locally. In this situation, we use thermodynamics which doesn't give any information about *rate* of the processes since *time* is not considered in thermodynamics. In most cases, however, chemical reactions occur on time scales comparable with that of the flow and of the transport processes (molecular or turbulent) which are also the processes of ICE field [1]. Therefore, information is needed about the rate of chemical reactions, i.e., chemical kinetics which considers time.

A chemical reaction with its general case is shown in as below:

$$\mathrm{A} + \mathrm{B} + \mathrm{C} + ... \xrightarrow{k} \mathrm{D} + \mathrm{E} + \mathrm{F} + ... \tag{3.9}$$

where A, B, …,D, E, … are the reactant and product species involved in the reaction, *k* is the reaction rate coefficient. First of all, chemical reactions rarely proceed in one stage such as written in (3.9). This is a conventional single-stage writing of the equation of chemical reactions and indicates only the initial and final stages of the system which in essence is a symbolic expression of the mass balance (the law of conservation of mass). In actual conditions, a reaction usually proceeds through a number of intermediate stages, in which, the rate of the reaction being determined by that of the slowest stage [45]. System conditions such as:

- concentration of reactants
- temperature, pressure
- radiation and turbulence effects
- presence of a catalyst or inhibitor

affect the reaction rate [13]. A rate law is based on the empirical formulation of the reaction rate [1]. The reaction rate may be expressed in terms of the concentration of any of the reacting substances or of any reaction product [13]. So, the reaction rate for (3.9) may be expressed as:

- the rate of decrease of concentration of reactants (e.g., A, B, C) or,
- the rate of increase of concentration of products (e.g., D, E, F).

In other words, it is sufficient to know the change in the concentration of only one of the reactant or product participating in a chemical reaction in time to find its rate, since the changes in the concentrations of all the remaining substances can be determined on the basis of stoichiometry (see Equation 3.9) [45]. To understand the reaction rate formulation, it will be useful to remember the very beginning of investigations in gas chemical kinetics; the physically obvious assumption was made that only molecules which collide react. The number of collisions is obviously directly proportional to the number of molecules; therefore the rate of a reaction should be proportional to the concentrations of the reactants, i.e., considering the consumption of species A, the reaction rate for (3.9) can be expressed according to

$$\frac{\mathrm{d}[\mathrm{A}]}{\mathrm{dt}} = -k \cdot [\mathrm{A}]^a [\mathrm{B}]^b [\mathrm{C}]^c \ldots \tag{3.10}$$

Here a, b, c … are reaction orders with respect to species A, B, C … and k is the rate coefficient of the reaction. The sum of all exponents ($a + b + c$…) is the overall reaction order. The (3.10) expression is the empirical formulation of the reaction rate and is called fundamental postulate of gas chemical kinetics.

Frequently some species are in excess and their concentrations do not change noticeably. If, e.g., [B], [C], … remain nearly constant during the reaction, an effective rate coefficient can be generated from the rate coefficient and the nearly constant concentrations of the species in excess, and using $k_{\mathrm{exp}} = k \cdot [\mathrm{B}]^b [\mathrm{C}]^c \ldots$, one obtains as a simplified version of (3.10)

$$\frac{\mathrm{d}[\mathrm{A}]}{\mathrm{dt}} = -k_{\mathrm{exp}} \cdot [\mathrm{A}]^a \tag{3.11}$$

The temporal change of the concentration of species A can be calculated by integrating (3.11) as it will be shown in the next chapter with some additional information about reaction orders.

3.1.4 Reaction Orders of Chemical Reactions

As it is described above, the order of a reaction with respect to a certain reactant (i.e., with respect to A, B, C in (3.10)) is defined, in chemical kinetics, as the power to which its concentration term in the rate equation is raised. And the total reaction order is the sum of all concentration terms' powers. If the reaction is an elementary reaction, then reaction order is related to the stoichiometric coefficients of the reaction. Otherwise, in complex (global) reactions, reaction orders may or may not be equal to stoichiometric coefficients. So it is not necessary that the reaction order is a whole number (zero and fractional values of order are possible) but they tend to be integers. Reaction orders can be determined by experiment and their knowledge allows conclusions about the reaction mechanism [46].

If one considers (3.11), for first-order reactions (a = 1), integration of (3.11) yields the concentration time behavior reads

$$\ln\frac{[\mathrm{A}]_t}{[\mathrm{A}]_0} = -k_{\exp}(t - t_0), \tag{3.12}$$

where $[\mathrm{A}]_0$ and $[\mathrm{A}]_t$ denote the concentrations of species A at time t_0 and t, respectively.

For second-order reactions (a = 2), the temporal behavior reads

$$\frac{1}{[\mathrm{A}]_t} - \frac{1}{[\mathrm{A}]_0} = k_{\exp}(t - t_0). \tag{3.13}$$

For third-order reactions (a = 3), the temporal behavior reads

$$\frac{1}{[\mathrm{A}]_t^2} - \frac{1}{[\mathrm{A}]_0^2} = 2k_{\exp}(t - t_0). \tag{3.14}$$

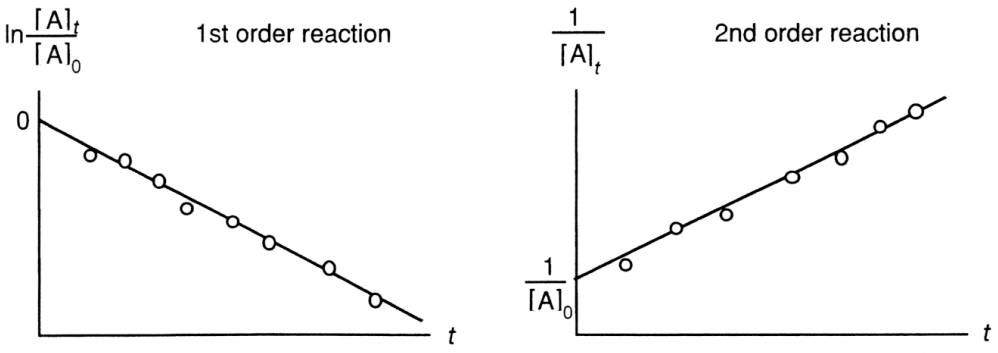

Figure 3.1 Time behavior of the concentrations for first- and second-order reactions [1]

If the time behavior is measured, the reaction order can be determined. Logarithmic plots of concentrations versus time for first-order reactions lead to linear dependences with the slope $-k_{exp}$ and plots of $1/[A]_t$ versus time for second order reactions lead to linear dependences with the slope k_{exp} (see Figure 3.1).

The unit of the reaction rate constant, k, depending on the reaction order a, will be $[(\text{concentration})^{a-1} \cdot (\text{time})]^{-1}$. So, the unit of k according to the order of reactions can be given as in Table 3.1 below.

Table 3.1 Unit of reaction rate coefficient, k

Reaction order	**Unit of reaction rate coefficient, k**
1	$[s^{-1}]$
2	$[mol \cdot cm^{-3} \cdot s^{-1}]$
3	$[mol^2 \cdot cm^{-6} \cdot s^{-1}]$

3.1.5 Relation of Forward and Reverse Reactions

In chemical kinetics, reactions that simultaneously and independently proceed in two directions (forward and reverse) at different rates are called reversible. For the reverse reaction of (3.9), the rate law for the production of A can be written analogous to (3.10)

$$\frac{d[A]}{dt} = k^{(r)} \cdot [D]^d [E]^e [F]^f \ldots \tag{3.15}$$

In fact, on the micro-scale (molecular level) chemical reaction (3.9) always progresses in both forward and reverse directions as mentioned above. It is characteristic of reversible reactions that in a certain time after they balance the rates of forward and the reverse reactions which become equal and a state of chemical equilibrium sets in. In other words, at chemical equilibrium, forward $^{(f)}$ and backward $^{(r)}$ reactions have the same rate on a microscopic level still progressing in both directions. However, on a macroscopic level, no net reaction can be observed. Therefore, at chemical equilibrium,

$$k^{(f)} \cdot [A]^a [B]^b [C]^c \ldots = +k^{(r)} \cdot [D]^d [E]^e [F]^f \ldots$$

or

$$\frac{[D]^d [E]^e [F]^f \ldots}{[A]^a [B]^b [C]^c \ldots} = \frac{k^{(f)}}{k^{(r)}} = K_c(T) \tag{3.16}$$

The expression in (3.16) corresponds to the equilibrium constant, K_c, of the reaction which can be calculated from thermodynamic data, and, thus, an important relation between the rate coefficients of forward and reverse reactions can be obtained,

$$K_c = \frac{k^{(\mathrm{f})}}{k^{(\mathrm{r})}} = \exp\left(-\Delta_R \overline{A}^0 / RT\right) \tag{3.17}$$

where,

K_c : equilibrium constant of the reaction

$k^{(\mathrm{f})}$: forward reaction rate constant

$k^{(\mathrm{r})}$: reverse reaction rate constant

$\Delta_R \overline{A}^0$: free energy of the reaction

R : universal gas constant

T : temperature.

All chemical reactions are reversible, but at definite conditions some of them can proceed only in one direction up to the practically complete disappearance of the reactants. Such reactions are called irreversible in which at least one product is removed from the sphere of the reaction, or which are attended by a great positive heat [45].

3.1.6 Elementary and Global Reactions and Reactions Molecularity

As it is mentioned in section 3.1.2, chemical reactions rarely proceed in one stage and we can classify them into two groups as elementary and global reactions.

3.1.6.1 Elementary Reactions

Open form of equation (3.7) can be written as below,

$$v_1' c_1 + v_2' c_2 + \ldots + v_S' c_S \xrightarrow{k} v_1'' c_1 + v_2'' c_2 + \ldots + v_S'' c_S \tag{3.18}$$

If one supposes that the reaction proceeds on a molecular level in one step, exactly in the way which is described by the reaction equation (3.18), such type of a reaction is called elementary reaction. The reaction of hydroxyl radicals (OH) with molecular hydrogen (H_2) forming water and hydrogen atoms is such an elementary reaction,

$$\mathrm{OH} + \mathrm{H_2} \longrightarrow \mathrm{H_2O} + \mathrm{H}. \tag{3.19}$$

Due to the molecular motion in the gas, hydroxyl radicals collide with hydrogen molecules. While most of these collisions are non-reactive in which, the molecules collide and bounce apart but some few collisions are reactive, the molecules react and products H_2O and H result from these collisions [1]. Some basic characteristics of elementary reactions;

- rate laws can always be specified for elementary reaction mechanisms,
- reaction order of elementary reactions is always constant (independent of time and of experimental conditions) and can be determined very easily, and
- reaction order of elementary reactions is equal to the molecularity of the reactions.

Molecularity is equal to the number of molecules that interact in the reaction step. If one molecule is transformed, the reaction is called a unimolecular; if two molecules participate in an elementary reaction, it is called bimolecular, etc. Since the probability of the simultaneous collision of a great number of particles is quite small, the molecularity of a one-step elementary reaction does not exceed three (trimolecular reactions).

Unimolecular reactions describe the rearrangement or dissociation of a molecule,

$$\mathrm{A} \longrightarrow \text{products.} \tag{3.20}$$

Unimolecular reactions have first-order time behavior and if the initial concentration is doubled, the reaction rate is also doubled.

Bimolecular reactions are the reaction type found most. They proceed according to reaction equations

$$\begin{aligned} &\mathrm{A} + \mathrm{B} \longrightarrow \text{products} \\ &\text{or} \\ &\mathrm{A} + \mathrm{A} \longrightarrow \text{products.} \end{aligned} \tag{3.21}$$

Bimolecular reactions have always a second-order rate law. Doubling of the concentration of each reaction partner quadruples the reaction rate.

Trimolecular reactions are usually recombination reactions. They obey a third-order rate law,

$$\mathrm{A + B + C} \longrightarrow \text{products}$$

or

$$\mathrm{A + A + B} \longrightarrow \text{products} \qquad (3.22)$$

or

$$\mathrm{A + A + A} \longrightarrow \text{products.}$$

After these definitions it is possible to formulate a general notation depending on the mass balance equation, (3.7), which is confirmed experimentally, and empirical formulation of reaction rate, (3.10), to define the rate of disappearance of a chemical reactant species *i*, defined as $\frac{\partial c_i}{\partial t}$, where each reactant concentration is raised to a power equal to the corresponding stoichiometric coefficient ($v_s^{'}$); i.e.,

$$\frac{\partial c_i}{\partial t} \approx \prod_{s=1}^{S} c_s^{\,v_s^{'}} \quad \rightarrow \quad \frac{\partial c_i}{\partial t} = k \prod_{s=1}^{S} c_s^{\,v_s^{'}}. \qquad (3.23)$$

Here, the order of a reaction with respect to a given reactant species *s* is $v_s^{'}$ and it is also the stoichiometric coefficient of this reactant species, *s*. The overall reaction order of an elementary reaction is equal to the sum of the stoichiometric coefficients of the reactant species, $\sum v_s^{'}$ = S. In other words this overall order is equal to the number of molecules participating in the reaction and is called molecularity.

In actual reacting system, considering both reactant and products, the rate of change of the concentration of a given species *i* in a reaction *r* is given by,

$$\left(\frac{\partial c_i}{\partial t}\right)_r = k_r \left(v_{ri}^{''} - v_{ri}^{'}\right) \prod_{s=1}^{S} c_s^{\,v_{rs}^{'}}. \qquad (3.24)$$

where,

$v_{ri}^{'}$: stoichiometric coefficient of the reactants

$v_{ri}^{''}$: stoichiometric coefficient of the products

c_s : concentration of species *s*

S : total number of species involved.

Then, for an example elementary reaction,

$$\mathrm{H + O_2} \longrightarrow \mathrm{OH + O} \qquad (3.25)$$

considering the definition (3.24) one can write the rate laws such as below:

$$
\begin{aligned}
\mathrm{d[H]}/\mathrm{d}t &= -k\,[\mathrm{H}]\,[\mathrm{O_2}] \\
\mathrm{d[O_2]}/\mathrm{d}t &= -k\,[\mathrm{H}]\,[\mathrm{O_2}] \\
\mathrm{d[OH]}/\mathrm{d}t &= k\,[\mathrm{H}]\,[\mathrm{O_2}] \\
\mathrm{d[O]}/\mathrm{d}t &= k\,[\mathrm{H}]\,[\mathrm{O_2}]\ .
\end{aligned}
\tag{3.26}
$$

And for the another elementary reaction (3.27) the rate laws are given in (3.28),

$$\mathrm{OH + OH \longrightarrow H_2O + O} \tag{3.27}$$

$$
\begin{aligned}
\mathrm{d[OH]}/\mathrm{d}t &= -2\,k\,[\mathrm{OH}]^2 \\
\mathrm{d[H_2O]}/\mathrm{d}t &= k\,[\mathrm{OH}]^2 \\
\mathrm{d[O]}/\mathrm{d}t &= k\,[\mathrm{OH}]^2\ .
\end{aligned}
\tag{3.28}
$$

3.1.6.2 Global Reactions

Contrary to the (3.25) the reaction below is not elementary, instead a global reaction.

$$\mathrm{2H_2 + O_2 \longrightarrow 2H_2O} \tag{3.29}$$

It is known that water is not produced by single collision between three reacting molecules as it is shown in (3.29). Instead of this many intermediates like H, O, and OH are formed. In fact there is no such a one-step reaction which is identical to any global reaction representation (e.g. reaction which is given in (3.29)). This is a symbolic representation of the result of large number of (e.g., several thousand, depending on the considered global reaction) different elementary reactions which are combined and formed so-called reaction mechanism. If this reaction mechanism is composed of all possible elementary reactions in the system (complete mechanism), then it is valid for all conditions (i.e., temperatures and mixture compositions) [1, 47]. Some basic characteristics of global reactions are summarized below;

- they have very complicated rate laws such as in (3.10) or even more complex,
- the reaction orders are usually not integers, can be even negative depending on time and reaction conditions,
- an extrapolation of the reaction orders to conditions where no experiments exist is not reliable or even completely wrong,
- they are a consequence of a large number of elementary reactions which resolution of them is hard and time-consuming task.

3.1.7 Temperature Dependence of Rate Coefficients (Arrhenius Law)

Chemical reactions' rate coefficients strongly depend on temperature in a nonlinear way. The Arrhenius equation is a simple, but remarkably accurate, formula for the temperature dependence of a rate coefficient, as this coefficient includes all magnitudes that affect reaction rate except for concentration. The equation was first proposed by the Dutch chemist J. H. van't Hoff in 1884; five years later, the Swedish chemist Svante Arrhenius provided a physical justification and interpretation for it [48]. This temperature dependence can be described empirically by a simple formula (Arrhenius Law)

$$k = A' \cdot \exp\left(-\frac{E_a'}{RT}\right). \tag{3.30}$$

k : reaction rate coefficient

A' : pre-exponential factor

E_a' : activation energy of the reaction

R : universal gas constant

T : temperature.

Recent accurate measurements showed a temperature dependence of the pre-exponential factor, A' also which the new form of Arrhenius equation becomes

$$k = AT^b \cdot \exp\left(-\frac{E_a}{RT}\right). \tag{3.31}$$

Basically Arrhenius equation consists of two parts. First term, A' is the gas kinetic collision frequency which includes the steric factor and all variables other than concentration of the species and gives the collision amount of the reactants. More detailed explanation will be given later. Second term is $\exp(-E_a/RT)$ which is Boltzmann factor. It gives the fraction of all molecules that possess energy greater than certain amount activation energy, E_a, which is necessary to initiate a reaction process when they collide (see Figure 3.2). Maximum value of this activation energy corresponds to the bond energies in the molecule (in dissociation reactions, e.g., the activation energy is approximately equal to the bond energy of the bond, which is split), but it can also be much smaller (or even zero), if new bonds are formed simultaneously with the breaking of old bonds.

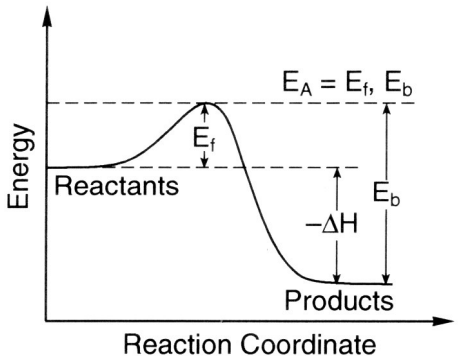

Figure 3.2 Energy as a function of a reaction coordinate for a reacting system [13]

Additionally to the stable reactants and products, there is also reacting species at the activated energy, E_a, which can be regarded as some intermediate complex that leads to the products [13]. In this figure both forward and backward (reverse) reactions' activation energy E_a is shown as E_f, and E_b, respectively. A reaction may occur in both directions (product species can revert to reactants by a reverse reaction). Note that E_b, activation energy for reverse reaction, is much larger than E_f.

Figure 3.2 shows an exothermic reaction behavior which characteristically release energy, $-\Delta H$, when reactants converted to products. Its opposite is endothermic reactions which characteristically reactants need specific amount of energy to be converted to products (i.e. backward reaction for this example need energy equal to E_b to occur). In global reactions energy release from an exothermic reaction can sustain other endothermic reactions such as backward reaction in Figure 3.2. If energy release from an exothermic reaction greater than the activation energy of the process, then it may sustain the backward reaction. For example acetylene decomposition is this type of reaction hence acetylene is considered an unstable species. On the contrary, for the benzene decomposition, the released energy is smaller than the activation energy and it will not be enough to sustain decomposition. For this reason benzene is considered stable species. Taking the natural logarithm of Arrhenius equation (3.30) results equation (3.32).

$$\ln(k) = \left(-\frac{E_a}{R}\right)\frac{1}{T} + \ln(A') \tag{3.32}$$

For elementary reaction, if one plots this logarithm of reaction rate constant according to reciprocal temperature as shown in Figure 3.3, the slope of this line will be equal to $(-E_a/R)$.

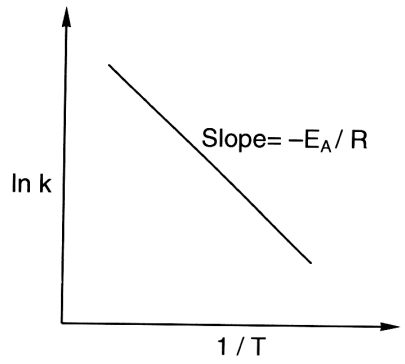

Figure 3.3 Arrhenius plot of the reaction rate as a function of the reciprocal temperature

So if the Arrhenius plot of a reaction is given then activation energy, E_a, can be determined easily according to the slope of the plot. At low temperatures, low activation energy processes proceed faster than high activation energy processes and they are much less temperature sensitive. At high temperatures, high activation energy reactions can be dominant because of this temperature sensitivity.

First term in Arrhenius equation, pre-exponential factor, A', is usually less effective in comparison to Boltzmann factor. It has a very mild $T^{1/2}$ temperature dependence which is often obscured by the experimental uncertainty (this temperature dependence is neglected in Arrhenius plots such as in Figure 3.3). But for very low activation energies, or for very high temperatures, Boltzmann factor goes to 1. Then the reaction rate is only governed by the pre-exponential factor A' or AT^b, respectively. It takes into account steric factor and collision frequency terms. When complex molecules are reacting every collision does not result with a reaction because of an activation energy barrier as mentioned in detail above. It is not enough to only exceed this activation energy level for the molecules which collide; also they must have the proper steric orientation for the specific reaction which is given by a constant, steric factor. Steric factor expresses the probability that the molecules contain a favorable orientation and will be able to proceed in a collision. It can be defined as the ratio between the pre-exponential factor and the collision frequency. Although it is most often less than unity, it can be greater than zero (10^{-8} < steric factor < 10^{+2} [45]). Usually when the reactant molecules are more complex, the steric factor is lower [49]. This pre-exponential factor has different meanings in uni-, bi- and trimolecular reactions:

For unimolecular reactions, 1/*A* corresponds to mean lifetime of an activated (reactive) molecule. In dissociation reactions, this lifetime is determined by the frequency of the vibration of the bond which is broken. Typically pre-exponential factor is equal to the twice the frequency of the bond vibration ($A' \sim 10^{14}$-10^{15} s^{-1}).

For bimolecular reactions, pre-exponential factor A' corresponds to a product of collision rate and probability of reaction. This collision rate is an upper limit for the reaction rate ($A' \sim 10^{13}$-10^{14} $cm^3mol^{-1}s^{-1}$) [1].

In trimolecular reactions, a third collision partner (M) has to remove the energy of the reaction. If, for example, two hydrogen atoms collide and form a hydrogen molecule for a short time, this molecule will dissociate immediately because of the excess of energy in the molecule. A three-body reaction is actually two bi-molecular reactions in rapid succession [1].

3.1.8 Pressure Dependence of Rate Coefficients

Dissociation (unimolecular) and recombination (trimolecular) reaction rate coefficients' depend on temperature, hence these reactions are not elementary; they are in fact a sequence of reactions. According to Lindemann, a unimolecular decomposition is only possible, if the energy in the molecule is sufficient to break the bond. Before the decomposition reaction, this required energy is added to the molecule by collision with other molecules M. This excited molecule may decompose into the products, or it can deactivate through a collision [1],

$$\begin{aligned} &\mathrm{A} + \mathrm{M} \xrightarrow{k_\mathrm{a}} \mathrm{A}^* + \mathrm{M} && \text{(activation)} \\ &\mathrm{A}^* + \mathrm{M} \xrightarrow{k_{-\mathrm{a}}} \mathrm{A} + \mathrm{M} && \text{(deactivation)} \\ &\mathrm{A}^* \xrightarrow{k_\mathrm{u}} \mathrm{P(products)} && \text{(unimolecular reaction).} \end{aligned} \tag{3.33}$$

According to (3.24) we can write rate equations for this case,

$$\frac{\mathrm{d}[\mathrm{P}]}{\mathrm{d}t} = k_\mathrm{u}[\mathrm{A}^*]$$

and (3.34)

$$\frac{\mathrm{d}[\mathrm{A}^*]}{\mathrm{d}t} = k_\mathrm{a}[\mathrm{A}][\mathrm{M}] - k_{-\mathrm{a}}[\mathrm{A}^*][\mathrm{M}] - k_\mathrm{u}[\mathrm{A}^*].$$

Assume that the concentration of the reactive intermediate is in a quasi-steady state,

$$\frac{\mathrm{d}[\mathrm{A}^*]}{\mathrm{d}t} \approx 0, \tag{3.35}$$

one obtains for the concentration of the activated species [A*] and the formation of the product P

$$[\mathrm{A}^*] = \frac{k_\mathrm{a}[\mathrm{A}][\mathrm{M}]}{k_{-\mathrm{a}}[\mathrm{M}] + k_\mathrm{u}}$$

and

$$\frac{\mathrm{d}[\mathrm{P}]}{\mathrm{d}t} = \frac{k_\mathrm{u} k_\mathrm{a}[\mathrm{A}][\mathrm{M}]}{k_{-\mathrm{a}}[\mathrm{M}] + k_\mathrm{u}}. \tag{3.36}$$

Now we can evaluate reaction rate for two extreme cases; very low pressure and very high pressure. For the low pressure range, the concentrations of the collision partners M is very small, thus, $k_{-\mathrm{a}}[\mathrm{M}] \ll k_\mathrm{u}$, one obtains a second-order rate law

$$\frac{\mathrm{d}[\mathrm{P}]}{\mathrm{d}t} = k_\mathrm{a}[\mathrm{A}][\mathrm{M}]. \tag{3.37}$$

Reaction rate is proportional to the concentrations of species A and collision partner M, because the activation is slow (i.e., rate limiting) at low pressures. For high pressure range, the collision partner M has a large concentration and, $k_{-\mathrm{a}}[\mathrm{M}] \gg k_\mathrm{u}$, one obtains first-order rate law

$$\frac{\mathrm{d}[\mathrm{P}]}{\mathrm{d}t} = \frac{k_\mathrm{u} k_\mathrm{a}}{k_{-\mathrm{a}}}[\mathrm{A}]. \tag{3.38}$$

Reaction rate does not depend on concentrations of collision partners, because at high pressures collisions occur very often and, thus, the decomposition of the activated molecule A* is rate-limiting instead of the activation [1].

So Lindemann mechanism illustrates the fact that the reaction orders of global reactions (i.e., non-elementary) depend on the conditions chosen.

The rate coefficients of unimolecular reactions depend on temperature and they show different temperature dependence at different values of pressure. The appropriate treatment of pressure-dependent reactions is important because many experiments on reaction kinetics are done at different pressures from the combustion processes which occur at elevated pressures. So it can be necessary to determine rate coefficients at specified temperature and pressure to treat combustion conditions properly.

3.1.9 Transition State (Activated Complex) Theory

For recombination (trimolecular) and low activation energy free-radical reactions, Arrhenius equation (2.24) is not suitable. For this low-activation free-radical case the transition state theory (TST) of reaction rates gives a more appropriate correlation of reaction rate data with temperature [13]. Both the Arrhenius and the TST describe the temperature dependence of the reaction rate. While the Arrhenius equation is founded on the empirical observation, TST is a theoretical approach [50].

The chemical reaction is represented by a path in the molecular coordinates space from the reactants' state into products. This path is called the reaction coordinate which is generally any parameter that shows the transformation of reactants into products. For one-dimensional representation, the reaction coordinate is considered as a one-dimensional coordinate against which the Gibbs energy of the reactants and products is plotted (Figure 3.4). In this figure, the horizontal axis is the reaction coordinate and the vertical axis is the potential/Gibbs energy. During the transition from reactants into products some transition state, activated complex, is formed. The transition state corresponds to the maximum of the Gibbs energy [50]. This makes the common representation of the reaction kinetics as passing through the activation barrier.

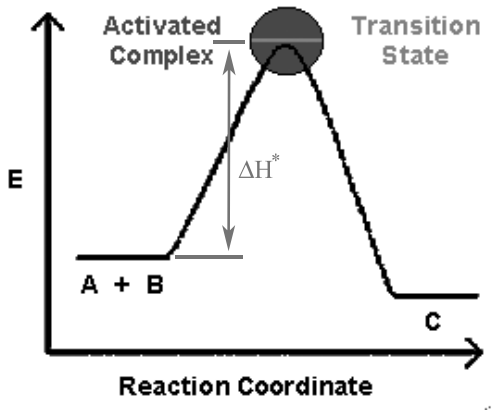

Figure 3.4 Energy profile [50]

Figure 3.4 shows the energy of the molecules along the reaction coordinate which measures the progress of the reaction. Along the flat at the left, the particles are approaching each other. During the approach, the particles slow down as their kinetic energies furnish the potential energy to climb the curve. If the reacting particles possess sufficient energy they can ascend the left side of the barrier all the way up to the summit. Then an activated complex AB^* or transition state is formed at the

potential energy maximum. The high-energy complex represents an unstable molecular arrangement, in which bonds break and form to generate the product C or to degenerate back to the reactants A and B. Once the energy barrier is surmounted, the reaction proceeds downhill to the product [50]. Briefly, the transition state is an unstable transitory combination of reactant molecules that occurs at a potential energy maximum [51]. Principles of the transition state theory:

- There is a thermodynamic equilibrium between the transition state and the state of reactants at the top of the energy barrier.
- The rate of chemical reaction is proportional to the concentration of the particles in the high-energy transition state.

So, one can write chemical reaction equation according to the TST in which, the reactants (A, B) are getting over into an unsteady intermediate (AB^*) state on the reaction pathway,

$$A + B \xleftarrow{k_a, k_{-a}} AB^* \xrightarrow{k_u} C. \tag{3.39}$$

The reactants are assumed to be in equilibrium with the intermediate species, activated complex. This complex can have several modes of molecular motion, with vibrational, rotational, translational and electronic contributions. These modes can be used to define the so-called molecular partition function, which can be thought as a measure of the average number of thermally accessible states available in the system at a given temperature [52]. The change in the concentration of the complex AB^* over time can be described by the following equation:

$$\frac{d[AB^*]}{dt} = k_a[A][B] - k_{-a}[AB^*] - k_u[AB^*]. \tag{3.40}$$

Due to the equilibrium between the activated complex, AB^* and the reactants A and B, the components the rate of the direct reaction is proportional to the concentration of AB^*,

$$-\frac{d[AB^*]}{dt} = k_u[AB^*] \tag{3.41}$$

k_u is given by statistical mechanics:

$$k_u = \frac{k_B T}{h} \tag{3.42}$$

where,

k_B : Boltzmann's constant (= $1.381 \cdot 10^{-23}$), J K^{-1}

T : temperature, K

h : Plank constant (= $6.626 \cdot 10^{-34}$), J s

k_u : universal constant for a transition state (~ $6.25 \cdot 10^{12}$), s^{-1} /molecule.

Additionally, [AB^*] can be derived from the quasi stationary equilibrium between AB^* and A, B by applying the mass action law:

$$\frac{[AB^*]}{[A][B]} = K_c \quad \text{and} \quad [AB^*] = K_c[A][B] \tag{3.43}$$

Here, K_c is thermodynamic equilibrium constant. Due to the equilibrium that will be reached rapidly, the reactants and the activated complex decrease at the same rate, from (3.41), (3.42) and (3.43),

$$-\frac{d[AB^*]}{dt} = \frac{k_B T}{h} K_c[A][B]. \tag{3.44}$$

We can write equilibrium constant, K_c, from thermodynamic definitions,

$$\Delta G^* = -R \cdot T \cdot \ln K_c$$
$$\text{and} \tag{3.45}$$
$$\Delta G^* = \Delta H - T \cdot \Delta S^*$$

R : universal gas constant (= 8.3145), J mol^{-1} K^{-1}

ΔG^* : free activation enthalpy, kJ mol^{-1}

ΔS^* : activation entropy, J mol^{-1} K^{-1}

ΔH^* : activation enthalpy, kJ mol^{-1}.

ΔH^* is the enthalpy difference between the transition state of a reaction and the ground state of the reactants. S is for the entropy, the extent of randomness or disorder in a system. The difference between the entropy of the transition state and the sum of the entropies of the reactants is ΔS^*. ΔG^* is the free activation enthalpy (Gibb's free energy) and it represents the determining driving power for a reaction. The sign of it determines if a reaction is spontaneous or not [50].

$\Delta G^* < 0 \rightarrow$ reaction is spontaneous

$\Delta G^* = 0 \rightarrow$ system at equilibrium, no net change occurs

$\Delta G^* > 0 \rightarrow$ reaction is not spontaneous

Excluding K_c from (3.45),

$$\ln K_c = -\frac{\Delta H^*}{R \cdot T} + \frac{\Delta S^*}{R}$$

and (3.46)

$$K_c = e^{-\frac{\Delta H^*}{R \cdot T}} \cdot e^{\frac{\Delta S^*}{R}}$$

So the reaction rate coefficient can be written,

$$k = \frac{k_B T}{h} \cdot e^{-\frac{\Delta H^*}{R \cdot T}} \cdot e^{\frac{\Delta S^*}{R}}$$

or (3.47)

$$k = \frac{k_B T}{h} \cdot e^{-\frac{\Delta G^*}{R \cdot T}}.$$

Remember that while the rate constant will increase monotonically with T for Arrhenius collision theory (see Figure 3.3), for the low activation energy processes represented by TST it will increase in nonmonotonic trend. Thus, data show curvature on Arrhenius plot probably represents a reacting system in which an intermediate complex forms and in which the activation energy is low. The value of ($k_B T/h$) term and pre-exponential factor, A' of Arrhenius equation are approximately the same (~ 10^{14} cm^3 mol s^{-1} at 1000 K). Thus one should generally expect pre-exponential values to fall in a range near 10^{13} to 10^{14} cm^3 mol s^{-1}. When quantities are far different from this range, one should conclude that the representative expression is an empirical fit to some experimental data over a limited temperature range.

The use of TST as a convenient expression of rate data is obviously complex and requires the presence of the temperature dependent partition functions. For this reason, most of the researches working in chemical kinetic modeling prefer a modified Arrhenius form which accounts for all the pre-exponential temperature dependent terms in (3.47).

3.2 Characteristics of Reaction Mechanisms

In chemistry, a reaction mechanism is the step by step sequence of large number of different elementary reactions (the elementary reaction theory has been explained briefly in section 3.1.6) which gives the overall chemical change. With the help of experiments, it is possible to make suggestions about the sequence of steps in a reaction mechanism. A mechanism describes in detail exactly what takes place at each stage of a chemical transformation. It describes the transition state and which bonds are broken and in what order, which bonds are formed and in what order, and what the relative rates of the steps are. A complete mechanism must also account for all reactants used, the function of a catalyst, stereochemistry, all products formed and the amount each. A reaction mechanism must also account for the order in which molecules react [53]. Remember that even the combustion of simple fuel, like hydrogen (global reaction $2H_2 + \rightarrow 2H_2O$), requires nearly 40 elementary reactions for a satisfactory chemical mechanism. The situation is much more complex for combustion of HC fuels with growing molecular size (see Table 3.2) such that, several thousand elementary reactions can influence the overall process [1].

Table 3.2 Reaction mechanism growth depend on molecular size [54]

Fuel	**H_2 (Hydrogen)**	**CH_4 (Methane)**	**C_3H_8 (Propane)**	**C_6H_{14} (Hexane)**	**$C_{16}H_{34}$ (Cetane)**
Number of species:	8	~ 30	~ 100	~ 450	~ 1200
Number of reactions:	30	~ 200	~ 400	~ 1500	~ 7000

Common formulation is to write a time dependent differential equation for the concentration or mole fraction of each chemical species for the considered system [55]. When we consider all differential equations set of the elementary reactions, which forms the global reaction mechanism, result will be a nonlinear ordinary differential equation (ODE) system. But these individual elementary reactions have greatly different reaction rates (time scales), see Figure 3.5. The maximal difference in the time scales is characterized as stiffness.

This wide variation in time scales brings severe problems for the numerical solution of these differential equation systems, which govern the reaction system. Usually the smallest time scales have to be resolved in numerical solution, even if one interested in the slow (rate-limiting) processes. Otherwise numerical solution tends to become unstable [1]. The first numerical solution method for stiff differential equations of

coupled chemical kinetics was developed by Curtiss and Hirschfelder in 1952 [56]. This was a milestone because stiff equation solvers were available and it had an enormous impact on computational combustion by moving kinetic modeling forward.

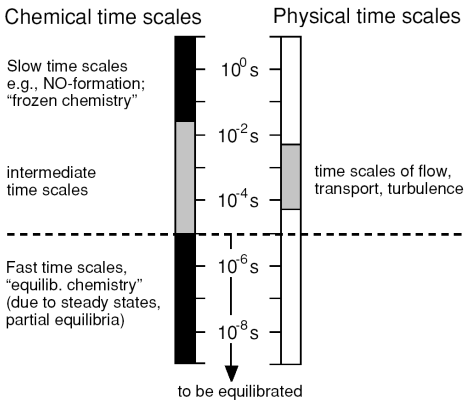

Figure 3.5 Classification of time scales in a chemically reacting flow [1]

The whole combustion is governed by the interaction of the elementary reactions. Also, the combustion system can be spatially inhomogeneous (distributed parameter system), where diffusion and convection also contribute to reaction dynamics, in which, simulation of it is not possible with chemical models of too many variables. On the other hand, independent of the specific properties of the fuel, all reaction mechanisms show some common characteristic properties in all combustion processes For example, only a few of the elementary reactions determine the rate of the overall process (rate-limiting reactions). Knowing the characteristic properties of mechanisms improves the understanding of the chemical reaction system and provides valuable information for the simplification of the mechanisms by eliminating irrelevant steps. Quasi-steady states and partial equilibrium simplifications are the two often used ones and they will be summarized below [1].

3.2.1 Quasi-Steady State Approximation (QSSA)

One of the methods of special importance to chemical kinetics for the lowering of the number of variables is the separation of different time scales. A method for such separation is called quasi-steady state approximation (QSSA) in chemistry [57]. The concept of quasi-steady state allows one to obtain results despite the fact that original equation system is coupled set of ordinary differential equations (ODE), which cannot be solved analytically.

Let's explain QSSA with a simple reaction chain, consisting of two elementary steps,

$$S_1 \xrightarrow{k_{12}} S_2 \xrightarrow{k_{23}} S_3 . \tag{3.48}$$

We will assume that S_2 is very active, and thus has a short life time ($k_{23} >> k_{12}$). But at first, without this assumption, one can write the rate laws of these species; S_1, S_2 and S_3 by the expressions,

$$\frac{d[S_1]}{dt} = -k_{12}[S_1], \tag{3.49}$$

$$\frac{d[S_2]}{dt} = k_{12}[S_1] - k_{23}[S_2], \tag{3.50}$$

$$\frac{d[S_3]}{dt} = k_{23}[S_2] . \tag{3.51}$$

An analytic solution can be obtained with the assumptions that at time $t = 0$ only S_1 is present and initial conditions $[S_1]_{t=0} = [S_1]_0$, $[S_2]_{t=0} = 0$ and $[S_3]_{t=0} = 0$. Details of solution are not given here because of lack of space, see [1] for details. And returning back to the QSSA that S_2 is very active ($k_{23} >> k_{12}$), the solution is illustrated in Figure 3.6a for $k_{12} / k_{23} = 0.1$.

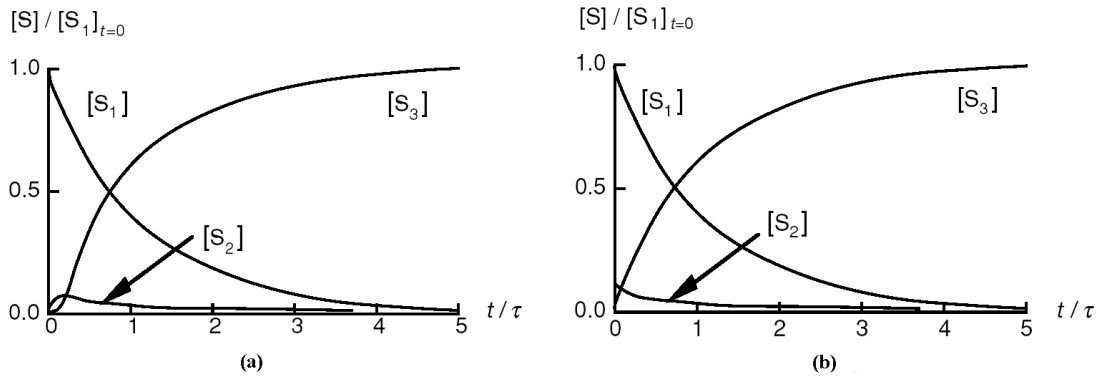

Figure 3.6 (a) Exact (b) With QSSA for $[S_2]$, temporal behaviors of the species concentrations in the reaction sequence $S_1 \rightarrow S_2 \rightarrow S_3$ are shown (τ is the characteristic life-time for $[S_1]_0$ to decay to $[S_1]_0/e$); $\tau = 1 / k_{12}$ [1]

The QSSA, S_2 is very active, means that the rate of consumption of S_2 is approximately equal to the rate of formation of S_2 allowing to write the following approximation

$$\frac{d[S_2]}{dt} = k_{12}[S_1] - k_{23}[S_2] \approx 0 , \tag{3.52}$$

hence,

$$k_{12}[S_1] = k_{23}[S_2] \quad . \tag{3.53}$$

If one is interested in the rate of formation of the product S_3, (3.51) express that only $[S_2]$ appears in the rate law for S_3. However, with QSSA above (3.52), one obtains (3.54) and writes the rate law for $[S_3]$ as

$$\frac{d[S_3]}{dt} = k_{12}[S_1] \; . \tag{3.54}$$

So, using this QSSA for S_2, obtained approximate results are illustrated in Figure 3.6b. It is clear that QSSA is very close to the exact solution of the process, if $k_{23} >> k_{12}$. Only at the beginning of the reaction are there some deviations (compare Figure 3.6 a-b) because of the needed time interval by the system to attain the QSS [1].

It is shown that, the concentrations of QSSA species, $[S_2]$, can be expressed algebraically in terms of other species since it is assumed that their rates of change can be decoupled from the set of ODE system and the right hand side is set to zero, $d[S_2]/dt = 0$. The number of differential equations is therefore reduced since some have been replaced by algebraic expressions [58].

3.2.2 Partial Equilibrium

Partial equilibrium assumption is very much like the QSSA. The difference is that in the QSSA one is concerned with a particular species and in the partial equilibrium assumption one is concerned with particular reactions. As already mentioned, reaction mechanisms have individual reaction steps which have widely varying time scales (reaction rates). It means that under certain circumstances a group of reactions will proceed rapidly and reach quasi equilibrium state, and one or more reactions may proceed slowly. And the forward and reverse reaction rates of partial equilibrium reactions are so high that their rates are affected very little with the change of a slow reaction's concentration. If one wants to determine the rate or rate coefficient of this slow reaction and if it requires to know the concentration of a species which is difficult to measure, then it is possible through a partial equilibrium assumption to express the unknown concentrations in terms of other measurable quantities [13].

The concept of partial equilibrium can be illustrated using the mechanism for hydrogen combustion. At high temperatures (T > 1800 K at p = 1 bar) the reaction rates of forward and reverse reactions are so fast that one obtains partial equilibrium

$$\mathrm{H} + \mathrm{O}_2 = \mathrm{OH} + \mathrm{O} \tag{3.55}$$

$$\mathrm{O} + \mathrm{H}_2 = \mathrm{OH} + \mathrm{H} \tag{3.56}$$

$$\mathrm{OH} + \mathrm{H}_2 = \mathrm{H}_2\mathrm{O} + \mathrm{H} \tag{3.57}$$

In this equation system O, H and OH are the reactive intermediates which are difficult to measure and H_2, O_2 and H_2O are stable species. Because each reaction is in equilibrium, forward and reverse reaction rates are equal,

$$\begin{aligned} k_1[\mathrm{H}][\mathrm{O}_2] &= k_2[\mathrm{OH}][\mathrm{O}] \\ k_3[\mathrm{O}][\mathrm{H}_2] &= k_4[\mathrm{OH}][\mathrm{H}] \\ k_5[\mathrm{OH}][\mathrm{H}_2] &= k_6[\mathrm{H}_2\mathrm{O}][\mathrm{H}] \,. \end{aligned} \tag{3.58}$$

Now, this equation system can be solved for the intermediates by three relations,

$$[\mathrm{H}] = \left(\frac{k_1 k_3 k_5^2 [\mathrm{O}_2][\mathrm{H}_2]^3}{k_2 k_4 k_6^2 [\mathrm{H}_2\mathrm{O}]^2} \right), \tag{3.59}$$

$$[\mathrm{O}] = \frac{k_1 k_5 [\mathrm{O}_2][\mathrm{H}_2]}{k_2 k_6 [\mathrm{H}_2\mathrm{O}]}, \tag{3.60}$$

$$[\mathrm{OH}] = \left(\frac{k_1 k_3}{k_2 k_4} [\mathrm{O}_2][\mathrm{H}_2] \right)^{\frac{1}{2}} . \tag{3.61}$$

Thus, one can obtain the concentrations of reactive species in terms of concentrations of the stable (and, thus, easier to measure) species H_2, O_2 and H_2O by using partial equilibrium assumption.

It is shown in Figure 3.7 mole fractions of H, O, and OH in premixed stoichiometric H_2-air flames as a function of the local temperature, which has been calculated using the detailed reaction mechanism and then recalculated using the partial equilibrium assumptions. Partial equilibrium assumption gives satisfactory results only at high temperatures (T > 1600 K). Below this certain temperature, partial equilibrium is not established, because the reaction times are slower than the mean gas velocity $\tau = d / \bar{v}$ (~1mm/1m·s^{-1} = 1 ms typically).

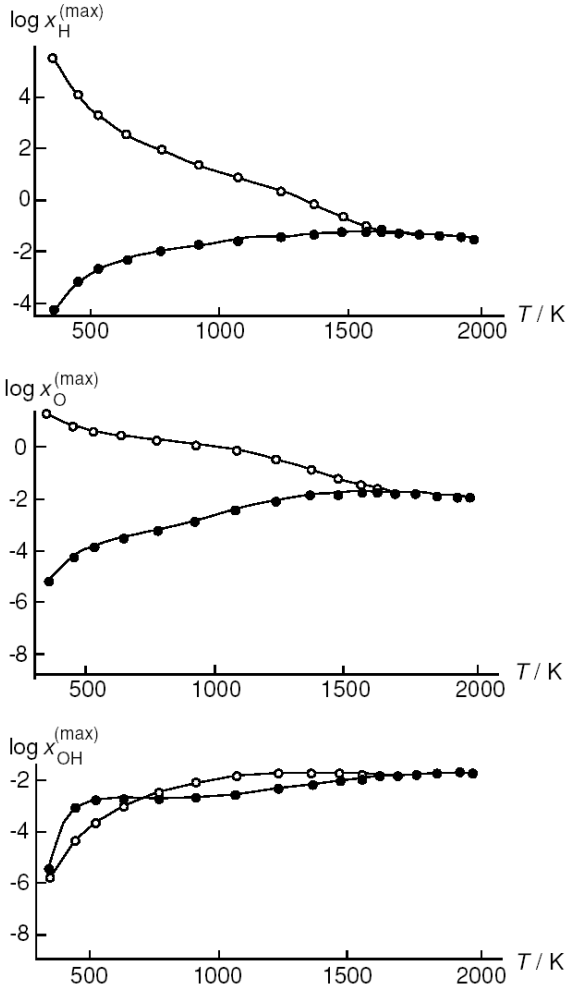

Figure 3.7 Maximum mole fractions of the radicals H, O and OH in premixed, stoichiometric H_2-air flames [59] at p = 1 bar, T_u = 298 K (unburnt gas temperature), calculated using a detailed mechanism (dark circles) and using the partial equilibrium assumption (light circles)

Hence, using partial equilibrium approach the rate expression can be written in terms of readily measurable stable species. In other words it eliminates measuring of the unstable species.

3.3 Analysis of Complex Chemical Mechanisms

Before developing a reaction mechanism, it is important to formulate its characteristics and size, maximum number of species and reactions [60]. Proper use of more species and reactions generally yields better accuracy. For instance, for the accurate pollutant predictions, a realistic approximation typically states that a complex HC combustion system contains 1000's of species with 10000's of reactions [61]. Using this many species and reactions is not possible today in a CFD application because of the available computational sources which can lead to

unacceptable execution time. It is therefore attractive to be able to include and handle a comprehensive chemical reaction mechanism, even if with limited size, which should accurately predict the ignition delay and reaction times for wide ranges of pressures, temperatures and equivalence ratios of engine operation.

For that reason, instead of using comprehensive reaction mechanisms in the computations, it is convenient to use reduced mechanisms, based on experience, sensitivity analysis or numerical evaluation. These reduced mechanisms can be validated in simple and well-defined laboratory conditions (i.e. plug-flow reactors, jet-stirred reactors, shock-tubes, premixed flames) [11].

Hence, a reaction mechanism that includes the important chemical steps of formation of soot precursors such as, acetylene (C_2H_2) and polyaromatic hydrocarbons (PAH), in general, can be used for realistic modeling of diesel fuel combustion. As mentioned in 2.1, DOS model used in this study is based on the mixture of 30% toluene (representing aromatic components in conventional diesel fuel which significantly contribute to soot formation) and 70% n-heptane (representing similar CN, ~ 56, with conventional diesel fuel). At first, detailed reaction mechanisms for n-heptane and toluene have been developed and validated by comparison of calculated ignition delay times with experimental shock tube data. For most sub-mechanisms (e.g. hydrogen, methane) the experimental data used was available for a wide range of pressures, temperatures and ERs. For DOS model, the validation of two most important sub-mechanisms, n-heptane and toluene was based on experimental shock tube data in the pressure range of 45-60 bar and 40-55 bar respectively in the temperature range of 650 K to 1500 K. Validation work is done by CHEMKIN [62] software. Also n-heptane and toluene oxidation chemistry is integrated with the kinetics of aromatic formation (up to four aromatic rings) developed for rich acetylene flames and then reduced on the bases of sensitivity analysis using the CHEMKIN software package. Finally, obtained reduced DOS mechanism implemented into the KIVA-3VR2 code [63]. Details of this process are given in the next chapter describing CHEMKIN software package.

3.4 CHEMKIN Package for Chemical Kinetics Calculations

CHEMKIN is a set of flexible and powerful tools for incorporating complex chemical kinetics into simulations of reacting flow. The software is a collection of

programs and subroutine libraries, which work together to facilitate the formation, solution, and interpretation of problems involving gas-phase and heterogeneous (gas-surface) chemical kinetics [64].

CHEMKIN Gas-phase Utility package (shortened as CHEMKIN) is one of the three basic elements in the CHEMKIN Collection, designed to facilitate the formation, solution, and interpretation of problems involving elementary gas-phase chemical kinetics in flowing systems. The other basic elements are the TRANSPORT property package and the surface chemistry package, SURFACE CHEMKIN. CHEMKIN Gas-phase Utility package is the part which is related with this study. Schematic view of CHEMKIN Collection is shown in Figure 3.8 for a reacting flow simulation.

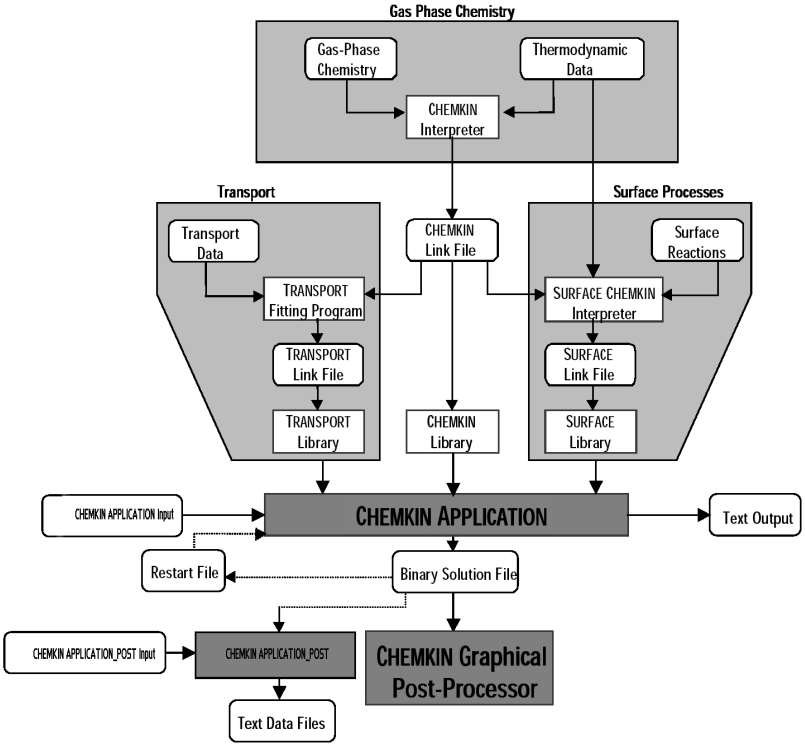

Figure 3.8 Schematic diagram showing the structure of the CHEMKIN Collection package and its relationship to its any application program [adapted from 65]

The CHEMKIN software architecture represents a modular approach that separates problem-specific information from problem-independent software. From the Figure 3.8: The CHEMKIN APPLICATION represents the general model description (typically includes conservation equations for mass, momentum, energy, and species) independent of what chemical species are included in a specific problem. CHEMKIN APPLICATION Input contain the input data that make the problem specific, i.e. species identity, species properties, reaction paths, and reaction rates. The

CHEMKIN software utilities, Interpreter and Gas-Phase Subroutine Library provide the interface between the problem-specific information and the problem-independent application [65].

The CHEMKIN Interpreter is a program that reads, Gas-Phase Chemistry, a symbolic description of a user-specified chemical reaction mechanism which includes species information, as well as reaction path and rate descriptions, then extracts the needed Thermodynamic Data for each species involved from the thermodynamic database.

The primary output from the CHEMKIN Interpreter is the CHEMKIN Link File. This file contains information that contains all required information about the elements, species, and reactions in the user's mechanism. The information in the CHEMKIN Link File is subsequently accessed by various subroutines to provide information on equation of state, thermodynamic properties, and chemical production rates.

The CHEMKIN Link File is read by an initialization subroutine in the Gas-Phase Subroutine Library, CHEMKIN Library, which is a collection of more than 100 modular FORTRAN subroutines. The purpose of the initialization is to create three data arrays (one integer, one floating point, and one character data type) for use internally by the other subroutines in the Gas-Phase Subroutine Library. CHEMKIN Library subroutines are called by CHEMKIN APPLICATION to return information on elements, species, reactions, equations of state, thermodynamic properties, and chemical production rates.

CHEMKIN has many applications that build on these basic elements to solve specific reacting-flow problems. Below related applications and numerical solution methods will be described for this study.

3.4.1 SENKIN Code to Analyze Chemical Mechanisms

SENKIN is a program that predicts the time-dependent chemical kinetics behavior of a homogeneous gas mixture in a closed system. In addition to predicting the species and temperature histories, the program can also compute the first-order sensitivity coefficients with respect to the elementary reaction rate parameters [66, 65].

SENKIN provides many options for defining a chemical kinetics problem for a wide variety of applications such as modeling combustion bombs, rapid compression machines, ICEs etc. Within SENKIN there are six problem type options available:

A. An adiabatic system with constant pressure

B. An adiabatic system with constant volume

C. An adiabatic system with the volume a specified function of time. This case includes the ability to model an ICE with the volume vs. time determined from specified engine parameters.

D. A system where the pressure and temperature are constant

E. A system where the volume and temperature are constant

F. A system where the pressure and temperature is specified functions of time.

These problem types are discriminated by the externally imposed thermodynamic conditions. Cases A through C are generally applicable to spontaneous ignition problems of combustion. Cases D and E are suitable for general type of homogeneous kinetics problems where heat release is not important. Condition E allows computation of mixture composition histories for specified temperature and pressure histories.

The program uses the DASAC [67] (Differential Algebraic Sensitivity Analysis Code) software to solve the nonlinear ODEs that describe the temperature and species mass fractions. In addition, DASAC solves the set of linear differential equations that describe the first-order sensitivity coefficients of temperature and species composition with respect to the individual reaction rates. The program runs in employs the CHEMKIN Utility software package, which handles the chemical reaction mechanism and species thermodynamic data.

3.4.1.1 Governing Equations

In this section, equations for mass and energy conservation are described for the problem types considered by the program. The reacting mixture is treated as a closed system with no mass crossing the boundary, so the total mass of the mixture

$$m = \sum_{i=1}^{S} m_i \tag{3.62}$$

is constant, and dm/dt=0. Here m_i is the mass of i-th species and S is the total number of species in the mixture. The individual species are produced or destroyed according to

$$\frac{\mathrm{d}m_i}{\mathrm{d}t} = V\dot{\omega}_i M_i \tag{3.63}$$

where,

t	: time
V	: volume of the system (may vary in time)
$\dot{\omega}_i$	: molar production rate of the i-th species by elementary reaction
M_i	: molecular weight of the i-th species.

Since the total mass is constant, this can be written in terms of mass fractions as

$$\frac{\mathrm{d}Y_i}{\mathrm{d}t} = v\dot{\omega}_i M_i \tag{3.64}$$

where Y_i=m_i/m is the mass fraction of i-th species and v=V/m is the specific volume. This species equation is true for all problem types, A-F. For the conditions A-C, the energy equation must be derived in light of specific constraints used in each case. The first law of thermodynamics for a pure substance in an adiabatic, closed system states that

$$\mathrm{d}e + p\mathrm{d}v = 0 \tag{3.65}$$

where e is the internal energy per mass and p is the pressure. For an ideal mixture of gases, internal energy of the mixture is given by

$$e = \sum_{i=1}^{S} e_i Y_i \tag{3.66}$$

where e_i is the internal energy of the i-th species. Differentiating the internal energy of the mixture leads to

$$\mathrm{d}e = \sum_{i=1}^{S} Y_i \mathrm{d}e_i + \sum_{i=1}^{S} e_i \mathrm{d}Y_i \ . \tag{3.67}$$

Assuming calorically perfect gases, we write de_i = $c_{v,i}$ dT, where T is the temperature of the mixture, and $c_{v,i}$ is the specific heat of the i-th species evaluated at constant volume. Mean specific heat of the mixture

$$c_v = \sum_{i=1}^{S} Y_i c_{v,i} \ . \tag{3.68}$$

Differentiating the internal energy of the mixture equation (3.67) and using (3.68) leads to

$$\begin{aligned} \mathrm{d}e &= \sum_{i=1}^{S} Y_i c_{v,i} \mathrm{d}T + \sum_{i=1}^{S} e_i \mathrm{d}Y_i \\ \mathrm{d}e &= c_v \mathrm{d}T + \sum_{i=1}^{S} e_i \mathrm{d}Y_i \end{aligned} \tag{3.69}$$

after substitution of (3.69) in to the energy equation (3.65), it gives

$$c_v \mathrm{d}T + \sum_{i=1}^{S} e_i \mathrm{d}Y_i + p\mathrm{d}\nu = 0 \tag{3.70}$$

and differentiating this energy equation with respect to time,

$$c_v \frac{\mathrm{d}T}{\mathrm{d}t} + \sum_{i=1}^{S} e_i \frac{\mathrm{d}Y_i}{\mathrm{d}t} + p\frac{\mathrm{d}\nu}{\mathrm{d}t} = 0 \ . \tag{3.71}$$

Substituting of (3.64) for the species production rate gives,

$$c_v \frac{\mathrm{d}T}{\mathrm{d}t} + p\frac{\mathrm{d}\nu}{\mathrm{d}t} + \nu \sum_{i=1}^{S} e_i \dot{\omega}_i M_i = 0 \ . \tag{3.72}$$

The ideal gas equation of state, (3.6) is used to calculate pressure. In case C, volume is provided as a function of time, hence specific volume and its rate of change are

$$\nu(t) = \frac{V(t)}{m} \tag{3.73}$$

and

$$\frac{\mathrm{d}\nu}{\mathrm{d}t} = \frac{1}{m}\frac{\mathrm{d}V}{\mathrm{d}t} \ . \tag{3.74}$$

In case B, the volume is held constant, so (3.72) reduces to

$$c_v \frac{\mathrm{d}T}{\mathrm{d}t} + \nu \sum_{i=1}^{S} e_i \dot{\omega}_i M_i = 0 \tag{3.75}$$

Equation (3.72) can be arranged according to particular specifications of other cases, i.e., for case A, the enthalpy of the mixture is constant. For the details, see [66].

The net chemical production rate $\dot{\omega}_i$ of each species results from a competition between all the chemical reactions involving that species. Each reaction proceeds according to the law of mass action and the forward rate coefficients are in the modified Arrhenius form, (2.25).

3.4.1.2 Numerical Solution Method

The system of ODEs described in the previous section is generally stiff, and thus is most efficiently solved by implicit techniques. DASAC performs the time integration and first-order sensitivity analysis. The DASAC package is based on the differential/algebraic system solver DASSL [68], which performs the time integration using a backward differentiation formula (BDF). These BDF methods are in regular use for solving a wide range of stiff problems, including chemical kinetics problems. The details of the numerical methods in DASSL are described by Petzold [68] and the DASAC enhancements by Caracotsios and Stewart [67].

3.4.1.3 Sensitivity Analysis

In nearly all models, the solutions depend both on initial and boundary conditions and on certain parameters that go into defining the model itself. Sensitivity analysis is a formal procedure for determining quantitatively how the solution to a model depends on certain parameters in the model formulation. In the cases considered here, the parameters are the elementary reaction rate constants. Sensitivity analysis allows one to understand how the model will respond to changes in these elementary reaction rate parameters, without requiring repetitive solution of the problem with different values for the rate constants. This type of analysis also provides insight about how important certain reaction pathways are to the model's predictions.

All the computationally efficient sensitivity analysis methods exploit the fact that the differential equations describing the sensitivity coefficients are linear, regardless of any non-linearities in the model problem itself. Furthermore, some of the methods, including the one used here, take advantage of the fact that the sensitivity equations are described in terms of the Jacobian of the model problem. In stiff ODE software, such as DASSL or LSODE [69] which are based on BDF methods, the Jacobian is required for solution of the model problem, so it is available for the sensitivity computation [66].

The system of ODEs that describe the physical problem are of the general form

$$\frac{\mathrm{d}c}{\mathrm{d}t} = F(c,t;a) \tag{3.76}$$

where, $c = (T, Y_1, Y_2, \ldots, Y_S)^{\mathrm{T}}$ is the vector of temperature and mass fractions and the parameter vector a represent the pre-exponential constants, $A_i^{'}$ in (3.30) for each of the elementary reactions.

The first order sensitivity coefficient matrix is defined as

$$w_{j,i} = \frac{\partial c_j}{\partial a_i} \tag{3.77}$$

where the indices j and i refer to the dependent variables and reactions, respectively. Differentiating (3.76) with respect to the parameters A_i yields,

$$\frac{\mathrm{d}w_{j,i}}{\mathrm{d}t} = \frac{\partial F}{\partial c} \cdot w_{j,i} + \frac{\partial F_j}{\partial a_i} \ . \tag{3.78}$$

This equation for the sensitivity coefficients is linear. The Jacobian matrix $\partial F/\partial$c is exactly the one that is required by the BDF method in solving the original model problem, so it is readily available for the sensitivity computation. Each column corresponds to the sensitivities with respect to one of the reaction pre-exponential constants. The solution proceeds column by column. Note that the Jacobian matrix is the same for each column of the $w_{j,i}$. However, since the $\partial F_j/\partial a_i$ matrix describes the explicit dependence F on each of the reaction parameters a_i, each of its columns must be formed prior to solving for a column of $w_{j,i}$.

3.4.1.4 Program Structure

Program structure of SENKIN program of the CHEMKIN obeys the general schematic view of the CEMKIN which is given in Figure 3.8. It is enough to replace CHEMKIN APPLICATION blocks of this schematic with the name SENKIN to get the program structure (Figure 3.9). To summarize the structure: At first, CHEMKIN Interpreter, “chem”, reads usersupplied information about the species and chemical reactions (see Gas-Phase Chemistry in Figure 3.9) for a particular reaction mechanism. It then extracts the species’ thermodynamic properties from a database file, “therm.dat” (see Thermodynamic Data in Figure 3.9). The user may also optionally input thermodynamic property data directly in the input file to the

CHEMKIN Interpreter to override or supplement the database information. The information from the user input and the thermodynamic properties is stored in the CHEMKIN Link File, “chem.asc”; a file that is later required by the CHEMKIN subroutine library, which will be accessed from the SENKIN program.

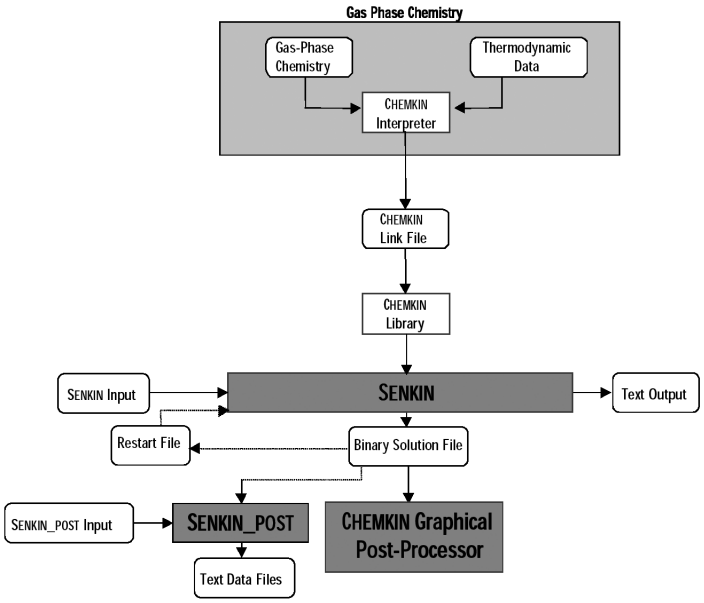

Figure 3.9 Schematic diagram showing the structure of the SENKIN [65]

SENKIN makes appropriate calls to the CHEMKIN Library to initialize the species- and reaction-specific information. The purpose of the initialization is to read the linking file and set up the internal working and storage space required by all subroutines in the libraries. SENKIN next reads the input, SENKIN Input, that defines a particular problem and any other needed parameters in a Keyword format from the input file, “senkin.inp”, or SENKIN begin its iteration from a previously computed solution. In this case the old solution is read from a binary Restart File, called “rest.bin”. SENKIN produces printed output, “senkin.out” (Text Output), and it saves the solution in a binary save file, “save.bin”. The Save File can be used to restart SENKIN to provide a starting estimate for a different problem that may have different constraints. A Restart File can be created simply by copying Binary Solution File, “save.bin” to the Restart File name, “rest.bin” (see Figure 3.9).

3.4.2 EQUIL Code to Anaylze Chemical Equilibrium

EQUIL [65] is a program that computes the chemical equilibrium state of an ideal gas or solution mixture. An established method for evaluating chemical equilibrium is the element-potential method embodied in the Stanford software STANJAN [70]

The EQUIL program provides an interface to the STANJAN library of routines, which allows users to specify species and thermodynamic data in CHEMKIN format.

For combustion systems, EQUIL can be used to determine adiabatic flame temperatures for constant pressure or constant volume conditions. To achieve this, one specifies the reactants as the initial species. EQUIL will determine the enthalpy (or energy) of this initial state. Then equilibrium calculation can be run that includes the combustion products as available species, to which the reactants can be converted. Running a constant pressure and enthalpy (or constant volume and energy) problem using the enthalpy (or energy) of the initial state will thus produce an equilibrium temperature, which is, by definition, the adiabatic flame temperature.

3.4.2.1 The Element-Potential Method Theory

The basic theory for the element-potential method of determining equilibrium is based on the minimization of Gibbs free energy [65]. The Gibbs function of a system

$$G = \sum_{i=1}^{S} \overline{g}_i n_i \tag{3.79}$$

$\overline{g}_i$: partial molal Gibbs function

n_i : the number of moles of each species i in the system

S : total number of species involved.

For ideal-gas mixtures or ideal solutions, the partial molal Gibbs functions are:

$$\overline{g}_i = g_i(T,P) + RT \ln x_i \tag{3.80}$$

where $g_i(T,P)$ is the Gibbs function for the pure species i, evaluated at the system temperature and pressure, x_i is the mole fraction of the i-th species.

The equilibrium solution at a given temperature and pressure is the distribution of n_i that minimizes the system Gibbs function, G, subject to atomic population constraints (and non-negative n_i). The atomic population constraints are:

$$\sum_{i=1}^{S} num_{ji} n_i = p_j,\ j = 1,...\text{NLM} \tag{3.81}$$

num_{jk} : number of j-th atoms in the i-th molecule

p_j : total population in moles of the j-th atom in the system

NLM : total number of different elements in the system.

Details regarding the relationship between the partial molal Gibbs functions and the elemental potentials for the atoms, as well as the explicit form of the equations solved in the STANJAN library are described in [65].

3.4.3 PSR Code to Analyze Reactor Premixed Flows

The stirred reactor consists of a small thermally insulated chamber that has inlet and outlet ducts. A steady flow of fuel and oxidizer are introduced in such a way that high intensity turbulent mixing causes the contents of the reactor to be nearly spatially uniform. This means that the rate conversion from reactants to products is controlled by chemical reaction rates and not by mixing processes. Thus, a well-stirred reactor can be modeled as a micromixed perfectly stirred reactor (PSR), where the mixing rates are assumed to be infinitely fast [71].

In addition to fast mixing, the modeling of well-stirred reactors requires certain assumptions such as, walls are noncatalytic and flow through the reactor has to be characterized by a nominal residence time, which has to be deduced from the flow rate and the reactor volume.

Modeling well-stirred reactor requires solving systems of nonlinear algebraic equations.

It is possible to define the processes in a PSR by relating the conservation of mass and energy to the net generation of chemical species within the reactor volume. The concept is represented schematically in Figure 3.10. The mixing in the reactor chamber is intense and assumed that temperature and compositon in the reactor is the same as that which exits the reactor volume. And the mass flow rate through the reactor $\dot{m}$ is a constant.

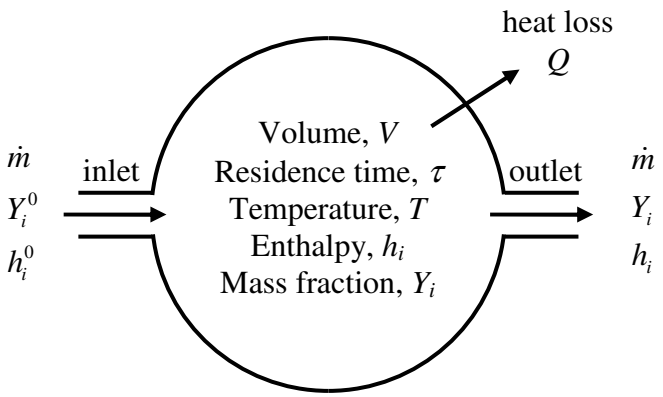

Figure 3.10 Schematic representation of a well-stirred reactor [71]

The species conservation equation

$$\dot{m}(Y_i - Y_i^0) - \dot{\omega}_i M_i V = 0 \ , \tag{3.82}$$

and conservation of energy is stated as

$$\dot{m}\sum_{i=1}^{S}(Y_i h_i - Y_i^0 h_i^0) + Q = 0 \, . \tag{3.83}$$

where h_i is the specific enthalpy of the i-th species and Q is the reactor heat loss. The superscript (^{0}) indicates the inlet conditions. The nominal residence time is related to the reactor volume, V, and the mass flow rate by

$$\tau = \frac{\rho V}{\dot{m}} \tag{3.84}$$

where the mass density ρ is calculated from (3.6). The residence time is preferred as a characteristic parameter of the reactor instead of the mass flow rate.

Equations form S+1 nonlinear algebraic equations, the solution of which is the temperature and mass fractions. The time dependent equation for mass conservation of each species is

$$\rho V \frac{\mathrm{d}Y_i}{\mathrm{d}t} = -\dot{m}(Y_i - Y_i^0) + \dot{\omega}_i M_i V \tag{3.85}$$

or

$$\frac{\mathrm{d}Y_i}{\mathrm{d}t} = -\frac{1}{\tau}(Y_i - Y_i^0) + \frac{\dot{\omega}_i M_i}{\rho} \ . \tag{3.86}$$

The energy balance for the reactor (assuming constant pressure) leads to

$$\rho V \frac{\mathrm{d}h}{\mathrm{d}t} = -\dot{m}\sum_{i=1}^{S}(Y_i h_i - Y_i^0 h_i^0) - Q \ , \tag{3.87}$$

or

$$\frac{\mathrm{d}h}{\mathrm{d}t} = -\frac{1}{\tau}\sum_{i=1}^{S}(Y_i h_i - Y_i^0 h_i^0) - \frac{Q}{\rho V} \ , \tag{3.88}$$

where h is the mass-weighted mean enthalpy. It is convenient to rewrite the energy equation in terms of temperature rather than enthalpy. Since

$$h = \sum_{i=1}^{S} Y_i h_i \text{ and } c_p = \sum_{i=1}^{S} Y_i c_{p_i} \tag{3.89}$$

$$\frac{\mathrm{d}h}{\mathrm{d}t} = c_p \frac{\mathrm{d}T}{\mathrm{d}t} + \sum_{i=1}^{S} h_i \frac{\mathrm{d}Y_i}{\mathrm{d}t} \ . \tag{3.90}$$

Combining (3.86), (3.88) and (3.90) gives the transient energy equation,

$$c_p \frac{\mathrm{d}T}{\mathrm{d}t} = \frac{1}{\tau} \sum_{i=1}^{S} Y_i^0 (h_i^0 - h_i) - \sum_{i=1}^{S} \frac{h_i \dot{\omega}_i M_i}{\rho} - \frac{Q}{\rho V} \ , \tag{3.91}$$

that is to be solved where c_p is the mass weighted mean specific heat.

The transient problem is a nonlinear ODE initial-value problem. The system of algebraic equations are solved by the damped modified Newton algorithm. If during the course of the iteration the Newton algorithm fails to converge, the solution estimate is conditioned by a time integration which provides a new starting point for the Newton algorithm that is closer to the solution. Eventually the problem is solved by convergence of Newton algorithm. One can find the details of the numerical solution method in [71].

3.4.4 PREMIX Code to Analyze Flame Propagation in Premixed Mixture

Many practical combustors, such as ICEs, rely on premixed flame propagation. Moreover, burner-stabilized laminar premixed flames are very often used to study chemical kinetics in a combustion environment. Also, laminar flame speed is often used to characterize the combustion of various fuel-oxidizer combinations. Therefore, the ability to model chemical kinetics and transport processes in these flames is critical to interpreting flame experiments and to understanding the combustion process itself [65]. PREMIX is capable of predicting temperature and species profiles in two laminar premixed flame configurations.

A. Analyzing species profiles in flame experiments such as burner-stabilized flame with a known mass flow rate. Two cases are considered for burner-stabilized flames,

   - temperature profile is known, measured by the experiments (gives better results),
   - temperature profile is determined by the energy conservation equation.

B. Flame speed calculation for freely propagating adiabatic flame (heat losses are neglected). The temperatures should be computed from the energy equation. Flame speed depends, in part, on the transport of heat, and predicting the temperature distribution is an integral part of the flame speed calculation.

The equations governing steady, isobaric, quasi-one-dimensional flame propagation may be written as follows:

Continuity:

$$\dot{m} = \rho u A \tag{3.92}$$

Energy:

$$\dot{m}\frac{\mathrm{d}T}{\mathrm{d}x} - \frac{1}{c_p}\frac{\mathrm{d}}{\mathrm{d}x}\left(\gamma A\frac{\mathrm{d}T}{\mathrm{d}x}\right) + \frac{A}{c_p}\sum_{i=1}^{S}\rho Y_i V_i c_{pi}\frac{\mathrm{d}T}{\mathrm{d}x} + \frac{A}{c_p}\sum_{i=1}^{S}\dot{\omega}_i h_i M_i = 0 \tag{3.93}$$

Species:

$$\dot{m}\frac{\mathrm{d}Y_i}{\mathrm{d}x} + \frac{\mathrm{d}}{\mathrm{d}x}\left(\rho A Y_i V_i\right) - A\dot{\omega}_i M_i = 0 \qquad (\mathrm{i} = 1,...,\mathrm{S}) \tag{3.94}$$

Equation of state:

$$\rho = \frac{p\overline{M}}{RT} \tag{3.95}$$

In these equations, x: the spatial coordinate; $\dot{m}$: the mass flow rate (which is independent of x); T: the temperature; Y_i: the mass fraction of the i-th species (there are S species); p: the pressure; u: the velocity of the fluid mixture; ρ: the mass density; M_i: the molecular weight of the i-th species; $\overline{M}$: the mean molecular weight of the mixture; R: the universal gas constant; γ : the thermal conductivity of the mixture; c_p: the constant-pressure heat capacity of the mixture; c_{pi}: the constant pressure heat capacity of the i-th species; $\dot{\omega}_i$: the molar rate of production by chemical reaction of the i-th species per unit volume; h_k the specific enthalpy of the i-th species; V_i: the diffusion velocity of the i-th species; and A: the cross-sectional area of the stream tube encompassing the flame (by default, the stream tube area is taken to be constant and equal to unity). For further details such as mixture-averaged and multicomponent transport properties, boundary conditions, etc … see [65].

3.5 Validation and Optimization of a Diesel Oil Surrogate Model Using CHEMKIN Package Routines

Before implementing the developed chemical kinetic mechanism, DOS model, into a CFD application, e.g. KIVA-3VR2 for this study, it is necessary to validate the model with the experimental results. Auto-ignition, adiabatic flame temperatures and laminar flame speeds of the model are the important characteristics which can present the general behavior and adequacy of the model.

3.5.1 Auto-ignition Shock Tube Data for Constituent Components

Shock tube ignition of various fuel-oxidizer mixtures provides essential data for development and validation of kinetic reaction mechanisms [55]. Considering ICE applications, there is not frequent experimental data in the literature for all possible constituents of any reaction mechanism at specified conditions, e.g., pressure and temperature to validate reaction mechanism. For example, there have been a greater number of shock-tube studies on paraffins than on aromatic species and experimental data on ignition delay times for paraffins have been available for a longer time than aromatic components. This can limit the development of a reaction mechanism [72]. The Gauther shock tube experiments were performed using a stoichiometric mixture of n-heptane and air under both low and high pressure conditions which are relevant enough to ICE simulations. In this study, detailed reaction mechanisms of DOS constituents, n-heptane and toluene oxidation which have been developed before (for improvement process and details see [73, 74, 75, 76, 77, 78, 79, 80]) are validated using available shock-tube auto-ignition data from Gauther and Davidsson [44, 81].

As mentioned above, there is no direct experimental data in the literature for DOS, which is represented in the fuel library as $C_{14}H_{28}$. For this reason, reaction mechanism starts with fuel surrogate, $C_{14}H_{28}$, decomposition into constituent components C_7H_{16} and C_7H_8 in which experimental data are available. In the course of the validation procedure, it was discovered that the experimental ignition delays in the temperature range 750-830 K are shorter for diesel fuel than for n-heptane. Since n-heptane is the most reactive component in the DOS fuel model, this behavior could not be reproduced. To account for this, a global oxidative pyrolysis reaction, possessing a relatively low activation energy, which will accelerate auto-ignition at low temperatures, is used [82]:

$$1.5C_{14}H_{28} + 0.5O_2 \Rightarrow 2C_7H_{16} + C_7H_8 + H_2O \quad (3.96)$$

Resulted detailed mechanism integrating the 70% n-heptane and 30% toluene oxidation chemistry with the kinetics of aromatics formation (up to four aromatic rings) for rich acetylene flames was reduced on the bases of sensitivity analysis (using the SENKIN code) to the mechanism consisting of ~ 72 species participating in ~ 332 reactions implemented into the KIVA-3VR2 code to simulate diesel spray combustion. The mechanism elaborates general high and low temperature oxidation paths for aliphatic hydrocarbons and a high temperature oxidation for toluene and was proved to predict the diesel oil auto-ignition (see Figure 3.11), combustion development and formation of PAHs till gaseous soot precursors based on acenaphthylene, A_2R_5, which are non-planar aromatic rings [38]. The ignition delay times at constant volume conditions were calculated using the SENKIN program which can represent the detailed chemistry in terms of the single-zone model [60]. Reaction rate parameters were taken from different sources, e.g., from LLNL [83] and MIT [84]. The low temperature toluene oxidation sub-mechanism was simplified since the auto-ignition of toluene in the mixture with n-heptane is mainly driven by the most reactive component. From Figure 3.11 it can be seen that the model reproduces the Negative Temperature Behavior (NTC) of the system well. Considering DOS, with the increase of equivalence ratio (ER), ignition delay times decreases till ER = 5, further increasing beyond this value has no considerable effect.

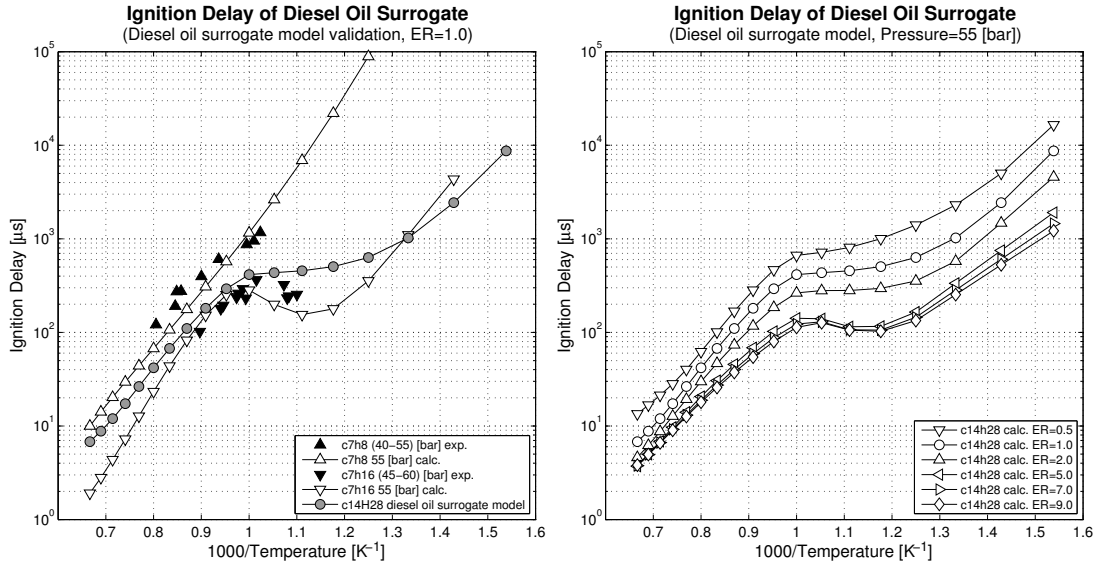

Figure 3.11 Calculated ignition delays vs. inverse temperature for DOS and its constituent components (70% n-heptane and 30% toluene): Left; comparison with shock-tube data and Right; comparison of calculations of DOS for different ERs

As mentioned before, comprehensive reaction mechanisms for HCs may consist of several thousand elementary reactions and depending on one's concern, many of these reactions can be neglected. So with the help of sensitivity analysis it is possible to identify the rate-limiting reaction steps and generate a simplified, or reduced, reaction mechanism by eliminating unimportant reactions. For the reaction mechanism which was used in this study, Figure 3.12 shows the temperature sensitivity analysis.

DOS sensitivity calculations were made with SENKIN code at constant volume for five different durations starting from 0.2E-03 s to 1.0E-3 s at high pressure. Initial conditions are T= 800 K, P = 60 bar and ER = 1 (stoichiometric mixture). Ignition delay temperature was accepted, 200 K increase from initial temperature, as 1000 K. Ignition delay time was calculated as 0.521E-03 s (where mixture temperature reached to 1000 K value). This analysis also proves the fact that reactions are most sensitive when they are close to the ignition delay times, e.g. at the moment of ignition, see Figure 3.12. From the figure one can see from the darkness of the bars that, sensitive reactions fall in the time range between 0.402E-03 s and 0.601E-03 s which includes ignition time inside. Numbers of the reactions are on the ordinate.

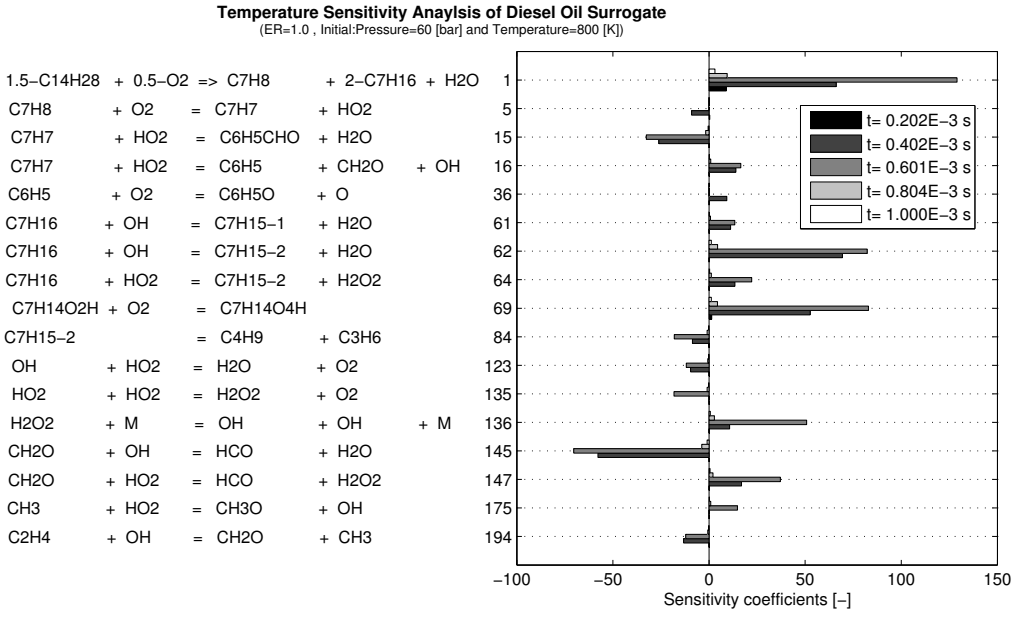

Figure 3.12 Sensitivity coefficients of the mechanism considering temperature of the mixture

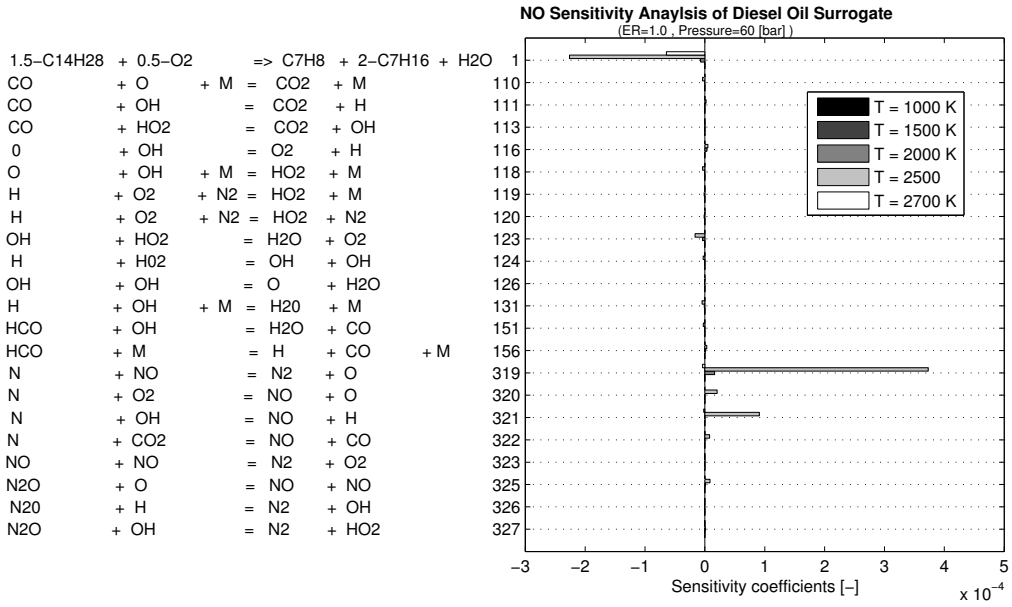

Figure 3.13 Sensitivity coefficients of the mechanism considering NO formation

Also it is very important for this study: How the reaction mechanism represents NO formation and which reactions are sensitive for NO production? NO sensitivity calculations are made at the conditions which is relevant to ICE operation, e.g. in the range of 1000 – 2700 K at five different temperatures. Initial conditions are P = 60 bar and ER = 1 (stoichiometric mixture). Analysis gives that noticeable NO formation is only possible at high temperatures (above 2000 K) and governed by well known Zel'dovich mechanism (Thermal NO mechanism) reactions, 319 and 321 for this analysis, in Figure 3.13. For both sensitivity analyses, global pyrolysis reaction (1st reaction) keeps its importance. One can see Edman's study [72] for further details of validation.

Although mechanisms for some HCs include thousands of elementary reactions, combustion rates are usually dependent on only a small subset of the many parameters in the kinetic model. These sensitivities are due to the roles, directly or indirectly, each reaction plays in contributing to the chain branching behavior of the reaction mechanism [55].

For example, at high temperatures (above about 1100 K) encountered in propagating flames, shock tube ignition, detonations, and pulse combustors, the primary chain branching is due to the single reaction,

$$H + O_2 = OH + O \tag{3.55}$$

which consumes one H atom radical and produces two new radicals, the O atom and the OH radical. Kinetic processes that increase the H atom population therefore will increase the rate of chain branching because those H atoms can react with O_2 through (3.55), resulting in more rapid overall reaction. Kinetic processes that reduce the amounts of H atoms will correspondingly lower the over all rate of reaction because the chain branching rate is reduced. The rate of reaction (3.55) is therefore found to be the most sensitive reaction in models of laminar flames and other high temperature systems. The second most sensitive reaction in high temperature combustion models is

$$CO + OH = H + CO_2 \ . \tag{3.97}$$

This reaction not only produces H atoms to react via (3.55), but also produces significant amounts of heat release through production of CO_2 at the reaction (3.97). Different fuels and classes of HCs react at different rates in the high temperature range because of their rates of production of H atoms and subsequent different rates of chain branching. This produces different laminar burning velocity, shock tube ignition delay and detonation properties such as cell size and initiation energy [55].

In conclusion, only a few elementary reactions are sensitive, e.g. rate limiting, in any mechanism. Other reactions are so fast that their rate coefficients have minor influence on the overall combustion process. This means that, the rate coefficients of sensitive elementary reactions have to be well known, because they have a great influence on the results. If reactions have low sensitivities, approximate values for the rate coefficients have to be known. Thus, sensitivity analysis reveals a few of the sensitive elementary reaction rates, which require accurate determination [1].

3.5.2 Analysis of Perfectly Stirred Reactor (PSR) Flows

Equilibrium calculations can be made by EQUIL code for the reaction mechanism. Basically, this kind of calculations can give useful results in two ways: First, it is possible to get an impression about the initial conditions, which affect the combustion temperature and pressure that are very important for the efficiency and emission products of the ICE, with the help of equilibrium calculations. Second, it gives the ability to examine the chemical nature of the product mixture which must be predicted or known before to help engine designers and developers in order to predict some potential emission products and amounts [85].

One of the chemical properties of the products is adiabatic flame temperature which can be obtained in two ways depending on how the process is completed: constant volume and constant pressure. Considering this reaction mechanism, adiabatic flame temperature calculations in air are made by EQUIL code for two cases; constant volume (initial P = 10 bar, T= 600 K) and constant pressure (initial P = 60 bar, T = 600 K), (see Figure 3.14).

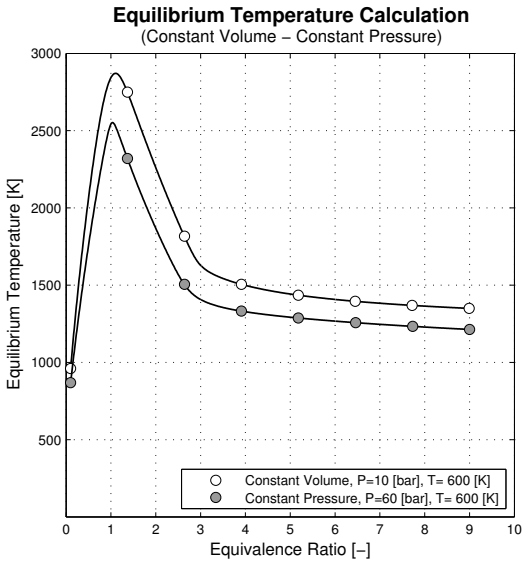

Figure 3.14 Equilibrium temperature calculation of the reaction mechanism for two cases; constant volume (initial P = 10 bar, T = 600 K) and pressure (initial P = 60 bar, T = 600 K)

The constant volume adiabatic flame temperature results from a complete combustion process that occurs without any work, heat transfer or changes in kinetic or potential energy. This is the maximum temperature that can be achieved for given reactants. But constant pressure adiabatic flame temperature occurs with work, hence its temperature is lower than the constant volume process because some of the energy is utilized generate work [86]. This difference can be seen clearly in Figure 3.14.

In the equilibrium calculation results of this study, maximum temperature is obtained in constant volume case while for both cases maximums occurred at slightly rich mixture conditions. This is an additional validation of the used reaction mechanism because ERs corresponding to maximum temperatures were in slightly rich area which is in consistence with the reality. Also these adiabatic flame temperature calculations will be useful in map construction process which will be explained in detail in the forthcoming chapters.

3.5.3 Flame Propagation Analysis in Premixed Mixtures

In order to validate mechanism's accuracy and test its range of applicability, it is important that kinetic model be compared with experimental data, such as the flame structure and response. For the flame response, a widely used parameter is the laminar flame speed that describes the propagation of the one-dimensional, planar, adiabatic, premixed flame in the doubly infinite domain. This response embodies the fundamental information on the diffusivity, reactivity, and exothermicity of a given mixture and has been extensively used to partially validate proposed kinetic models. If a proposed model could not reproduce such an important response as the laminar flame speed, its comprehensiveness and utility would obviously require further examination [87]. In Figure 3.15 the results of the laminar flame speed calculations for, one of the constituent of DOS, premixed n-heptane/air mixtures at different equivalence ratios are presented.

Figure 3.15 compares the experimentally determined flame speeds of n-heptane-air mixtures to the calculated flame speeds. The calculations were carried out using the present mechanism in the flame propagation code PREMIX. The results show that the mechanism predicts the n-heptane-air flame speeds well in lean mixtures and satisfactorily in rich mixtures of experimental data of Davis et al. [87]. In Figure 3.16 calculations for the other constitute of DOS, toluene are also presented.

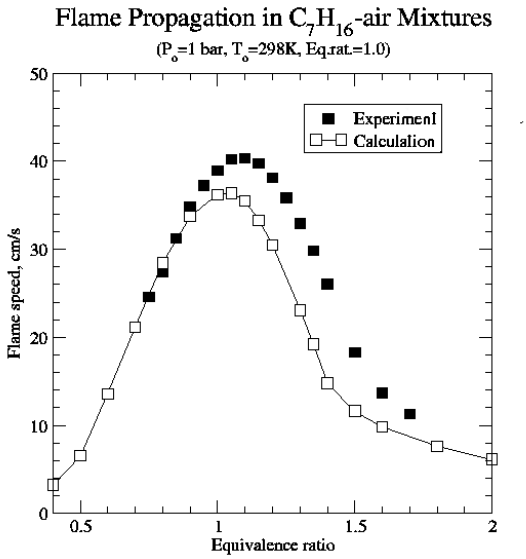

Figure 3.15 Comparison of experimental (filled squares) and computed (empty squares) laminar flame speeds of n-heptane-air mixtures at 1 bar.

Although laminar flame speed calculations in Figure 3.16 does not cover all the experimental data range, available results show that the mechanism predicts the toluene-air flame speeds well in both lean and rich mixtures of experimental data.

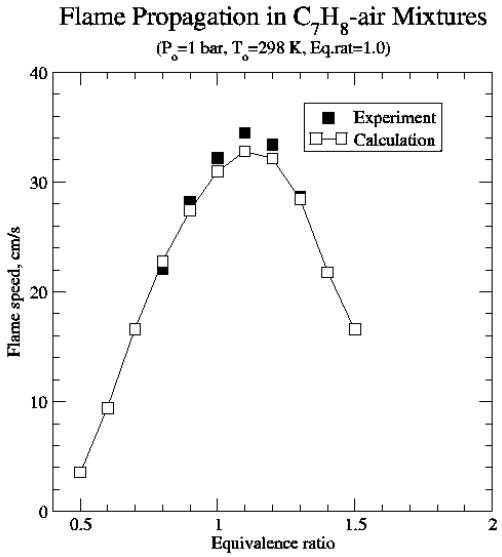

Figure 3.16 Comparison of experimental (filled squares) and computed (empty squares) laminar flame speeds of toluene-air mixtures at 1 bar.

The fact that the mechanism gives accurate predictions for flame propagation velocities confirms the mechanism's applicability for engine simulations [60]. Actual peak flame temperatures closely correspond to trends predicted by adiabatic flame calculations with maximum values near stoichiometric reactant conditions [10].

For an example of more complex diesel fuel-model, one can see Dagaut's model [11] represented as $C_{15.5}H_{30}$ compared with the experimental data. The oxidation of the model fuel was studied experimentally in a Jet Stirred Reactor (JSR) in ER = 0.5, 1 and 1.5 conditions. The kinetic modeling was performed by merging the kinetic reaction mechanisms proposed for the oxidation of n-hexadecane, iso-octane, n-propylcyclohexane and n-propylbenzene yielding a kinetic reaction mechanism involving 298 species and 2352 reactions (mostly reversible). While the proposed model could predict maximum mole fraction of most of the measured intermediates and products reasonably well (see Figure 3.17), it could not fully represent the oxidation of this diesel fuel according to Dagaut.

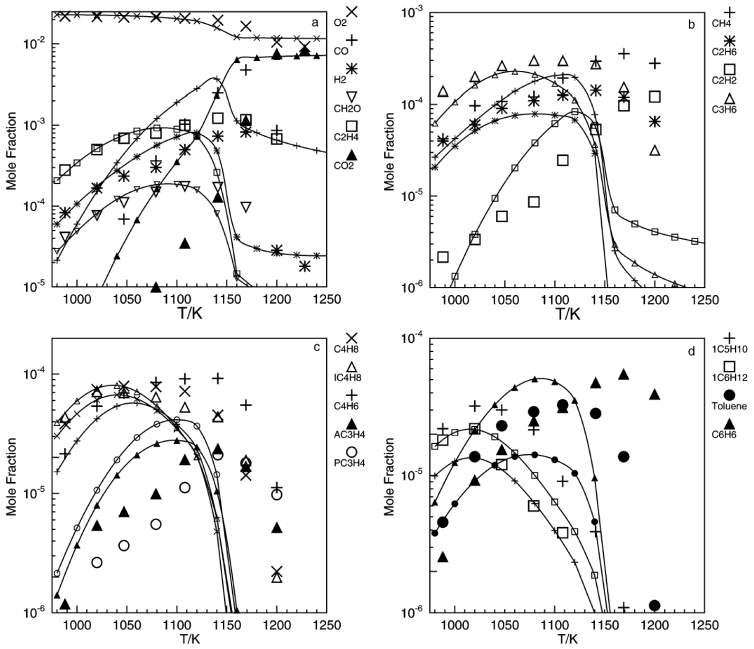

Figure 3.17 The oxidation of a diesel fuel ($C_{15.5}H_{30}$) at 1 atm in a JSR (0.05% of fuel, ER = 0.5, τ = 0.10 s). The experimental data (large symbols) are compared to the computed mole fractions (lines and small symbols) [11].

According to Dagaut, the model-fuel may be too simplistic and the inclusion of polyaromatics could be necessary, so more complex model-fuels are required for the modeling of the kinetics of oxidation/combustion of diesel fuels in detail.

3.6 Chemical Mechanism of Emission Formation

A general view about emission formation from diesel engine is given in section 1.1 before. On the other hand this section is restricted with only NO_x and soot emissions and denoted to explain basic mechanisms of these two pollutants. In general, the concentrations of these pollutants in ICE exhaust differ from values calculated assuming chemical equilibrium. Thus, it is necessary to know the detailed chemical mechanisms describing the formation of these pollutants and the kinetics of these processes to be able to determine emission levels. For soot, the formation and destruction reactions are internally coupled with the primary fuel combustion process. On the contrary, for NO_x, the formation and destruction processes are not part of the fuel combustion process. However, the reactions which produce nitrogen oxides (NO_x) take place in an environment resulting from combustion reactions, so the two processes are still internally but indirectly linked [7].

3.6.1 Mechanisms of NO_x Formation and Reduction

NO_x is a generic term for mono-nitrogen oxides. These oxides are produced during combustion, and are of interest as air pollution. They are believed to aggravate asthmatic conditions, react with the oxygen in the air to produce ozone, which is also an irritant, and eventually form nitric acid when dissolved in water. When dissolved in atmospheric moisture the result can be acid rain which can damage both trees and entire forest ecosystems [88].

In engine combustion, nitrogen oxides (NO_x) represent NO and NO_2 species. Considering NO_x emissions, ICE combustion emits mainly NO. NO_2/NO ratio can range between 10 and 30% in diesel engines. However, even if the NO_2-fraction within the NO_x is close to the upper limit, 30%, after a longer period of time it is converted almost completely into nitrogen dioxide (NO_2) under atmospheric conditions, e.g. by the reaction [7, 8]:

$$NO + HO_2 \longrightarrow NO_2 + OH \ . \tag{3.98}$$

For this reason, NO_x formation and modeling in ICE is most often reduced to NO formation.

Like as the general pollutant formation process, NO formation processes are strongly dependent on the fuel distribution and mixing of the combustion. For that reason, fuel spray and flame properties of premixed and mixing-controlled phases of diesel combustion will affect NO formation in a DI engine. Although global excess air ratio, λ, of the total mixture is lean (most often $\lambda > 1.2$), spray combustion (diffusion combustion) process occurs in local stoichiometric conditions ($\lambda \cong 1.0$) in diesel engine. Hence, one must consider this stoichiometric combustion conditions instead of global mixture λ while evaluating NO formation [89]. For ICE combustion, NO can be formed in three different ways [7, 8]:

1. Thermal NO: It is the major part of the NO and formed from atmospheric (molecular) nitrogen at high temperatures under slightly lean (local $\lambda > 1.0$) conditions within the burned products according to the Zel'dovich mechanism.
2. Prompt NO: It is formed from the reaction of the atmospheric nitrogen with HC radicals in the flame front of the fuel-rich regions (local $\lambda < 1.0$).

3. N_2O-intermediate: It is activated at lower temperatures than the thermal NO in a fuel-lean (local $\lambda > 1.0$) and high pressure environment. Although it has a minor effect in conventional diesel engine combustion, it is considered in the NO mechanism to model NO formation for LTC combustion conditions.
4. Fuel NO: If the fuel contains significant nitrogen, then fuel NO is formed from the oxidation of the fuel nitrogen-containing compounds. But diesel fuel does not contain significant amount of nitrogen, hence fuel NO is most often neglected in modeling.

As mentioned before, major fraction of NO is formed via the thermal part (80% to 95% according to literature [8]). For this reason numerical studies are mainly based on the thermal NO formation neglecting the remaining mechanisms. Prompt NO is effective within the flame region (it has 5% to 20% contribution) and it needs a detailed chemical mechanism to determine the intermediate species which take place in prompt NO mechanism to be able to get yield useful results. Although thermal and prompt NO mechanisms are the most important ones, all four type of NO formation mechanisms are considered in the detailed chemical mechanism (see Appendix I).

3.6.1.1 Thermal NO

Thermal NO formation process is basically well understood and simple. In fact, it needs three conditions at the same time, independent from the combustion application. These conditions are:

- high temperature
- oxygen availability
- time

When atmospheric air encounters with all these three conditions at the same time, no matter it is ICE combustion or any other process, NO forms. So, diesel combustion only prepares proper environment for thermal NO formation, e.g. indirectly causes thermal NO formation. This simple but very important knowledge and its mechanism were first discovered and explained by the great prolific Soviet physicist, Yakov Borisovich Zel'dovich in the year of 1946 [90], hence thermal NO mechanism is actually Zel'dovich mechanism. It consists of two elementary reactions, first breakup of a nitrogen molecule by an oxygen atom, and second the subsequent oxidation of N

atoms. Due to underestimations of NO levels, the third NO-creating elementary reaction was later added to the Zel'dovich mechanism by Lavoie et al. [91] and after then it is called extended Zel'dovich mechanism which is given below:

$$O + N_2 \xleftrightarrow{k_1} NO + N \tag{3.99}$$

$$N + O_2 \xleftrightarrow{k_2} NO + O \tag{3.100}$$

$$N + OH \xleftrightarrow{k_3} NO + H \tag{3.101}$$

From Table 3.3, it is evident that reaction (3.99) has a very high activation energy; e.g., ~ 38000 J which is much higher than the activation energy, ~ 3000 J of (3.100) and ~ 400 J of (3.101) due to the strong triple bond in the N_2 molecule in the reaction (3.99), hence, this reaction is sufficiently fast only at high temperatures. For this reason (because of the high temperature need) this mechanism is also called "Thermal NO". This thermal NO mechanism has been one of the most investigated of all reaction mechanisms. The forward reaction rate coefficients from different sources are summarized in Table 3.3.

If one calculates forward reaction rate coefficients at T = 2000 K, according to i.e, Warnatz, then:

$k_1 = 0.89\ 10^6$, $cm^3\ mol^{-1}\ s^{-1}$,
$k_2 = 2.68\ 10^{12}$, $cm^3\ mol^{-1}\ s^{-1}$,
$k_3 = 3.80\ 10^{13}$, $cm^3\ mol^{-1}\ s^{-1}$,
were obtained.

Since reaction rate coefficient of the reaction (3.99), k_1, is much lower than k_2 and k_3, reaction (3.99) is the slowest and rate-limiting step of this Zel'dovich mechanism. So, thermal NO formation is relatively slow process (see Figure 3.18).

Concentration-time profiles in the kinetic calculation of the CH_4/air at an inlet temperature of 1000 K, pressure of 10 atm, ER = 1.0 and T = 2477 K were given in Figure 3.18. This figure shows that all the energy release reactions are equilibrated before any significant amounts of NO formed (i.e., $t = 5\ 10^{-5}$ s moment). And it takes even more than 10^{-2} s for NO to reach equilibrium concentration at such a high temperature T = 2477 K [13]. In conclusion, thermal NO formation reaction is the slowest one among the others and this was clarified also with Figure 3.18.

Table 3.3 Rate coefficients for the forward reactions of extended Zel'dovich mechanism (revised and enhanced from [8])

Reaction coefficient	$cm^3\ mol^{-1}\ s^{-1}$	Source
k_1	$1.80\cdot10^{14}\exp\left[-\frac{38247}{T}\right]$	Warnatz et al., [1]
	$1.80\cdot10^{14}\exp\left[-\frac{38400}{T}\right]$	Baulch et al., 1991 [92]
	$0.54\cdot10^{14}\exp\left[-\frac{38020}{T}\right]$	GRI-MECH 3.0, 2000 [93]
	$0.76\cdot10^{14}\exp\left[-\frac{38000}{T}\right]$	Heywood, 1988 [7]
		APPENDIX I
k_2	$6.40\cdot10^{9}T\exp\left[-\frac{3127}{T}\right]$	Warnatz et al., [1]
	$1.48\cdot10^{8}T^{1.5}\exp\left[-\frac{2860}{T}\right]$	Pattas, 1973 [94]
	$9.00\cdot10^{9}T\exp\left[-\frac{3271}{T}\right]$	GRI-MECH 3.0, 2007 [93]
	$6.40\cdot10^{9}T\exp\left[-\frac{3150}{T}\right]$	Heywood, 1988 [7]
	$2.65\cdot10^{12}\exp\left[-\frac{3221}{T}\right]$	APPENDIX I
k_3	$3.80\cdot10^{13}$	Warnatz et al., [1]
	$3.00\cdot10^{13}$	Baulch et al., 1991 [95]
	$3.36\cdot10^{13}\exp\left[-\frac{385}{T}\right]$	GRI-MECH 3.0, 2007 [93]
	$4.10\cdot10^{13}$	Heywood, 1988 [7]
	$7.33\cdot10^{13}\exp\left[-\frac{564}{T}\right]$	APPENDIX I

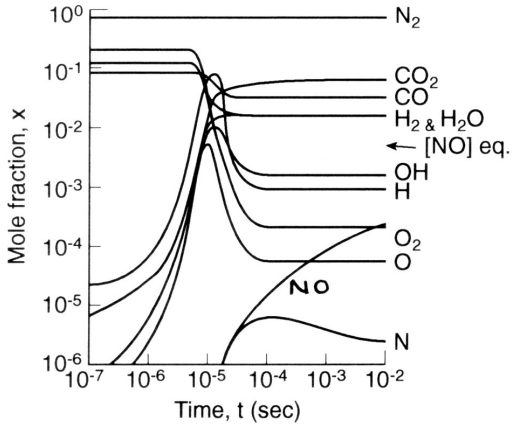

Figure 3.18 Concentration-time profiles in the kinetic calculation of the CH_4/air at an inlet temperature of 1000 K. P_2 = 10 atm, ER = 1.0, and T = 2477 K [96]

Naturally it is same for diesel engine combustion, it is not possible to reach chemical equilibrium conditions for NO, e.g., chemical reaction kinetics at the temperatures in the combustion chamber is slow in comparison to physical processes of the flow field. Figure 3.19 explains this phenomenon. NO concentrations versus Crank Angle (CA), under assumption of equilibrium and under consideration of kinetics are qualitatively illustrated according to Zel'dovich mechanism. At first, kinetically controlled process produces less NO (Δ1) than under equilibrium, but in the late combustion phase (expansion stroke), temperature decreases in the combustion chamber and [NO] "freezes" due to the slow reverse reactions in comparison with the engine speed. So at the late stage of combustion NO concentration remains higher (Δ2) than equilibrium concentrations [1, 97].

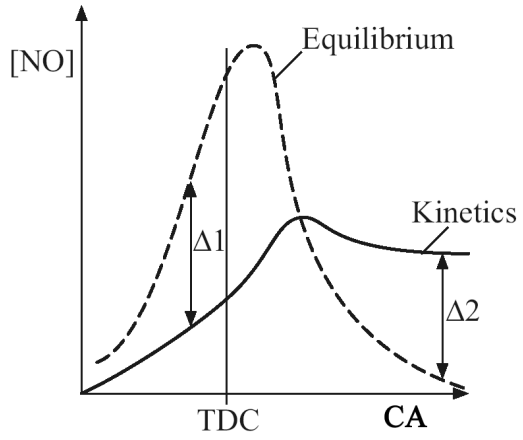

Figure 3.19 Equilibrium and kinetically controlled NO-formation for ICE [8]

This brings one to a conclusion that, if once combustion produces NO emission, it will not be possible to reduce it with the internal combustion process because of "freezing" process as in Figure 3.19. In order to avoid NO emission, it is necessary to shape combustion development process. Otherwise after-treatment will be necessary.

For NO formation rate, from (3.99) to (3.101)

$$\begin{aligned}\frac{\mathrm{d}[\mathrm{NO}]}{\mathrm{d}t} = {} & k_1[\mathrm{O}][\mathrm{N}_2] + k_2[\mathrm{N}][\mathrm{O}_2] + k_3[\mathrm{N}][\mathrm{OH}] \\ & - k_1[\mathrm{NO}][\mathrm{N}] - k_2[\mathrm{NO}][\mathrm{O}] - k_3[\mathrm{NO}][\mathrm{H}] \,,\end{aligned} \tag{3.102}$$

and for temporal change of nitrogen atom concentration

$$\begin{aligned}\frac{\mathrm{d}[\mathrm{N}]}{\mathrm{d}t} = {} & k_1[\mathrm{O}][\mathrm{N}_2] - k_2[\mathrm{N}][\mathrm{O}_2] - k_3[\mathrm{N}][\mathrm{OH}] \\ & - k_1[\mathrm{NO}][\mathrm{N}] + k_2[\mathrm{NO}][\mathrm{O}] + k_3[\mathrm{NO}][\mathrm{H}] \,.\end{aligned} \tag{3.103}$$

Remember that the forward rate of the both reactions (3.100) and (3.101) are much faster than (3.99), hence, N formed in (3.99) is immediately further converted to NO in the (3.100) and (3.101) reaction steps. The concentration of N thus remains constant after a short initial phase. For this reason, the concentration of N can be assumed to be quasi-steady, see section 3.2.1, d[N]/dt = 0. Then with this assumption and relation between (3.102) and (3.103):

$$\frac{\mathrm{d}[\mathrm{NO}]}{\mathrm{d}t} = 2k_1[\mathrm{O}][\mathrm{N}_2] - 2k_1[\mathrm{NO}][\mathrm{N}] \,. \tag{3.104}$$

If [NO] << $[NO]_{eq}$ then (3.104) can be simplified as

$$\frac{\mathrm{d}[\mathrm{NO}]}{\mathrm{d}t} = 2k_1[\mathrm{O}][\mathrm{N}_2] \,, \tag{3.105}$$

and in order to have this equation with oxygen molecule rather than oxygen atom, considering equilibrium conditions,

$$\frac{1}{2}[\mathrm{O}_2]_{\mathrm{eq}} \leftrightarrow [\mathrm{O}_{\mathrm{eq}}] \quad \text{and} \quad \mathrm{K}_{\mathrm{c,f,O}} = \frac{[\mathrm{O}]_{\mathrm{eq}}}{[\mathrm{O}_2]_{\mathrm{eq}}^{1/2}} \,. \tag{3.106}$$

Now, final form of NO formation rate, (3.105) is

$$\frac{\mathrm{d}[\mathrm{NO}]}{\mathrm{d}t} = 2k_1 \cdot \mathrm{K}_{\mathrm{c,f,O}}[\mathrm{O}_2]_{\mathrm{eq}}^{1/2}[\mathrm{N}_2] \,. \tag{3.107}$$

In conclusion, NO formation can be minimized by decreasing N_2, O_2 and k (temperature). From (3.107) it is evident that NO formation strongly depends on temperature, less depends on O_2 concentration. Hence, for ICE, the best way of controlling NO is to reduce combustion gas temperature and to a lesser extent O_2 concentration.

3.6.1.2 Prompt NO

Experimental measurements on flat HC flame by C. P. Fenimore [98] revealed that NO concentration in the flame, especially in fuel rich flames, is not zero. Fenimore understood that reactions other than Zel'dovich mechanism were playing role in the flame which forms some NO. He called this NO, "prompt NO". Also Fenimore noted that prompt NO was not found in non-HC flames [13]. Reactions that are promptly producing NO at the flame front is more complicated than thermal NO, because the prompt NO results from the radical CH that is generated through a complex reaction

mechanism. CH radical is formed as an intermediate at the flame front only (see Figure 3.20). Figure 3.20 shows quantitative measurements: Absolute concentrations of OH and NO, relative concentrations of CH in a premixed laminar flat CH_4-air flame at low pressure. Note that relative concentration profile provides valuable information on the shape and position of the CH-radical profile [1].

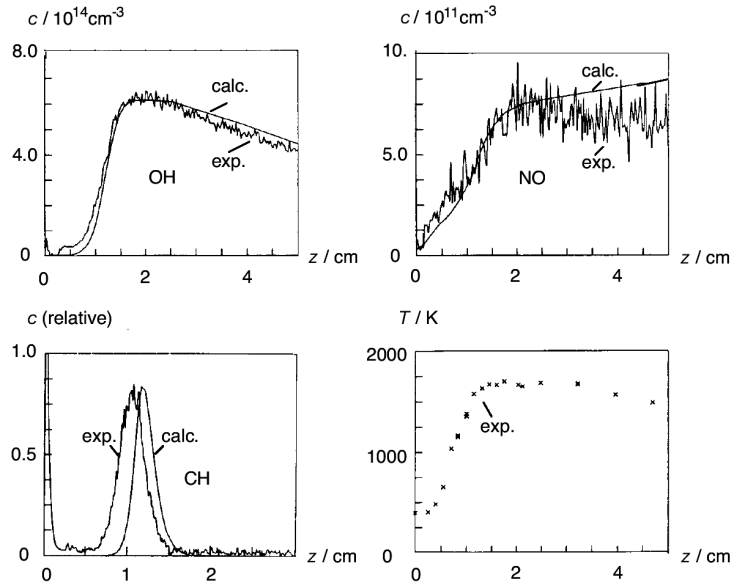

Figure 3.20 LIF measurements of profiles of temperature, OH and NO absolute concentrations and CH relative particle concentration in a premixed laminar flat CH_4-air flame [1]

CH radical reacts with the nitrogen of the air, forming hydrocyanic acid (HCN), which reacts further to NO,

$$CH + N_2 \longrightarrow HCN + N \Rightarrow \cdots \Rightarrow NO, N_2 \qquad (3.108)$$

Precise information about the rate-limiting step $CH + N_2 \rightarrow HCN + N$ is rather rare in the literature, thus, predictions of Fenimore NO are less accurate. The activation energy of this reaction, ~ 9000 K, is lower than the activation energy of the thermal NO reaction, ~ 38200 K, therefore, in contrast to thermal NO, prompt NO is formed at relatively low temperatures about 1000 K. Also there is another requirement for prompt NO formation, C_2H_2, which is a CH-radical precursor, accumulates under fuel-rich conditions, so, prompt NO is favored in rich flames.

In typical engine combustion, ~ 5-10% of NO_x is formed via the Fenimore mechanism, prompt NO, and 90-95% NO_x is formed via the Zel'dovich mechanism, thermal NO [8].

3.6.1.3 NO formed via N_2O

The nitrous oxide (N_2O) mechanism is analogous to the thermal mechanism in that O atoms attack molecular nitrogen with the presence of a third molecule M. This reaction is first postulated by Wolfrum [99],

$$N_2 + O + M \longrightarrow N_2O + M \ . \tag{3.109}$$

Then N_2O may subsequently react with O atoms to form NO,

$$N_2 + O \longrightarrow NO + NO \ . \tag{3.110}$$

In fact, this reaction is an insignificant contributor to the total NO sourced from engine combustion. However, for very some specific circumstances such as, lean conditions which suppress the formation of CH and, hence, Fenimore NO and low temperatures which suppress Zel'dovich NO, it remains only N_2O generated NO, that is promoted at high pressures because of the three-body reactions. N_2O route can be major source of NO in lean premixed high pressure combustion circumstances, i.e., mostly gas turbine engines [1].

3.6.1.4 Fuel NO

The conversion of fuel-nitrogen, fuel-bound nitrogen (FBN) into NO does not play a role in engine combustion, because fuels for internal combustion engines contain hardly any nitrogen. It is mainly observed in coal combustion, because even "clean" coal contains about 1% mass of chemically bound nitrogen.

The rate-limiting steps are both of the reactions competing for nitrogen atoms known from the Zel'dovich mechanism,

$$N + NO \longrightarrow N_2 + O \ , \tag{3.99}$$

$$N + OH \longrightarrow NO + H \ , \tag{3.101}$$

so that, they are extensively studied and known reactions, hence, NO formation from N_2O also is well understood [8].

3.6.1.5 Mechanisms of NO_x Reduction Using Ammoniac (Urea) Compounds

The effect of ammoniac deoxidizing agent (Urea) on the reduction of NO_x produced in the diesel engine was investigated numerically by Golovitchev et al., in which urea dissolved in water was directly injected into the engine cylinder during the expansion

stroke [100]. The NO_x deoxidizing process was described using a simplified chemical kinetic model coupled with the comprehensive kinetics of DOS combustion. The deoxidizing reactants could be delivered in a controlled amount directly into the flame plume zones, where NO_x are forming. Numerical simulations for the Isotta Fraschini DI Diesel engine are carried out using the KIVA-3VR2 code showed that the amount of NO_x could be substantially reduced up to 80% with the injection timing and the fraction of Urea in the solution optimized.

The high temperature submechanism of NO reduction by Urea is given below (see [100] for details). The process begins with Urea decomposition. In the presence of water vapor, Urea decomposes through the following path:

$$(NH_2)_2CO + H_2O + M \longrightarrow 2NH_3 + CO_2 \qquad (3.111)$$

The key species for NO reduction is the radical NH_2 formed from NH_3 by hydrogen abstraction:

$$NH_3 + OH \longrightarrow (NH_2) + H_2O \qquad (3.112)$$

and the major reaction channels of NO conversion are,

$$NH_2 + NO = N_2 + H_2O \ , \qquad (3.113)$$

$$NH + NO = N_2 + OH \ . \qquad (3.114)$$

One can find more details of the mechanisms in [101].

3.6.1.6 NO_x Reduction by Combustion Modifications

In any combustion system, for longer high temperature residence time and close to the equilibrium, NO formation will be favored. Thus the aim is to define an optimum time such that all of the fuel will be oxidized, as well as intermediates such as CO and the formation of NO is terminated by rapid cooling. Combustion modifications which are suitable to this theoretical approach are called primary measures. Primary methods are typically applicable to new combustion devices because they need extensive geometrical modifications and it is very difficult to change old combustion devices to meet these requirements. In old combustion devices there is possibility to use secondary methods, after-treatments [8].

According to the obtained information of NO formation mechanisms which are described in detail above, one can see Figure 3.21 for various combustion modification visualizations that is offered by Warnatz [1] to reduce NO formation.

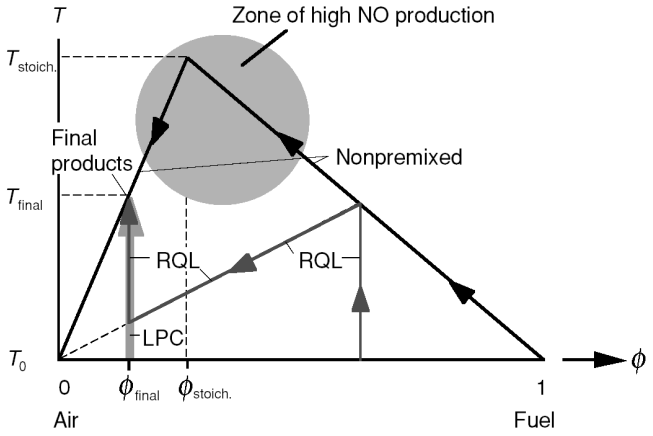

Figure 3.21 Schematic representation of mixing and reaction; LPC = lean premixed combustion, RQL = rich-quick-lean approach

Here, right edge of the x-axis is pure fuel ($\phi = 1$, $T = T_0$) and origin is pure air ($\phi = 0$, $T = T_0$). Fuel mixing with air is represented by movement from right to left and chemical reaction is represented by upward movement in this diagram. In non-premixed flames, the fuel evolves from the right ($\phi = 1$, $T = T_0$) to maximum temperature at $\phi = \phi_{\text{stoich.}}$, $T = T_{\text{stoich.}}$ to the final composition $\phi = \phi_{\text{final}}$, $T = T_{\text{final}}$. NO generation is largest in the zone near the maximum temperature $T = T_{\text{stoich.}}$, so, this way is to be avoided. Instead, it is possible to use EGR and dilute the air with inert products to reduce the maximum temperature, $T = T_{\text{stoich.}}$, hence, to decrease the NO generation. Figure 3.22 shows the effect of dilution of the intake air with N_2, CO_2, and exhaust gas on NO_x emissions. Note that, the heat capacity of CO_2 (per mole) at the temperatures relevant to diesel combustion is about twice that of N_2 and of the exhaust gas is slightly higher than that of N_2. Additions of these diluents reduce peak flame temperatures and NO_x emissions; addition of oxygen is vice versa [7]. So, according to Figure 3.21, it is possible to follow two ways:

- LPC: NO production zone is avoided by mixing fuel ($\phi = 1$, $T = T_0$) with air ($\phi = 0$, $T = T_0$) without reaction, following by reaction (vertical movement) to low NO products at $\phi = \phi_{\text{final}}$, $T = T_{\text{final}}$.
- RQL: In this approach, rich products are rapidly mixed with air along the mixing line connecting with $\phi = 0$, $T = T_0$ with the goal of reacting $\phi = \phi_{\text{final}}$, T

= T_{final} . Application example for this approach can be seen in Mehdiyev et al.'s studies, MR-Process [9], Bi-Modal Combustion [102] and stratified combustion strategy [103, 104].

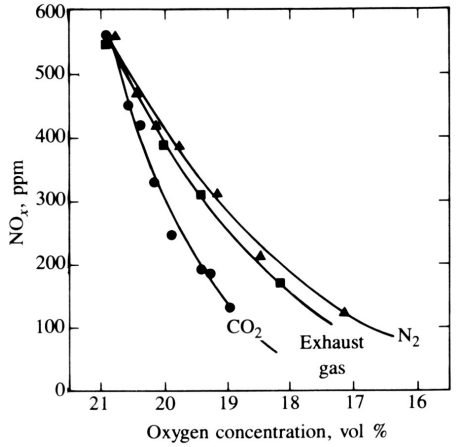

Figure 3.22 Effect of dilution on NO_x emission in DI diesel engine. Bore = 140 mm, stroke = 152 mm, CR=14.3, n = 1300 rpm, fuel rate = 142 mm^3/stroke, SOI = 4 CA BTDC [7]

3.6.2 Mechanism of Soot Formation and Oxidation

3.6.2.1 The Nature and Chemical Composition of Soot

Soot is carbonaceous particulates formed in gas-phase combustion at high temperature that often contains soluble organic fraction whose constituents include aromatic compounds as well as various other unburned HCs [105]. Although primary soot particles and graphite are similar in terms of morphology, soot is not uniquely defined, chemically as graphite. The characteristics of soot are well defined by Palmer and Cullis [106]. It contains at least 1% by weight (10% by atomic fraction) of H and can be represented with an empirical composition formula of C_8H [105].

3.6.2.2 Formation of Soot

Mechanism of soot formation is not simple and independent from the physical processes, such as NO formation case; hence it is not well understood yet and modeling of soot formation is problematic. Basically, soot formation is a kinetically controlled process [1] and it is affected from the flame type, various chemical and physical parameters of a given fuel and physical processes occurring in the combustion chamber [13]. According to the present knowledge, soot formation is divided into several stages as follows (see Figure 3.23):

– Particle inception: Formation of particle like structures by homogenous inception of large molecular precursors by coagulation of PAH molecules [107] or PAH molecule growth into the third dimension via addition of 5-membered ring structures [1, 105].

– Particle surface growth: Nearly all soot (> 95%) is formed by surface growth rather than particle inception [108, 109]. Surface-growth is not a gas-phase reaction of small molecules; it is a heterogeneous process where condensing and formation of soot kernels, dimensions of ~ 1 nm to 2 nm, occurs by picking up growth agents from the gas phase [8].

– Particle coagulation: Coagulation of relatively small particles, which are characterized by high rates of growth, i.e., up to ~ 10 nm diameter in low pressure premixed systems [110].

– Particle agglomeration: Agglomeration of the primary particles to form chain-like aggregates.

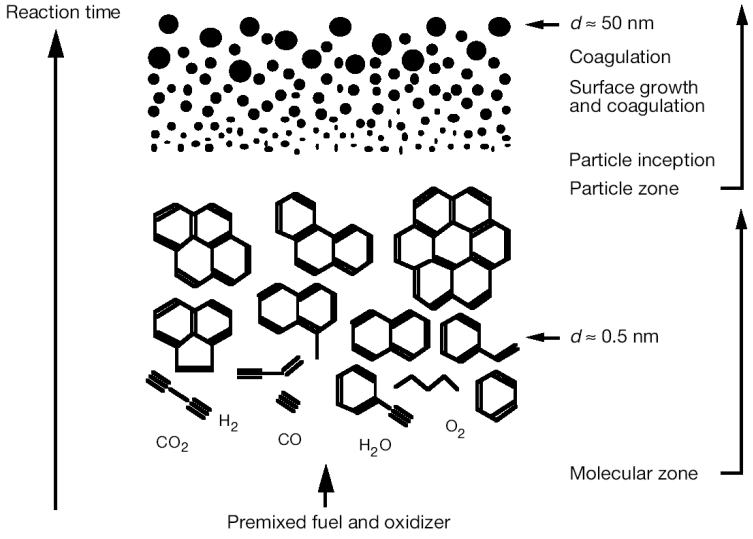

Figure 3.23 Schematic reaction path for soot formation in homogenous mixtures or pemixed flames [1]; ≡ is an acetylenic triple bond

From Figure 3.23, one can see that soot formation develops in two different stages as molecular and particle zones. The formation of molecular precursors which reactions take place in the gas phase is very important. It explains the origin of soot formation which is the subject of many soot studies. In this study, only formation of soot precursors (particle inception) and, global carbon "graphitization", for the oxidation process of solid soot, are considered via a sub-mechanism.

First step should be to decide on the molecular soot precursors which will be considered in the modeling. Regardless of the type of the flame and initial fuel involved, the HC fuel undergoes either pure or oxidative pyrolysis, degrading into small HC radicals. Under fuel-rich conditions, these small radicals react, leading to the formation of smaller HCs, particularly acetylene, C_2H_2. Then, large HC molecules containing large number of atoms such as polyynes ($C_{2n}H_2$, n=2, 3,...) and PAH are built up [105]. These,

- acetylene, C_2H_2
- polyynes, C_4H_2, C_6H_2, C_8H_2, ...
- PAH

are regarded as the molecular soot precursors. From the soot formation stages above, the particle inception chemistry used in this study is represented by the detailed fuel oxidation mechanism that includes the formation of acetylene (which is main sooting agent) and other generic soot precursors, polyynes and PAH. Large PAH are included in the mechanism to approximate the tendency to form soot. Such an approach is reasonable for the combustion of low HCs, but could fail to describe the soot formation processes in realistic diesel fuels, because practical diesel fuels contain significant amount of aromatics. So, toluene, representing aromatic components of real diesel fuel, is also added to the DOS model (see section 2.1). The mechanism consists of series of elementary reaction steps leading from acetylene, C_2H_2, and hydrogen, H_2, to the formation of the first aromatic ring, benzene, A1 which is building block for aromatic hydrocarbons (see section 1.2.1.5) [111]. Formation of the first aromatic ring is very important because this step is recognized as the rate-limiting step in the reaction sequence to larger aromatics [112]. Furthermore, Also toluene can form the A1 ring without interactions with acetylene. These reaction steps are followed by the successive stages of H-abstraction, C_2H_2-addition (HACA-mechanism), thus, yielding a chain of aromatic rings which connect the main combustion zone chemistry with the soot formation. The model predicted features are simulated shock-tube experiments for both n-heptane and toluene, time evolutions of fuel surrogate and its constituents, and soot formation/oxidation in the course of combustion. The electronic version of the mechanism can be found on the web site [113]. Below, A1 formation and PAH growth which is consider in the mechanism are described.

3.6.2.3 Formation of First Aromatic Ring, Benzene and Phenyl Radical

Benzene, A1 and the phenyl radical, A1-, is supplied from two reaction paths, the acetylene and the ion hypotheses described by the alkane and toluene sub mechanisms respectively. The first path, acetylene hypothesis, is independent from the existence of aromatic content in the initial fuel composition and consists of cyclization of smaller straight-chain HCs. The acetylene hypothesis assumes that several molecules of acetylene, which originated in rich combustion, join together to a first aromatic ring, benzene, with the addition of $H^{\bullet}$ and the splitting off of H_2. (see Figure 3.24) In this case, two different reaction paths are possible according to the local temperature, e.g., high and low temperature routes.

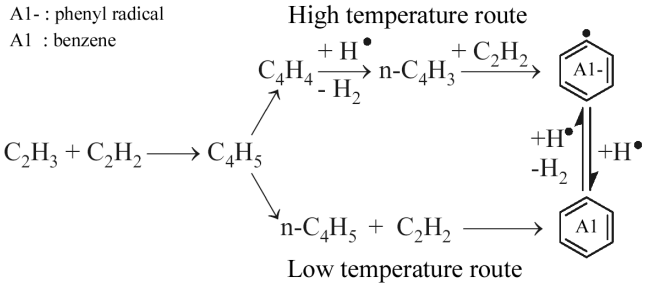

Figure 3.24 Acetylene hypotheses; reaction routes forming the first aromatic ring, benzene and phenyl radical [114]

The ion hypothesis states that the combination of propargyl, C_3H_3, radicals can also contribute to the formation of benzene or phenyl radicals. Benzene can be converted to a phenyl radical by H-abstraction or vice-versa (see Figure 3.25).

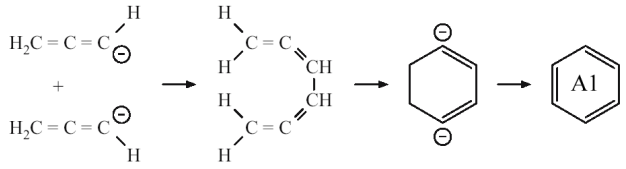

Figure 3.25 Ion hypotheses; reaction routes forming the first aromatic ring via the combination of propargyl, C_3H_3, radicals [115]

Acetylene hypothesis (see Figure 3.24) is considered in the DOS model by the acetylene addition to C_4- species,

$$C_4H_3 + C_2H_2 = \text{A1-} \tag{3.115}$$

$$C_4H_5 + C_2H_2 = \text{A1}\ , \tag{3.116}$$

and ion hypothesis combination of propargyl radical reaction (see Figure 3.25),

$$C_3H_3 + C_3H_3 = A1 \ . \qquad (3.117)$$

Based on benzene and phenyl radical, two and higher order aromatic ring species are formed through a variety of reaction paths, e.g. Hydrogen-Abstraction-C_2H_2-Addition (HACA) mechanism and/or polyyne polymerization [114].

3.6.2.4 PAH Growth via HACA Mechanism

HACA model has the ability to model the particle inception and surface growth processes in soot formation but not particle coagulation and agglomeration processes (under section 3.6.2.2). According to HACA mechanism, acetylene is the most important building block for PAH growth and subsequent soot formation [72]. HACA mechanism assumes a sequential two-step process for the aromatic ring formation:

- H-abstraction, which activates the aromatic molecules
- C_2H_2 addition to promote continuing molecular growth and cyclization of PAH (see Figure 3.26)

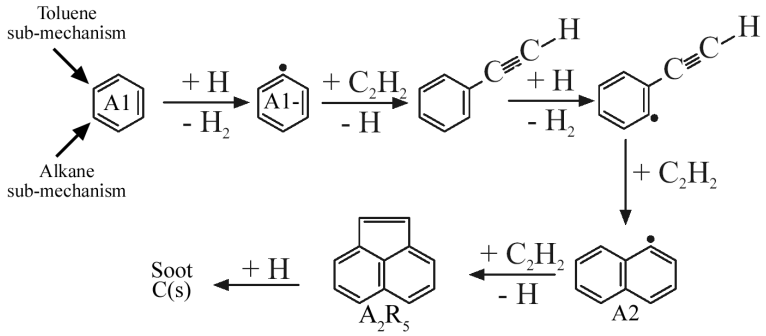

Figure 3.26 PAH growth via HACA mechanism (combined from [8] and [72])

Formation of first aromatic ring, benzene, as described in the previous section, takes place via toluene or alkane sub mechanisms. After these reaction steps, the HACA mechanism follows with the successive stages of H- abstraction and C_2H_2- addition and results with the formation of PAHs as the gaseous soot precursors represented by acenaphthylene species, A_2R_5, which are non-planar aromatic rings (see Figure 3.26). Here, one can see the soot model from the formation of first aromatic ring, benzene, to the soot precursor, acenaphthylene, A_2R_5 via HACA mechanism and finally graphitization step of the acenaphthylene to soot, C(s) [72]. Reactions of these steps till soot precursor, A_2R_5, are given below:

$$A1 + H = A1\text{-} + H_2 \quad (3.118)$$

$$A1\text{-} + C_2H_2 = A1C_2H + H \quad (3.119)$$

$$A1C_2H + H = A1C_2H\text{-} + H_2 \quad (3.120)$$

$$A1C_2H\text{-} + C_2H_2 = A2\text{-} \quad (3.121)$$

$$A2\text{-} + C_2H_2 = A_2R_5 + H \quad (3.122)$$

And graphitization of the acenaphthylene,

$$A_2R_5 \longrightarrow 12C(s) + 4H_2 \ . \quad (3.123)$$

The term "graphitization" is used because the thermal properties of soot particles are taken as solid graphite.

3.6.2.5 PAH Growth via Polyyne Polymerization

Some other researchers propose another approach considering linear polymers, polyynes, as gaseous soot precursors. They support their idea on that polyyne group grows faster than other HCs at higher temperatures and that soot is formed in large amounts even under flame/pyrolysis conditions with low PAH production. Polymerization of polyynes includes cyclization and breeding at surface radical sites so that the polyyne complex grows irreversibly to polymeric globule, a primary soot particle. Graphitization of these particles is represented by the reaction,

$$C_6H_2 \longrightarrow 6C(s) + H_2 \ . \quad (3.124)$$

For aromatic ring growth, (see graphitization reactions, (2.115) and (2.116)) it is stopped at C_6H_2, long-chain acetylene, and A_2R_5, acenaphtylene, assuming that soot inception can be simulated via fast "graphitization" processes [116]. Carbon produced includes both vapor and solid phases, but, since the density of the vapor is in orders of magnitude smaller than that of the solid phase, the vapor concentration can be ignored. Since carbon is solid, it cannot contribute to the Arrhenius rates or gas pressure calculations. PAH growth part of the DOS model is based on work by Wang and Frenklach [117] and to limit the PAH growth, the oxidation by OH and O_2 is included into the mechanism [111].

3.6.2.6 Oxidation of Soot

Unlike soot formation route, soot oxidation occurs over the entire course of soot formation and it is a heterogeneous process in which oxidation reactions take place on the surfaces of soot particles, depleting the carbon mass accumulated in the soot particles [105]. Soot particles in principle can be oxidized by O atoms, OH radicals, O_2 and, furthermore, NO. Because of the low concentration of O in sooting flames ([O] = 0.01·[OH]) and its limited reaction probability on soot surfaces at flame temperatures, the oxidation of soot is considered to be primarily due to OH, O and O_2 [1, 118]. This is also supported with the fact that, in the flame environment, about 10% of collisions with OH radicals are effective in gasifying C(s), hence, OH radicals may be very important in soot oxidation in flames, even in the presence of significant concentrations of O_2 [105]. Solid soot oxidation reactions in the DOS model used,

$$C(s) + O_2 \longrightarrow O + CO \tag{3.125}$$

$$C(s) + H_2O \longrightarrow CO + H_2 \tag{3.126}$$

$$C(s) + OH \longrightarrow CO + H \tag{3.127}$$

$$C(s) + OH + OH \longrightarrow CO_2 + H_2 \tag{3.128}$$

$$C(s) + OH + O \longrightarrow CO_2 + H \tag{3.129}$$

$$C(s) + NO_2 \longrightarrow CO + NO \ . \tag{3.130}$$

Influence of temperature both on soot formation and oxidation process is given in Figure 3.27. Soot yield is represented upon the temperature and excess air ratio, λ. Soot is rapidly formed after some induction period reaching its maximum and it is equaly rapidly oxidized [119]. There is a temperature window 1,500 K < T < 1,900 K which is critical for soot formation. High temperature favors both soot formation (pyrolyse) and oxidation. Extreme increase in soot emission is visible for $\lambda < 0.6$ [8].

This appearance is the result of the fact that at low temperature the radical precursors of soot (such as C_3H_3) are not formed, and that at high temperature the reverse decomposition reactions of the soot precursors are initiated and they dominate the process, e.g., decrease the soot amount.

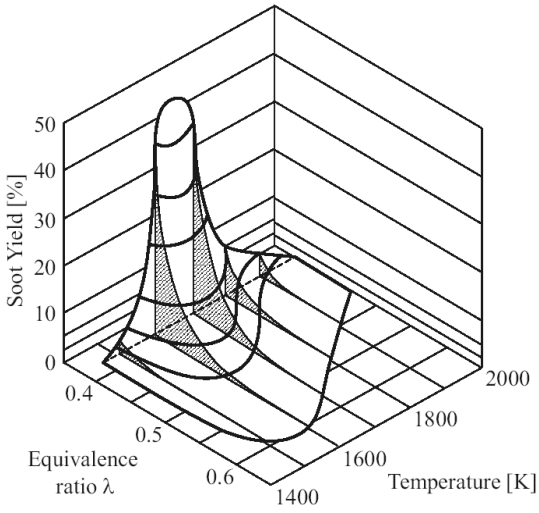

Figure 3.27 Soot yield as a function of λ and *T* [8]

The pyrolyse-oxidation problem for ICE is shown schematically in Figure 3.28. At the beginning of combustion, a relatively large amount of soot is produced, which is however for the most part oxidized again during the main and post-combustion phases. At some point during the expansion stroke, the oxidation of previously formed soot comes to a stop because the concentration of O-atoms and OH-radicals becomes too small to attack the soot particles. This freezing of the oxidation occurs approximately between 1300 K and 1400 K. So, a certain fraction of the soot, which cannot be oxidized, is emitted into the exhaust. The amount of particles measured in the exhaust gas is thus only a fraction (~ 0.1 to 1%) of the maximum formed particles. This very much problematizes the understanding and the coverage of the dominating chemical and physical processes in soot formation. This represents a principal mathematical problem in this way that since the soot mass in the exhaust is only a very small difference between two large, formation and oxidation, quantities, a significant relative error will result if there is only a slight deviation in either the production or oxidation rate.

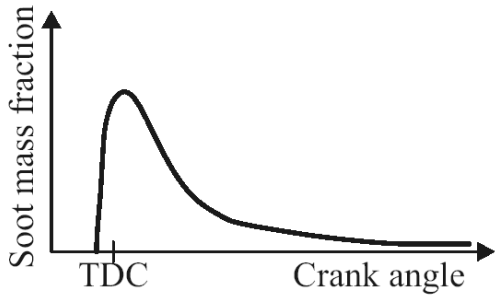

Figure 3.28 Example for soot evaluation vs. CA in ICE [8]

For the above reasons soot models can today mostly be utilized in order to make qualitative assessments with high relative errors (i.e., > 100%). and they are most useful in fundamental studies with simpler boundary conditions. They are not yet a standard in 3D-CFD diesel engine modeling [120].

4 APPLICATION OF PARAMETRIC ϕ-T MAPS TO THE ANALYSIS OF EMISSIONS FORMATIONS IN DIESEL ENGINES

4.1.1 Parametric ϕ-T Map Technique (Static Map)

The so-called parametric ϕ-T map (ϕ: local fuel/air ratio and T: local temperature), two dimensional (2D) graphical representation, was first introduced by Kamimoto and Bae [121] in 1988 (see Figure 4.1).

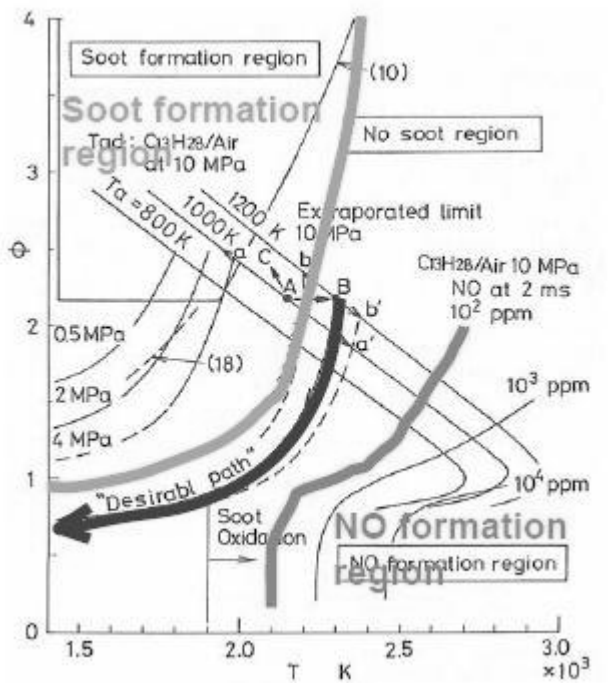

Figure 4.1 First ϕ-T map introduced by Kamimoto et al. (modified from [121])

From Figure 4.1, it is seen two peninsulas for soot and NO_x concentrations as a function of certain amount of ϕ and T value pairs which are consistent with the diesel engine combustion conditions (ϕ = 0.0, 0.5,…, 4.0 and T = 1400, 1500,…, 3000 K). The idea of this map technique is to make simulations for the formation of the desired species at lots of ϕ-T combinations in a zero-dimensional, 0D, closed Perfectly Stirred Reactor, PSR, using certain elapsed reaction times, pressures and initial conditions (i.e. EGR). Then, results of these calculations, corresponding to those intended amount of ϕ-T value pairs, are drawn on 2D ϕ-T plane showing the

amount of the related species (volume ratio, molar fraction, etc…) for the given pressure, initial conditions and elapsed reaction time. Note that calculations of the all ϕ-T range of a single map corresponds to only one pressure value, initial condition and elapsed reaction time. For example, Figure 4.1 shows first example, Kamimoto's work, in which $C_{13}H_{28}$ /air mixture and its equilibrium states were calculated at constant high pressure, 10 MPa, and for 2 ms elapsed reaction time after the SOI. While soot emissions were based on the published data, NO formation was calculated by the extended Zel'dovich mechanism. The amount of calculations of those ϕ-T points can change according to the intended intensity.

After thirteen years passed from the introduction of first ϕ-T map idea by Kamimoto, Akihama et al. [122] introduced this static map technique into Low Temperature diesel Combustion, LTC, regime by the presence of high EGR loads using this ϕ-T map technique coupled with a simplified 3D engine combustion simulation. Then Kook et al. [123] optimized LTC regimes using the technique based on the simplified emission map and Shimo et al. [124] optimized a new Premixed Charge Compression Ignition, PCCI, regime using the simplified maps with the 3D engine simulations and also Kim et al. [125] investigated the soot emissions tendency using the map analysis coupled with the chemical mechanism of the diesel surrogate oil. In all these studies, elapsed reaction times and pressures were always kept constant, e.g. an identical map was used as background, for analyzing the whole engine cycle. Hence, Golovitchev called these first generation map technique "static maps". Although it is easier and simpler to develop this kind of static maps, it is better to use dynamic maps where calculation pressures and elapsed reaction times change with respect to varying pressure and elapsed reaction times of real ICE combustion.

4.1.2 Unique Parametric ϕ-T Dynamic Map Technique

Different from those previous static maps, the unique parametric ϕ-T dynamic map technique (ϕ-T dynamic map) used in this study was first introduced by Golovitchev and co-workers [126]. The maps were dynamic in that sense that when constructed, the pressures and the elapsed times after SOI were taken same as those in the 3D engine simulations. Golovitchev developed this technique and applied into the simulations of different type ICEs, e.g., Free Piston, FP, engines [127, 128]; High Speed Direct Injection, HSDI, engine [129]; Dimethyl Ether, DME, diesel engine

[130] and Modulated Kinetics, MK, combustion engines [38, 119]. This ϕ-T dynamic map technique consists of two independent routes, 3D-CFD and 0D, which their calculation results are coupled and used for the scientific evaluation of engine combustion and emission formation (see Figure 4.2). There is no direct coupling between those two 3D and 0D simulation routes. Results of KIVA-3VR2 simulation, e.g., initial conditions, ϕ, T, pressure and elapsed reaction time are properly organized for the 0D SENKIN code simulation.

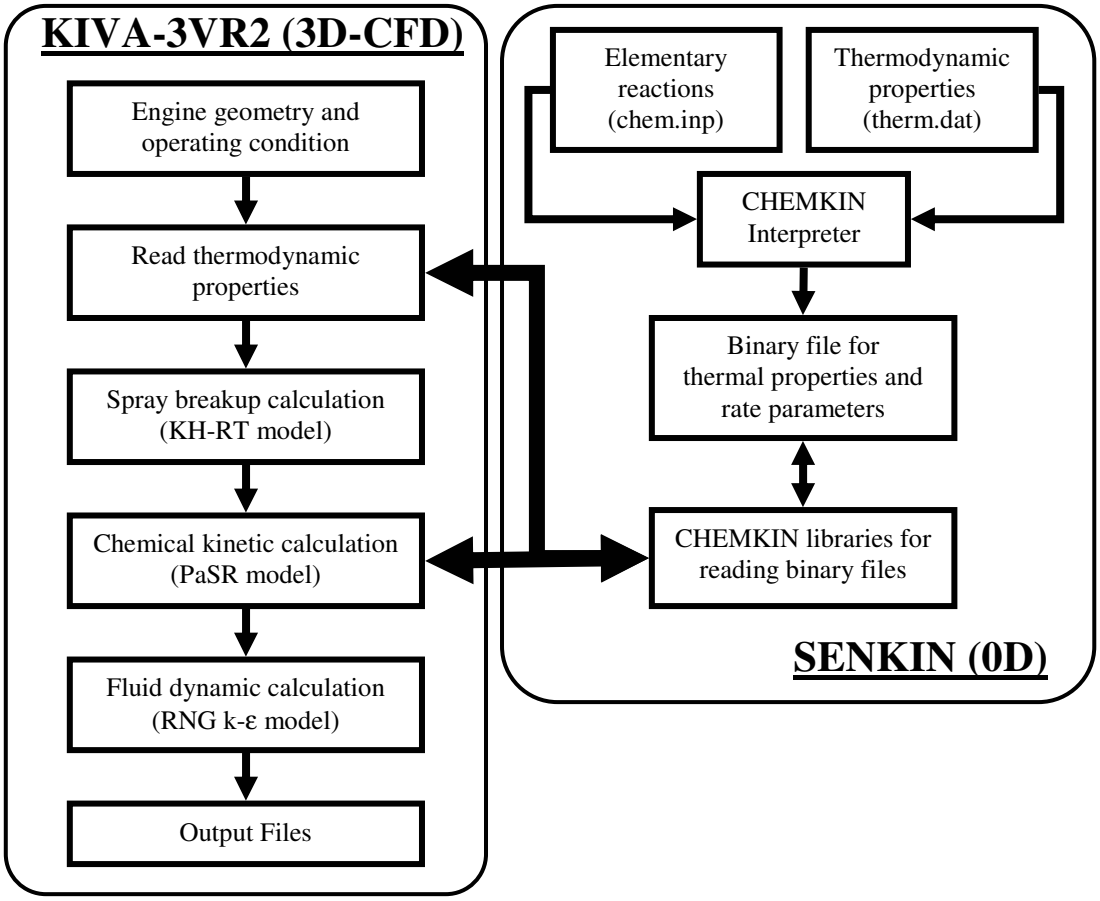

Figure 4.2 Two routes 3D-CFD KIVA-3VR2 and 0D SENKIN codes and their interaction for ϕ-T dynamic map construction

4.1.2.1 0D (SENKIN) Background Simulation Part

Actually, 0D SENKIN map calculations forms background view showing species mole fractions presented with iso-lines (see Figure 4.3 for soot-NO map background example). The maps were constructed using the constant pressure and temperature option (TTIM) of the 0D SENKIN code. This is a feasible approach to analyze the formation mechanism of mixture components at any point of the map. The temperature and pressure are held constant at each ϕ-T calculation point of the map.

The temperature before and after combustion are superimposed to be the same, which means that the conditions are non-isochoric and non-adiabatic. Therefore, for some regions of the map, the actual ϕ-T combination will never be obtained in practice from combustion with a certain ϕ [127]. In principle, one can create similar maps for other desired species such as CO_2, OH, C_2H_2… Also see [127] for detailed application examples.

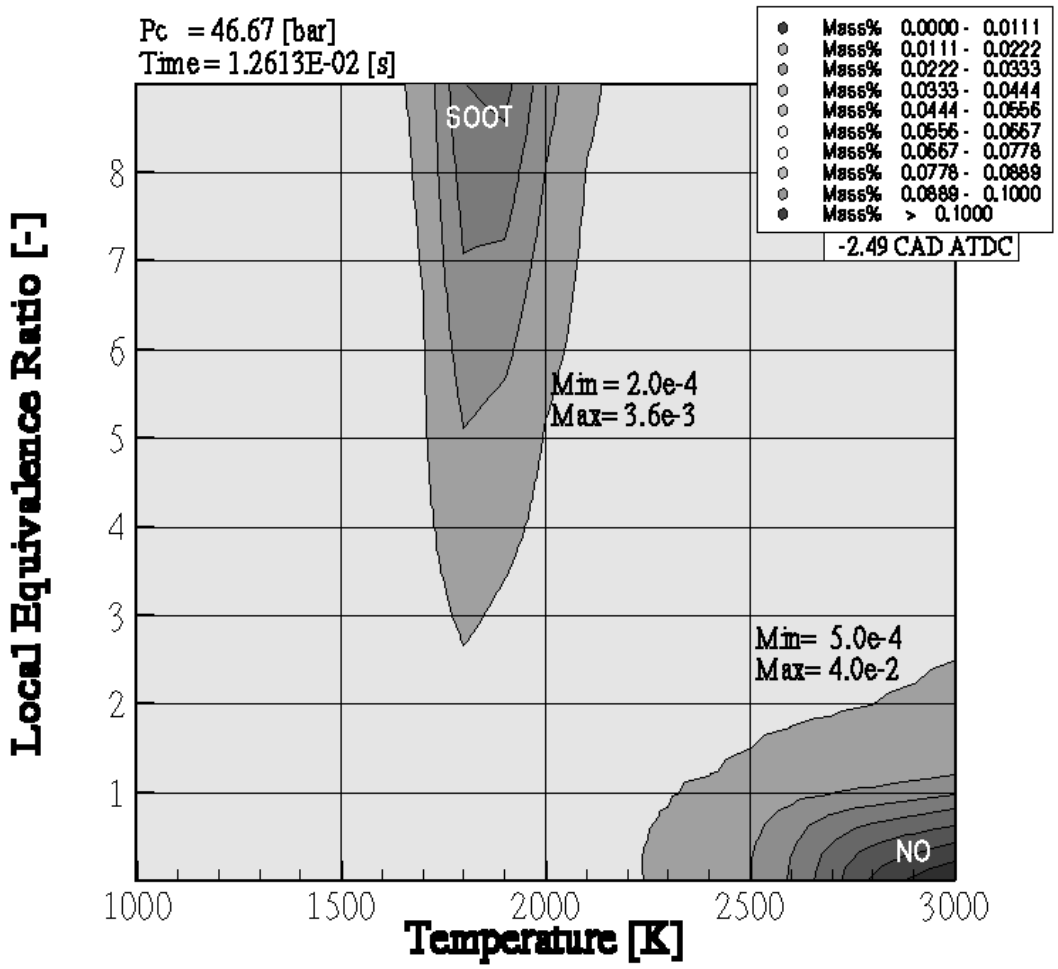

Figure 4.3 An example soot-NO map calculation for one case

For the 0D background calculation example in Figure 4.3, one can see that pressure = 46.67 bar (kept constant) and exact simulation time = 1.2613E-2 s values are used. Those pressure and time values used in this background correspond to the moment of -2.49 crank angle degree (CAD) after top dead centre (ATDC) of the considered ICE simulation which was made by 3D-CFD code, KIVA-3VR2. At the top right corner, it is given a mass distribution scale of the all mixture in the KIVA-3VR2 simulation. Later, it will be explained in detail over

the pressure curve of the KIVA-3VR2 simulation. Since calculation local temperature range is 1000 K < T < 3000 K with 100 K increment and, local ER range is 0.0 < ϕ < 9.0 with 0.25 increment, the number of calculation points, $SENKIN_{number}$, can be calculated as 777. So for those temperature and pressure ranges and increments, each background map calculation will have 777 ϕ-T calculations. See below for the derivation of the total number of map calculation points.

T_{number} = (3000-2000) / 100 + 1 = 21

ϕ_{number} = (9.00-0.00) / 0.25 + 1 = 37

$SENKIN_{number}$ = 21 x 77 = 777

where,

T_{number} : number of local temperature points,

ϕ_{number} : number of local equivalence ratio points

4.1.2.2 3D-CFD (KIVA-3VR2) and 0D (SENKIN) Simulations

ϕ-T dynamic maps were constructed according to the pressure curve from 3D-CFD simulations [127]. The number of the maps depends on the considered CA range, map interval and operating conditions of the engine. Although there is no any limitation, for optimum, it can be advised at most 40 maps in order to have a reasonable idea about emission formation and/or efficiency of a cycle. Figure 4.4 shows a pressure curve example from KIVA-3VR2 simulation with the selected three soot-NO ϕ-T dynamic maps from certain moments of this pressure curve. Those maps belong to early, developed and late combustion stages, respectively. With the help of this schematic figure, basic approach of ϕ-T dynamic map construction can be explained. Note that the number of maps in this example is only three and not enough to judge the emission and efficiency characteristics of the cycle. They are just arbitrarily chosen for explanation of the ϕ-T dynamic map technique. Basic data of these maps are given in Table 4.1.

Table 4.1 lists basic data of the three points considered in Figure 4.4. In ϕ-T dynamic map construction, one of the most important feature of the 0D SENKIN simulations is that, except first map, initial mixture composition of each map are taken as same with the product composition of the previous map. For example, in Table 4.1, Map 1 calculation starts with an initial mixture composition, $(C_{14}H_{28}, O_2, N_2)_{1r}$, and results

with the products such as $(CO_2, O_2, N_2\ldots)_{1p}$ and Map 2 calculation starts with Map 1's product composition, $(CO_2, O_2, N_2\ldots)_{1p}$, and so on.

Table 4.1 Basic data of the maps given in Figure 4.4.

	3D-CFD RESULTS			0D SIMULATIONS		
Map No	**CAD** ATDC	**Exact Time** s x 10^{-3}	**Pressure** bar	**Elapsed time** s x 10^{-3}	**Reactant species**	**Product species**
1	-7.99	7.5645	54.92	0.5645	$(C_{14}H_{28})_{1r}$, $(O_2)_{1r}$, $(N_2)_{1r}$	$(CO_2)_{1p}$, $(H_2O)_{1p}$, $(CO)_{1p}$, $(OH)_{1p}$,…
2	+0.01	8.2602	82.05	0.6957	$(CO_2)_{1p}$, $(H_2O)_{1p}$, $(CO)_{1p}$, $(OH)_{1p}$,…	$(CO_2)_{2p}$, $(H_2O)_{2p}$, $(CO)_{2p}$, $(OH)_{2p}$,…
3	+20.00	9.9977	32.55	1.7375	$(CO_2)_{2p}$, $(H_2O)_{2p}$, $(CO)_{2p}$, $(OH)_{2p}$,…	$(CO_2)_{3p}$, $(H_2O)_{3p}$, $(CO)_{3p}$, $(OH)_{3p}$,…

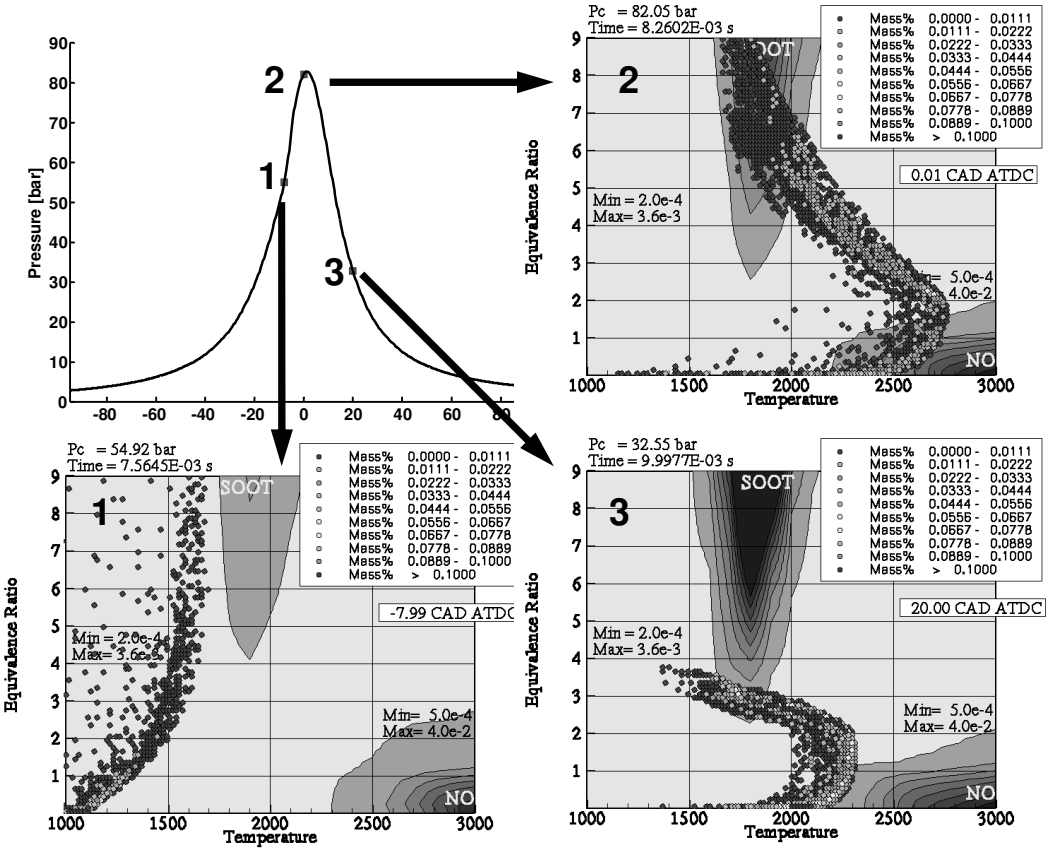

Figure 4.4 The schematic of soot-NO ϕ-T dynamic map construction, maps 1-3 correspond to different positions on the compression/expansion pressure curve

First map in Figure 4.4 must appear at a moment after SOI of the 3D-CFD engine simulation. In order to start map calculations, a virtual reference time, allowing enough duration after SOI for the evaporation of fuel, is accepted (i.e., assume that reference time = 7.0000E10^{-3} s here). This virtual reference time is used to determine

elapsed reaction time used in 0D simulation for the only first map. Hence, elapsed reaction time for the first map is equal the difference between exact simulation time and the virtual reference time (7.5645E10-3 s - 7.0000E-3 s) = 0.5645E-3 s, see "Exact time" in Table 4.1). For the forthcoming maps, exact time differences between the consequent two maps (i.e., time of map 2 - time of map 1) are taken as the elapsed reaction time for 0D simulations (see Table 4.1). As can be seen from Table 4.1, CAD, exact simulation time and pressure data are taken from 3D-CFD simulations. Then, by using this pressure (kept constant), initial conditions and calculated elapsed reaction times; reactant and product species compositions are calculated with 0D background map simulations (see Table 4.1).

Different from the Figure 4.3, one can see additional points plotted on the each background map in Figure 4.4. Those points show the mass fraction of the ϕ-T conditions corresponding to all computational cells of the 3D-CFD simulation. In other words, predicted in-cylinder conditions using the KIVA-3VR2 code (represented by the computational cells' elapsed reaction time, mass, with ϕ, T and P values) were plotted on the background maps, identifying combustion trajectories helping to navigate between the regions of emissions formation by varying different engine and injection parameters (see Figure 4.4). The CFD simulations were performed using a modified version of the KIVA-3VR2. For each ϕ-T dynamic map construction, all of the computational cells of the gas mixture in the 3D-CFD simulation are scanned and cells' individual masses are grouped and summed up with respect to their ϕ-T values which are used to construct the background map. Then, these mass groups' data are written into special output files to be processed by the help of graphic and plotting software, TECPLOT, and accessory FORTRAN codes. Processing of those mass groups makes them colored according to the predefined mass fraction ranges and then they are plotted over background maps with the specially designed layout options of TECPLOT. A 10 stepped mass scale is used in the map construction in this study. These colored ranges are placed in a box at top right of each map. One can see CAD value below this box, also pressure and exact simulation time values are seen at the top left in each map.

So, linkage between 3D-CFD simulations and 0D background calculations are obtained by plotting these ϕ-T points from CFD simulations on the calculated background maps. When these points intersect with the peninsulas of emissions

formation (NO_x or soot), see Figure 4.4, it characterizes their formation. Note that, each time different background maps are used for every point over the pressure curve of the 3D-CFD simulation (because pressure and elapsed time values change). This is why Golovitchev [126] called these transient map construction technique, as "ϕ-T dynamic map". Same reaction mechanism, DOS model, with the one which is implemented in KIVA-3VR2 code is used in the 0D SENKIN simulations to construct ϕ-T dynamic maps.

Figure 4.5 shows another ϕ-T dynamic map application example, for soot-NO emissions in diesel combustion. On the left side NO distribution, on the right side soot distribution of the KIVA-3VR2 simulation (both in the sector mesh) and in the middle, related ϕ-T dynamic map of the SENKIN simulation are presented [131]. This is a LTC regime, SOI=9 CA ATDC, CR=14.00 and these figures correspond to 0.03 CA ATDC. One can see high amount of NO emissions both on the map and on the 3D-CFD simulation images (Figure 4.5 a, b). While most of the points representing KIVA-3VR2 simulation intersect with the NO formation peninsula, fewer points intersect with the soot formation peninsula of the map. This is only one example of the possible ϕ-T maps of this cycle. It is not correct to judge the amount of emissions only looking at one map such as here, instead it is necessary to produce more maps (i.e. 20) covering whole CA range to come to a reasonable decision about emission formation.

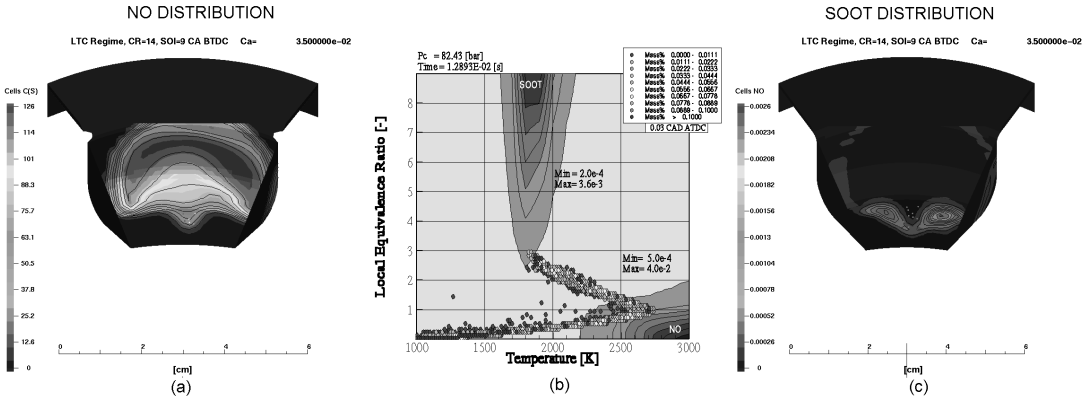

Figure 4.5 Soot-NO emission distributions in the CFD and ϕ-T map modeling

Although, one can get an idea about the emission formation and/or efficiency, it is not possible yet to get accurate emission values from ϕ-T dynamic maps because:

– The effects of the interactions between cells of the 3D-CFD simulation cannot be considered in 0D SENKIN simulation. In fact, local fuel/air ratio and species concentrations and cell temperatures are affected and changed because of the diffusion between neighbor cells in 3D-CFD simulations.

– The number of the maps is limited to stay in applicable level. To get accurate, comparable to 3D-CFD simulations, emission values, the number of the ϕ-T dynamic maps should be a lot higher.

– Although its effect is minor, there is still a problem for calculating exact local air/fuel ratio in the 0D SENKIN calculations. Fuel/air ratio values are corrupted very little, especially in the calculations of the EGR cases because of the Saturated Stoichiometric Products, SSP, of the initial EGR composition such as CO_2 and H_2O. Hence definition of the local ER is critical.

4.1.3 Definition of the Local (Chemical) Fuel/Air Equivalence Ratio

One of the main problems in developing ϕ-T dynamic map technique is to calculate fuel/air ratio at all conditions, .i.e., after the evaporation of the main fuel, $C_{14}H_{28}$, into its constituent components C_7H_{16} and C_7H_8 (see pyrolysis reaction (3.96)). Because of the DOS model's structure, the fuel will disappear by the decomposition reaction (3.96) after a certain time. Hence, conventional fuel to oxygen equivalence ratio, ϕ_{conv}, cannot be valid to define fuel/air equivalence ratio when fuel disappears.

$$\phi_{conv} = \frac{(f/o)}{(f/o)_{stoich.}} \ , \tag{4.1}$$

where $(f/o)_{stoich.}$ is the fuel/oxygen mass ratio at the stoichiometric condition. Equation (4.1) is applicable to hydrocarbon-air mixtures before reactions have begun. However, when dynamic maps are constructed, the initial mixture composition is each time represented by reactants and combustion products taken from the previous stages as mentioned in section 4.1.2 above. When main fuel disappears, Equation (4.1) is not applicable anymore. For this reason, the chemical equivalence ratio, ϕ_{chem}, based on element oxidation states was used to calculate the equivalence ratio (see equation (4.2)). Both definitions ϕ_{conv} and ϕ_{chem} are identical for the stoichiometric condition and for the initial mixture consisting of only fuel and oxygen elements [132].

Chemical equivalence ratio is defined as,

$$\phi_{chem} = \left[\frac{\sum_{i=1}^{NLM} V_i^{+} b_i}{\sum_{i=1}^{NLM} V_i^{-} b_i} \right] \tag{4.2}$$

and b_i,

$$b_i = \sum_{j=1}^{NS} a_{ij} n_j \quad (i = 1,..., NLM;\ j = 1,..., NS) \tag{4.3}$$

where,

V_i^+ and V_i^- : positive and negative oxidation states of the *i*-th element in the species representing combustion of HCs. At least one of these states must be zero,

NLM : number of elements,

NS : number of species,

a_{ij} : number of kg-atoms of element per kg-mole of species j,

n_j : kg-mole number of species j in the mixture, $(\text{kg-mole})_j$ / kg.

One can apply this equation considering DOS fuel global oxidation reaction.

$$C_{14}H_{28} + 21O_2 \rightarrow 14CO_2 + 14H_2O \tag{4.4}$$

For this reaction, the oxidation numbers of elements are given Table 4.2.

Table 4.2 Oxidation numbers of elements representing combustion of DOS

Element	***i***	$\mathbf{V_i^+}$	$\mathbf{V_i^-}$
Carbon, C	1	4	0
Hydrogen, H	2	1	0
Oxygen, O	3	0	2
Nitrogen, N	4	0	0

And also numbers of kg-atoms of elements per kg-mole of species j are summarized in Table 4.3 below considering equation (4.4).

Table 4.3 Number of kg -atoms of element *i* per kg-mole of species *j*, a_{ij}

	$\mathbf{a_{ij}}$		**elements**			
			C	**H**	**O**	**N**
		j i >	1	2	3	4
species	$\mathbf{C_{14}H_{28}}$	1	14	28	0	0
	$\mathbf{O_2}$	2	0	0	2	0
	$\mathbf{N_2}$	3	0	0	0	2

Assuming mole numbers of species as; $n_1 = n_{C_{14}H_{28}} = n_{fu}$, $n_2 = n_{O_2} = n_{ox}$, $n_3 = n_{N_2} = n_{SSP}$ for fuel, oxidizer and zero valency species respectively, one can apply the chemical fuel/air ratio equation which is given by the equations (4.2) and (4.3).

$$\phi_{chem} = \frac{\begin{array}{l} V_1^+\left(a_{11}n_1 + a_{12}n_2 + a_{13}n_3\right) + V_2^+\left(a_{21}n_1 + a_{22}n_2 + a_{23}n_3\right) \\ + V_3^+\left(a_{31}n_1 + a_{32}n_2 + a_{33}n_3\right) + V_4^+\left(a_{41}n_1 + a_{42}n_2 + a_{43}n_3\right) \end{array}}{\begin{array}{l} V_1^-\left(a_{11}n_1 + a_{12}n_2 + a_{13}n_3\right) + V_2^-\left(a_{21}n_1 + a_{22}n_2 + a_{23}n_3\right) \\ + V_3^-\left(a_{31}n_1 + a_{32}n_2 + a_{33}n_3\right) + V_4^-\left(a_{41}n_1 + a_{42}n_2 + a_{43}n_3\right) \end{array}}$$

$$= \frac{\begin{array}{l} 4\left(14n_{fu} + 0n_{ox} + 0n_{SSP}\right) + 1\left(28n_{fu} + 0n_{ox} + 0n_{SSP}\right) \\ + 0\left(0n_{fu} + 2n_{ox} + 0n_{SSP}\right) + 0\left(0n_{fu} + 0n_{ox} + 2n_{SSP}\right) \end{array}}{\begin{array}{l} 0\left(14n_{fu} + 0n_{ox} + 0n_{SSP}\right) + 0\left(28n_{fu} + 0n_{ox} + 0n_{SSP}\right) \\ + 2\left(0n_{fu} + 2n_{ox} + 0n_{SSP}\right) + 0\left(0n_{fu} + 0n_{ox} + 2n_{SSP}\right) \end{array}} \qquad (4.5)$$

$$= \frac{14n_{fu} + 28n_{fu}}{4n_{ox}} = 21\frac{n_{fu}}{n_{ox}},$$

When ϕ_{chem}=1 then,

$$\left(\frac{n_{fu}}{n_{ox}}\right)_{stoich} = \frac{1}{21} \ . \qquad (4.6)$$

Note that same result will be obtained for reaction (4.4) with the conventional fuel/air ratio, ϕ_{conv}, definition. So, it is proven that ϕ_{conv} and ϕ_{chem} are identical for the stoichiometric condition.

However, in contrast to ϕ_{conv}, ϕ_{chem} holds the initial mixture stoichiometry true in the course of all stages of combustion, i.e. $d(\phi_{chem})/dt = 0$, and product concentrations are used to calculate the chemical ER. This facilitates the ϕ-T dynamic map construction. Before the map construction, each species in the mixture composition must be classified as a fuel, an oxidizer and species with zero valency, so called SSPs, Saturated Stoichiometric Products, [133]. The effect of the SSP species in the initial composition on the chemical equivalence ratio must be avoided, e.g., for initial mixtures with EGR components such as CO_2 and H_2O.

4.1.4 Uses of the ϕ-T dynamic map technique

In conclusion, we can classify the uses of the ϕ-T dynamic map technique in three main titles:

It helps understanding how the formation of species are affected from various parameters such as ϕ, T, P, elapsed reaction time and initial conditions of the mixture. Looking at the map, one can see the regions which favor high emissions and/or low efficiency. Hence, the results of this map technique can help to decide on a combustion regime, a suitable ϕ-T route, with low emissions and high efficiency.

It is possible to obtain the maps of different chemical species characterizing, for example, the formation of soot precursors, e.g. acetylene, C_2H_2, and products of non-complete combustion such as CO.

It is possible to express the spatially complex 3D-CFD results of the species into relatively simple planar 2D distributions, map, and to group the conditions (ϕ, T...) according to their contributions to the formation of the species. This can give a different tool to the one who should comment and decide on emission formation and efficiency behavior of any combustion process.

One can reduce 3D-CFD calculations to a simplified form by eliminating detailed chemical calculations part and use this simplified CFD calculation results in ϕ-T dynamic map simulations with detailed chemical kinetic calculations for the formation of the species. By this way it can be possible to make detailed chemistry calculations after and independent from the 3D-CFD simulations. This gives an opportunity to use a wide range of 3D-CFD simulations, no matter how powerful and accurate their detailed chemistry part and eliminates their well known restrictions (i.e., long calculation times) which constrain their selection and use.

5 CFD MODELING OF INTERNAL COMBUSTION ENGINES WITH KIVA-3VR2 CODE

The engine combustion process is exceedingly complex. It occurs in a 3D time-varying turbulent flow, concerning a fuel which is a blend of hundreds of different organic compounds whose combustion chemistry is poorly understood and takes place in a space, combustion chamber, whose shape varies with time and whose walls directly influence the process [134]. Without doubt, our present knowledge level is still far away from describing these processes exactly.

Before the details, it will be useful to remember those general descriptions about ICE modeling which was previously discussed by Heywood [134]. According to Heywood, modeling activities can contribute to engine developments in three general areas.

1. The development of a more complete understanding of the important physical processes that emerges from the requirements of formulating the model.
2. The identification of key controlling variables which provide guidelines for more rational and therefore less costly experimental programs, and for data reduction.
3. The ability to predict behavior over a wide range of design and operating variables which can be used to screen concepts prior to major hardware programs, to determine the trends and trade-offs, and if the model is sufficiently accurate, to optimize design and control.

Today it is possible to say that modeling activities can make contribution mostly to the first and second fields and lesser to the third field. A current example is HCCI combustion where combustion modeling is wholly used and revolutionized overall HCCI research plan in industry [55].

For diesel engine, the target is to meet future environmental legislations where both soot and NO_x emissions must be reduced drastically. Although developing and testing a new diesel engine has been, and still is, done by experiments, which is a

time consuming and expensive task, the role and contribution of combustion modeling increases. Experimental research is reliable but it offers little feedback (in terms of what can be improved and how to improve it) as the engine essentially is a black box, e.g., important process inside the engine is not well known. By using CFD in conjunction with experiments it is possible to drastically reduce the time and cost of the engine development procedure. Even though CFD is still not reliable enough to be trusted exclusively, its value cannot be argued. Reliable CFD models are, therefore, the key to better and more predictive computations [61].

5.1 Brief Description of KIVA-3VR2 Code

5.1.1 Background

The KIVA-3VR2 [135] computer code, developed by Amsden from the previous versions KIVA [136], KIVA-II [137], KIVA-3 [138] and KIVA-3V [41], has been selected for the reason that the code source is available, thus, representing an ideal platform for model modification, validation and evaluation.

The in-cylinder dynamics of advanced ICEs such as the DI diesel engine, involve a number of complex, closely coupled physical and chemical processes. These include the transient 3D dynamics of evaporating fuel sprays interacting with flowing multi-component gases undergoing mixing; ignition; chemical reactions, and heat transfer. The KIVA-3VR2 code has the ability to calculate such flows in engine cylinders, solving the conservation equations for evaporating fuel sprays coupled with the 3D turbulent fluid dynamics of compressible, multicomponent, reactive gases in engine cylinders with arbitrary shaped piston geometries, including the effects of turbulence and wall heat transfer [139]. The gas-phase solution procedure is based on a finite volume method called the arbitrary lagrangian-eulerian, ALE, method. The code treats differently “fast” chemical reactions, which are assumed to be in equilibrium, and “slow” reactions proceeding kinetically, albeit the general tri-molecular processes with different third bodies are not incorporated in the mechanism. The turbulent combustion is realized in a form of the classic Magnussen-Hjertager model not accounting for self-ignition and chemistry/turbulence interaction [140]. This is why the chemical routines in the original code were replaced with specialized models. The code fuel library has been also updated using property data compiled in

[141]. All these measures extend the capabilities of the KIVA-3VR2 to predict spray combustion of real HC fuels with the particulate emission [111].

5.1.2 The Governing Equations

Equations of motion for both the Eulerian and Langrangian representation of gas and liquid phase are based on the conservation laws of physics. These fundamental physical principles simply states that mass, momentum and energy are conserved during the fluid motion [142]. The equations of motion for the fluid phase are given below. Vector and tensor quantities are written with bold symbols. The unit vectors in the x-, y- and z-directions are denoted by **i**, **j** and **k** respectively. The position vector **x** is defined by,

$$\mathbf{x} = x\mathbf{i} + y\mathbf{j} + z\mathbf{k} \ , \tag{5.1}$$

the vector operator ∇ is given by,

$$\nabla = \mathbf{i}\frac{\partial}{\partial x} + \mathbf{j}\frac{\partial}{\partial y} + \mathbf{k}\frac{\partial}{\partial z} \ , \tag{5.2}$$

and the fluid velocity vector **u** is given by,

$$\mathbf{u} = u(x, y, z, t)\mathbf{i} + v(x, y, z, t)\mathbf{j} + \mathrm{w}(x, y, z, t)\mathbf{k} \ . \tag{5.3}$$

5.1.2.1 The Continuity Equation (Conservation of Mass)

The continuity equation, or rather species transport equation, for one component (species *m*) in a multi component mixture is written as [137];

$$\frac{\partial \rho_m}{\partial t} + \nabla \cdot (\rho_m \mathbf{u}) = \nabla \cdot \left[\rho D \nabla \left(\frac{\rho_m}{\rho} \right) \right] + f_m + \dot{\rho}_m^s \delta_{m1} \ , \tag{5.4}$$

ρ_m : mass density of species *m*

ρ : total gaseous mass density

u : gas velocity

D : mass diffusion coefficient including turbulent diffusivity where all species diffuse equally (modeled using Ficks law of binary diffusion with a single diffusion coefficient)

f_m : creation or consumption of a species due to chemistry (PaSR model)

$\dot{\rho}_m^s$: source term due to the evaporation of liquid fuel spray causing the addition of species *m* to the gas phase (note that single component fuel is used and by convention the fuel is set to species 1)

δ_{m1} : Dirac delta function (since single component fuels were generally chosen for modeling, *j* is 1, in general case it is δij)

Global continuity equation with the sum of Equation (5.4) over all species,

$$\frac{\partial \rho}{\partial t} + \nabla \cdot (\mathbf{u}\rho) = \dot{\rho}^s \quad . \tag{5.5}$$

The equation for the liquid evaporation rate, $\dot{\rho}^s$, is given by the relation,

$$\sum_V N_p \dot{m}_d = \int_V \dot{\rho}_s dV = -V\dot{\rho}_s \tag{5.6}$$

where,

V : volume of the cell

N_p : statistical number of liquid droplets in the parcel

$\dot{m}_d$: evaporation rate of a single droplet.

The left hand side, LHS, sum of Equation (5.6) is the sum over the all spray parcels in the cell volume.

5.1.2.2 The Momentum Equation (Newton's Second Law)

The averaged momentum equation for the gas mixture is modified to account for the phenomena associated with spray modeling. This is done through the term $\mathbf{F^s}$, in momentum equation, which describes the rate of momentum gain, delivered to the gas phase by the spray droplet drag and gravity forces [72]. So, momentum equation becomes [137],

$$\frac{\partial(\rho \mathbf{u})}{\partial t} + \nabla \cdot (\rho \mathbf{u}\mathbf{u}) = -\nabla p + \nabla \boldsymbol{\sigma} + \mathbf{F^s} + \rho \mathbf{g} - \cdot \nabla \left(\frac{2}{3} \rho k \right) , \tag{5.7}$$

where,

p : gas pressure

$\boldsymbol{\sigma}$: viscous stress tensor (defined below)

$\mathbf{F^s}$: rate of momentum gain/loss per unit volume due to the spray

$\mathbf{g}$: specific body force, which is assumed to be constant

k : turbulent kinetic energy ($=1/2\sqrt{\mathbf{u}' \cdot \mathbf{u}'}$)

The viscous stress tensor is in Newtonian form,

$$\boldsymbol{\sigma} = 2\mu \mathbf{S} + \beta \nabla \mathbf{u} \mathbf{I} \tag{5.8}$$

$$\mathbf{S} = \frac{1}{2}\left[\nabla \mathbf{u} + (\nabla \mathbf{u})^T\right] \tag{5.9}$$

and,

μ : first coefficient of viscosity

β : second coefficient of viscosity (β = -2/3μ) [137]

S : mean strain rate tensor,

I : unit dyadic, simply 3x3 identity matrix

In a turbulence model, equation (5.7) governs the averaged momentum and is based on the separation of a mean ($\mathbf{u}$) and fluctuating ($\mathbf{u}'$) velocity contribution to the actual velocity ($\mathbf{U} = \mathbf{u} + \mathbf{u}'$) in a point in time and space. This is called Reynolds decomposition and it necessitates the use of a turbulence model, as it introduces additional unknowns (Reynolds stresses: $\rho \mathbf{u}_i' \mathbf{u}_j'$) into the system of equations so that it contains more unknowns than independent equations. Thus, turbulence models, i.e. k-ε model, are required to close the system [72].

5.1.2.3 The Energy Equation (First Law of Thermodynamics)

The internal energy equation [137, 136],

$$\frac{\partial(\rho e)}{\partial t} + \nabla \cdot (\rho \mathbf{u} e) = -p \nabla \mathbf{u} - \nabla \mathbf{J} + \rho \varepsilon + Q^c + Q^s \tag{5.10}$$

where,

e : specific internal energy (excluding chemical energy)

J : heat flux vector which is the sum of contributions due to heat conduction and enthalpy diffusion

$$\mathbf{J} = -\kappa_{hc} \nabla T - \rho D \sum_m h_m \nabla \left(\frac{\rho_m}{\rho} \right) \tag{5.11}$$

The first term of the right hand side, RHS, of the equation (5.11) is the heat conduction where,

κ_{hc} : coefficient of the heat conduction

T : gas temperature.

The second term of the RHS of the equation (5.11) is the diffusion of specific enthalpy h_m of species m. The last two terms of equation (5.10), $\dot{Q}^c$ and $\dot{Q}^s$, are the source terms related to chemical heat release and spray/gas-phase interaction,

respectively. The chemical heat release depends on the chemical kinetics and takes the form [72],

$$\dot{Q}^c = \sum_{r=1}^{NR} q_r \dot{\omega}_r \tag{5.12}$$

where, $\dot{\omega}_r$ is the reaction rate and q_r is the heat of reaction r at the reference temperature. The heat of reaction is

$$q_r = \left(\sum_{s=1}^{NS} (v^{'} - v^{"})(h_s)_f^{ref} \right) \tag{5.13}$$

where,

NR : number of reactions

NS : number of species in reaction r

$(h_s)_f^{ref}$: heat of formation of the species s at the reference temperature

5.1.3 KIVA-3VR2 File Structure

The KIVA-3VR2 computer program consists of a set of subroutines controlled by a short main program. Detailed information about the general structure can be found in [136]. Basically the code is formed in three different groups; pre-processor, main-code and post-processor, respectively. It is possible to use different codes for pre-processor and post-processor stages. Pre-processor is responsible for generating mesh of the problem and although it is not flexible and not easy to use, one can get satisfactory results generating structured relatively simple meshes by using the pre-processor k3prep. There are also other mesh generators which can be used to generate KIVA-3VR2 compatible meshes, i.e., ICEM-CFD™ (trademark used by ANSYS, Inc. under license) [143]. In this study, mostly k3prep is used to generate meshes. For post-processing it is more convenient to use a post-processor other than KIVA-3VR2 post-processor, k3post. General Mesh Viewer, GMV [144] (used in this study), is one of the free software for general post processing. Figure 5.1 shows file structure of standard version of KIVA-3VR2. Thin arrows represent passing between pre-, main- and post phases.

Standard KIVA-3VR2 file structure with GMV

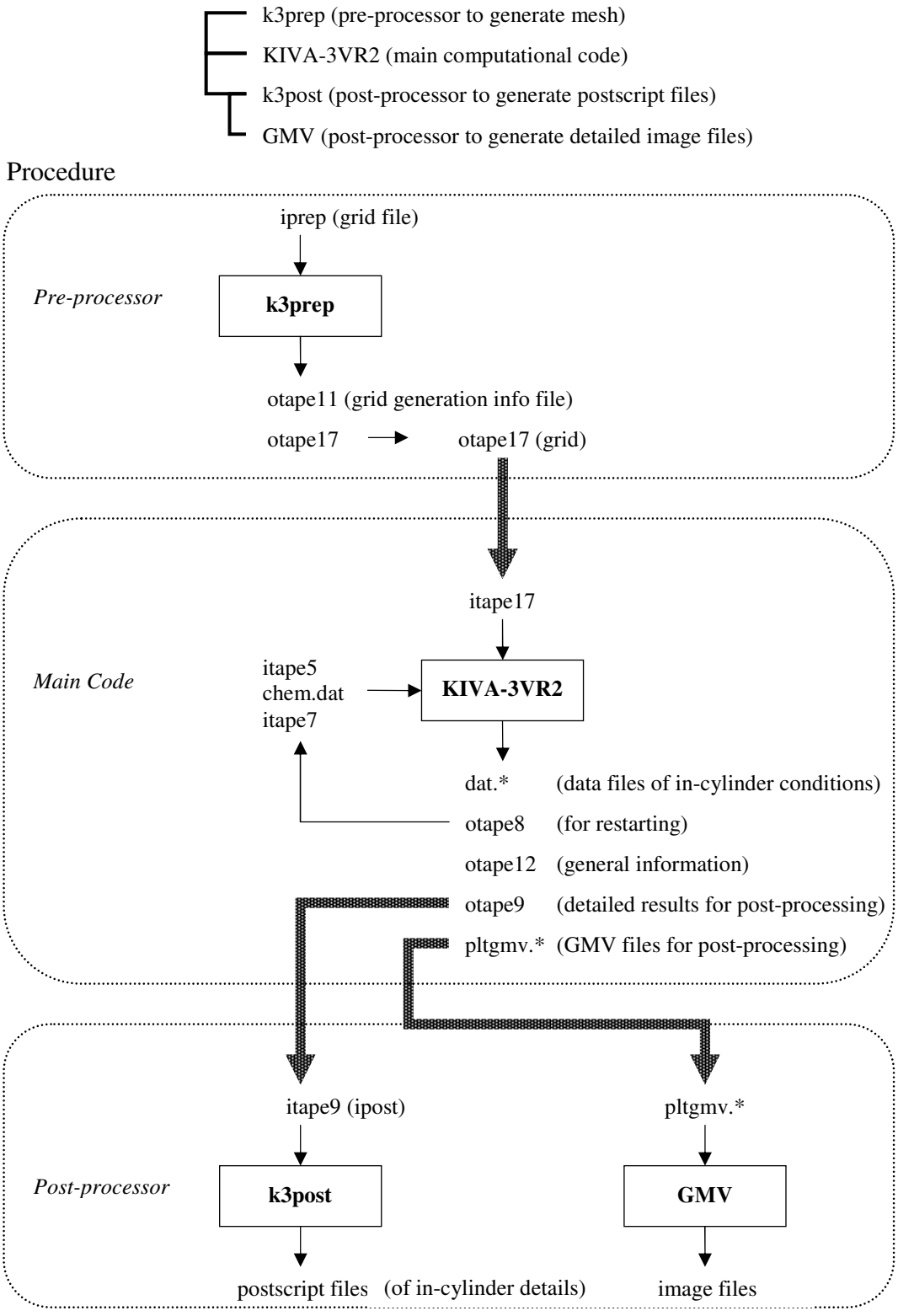

Figure 5.1 Standard KIVA-3VR2 code file structure with added GMV post-processing

A fresh simulation work starts with creating the mesh. Specially prepared iprep file is processed by k3prep and two output files, otape11 and otape17, are produced. otape11 is an information file about mesh generation process, and otape17 is the result grid file. otape17 must be renamed as itape17 for KIVA-3VR2.

Additionally itape5, which describes simulation conditions and chem.dat, which includes reaction mechanism data are needed for the simulation.

dat.* files are properly organized specific output files such as emissions, injection data, pressure-temperature data, etc… otape12 is general output file which includes all information (except mesh data) of the simulation. If the nctap8 parameter in itape5 file is set to a certain cycle value before starting a simulation, then the simulation produces a restart file, otape8, when it reaches to this designated cycle. If the simulation continues, for each nctap8 cycle a new restart file is produced replacing with the former one (i.e. if nctap8 = 800, then first restart file will be produced at 800^{th} cycle and at 1600^{th}, 2400^{th},… cycles new restart files will be generated replacing the previous ones). If the simulation stops, with any reason, after this restart file, otape8, is produced then one can restart the simulation from this cycle by setting irest parameter to 1 in itape5 file. Note that otape8 must be renamed as itape7 to restart a simulation. pltgmv.* files are the special mesh files which are produced for GMV. In this study GMV is used for post-processing task. Also otape9 file is the most detailed standard output data file which can be processed by k3post.

5.2 The Grid Generation for Diesel Engines

KIVA-3VR2 formulation is based on (x, y, z) Cartesian coordinates, which is applicable to cylindrical or planar calculations in either two or three space dimensions, as it is in previous versions of the code [137]. But rather than being confined to one logical block of cells in (i, j, k) space to encompass the entire region to be modeled, now, the KIVA-3VR2 mesh is composed of any arbitrary number of logical blocks that are patched together in a completely seamless fashion [138]. The number of cells in (x, y, z) directions are NX, NY, NZ, respectively.

The mesh generation logic allows the computational region to include cupped pistons and domed cylinder heads and to offset these relative to the axis of the cylinder. In addition to two- and three-dimensional Cartesian and cylindrical meshes, the code

allows the calculation of the flow in a single "sector" of certain 3D cylindrical configurations in which there is an n-fold symmetry about the axis of the cylinder. This symmetry is often found in engine cylinders with multihole injectors. For initial conditions, one can specify an axisymmetric swirl-velocity field with a Bessel function profile and a specified swirl ratio. Standard boundary conditions and rezone logic allow the mesh to follow the motion of a piston.

KIVA-3VR2 [135] can model any number of valves in the cylinder head. Each valve can have its own size and profile, and its own lift history. The valves may be vertical, with the valve axis parallel to the cylinder axis, or canted at some angle with respect to the cylinder axis. In logical space, valves can move only in a bottom-top direction.

If one is not so experienced, it is not easy to generate an optimum mesh, with k3prep, which can decrease the calculation time (increase calculation speed) because the number of cells and their dimensions, especially in the piston bowl region, are manually specified. It is not easy to find the best cell arrangement manually. A comparison is also made in order to see the difference between k3prep and ICEM-CFD^{TM} generated meshes and it is experienced that ICEM-CFD^{TM} mesh is 4-5 times faster than k3prep mesh. One can see Imren et al.'s study [145] for ICEM-CFD^{TM} application. Anyway, k3prep pre-processor is used for grid generation in this study.

Initial simulations were at first performed on a 360° full mesh (Figure 5.2a) covering the space occupied by six sprays of the six-hole injector of the Volvo D12C engine and then, compared with a 60° sector mesh (Figure 5.2b) for the one spray.

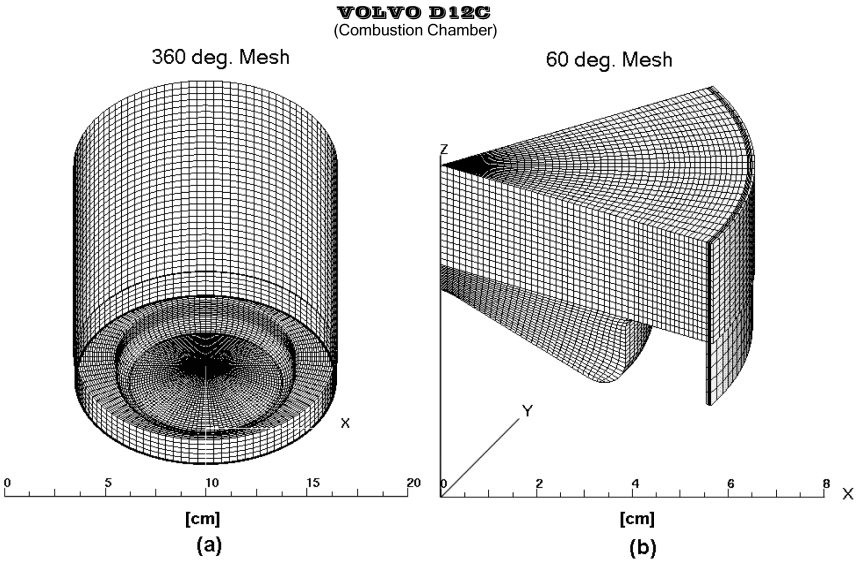

Figure 5.2 Volvo D12c engine a) 360° full and b) 60° sector meshes

According to a previous detailed investigation which was made by Edman and Golovitchev for the full and sector grid comparison [146]:

- poor grid resolution enhances the sector and full mesh difference,
- reasonable azimuthal resolution (in Y-direction) in engine combustion simulation were investigated and set to 2.4° per cell (2° gives better result),
- mean combustion temperature increases for the full 360 grid relative to the sector grid, especially for the bad azimuthal grid resolution cases.

The 360 deg. full mesh is composed from 272,899 hexagonal cells collected in six blocks, bowl (NX=32, NY=100, NZ=20), squish (NX=53, NY=100, NZ=34) and in crevices regions (see Figure 5.3). The 60 deg. sector mesh was made up by 82,912 cells partitioned as in the 360 deg mesh.

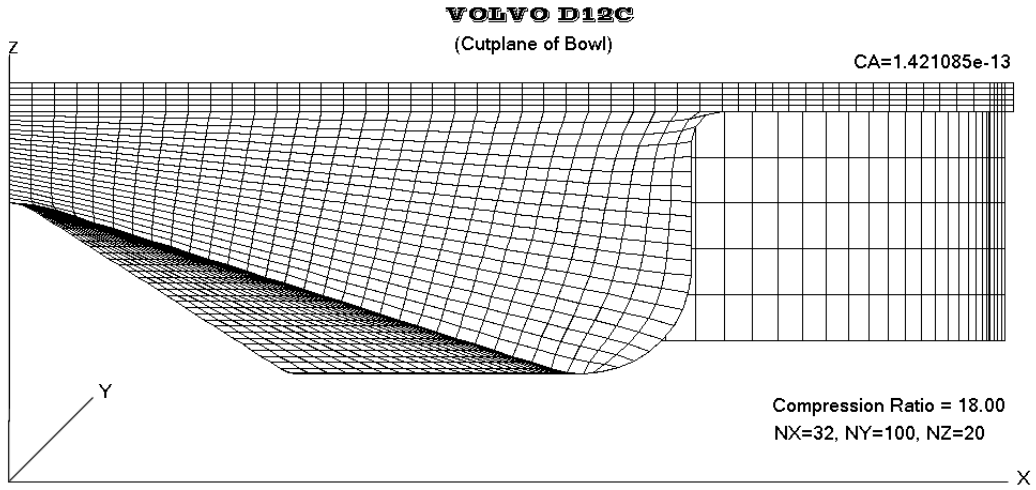

Figure 5.3 Bowl cutplane view of the Volvo D12C mesh at TDC

Because the simulation results of both full and sector mesh are in a reasonable agreement, sector mesh is used in the simulations in order to decrease the calculation time. Both meshes are generated by k3prep and they account for the crevice volumes. Considering the experimental engine data, fine tuning of CR is realized by changing the crevice volume (see the circumferential thin flange in Figure 5.2) while the TDC squish clearance is kept constant and same with the real engine (0.185 mm). Figure 5.3 shows the cutplane of the bowl for the one of the meshes used in the study. Considering intake valve closing, IVC, and exhaust valve opening, EVO, as simulation range, approximate simulation durations vary between 20-30 hours with this grid resolution.

5.3 Spray Models of Diesel Spray Combustion

There is no doubt that fuel injection; hence, spray modeling is the most important event in the DI diesel engine combustion and its modeling because nearly all processes in the engine start with the introduction of the fuel into the combustion chamber and develops according to the ongoing spray injection phenomenon. These processes are extremely complex and so involved that, most often, fuel injection continues after the start of combustion and in addition to the spray/mixture interaction, also spray/flame interaction occurs and brings additional unknowns of combustion process. The timing of the injection, the mass injected and the rate of injection all together control engine characteristics such as the combustion mode, heat release, HR, engine efficiency and, not least, pollutant formation. Aside these variables, other factors; nozzle geometry (i.e. spray direction, orifice size and shape etc.) and ambient conditions (injection and cylinder pressure, temperature, etc.) affect the spray. So, all these complex and dynamic system of variables determine the behavior of the spray [72]. For those regions, tuning of the spray models is particularly important and critical and properly tuned spray models will be very useful and will enhance the reliability of the whole diesel spray combustion simulation [39, 72]. Before describing the used spray models, it is better to look at the appearance of diesel spray combustion under the supervision of the current knowledge level.

5.3.1 Dec's Conceptual Model of Diesel Combustion

Instead of the previously accepted diesel spray combustion models, in the lack of laser-based imaging diagnostics, a reliable conceptual model of diesel combustion was eventually developed by Dec and colleagues at Sandia/Livermore [147] on the basis of complex, multiple laser in-cylinder diagnostics [55]. They traced some reacting intermediate species such as OH, CH, NO and PAHs which are the important process markers of combustion. This improved the understanding of diesel spray auto-ignition, flame propagation and emission (soot and NO_x) formation [148]. Later, this conceptual model was analyzed with proven chemical kinetic models and it was expressed the two-stage nature of diesel combustion [37]. Figure 5.4 shows a generalized schematic view of Dec's spray model.

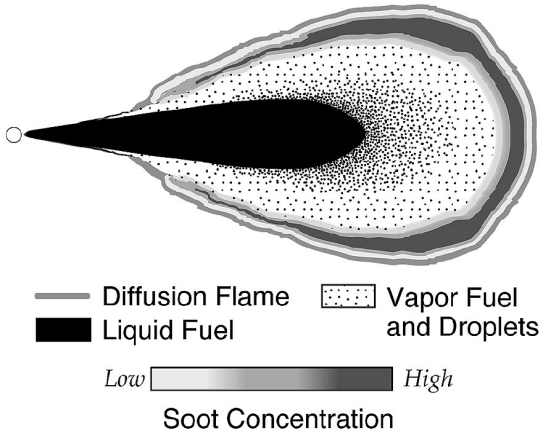

Figure 5.4 Schematic view of Dec's spray model [37]

In this conceptual model, the overall diesel process is described as a cold fuel spray entraining hot ambient air and supplying hydrocarbon fragments to a lifted diffusion combustion flame [148]. In real diesel spray, the flame front stabilizes at a certain location significantly downstream of the fuel injection region and the distance from the injector tip to the flame visible location is referred to the flame lift-off. The lift-off length is dependent on the injector parameters and undergoes considerable fluctuations as a result of coupling between the atomization/evaporation processes. Due to the fact that complex hydrocarbon fuels have shortest auto-ignition delays for substantially rich mixtures, the diesel spray flame stabilization occurs not along the stoichiometric mixture surface, but in a rich, distributed reaction zone located in the central region of the spray. The structure of the reaction zone close to the lift-off location can include either branches of a triple flame as reported in Chomiak and Karlsson [149] or a single pulsating rich premixed flame as hypothesized by Dec in his conceptual model. Since many of the details of flame stabilization are not well established yet, the evaluation of the flame lift-off role in spray combustion development and emission formation processes is of significant practical importance for Diesel engine [150]. Here, the injected liquid fuel jet breaks up to form a cloud of fuel droplets that subsequently vaporizes. For the quasi-steady period of diesel combustion depicted, the central part of the jet was generally thought to consist mainly of fuel as either droplets or vapor. Combustion was thought to occur as a diffusion flame where this fuel met the air at the jet periphery. Since soot formation requires combustion heating to pyrolyze the fuel, soot production would occur in a shell-like region on the fuel-rich side of the diffusion flame, see Figure 5.4 [37].

Figure 5.5 shows a sequence of idealized schematics of the early stages of the diesel combustion event, begins shortly after the start of fuel injection, ASI, and continues through the premixed burn and into the start of quasi-steady combustion. Shortly after combustion begins, the reacting diesel fuel jet enters a "quasi-steady" phase in which the general features of the jet are preserved, although it continues to grow penetrating across the chamber. For Figure 5.5, quasi-steady conditions are established 8-10 CAD after the start of injection [37].

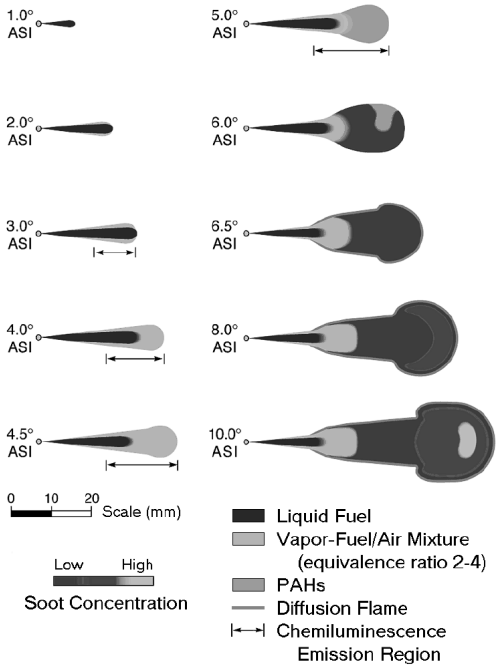

Figure 5.5 Schematics of early flame images from laser measurements [37]

And finally, Figure 5.6 presents the schematic view of the quasi-steady phase of diesel combustion. In addition to the features determined from laser sheet imaging, this schematics shows some hypothesized features:

First, as liquid fuel leaves the nozzle and travels down the jet, it rapidly entrains hot in-cylinder air, which initiates fuel vaporization. This leads to the formation of a sheath of fuel-vapor/air mixture in the shear layer along the sides of the jet.

Next, the initial part of the fuel oxidation process takes place as the fuel-vapor/air enters the jet and the final oxidation process takes place around the periphery of the jet. This two-stage nature of fuel oxidation is a key concept presented in Figure 5.6.

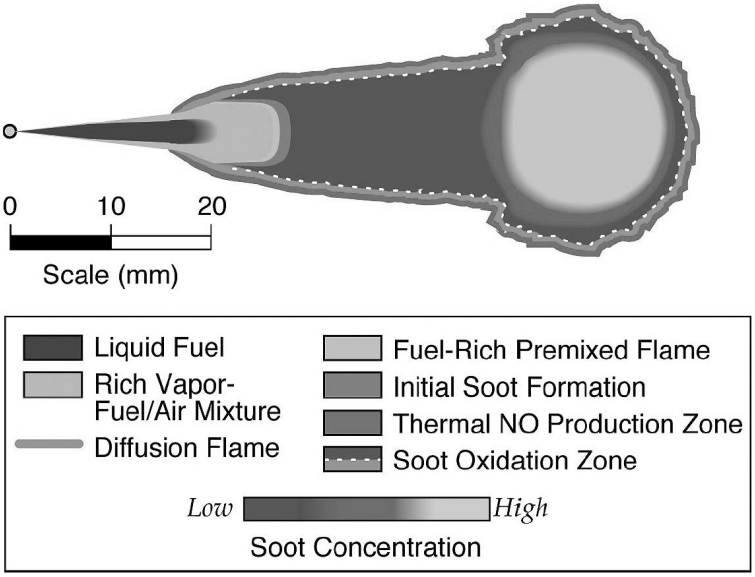

Figure 5.6 Schematic of quasi-steady structure of diesel spray combustion zone according to the conceptual model proposed by Dec [147] and reprinted version by Tao [151]

One of the surprising aspects of this new image was the limited penetration of fuel droplets in the combustion chamber. This conceptual schematic figure provides a spatial definition of liquid disappearance and zones where reactions occur in the fuel-vapor/air mixture [37]. Contrary to classical spray models, in which soot is assumed to be formed along the stoichiometric surface on the rich side of diffusion flame, Dec's conceptual model locates the soot cloud formation downstream of the fuel jet, prior to the main combustion zone [148]. The difference between the earlier theoretical predictions and Dec's experimental observation reveals a weak point of classical diesel combustion models. After this introduction about the diesel combustion spray, below it is given the modeling approach of the problem.

5.3.2 Spray Modeling

The Diesel spray creates a highly turbulent field with very strong gradients. The diameter of the liquid spray is on the order of 0.1 mm and the liquid velocity around 200-600 m/s [61]. In general, injection pressures can vary around 300-2000 bar and combustion chamber pressure and temperature at TDC is about 50 bar and 800-900 K respectively for DI diesel combustion. Note that these values can vary greatly, even out of these ranges, in accordance to operating conditions. The aim of spray modeling is to imitate the fuel introduction into the combustion chamber as close as possible to the real engine. Gaseous components for combustion are delivered into the cylinder in accordance with what happens in a real engine [72].

Since the fuel enters the computational domain in liquid form, models are needed to convert liquid into the vapor phase. In the numerical treatment, the entry of the spray is treated in a straightforward manner. Droplet is introduced at only one point in space, with a set direction, speed, size etc. The main reasons of this simplification are the lack of enough computational power and physical principals which describe the spray modeling. Considering Eulerian or Lagrangian numerical methods, in Eulerian way, nozzle must be resolved and because of the large difference in scale between the injector orifice and the bore of the cylinder, and limitations in computer power, the computational time using this approach is much longer and often too long for practical purposes. On the contrary, in Lagrangian way, nozzle region is not required to be fully resolved by the computational mesh. The spray is represented by points, often referred to as parcels or droplets. These points are then assigned properties which may be as many as desired (i.e., location, velocity, diameter, mass, temperature and fuel composition). Since these points are of zero dimension and do not occupy any space in the domain, they only serve one purpose: To act as a marker. The Eulerian equations, for the gas phase modeling, need to know in which cell the liquid/gas exchange takes place, so that the interaction terms can be distributed in the correct position. These points are then tracked through the domain, in which they move from cell to cell, according to the implemented physics and distribute mass, momentum and energy. This, tracking of the fuel parcels in the computational domain, adds extra numerical complexity [61].

In conclusion, model equations for the known spray properties are constructed in the lagrangian framework and coupled to the Eularian phase through corresponding source terms. Traditionally, five basic models are incorporated into the CFD spray code;

- spray atomization
- droplet break-up (primary and secondary break-up)
- collision
- evaporation
- dispersion by turbulence

Before discussing those sub-processes given above, it should be mentioned that actually spray injection starts inside the injector nozzle hole which is not taken into

account in this study. So the effect of hydro grindings of this nozzle hole is a question. Experiments performed under realistic engine operating conditions, using real-size nozzles with different inlet hydro grindings, but the same momentum, revealed that despite the differences in internal turbulence and discharge coefficients due to cavitations, no major differences could be seen in the spray parameters, ignition delay, flame temperature and soot distribution between the two nozzles. It was concluded that the Diesel sprays are mainly controlled by its momentum, and the internal nozzle flow structure is only significant if it changes the jet momentum or distribution in time and space [152].

5.3.2.1 The Atomization Model

The spray atomization depends on the spray's interaction with the ambient gas, leading to the formation of ligaments close to a liquid core that further disintegrates into parent droplets [38], see Figure 5.7. As mentioned before, in the Lagrangian way, nozzle is not resolved; hence, the initial conditions for the spray parcels must be specified. This can be done by using either an atomization model or by specifying the initial size and spray angle as constants which can be seen as a very simple atomization model. The latter approach which is simpler, faster and more straightforward has been used in this study [61].

5.3.2.2 The Droplet Breakup (Hybrid KHRT) Model

In order to improve the accuracy of predictions, the original KIVA-3VR2 sub-models describing the fuel injection and mixture formation were modified. Instead of Taylor Analogy Breakup, TAB, model standard in KIVA-3VR2 code, Kelvin-Helmholtz Rayleigh-Taylor, KHRT, breakup model [153] coupled with the "blob" injection model was modified, validated and applied to the code. KHRT breakup model can be divided into two modes Kelvin-Helmholtz, KH (primary breakup), and Rayleigh-Taylor, RT (secondary breakup). The spray core is represented as a region close to the injector orifice with large droplets (blobs) to the size equal to the effective nozzle diameter (see Figure 5.7). When the liquid parcels, r_{p0}, have been injected they start to deform and breakup. If the Weber number is high enough ($We > 6.0$) it happens [61].

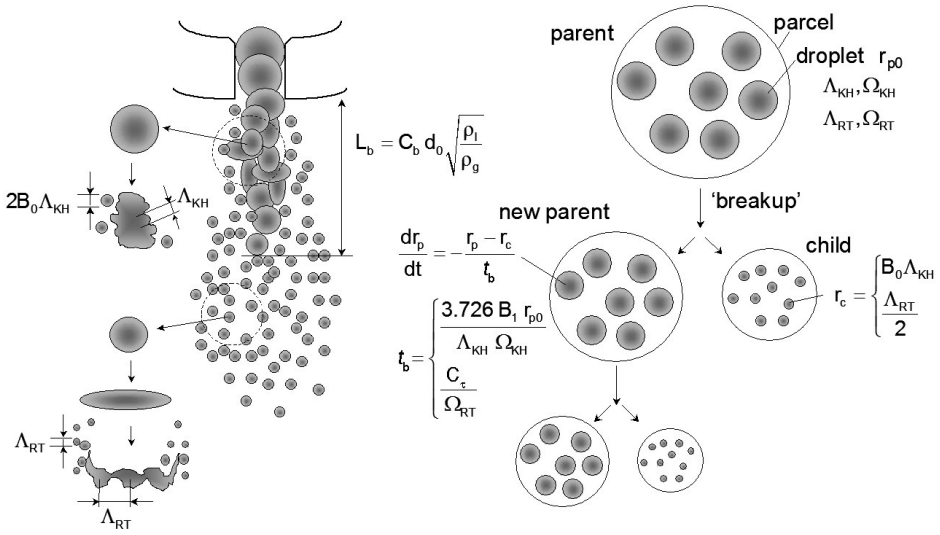

Figure 5.7 Spray Breakup: Hybrid Kelvin-Helmholtz Rayleigh-Taylor, KH-RT, Model [154]

Based on aerodynamic theory of instability wave growth, new droplets are formed from a parent droplet or a blob. KH instability is caused by the viscous forces due to the relative motion of the liquid and the ambient gas [128]. It is assumed that small droplets, r_c, are formed from the parent drops with a size proportional to the KH wavelength, Λ_{KH}. This can bee seen in Figure 5.7 where in KH breakup mode new child parcels, r_c, are stripped off from the larger sized parent parcels, r_p. The radius of the new droplets in the child parcel

$$r_c = B_0 \Lambda_{KH} \tag{5.14}$$

and the radius of the droplets, r_p, in parent parcel reduce according to the rate expression

$$\frac{dr_p}{dt} = -\frac{r_p - r_c}{t_b}, \quad t_b = \frac{3.726 B_1 D}{\Lambda_{KH}\Omega_{KH}} \tag{5.15}$$

where B_0=0.61, B_1=2.00 are model constants and Λ_{KH} is the wavelength of the fastest growing wave, Ω_{KH}, which are given below.

$$\Omega_{KH} = \frac{0.34 + 0.38 We^{1.5}}{(1+Oh)(1+1.4T^{0.6})} \sqrt{\frac{\sigma}{\rho_d (r_p)^3}} \tag{5.16}$$

$$\Lambda_{KH} = 9.02 r_p \frac{(1+0.45\sqrt{Oh})(1+0.4T^{0.7})}{(1+0.865 We^{1.67})^{0.6}} \tag{5.17}$$

In the (5.16) and (5.17) equations, the Weber number for the gas is defined as

$$\mathrm{We} = \frac{\rho \left|\mathbf{u}_{\mathrm{rel}}\right|^2 \mathrm{r_p}}{\sigma} \ , \tag{5.18}$$

the Ohnesorge number is defined as

$$\mathrm{Oh} = \frac{\sqrt{\mathrm{We}_l}}{\mathrm{Re}_l} \ , \tag{5.19}$$

and the Taylor number

$$\mathrm{T} = \frac{\mathrm{Oh}}{\sqrt{\mathrm{We}}} \ . \tag{5.20}$$

The liquid Weber number We_l is similar to We, only the gas density replaced by liquid density. The liquid Reynolds number is defined as

$$\mathrm{Re} = \frac{\rho_l \left|\mathbf{u}_{\mathrm{rel}}\right|^2 \mathrm{r_p}}{\mu_l} \ . \tag{5.21}$$

This KH break-up process which produces new parcel containing child droplets with the radius of $\mathrm{r_c}$ continues until the liquid mass removed from the parent droplet, $\rho_l 4/3\pi\left(r_{p0}^3 - r_p^3\right)$, reaches 1-3% of the parent parcel mass, and if the number of child droplets is greater than the number of parent droplets. While waiting for sufficient child droplets to accumulate, the parent droplet number, N, was adjusted so that $\mathrm{N} = \mathrm{N}_0 (\mathrm{r_{p0}}/\mathrm{r_p})^3$ where N_0 is the initial parent droplet number. The parent droplet number was restored following the formation of the new product parcel [128].

After primary atomization has been completed, a secondary stage, RT breakup mode, starts dependent on the parent droplet parameters (sizes, velocities, etc.). The RT mode works slightly in different way. RT instability is due to the inertia of the more dense fluid opposing mass acceleration in a direction normal to the dense fluid interface [128].The size of the child parcels,

$$\mathrm{r_c} = \frac{\Lambda_{\mathrm{RT}}}{2} \tag{5.22}$$

where,

$$\Lambda_{\mathrm{RT}} = \pi / \mathrm{K} \tag{5.23}$$

and

$$K = \sqrt{\frac{|g_t(\rho_l - \rho)|}{3\sigma}} \ , g_t = (\mathbf{g} + \frac{d\mathbf{u}_d}{dt}) \cdot \frac{\mathbf{u}_d}{|\mathbf{u}_d|} \tag{5.24}$$

If $\Lambda_{RT} < r_p$, it is assumed that RT waves have started to grow on the surface of the droplets. The life time of the growing RT waves is then tracked from then on, and when the life time exceeds the characteristic RT time, t_b

$$t_b = \frac{C_\tau}{\Omega_{RT}} \tag{5.25}$$

$$\Omega_{RT} = \sqrt{\frac{2}{\sqrt{27\sigma}} \frac{|g_t(\rho_l - \rho)|^{1.5}}{\rho_l + \rho}} \tag{5.26}$$

then catastrophic breakup occurs creating much smaller droplets. The secondary droplet break-up regimes that follow the primary atomization process are classified as bag, stripping or catastrophic, depending on the increasing value of the Weber number. In high-pressure diesel sprays, the droplets span a wide range of Weber numbers, so the contributions of all breakup mechanisms must be approximated in the modeling. After the RT breakup mode, no new drop parcels are created and droplet velocities are assumed to remain constant. However, the droplet number, N_{drop}, in a given parcel changes to $N_{drop} = N_{par}\left(r_{par} / \Lambda_{KH}\right)^3$ due to the change in the sizes of the parent and child droplets (N_{par} is the number of previous droplets) [128].

The hybrid KHRT model was realized in such a way that it only affects droplets beyond the breakup length, L_b, determined using the empirical correlation

$$L_b = C_b d_0 \sqrt{\frac{\rho_l}{\rho_g}} \ , \tag{5.27}$$

where,

C_b : fitting parameter (=12)

d_0 : the nozzle diameter

ρ_l, ρ_g : liquid and ambient gas mass density respectively [126]

Consequently, the liquid core is not influenced by the RT instability yielding a correct spray tip penetration length almost regardless of the grid used [128].

5.3.2.3 The Collision Model (Nordin)

Standard droplet collision model implemented in the KIVA-3VR2 code is inherently grid dependent due to the collision frequency depending on a computational cell size:

- collision occurs when only two parcels occupy the same computational cell
- probability for collision is higher than a threshold value based on collision frequency
- probability for collision does not take account, moving parcels' directions, e.g., parcels are moving towards or away from each other have the same collision probability [61]

Consequently, in the standard collision procedure, the probability P_n that a droplet undergoes n collisions with other droplets is calculated according to the Poisson distribution law, which parameter explicitly depends on the grid size. Because of these reasons the standard formulation by O'Rourke, integrated in the KIVA-II code is grid dependent [146]. Nordin [61] proposed a new formulation for the binary collision condition, in which, the droplet collision is impending if and only if the directional and geometric collision requirements are satisfied (see Figure 5.8):

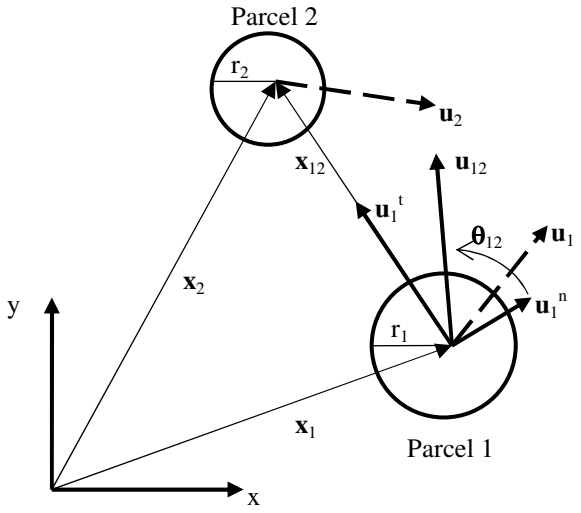

Figure 5.8 Two parcels traveling towards each other (source [61] and [72])

In order for two parcels such as in Figure 5.8 to collide they have to travel towards each other, which is formulated in (5.28) as

$$u_{12} > 0,\ u_{12} = (\mathbf{u}_1 - \mathbf{u}_2)\frac{\mathbf{x}_2 - \mathbf{x}_1}{|\mathbf{x}_2 - \mathbf{x}_1|}\ . \tag{5.28}$$

The second condition is that the parcel's relative displacement must be larger than the distance between them, which is formulated in (5.29) as

$$u_{12}\Delta t > \left|\mathbf{x}_2 - \mathbf{x}_1\right| - (r_1 + r_2) \ . \tag{5.29}$$

The modified droplet collision model, based on the geometrical conditions of a binary collision, accounts for two outcomes: droplet bouncing or coalescence. With this formulation of Nordin, grid dependence of the collision model is much more reduced compared with the original KIVA-3VR2 model formulation. The wall film model was modified, preventing droplets heating to a temperature higher than the critical temperature of the fuel. In order to improve the description of the droplet motion, the cell gas velocity interpolation is used when droplet/gas interaction is accounted for. This removes a computer artifact known as the "clover leaf" spray pattern [38]. One can see for further details, applications and grid dependence comparisons of this modified collision model of Nordin with others in Nordin's [61] and Edman's (Gustavsson) [146, 155] studies.

The heat transfer model is based on the wall/film function formalism, as in the original version of the KIVA-3VR2 code. Temperatures were assigned to the piston, the cylinder head, and the cylinder walls in accordance with experiments [38].

5.4 The Turbulence/Chemistry Interaction Model

Diesel spray combustion is one of the most difficult problems of applied macroscopic physics as it involves the most difficult problems of turbulence, chemistry and two phase flows. These are problems that are tightly coupled and highly non-linear, with time and length scales that are so small that it's questionable if they will ever be possible to resolve. The turbulence/chemistry interaction is very strong and it is therefore essential to have a reliable interaction model for this process if accurate predictions of emissions are to be performed [61]. For those reasons, modeling the diesel process requires a turbulence/chemistry interaction model that can cover full range from distributed slow chemical reactions to turbulence mixing controlled fast chemical reactions. Furthermore the model must be able to deal with both premixed and diffusion controlled combustion and the mixed case in partially premixed combustion as well as complex chemistry [156].

In terms of mathematics, the turbulence/chemistry interaction modeling deals with how the chemical source terms in the continuity equation (5.4) have been modeled. The modeling approach uses a special technique, in which a reference species is introduced to compute both the reaction rate and the characteristic chemical time. Because of the thinness and complex structure of the flame, present computer technology cannot resolve the flame structure, e.g., the computational cell size has to be several orders of magnitude larger than required. And since it is only possible to resolve variables, e.g., species concentrations, on a scale which is of the same order as the cell size, the conditions in the combustion zone are thus, in principle, unknown. And since the source term, f_m, in the continuity equation (5.4) is a function of the combustion zone parameters; it is dependent on variables, not on a grid level, but on a sub-grid level. Because of this, correlating the sub-grid conditions with grid level conditions is a necessity, since the grid level conditions are the only information available [61].

5.4.1.1 Background

With the introduction of the Eddy Break-Up model (EBU) by Magnussen and Hjertager in 1976, it became possible to treat turbulent diffusion combustion in a successful manner. Since then, the EBU model has become widespread and widely used in many CFD codes. The success of the model can mainly be attributed to two things, the simplicity of the model, plus, at the time, lack of other diffusion flame models. Since the introduction of the EBU model, other models have been derived, based on other principles, such as the probability density function (PDF) approach, the Lagrangian approach or the flamelet concept. There have also been extensions to the EBU concept. However, all of these approaches, except for the Lagrangian, have difficulties handling complex chemistry. One can see [61] for the main characteristics of these approaches. The standard EBU only uses one global reaction. Although it is possible to extend it for complex chemistry, it is not clear how to do this [61]. In this study, Partially Stirred Reactor (PaSR) concept by Karlsson [156] which is an extension of the EBU approach is used. It has proven to work very well for turbulent Diesel spray combustion and provides the first complex chemistry treatment of the problem [61]. Before expressing the main idea of the PaSR model, reference species technique which is used in PaSR concept is given below.

5.4.1.2 The Reference Species Technique

Solving a chemical system in a fully coupled fashion, when the number of reactions is of the order of about 100, is far too expensive. Hence, to treat a detailed mechanism, another approach has been developed in which the reaction set is solved sequentially, i.e., the reactions are accounted for one after another and the species are updated after each reaction and fed into the next reaction. Due to the stiffness of the system a special technique, using a reference species for each reaction, has been applied. In this approach, the definition of the chemical time scale is based on the reference species and both reaction rate and the characteristic chemical time are computed by the reference species technique. This approach is appropriate when the integration step is larger than the smallest chemical time scale, since the same algorithm can be applied to all reactions without checking whether they are slow or fast (equilibrium). By using this approach, the integration step is restricted because of the species which are in danger of being driven to negative concentration.

Consider the following elementary reaction (stoichiometric coefficients = 1)

$$c_1 + c_2 \xleftrightarrow{k_f, k_r} c_3 + c_4 \ . \tag{5.30}$$

The rate equation for (5.30) is

$$\dot{\omega} = k_f [c_1][c_2] - k_r [c_3][c_4] \tag{5.31}$$

and,

$$\frac{\mathrm{d}[c_1]}{\mathrm{d}t} = \frac{\mathrm{d}[c_2]}{\mathrm{d}t} = -\dot{\omega}, \ \frac{\mathrm{d}[c_3]}{\mathrm{d}t} = \frac{\mathrm{d}[c_4]}{\mathrm{d}t} = \dot{\omega} \ . \tag{5.32}$$

Equation (5.32) is solved by implicit scheme, since the reaction rate $\dot{\omega}$ is dependent on both temperature and concentration, it can differ in value by several orders of magnitude when the reactions proceed. The problem is illustrated by discretizing (3.32) for the forward reaction and assuming $\dot{\omega} > 0$

$$\frac{[c_1]^{n+1} - [c_1]^n}{\tau} = -\dot{\omega}^x \ \Rightarrow \ [c_1]^{n+1} = [c_1]^n - \tau \dot{\omega}^x \tag{5.33}$$

where $\dot{\omega}^x$ is either evaluated at x = n, x = n+1 or a combination of both.

From the above it is clear that, if $\dot{\omega}^x$ is evaluated at x = n, then the integration step τ is restricted because $[c_1]^{n+1}$ can be negative after a certain value of τ. Obviously, this

is physically impossible and incorrect because the concentrations should tend towards the equilibrium solution ($\dot{\omega} = 0$), which for $i = 1$ yields

$$[c_1]^{\mathrm{eq}} = \left(\frac{k_r [c_3][c_4]}{k_f [c_2]} \right)^{\mathrm{eq}} \quad . \tag{5.34}$$

To overcome this deficiency, $\dot{\omega}^{\mathrm{x}}$ is evaluated at x = n+1 semi-implicitly in the following way:

Differentiating $\dot{\omega}^{\mathrm{x}}$ with respect to time yields (k_f and k_b are hold constant):

$$\frac{\mathrm{d}\dot{\omega}}{\mathrm{d}t} = k_f \left(\frac{\mathrm{d}[c_1]}{\mathrm{d}t}[c_2] + [c_1]\frac{\mathrm{d}[c_2]}{\mathrm{d}t} \right) - k_b \left(\frac{\mathrm{d}[c_3]}{\mathrm{d}t}[c_4] + [c_3]\frac{\mathrm{d}[c_4]}{\mathrm{d}t} \right), \tag{5.35}$$

by using (5.32),

$$\frac{\mathrm{d}\dot{\omega}}{\mathrm{d}t} = k_f \left(-\dot{\omega}[c_2] + [c_1](-\dot{\omega}) \right) - k_b \left(\dot{\omega}[c_4] + [c_3]\dot{\omega} \right) \tag{5.36}$$

$$\frac{\mathrm{d}\dot{\omega}}{\mathrm{d}t} = -\underbrace{\left(k_f \left([c_2] + [c_1] \right) + k_b \left([c_4] + [c_3] \right) \right)}_{\alpha} \dot{\omega} \tag{5.37}$$

$$\frac{\mathrm{d}\dot{\omega}}{\mathrm{d}t} = -\alpha\, \dot{\omega} \,. \tag{5.38}$$

Introducing α and discretizing (5.38) semi-implicitly, results in:

$$\frac{\dot{\omega}^{\mathrm{n+1}} - \dot{\omega}^{\mathrm{n}}}{\tau} = -\alpha^{\mathrm{n}} \dot{\omega}^{\mathrm{n+1}} . \tag{5.39}$$

$$\dot{\omega}^{\mathrm{n+1}} = \frac{\dot{\omega}^{\mathrm{n}}}{1 + \alpha^{\mathrm{n}} \tau} . \tag{5.40}$$

Then, inserting (5.40) into (5.33) gives

$$[c_1]^{\mathrm{n+1}} = [c_1]^{\mathrm{n}} - \tau \frac{\dot{\omega}^{\mathrm{n}}}{1 + \alpha^{\mathrm{n}} \tau} \tag{5.41}$$

which can be written in open form (assuming $\tau \to \infty$),

$$[c_1]^{n+1} = [c_1]^n - \tau \frac{\dot{\omega}^n}{1+\alpha^n \tau} \xrightarrow{\tau \to \infty} [c_1]^n - \frac{\dot{\omega}^n}{\alpha^n}$$
$$= [c_1]^n - \left(\frac{k_f [c_1][c_2] - k_r [c_3][c_4]}{k_f ([c_2]+[c_1]) + k_r ([c_4]+[c_3])} \right)^n , \quad (5.42)$$

does not tend toward equilibrium concentration $[c_1]^{eq}$, see (5.34). In order to overcome this deficiency, the reference species concept is introduced. The reference species is defined as the species most in danger of being driven negative, thus, it is the species which is being consumed by the reaction and has the lowest concentration. For the sake of argument let's assume the reference species to be $c_r = c_1$, i.e., species one. The partner to species one is, thus, c_2. Note that $[c_2] > [c_1]$ and by assuming that $k_f [c_2]$ is the largest of the terms in the expression for α, we have

$$\alpha^n \approx \left(k_f [c_2] \right)^n , \quad (5.43)$$

Now considering (5.43), for the reference species (5.42) becomes

$$[c_1]^{n+1} = [c_1]^n - \tau \frac{\dot{\omega}^n}{1+\alpha^n \tau} \xrightarrow{\tau \to \infty} [c_1]^n - \frac{\dot{\omega}^n}{\alpha^n}$$
$$= [c_1]^n - \left(\frac{k_f [c_1][c_2] - k_r [c_3][c_4]}{k_f [c_2]} \right)^n = \left(\frac{k_r [c_3][c_4]}{k_f [c_2]} \right)^n \quad (5.44)$$

which is same with the (5.34). This way, the equilibrium condition for each reaction is automatically ensured and there is no need to treat equilibrium reactions separately from the slow, kinetically controlled reactions. Also reference species assumption gives the relevant chemical timescale, τ_c, which is the reciprocal value of α [72]:

$$\tau_c = \alpha^{-1} = \frac{1}{k_f [c_2]} . \quad (5.45)$$

5.4.1.3 The Original Interaction by Exchange with the Mean (IEM) Model

Most methods in simulating reacting flows involve numerical solutions of the unsteady RANS, Reynolds Averaged Navier Stokes, equations. The key element of any reliable turbulent combustion model is the incorporation of two distinct mechanisms in the turbulent mixing, macro- and micro-mixing. To account for the effect of mixture imperfections, the generalized PaSR, Partially Stirred Reactor, model has been employed. The original PaSR model introduced by Villermaux [157] is a simple form of the IEM, Interaction by Exchange with the Mean, approach. Let

us describe briefly the original IEM model accounting for a Lagrangian particle age repartition inside the reactor. Particles injected into the reactor are heated by mixing with the more aged ones and reacting in the reactor zones with the premixed mixture. The particle mixing rate depends on τ_{mix}, the micro-mixing time scale. The set of the time dependent equations governing the species concentrations in the reactor zone:

$$\frac{\mathrm{d}c}{\mathrm{d}t} = \frac{< [c] > - [c]}{\tau_{\text{mix}}} + f_r(c,T);\ c(t=0) = c_0 \tag{5.46}$$

where, c is the instantaneous species molar density, T is the mixture temperature, and $f_r(c,T)$ is the chemical source term; the brackets denote an averaging procedure, species indices are omitted for simplicity. The mean value $< c >$ is the integral weighted by the PDF $p(c)$ describing the species repartition in the reactor, i.e

$$< c >= \int_0^1 c \cdot p(c) \cdot \mathrm{d}c \tag{5.47}$$

By assuming ergodicity for the concentration repartition for a given time and the particle age repartition in the reactor, it follows:

$$p(c) \cdot \mathrm{d}c = \phi(t) \cdot \mathrm{d}t \tag{5.48}$$

where $\phi(t)$ is a random function of a deterministic variable such as time, t. This function was taken in a form of the exponential distribution $\phi(1/\tau_r, t) = e^{-t/\tau_r} / \tau_r$, where τ_r is a mean residence time of particles in the reactor. The exponential distribution is a reduced form of the Poisson distribution with one discrete occurrence or "arrival" in the course of the residence time. Finally, the averaging procedure is defined as:

$$< c >= \int_0^\infty c(t) \cdot \phi(t) \cdot \mathrm{d}t \tag{5.49}$$

This model is known as the PaSR model.

5.4.1.4 The Partially Stirred Reactor (PaSR) Model

In the extended PaSR model [76], the averaging procedure described by equations (5.47)-(5.49) is replaced by numerical solution of the conservation equations of spray combustion obtained on the computational grid, thus giving the values of $< c >$ and

other flow parameters. The cells of the computational grid can be interpreted as the particles representing the mixture composition in the original IEM model. The PaSR concept assumes the combustion process to be a sequential process in which mixing is followed by chemical reactions [77] (see Figure 5.9).

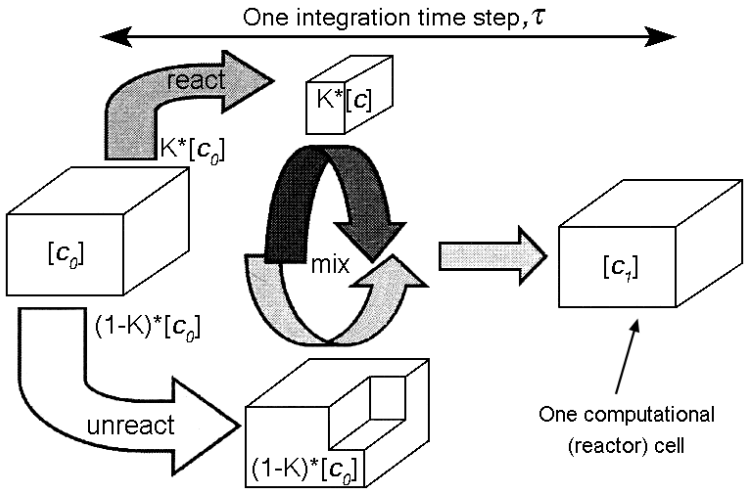

Figure 5.9 Schematic representation of PaSR [72]

In the PaSR approach, a computational cell is split into two different zones, one zone, in which all reactions occur, and another, in which no reactions occur. Among these two zones, the reacting zone is treated as a perfectly stirred reactor (PSR), in which the composition is homogeneous (every species is assumed to be perfectly mixed with the other ones). This allows us to disregard any fluctuations when calculating the chemical source terms [61]. The composition changes due to mass exchange between the reacting and non-reacting zones reflect the turbulence effects that produce transient localized regions favorable to combustion [72].

PaSR model distinguishes between three molar concentrations (see Figure 5.9):

- $[c_0]$ is the averaged concentration in the feed of the cell and may be considered as the initial averaged concentration in the cell, here, the state of the particles is assumed as not mixed yet (composed of only one reactant)
- $[c]$ is the unknown concentration in the reaction zone on a sub-grid level in the unknown reactive fraction of the cell material (virtual concentration), here, the state of the particles is assumed as mixed and reacting (composed of both reactants)

– $[c_1]$ is the sought for, time averaged reactor-exit concentration. This is also the averaged concentration in the cell, here, the state of the particles is assumed as mixed and burnt (composed of products only),

where K^* is the mass fraction of the initial mixture, $[c_0]$, that reacts. After each computational step, $[c_1]$ trades place for $[c_0]$. In order to minimize the computational work required to track and solve the complex chemistry in all particles, the assumption is made that all reacting particles have the same composition and the interaction of all particles occurs by IEM [156].

PaSR concept can be illustrated for the mass conservation of species, in a linear, one dimensional form (averaging symbol "< >" is omitted hereafter)

$$\frac{\mathrm{d}[c]}{\mathrm{d}t} = \underbrace{D_{\mathrm{sgs}} \frac{\mathrm{d}^2[c]}{\mathrm{d}x^2}}_{\text{subgrid diffusion term}} + f_r([c]) \,, \tag{5.50}$$

D_{sgs} : corresponding subgrid diffusivity

f_{r} ([c]) : reaction rate

Here a subgrid diffusion term is used to describe the mixing in the PaSR and the role of subgrid diffusivity, D_{sgs}, is quite similar to that of the RNG subgrid viscosity to the total turbulent viscosity. But, D_{sgs} is a very important parameter in the PaSR because it influences chemical reactions in the reactor. The discretization of the subgrid diffusion term in (5.50) can be achieved by means of the IEM concept as:

$$D_{\mathrm{sgs}} \frac{\mathrm{d}^2[c]}{\mathrm{d}x^2} = \frac{[c]-[c_1]}{\tau_{\mathrm{mix}}} \,. \tag{5.51}$$

Applying Vulis' rate balance concept to the PaSR together with the operator-splitting technique to (5.50), a generalized relation yields

$$\frac{[c_1]-[c_0]}{\tau} = f_r(c) = \frac{[c]-[c_1]}{\tau_{\mathrm{mix}}} \,. \tag{5.52}$$

Above, while the chemical source term (Arrhenius reaction term), f_r ($[c]$, T), is calculated at the reactor virtual concentrations, τ is the integration time step (as used in KIVA-3VR2), τ_{mix} is the micro-mixing time which can change from the break-up time of the large eddies to the Kolmogorov time of small eddies. τ_{mix} is calculated from k, ε values in the computational cell and a fitting parameter [126]. The three equations in (5.52), clearly express the idea that the combustion in the PaSR is a

sequential process where mixing is followed by chemical reaction and, for a stationary regime, the rates of these individual steps are equal [73]. One can plot the equations in (5.52) with the concentrations of c_0, c and c_1 as in Figure 5.10.

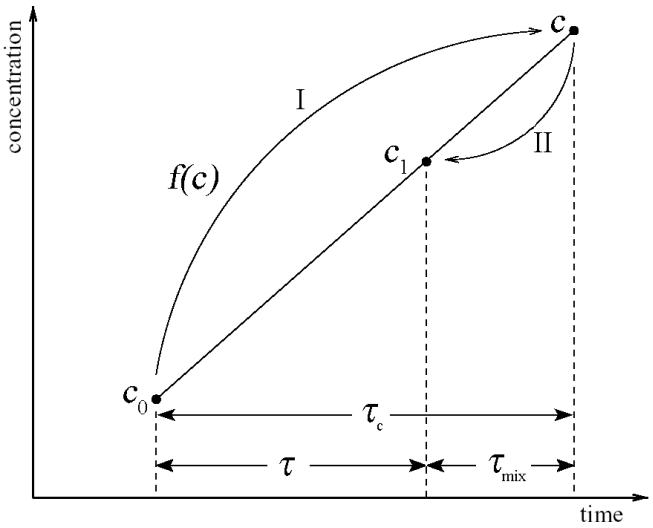

Figure 5.10 The reaction/mixing procedure of PaSR approach [61]

The whole process in PaSR can be divided into two sub-steps, proceeding in parallel. In Figure 5.10 they are marked as I and II:

I The initial concentration in the reaction zone changes from [c_0] to [c] as it reacts,

II The reactive mixture, c, is mixed with the unreactive mixture, c_0, by turbulence, resulting in the averaged concentration c_1.

The key issue in the PaSR approach is how to split the cell into the reacting and non-reacting part. In other words, how large is the mass fraction of the mixture (K^* in Figure 5.9) taking part in the combustion, and what governs the composition of it? Answers of this question describe the connection between the sub-grid information and the grid level information.

The reactor exit concentration can be obtained, from mass conservation considerations, looking at Figure 5.9, as

$$[c_1] = K^*[c] + (1 - K^*)[c_0] \tag{5.53}$$

In the case of [c] ≡ [c_1], the system (5.52) can be solved by conventional numerical methods, e.g. by the kinetics program of the CHEMKIN package. Otherwise, these equations are "unclosed", since two sets of unknowns, [c_1] and [c] must be found.

Here, the reaction zone concentration, [c], is sub-grid information and it must be expressed in terms of resolved grid level information [c_0] and [c_1]. To achieve this, subgrid information, c, in (5.53) is eliminated considering (5.52) and by rearranging these equations for an expression of c_1, the reactive mass fraction of the mixture can be defined as

$$\mathrm{K}^* = \frac{\tau}{\tau + \tau_{mix}} \ . \tag{5.54}$$

According to the effectiveness of τ and τ_{mix}:

- if the integration step, $\tau = 0$ then $\mathrm{K}^* = 0$, no mixing and reaction
- if the turbulent mixing time, $\tau_{\mathrm{mix}} = 0$ then $\mathrm{K}^* = 1$, the model reduces to PSR

In the case of the linear Arrhenius kinetics, f_r ([c], T) ≡ -[c]/τ_{c}, one can rewrite (5.52)

$$\frac{[c_1]-[c_0]}{\tau} = \frac{[c]-[c_1]}{\tau_{mix}}, \frac{[c]-[c_1]}{\tau_{mix}} = -\frac{[c]}{\tau_c} \ , \tag{5.55}$$

where τ_{c} is the chemical reaction time. The second equation of (5.55) expresses the main idea of the Eddy Dissipation Concept, EDC, model [158] which suggests that the fastest chemical reaction is constrained by the micro-mixing in a form of "mixing–reacting" [159].

The Taylor expansion of f_{r} ([c]) at $c = c_1$ can be used to remove subgrid value c:

$$f_r([c]) = f_r([c_1]) + \frac{\partial f_r}{\partial [c]}([c]-[c_1]) + \frac{1}{2}\frac{\partial^2 f_r}{\partial [c]^2}([c]-[c_1])^2 \ . \tag{5.56}$$

In (3.56), it is assumed that the dominating term is the first order derivate concerns the reference species, hence, the second order derivate is neglected. In this way, the chemical time scale can be defined as:

$$\frac{1}{\tau_{\mathrm{c}}} = -\frac{\partial f_r}{\partial [c_{\mathrm{r}}]} \tag{5.57}$$

Combining (5.56) and (5.57) yields the following expression:

$$f_r([c]) = f_r([c_1]) + \frac{[c_1]-[c]}{\tau_{\mathrm{c}}} \tag{5.58}$$

After algebraic manipulations and using (5.53), the above expression yields in a form

$$f_r([c]) = f_r([c_1]) \cdot \mathrm{K} = -\frac{[c_1]}{\tau_c} \cdot \mathrm{K} \quad , \text{where } \mathrm{K} = \frac{\tau_c}{\tau_c + \tau_{mix}} \ . \tag{5.59}$$

Equation (5.59) shows that the turbulent combustion time is the sum of the mixing and reaction times if the reaction rate is expressed in terms of the reactor exit parameters. This is the main consequence of the PaSR model. Here, $-[c_1]/\tau_c$ is a linear approximation of the Arrhenius reaction source term calculated using the exit parameters of the reactor rather than the parameters of the reaction zone as in the original Vulis' model (see (5.55)).

If the reaction time is defined as (see [61] for the detailed derivation)

$$\frac{1}{\tau_c} = \frac{f_r^0}{\left([c_0]_s + term_r^- \tau\right)} \tag{5.60}$$

Then, for the detailed chemical mechanism, the net production rate of the reference *s*-species due to the chemical reaction with accounting for the micro-mixing effect can be given in a form

$$\frac{[c_1]_s - [c_0]_s}{\tau} = f_r([c_1]) \cdot \mathrm{K} = \frac{[c_0]_s f_r^0}{[c_0]_s + term_r^- \tau + term_r^- \tau_{mix}} \tag{5.61}$$

where f_r^0 and $term_r^-$ are the net chemical production rate and the term representing mass depletion rate.

The species production rate due to the particular r-chemical reaction is defined by Arrhenius reaction term such as below,

$$f_r([c]) = (\upsilon_r'' - \upsilon_r')\dot{\omega}_r(c) = term_r^+ - term_r^- = \\ = term_r^+ - c_s / \tau_c \tag{5.62}$$

Above, υ_r'' and υ_r' are stoichiometric coefficients of the backward and forward stages, $\dot{\omega}_r$ is the rate progress variable of the r-reaction, respectively.

The equation (5.61) can be deduced, if the chemical reaction times τ_c are formally defined as characteristic times of the species destruction rates, when the species chemical production terms are presented as in the equation (5.62). Micro mixing time is described in terms of Kolmogorov's time definition [38].

5.4.1.5 Micro-mixing Time Definition

The correct definition of the micro-mixing time is a matter of importance for any EDC turbulent combustion model. The basic assumption of the EDC is that chemical reactions occur only in the turbulence fine structure, i.e., Kolmogorov size eddies and that the reactions are quenched, if the characteristic chemical times for limiting species are longer than the Kolmogorov time. Thus, the classic EDC model does not allow the reaction zone broadening beyond the Kolmogorov limit for slow reactions [160]. The approach used in this study is based on the Kolmogorov expression for the micro-mixing time with the molecular viscosity replaced by a fraction of the effective viscosity assumed to be responsible for micro-mixing. If, for example, the RNG *k*-ε model is employed, the turbulent viscosity related to *k*, turbulent kinetic energy, and *ε*, dissipation rate of *k*, is given by the general expression:

$$\mu_t = \mu_l \left(1 + \sqrt{\frac{c_\mu \rho k^2 / \varepsilon}{\mu_l}} \right)^2 = \rho \left(\upsilon_l + \upsilon_t^s + 2\sqrt{\upsilon_l \upsilon_t^s} \right) \tag{5.63}$$

where υ_t^s is the "standard" *k*-*ε* kinematic viscosity.

Provided that the first two terms in expression (5.63) contribute to conventional diffusion transport, the geometrical mean term can be assumed to determine the characteristic time scale for micro-mixing in the turbulence/chemistry interaction model. When written in a form similar to the Kolmogorov time definition, $\tau_k = (\upsilon_l / \varepsilon)^{1/2}$, it replaces the molecular viscosity by a corresponding value of the turbulent viscosity:

$$\tau_{mix} = \left(2\sqrt{\upsilon_l \upsilon_t^s} / \varepsilon \right)^{1/2} = \left(2\sqrt{c_\mu} \frac{k}{\varepsilon} \tau_k \right)^{1/2} \tag{5.64}$$

where c_μ=0.09 is the constant of the *k*-*ε* model of turbulence. Equation (5.64) gives only a provisional value of τ_{mix} that must be refined in comparing predictions with experiments [38].

6 THE ADVANCED REGIME OF TURBULENT COMBUSTION FOR DIESEL ENGINE APPLICATIONS

6.1 Conventional Diesel Spray Combustion

In a direct injection diesel engine, the fuel is injected into the hot compressed air inside the combustion chamber. Due to the increasing gas temperature during compression, the combustion process is initiated by auto-ignition. The start of combustion is controlled by injection timing, and the desired engine torque is adjusted via the amount of fuel injected per cycle. Due to the short time available for mixture formation, the fuel-air mixture always consists of fuel-rich and lean regions, and thus it is strongly heterogeneous. Figure 6.1 shows three phases of a conventional diesel combustion process, which will be discussed in detail [161].

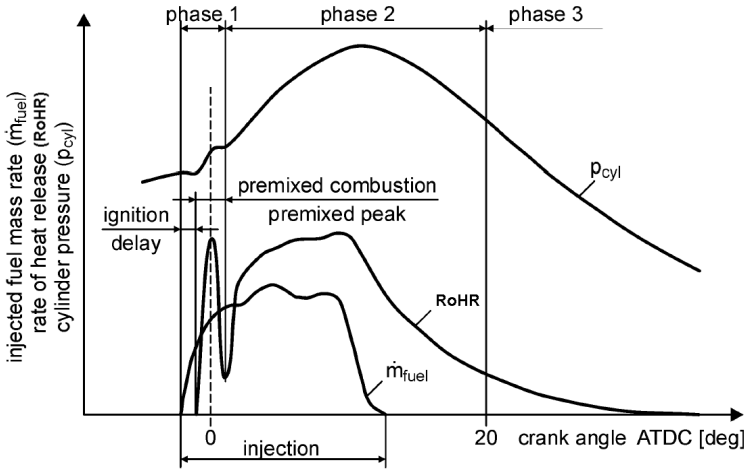

Figure 6.1 Phases of conventional diesel combustion process [161]

The first phase begins with the start of injection and ends after the so-called premixed combustion. The direct injection of fuel into the cylinder usually starts some degrees of crank angle before top dead center, the exact timing is depending on engine speed and load. The injection duration depends on the amount of fuel that has to be injected per cycle. As soon as the cold fuel jet starts to penetrate into the combustion chamber, it begins to mix with the hot compressed air. As penetration

increases, more and more hot air is entrained, the droplets begin to vaporize, and a sheath of vaporized heated fuel-air mixture forms around the jet's periphery [161].

When the temperatures inside this fuel-rich zone reach about 750 K, the first reactions resulting in a breakdown of high cetane fuel begin to occur. These reactions as well as the further entrainment of hot air and the additional compression of the cylinder charge increase the temperature and the rate of the reactions. The products of these basic reactions are largely C_2H_2, C_2H_4, and C_3H_3 fuel fragments as well as CO and H_2O [37]. Now temperature and reaction rate increase quickly, resulting in a burning of the complete fuel-air mixture that has been formed during the ignition delay, which is the time between start of injection and ignition. This sudden combustion of well-prepared fuel-air mixture results in a strong and sudden increase of heat release and cylinder pressure, the so-called premixed peak [161].

The strong pressure gradients ($dp/d\alpha$) cause considerable noise, and the high temperatures in the premixed zone are responsible for production of NO_x (Zeldovich mechanism). The heat being released during the premixed combustion depends on the amount of fuel being injected and evaporated during the ignition delay.

The premixed combustion consumes all fuel-air mixture around the inner spray region. The temperatures of the inner spray region increases to about 1600–1700 K, and all available oxygen in this region is consumed by partial oxidation of the fuel fragments. From now on, air and partial burnt products, which diffuse from inside the spray to the outer regions, are burnt in a very thin reaction zone at the periphery of the spray, the so-called diffusion flame, Figure 6.2.

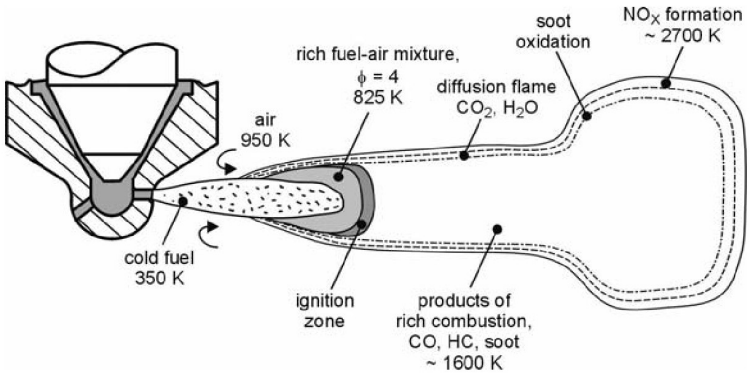

Figure 6.2 Conventional diesel spray combustion and production [161]

This kind of combustion, so-called diffusion burning, characterizes phases 2 and 3 in Figure 6.1, and is limited by the mixing of partial burnt products and air, resulting in

a slower reaction compared to the premixed one. During phase 2, the fuel drops being injected heat up due to the entrainment of hot air and combustion products into the jet near the nozzle. As the evaporated fuel further penetrates into the spray, it breaks down into small molecules, which are then subject to partial oxidation due to the lack of sufficient oxygen inside the hot spray cloud. The partial oxidation reactions and the heat transferred form the diffusion flame keep the temperature of the inner zone at values of about 1600–1700 K [37]. These high temperatures in combination with the low oxygen content are ideal conditions for the formation of soot, and large amounts of soot are produced in the inner cloud. The products from inside this partial oxidation zone diffuse to the boundary and are consumed by the diffusion flame. While only 10–15% of the fuel energy is released in the partial burning zone [37], the diffusion flame releases the rest of the energy. The diffusion flame is fed with oxygen from the surrounding of the burning spray, and near stoichiometric equivalence ratios are reached at its outer zone. Due to the very high temperatures of about 2700 K, nearly all soot entering the diffusion flame is consumed. At the outer boundary of the hot diffusion flame, there is enough oxygen to produce large amounts of NO_x [161].

After the end of the injection process, the partial burning zone is no longer fed with fuel vapor, and it can now be consumed by the diffusion flame. The reduction of soot finally becomes stronger than the production, and the overall amount of soot inside the combustion chamber decreases. As given before, one can see in Figure 3.28 the overall soot concentration inside a combustion chamber as a function of crank angle. Most of the large amount of soot produced at early crank angles is consumed again at later crank angles, and the remaining mass of soot, which is finally detected in the exhaust gases, is only a very small fraction of the initial one. At the end of injection, it is very important to achieve a complete closing of the injector, because unintended post-injections of low-speed large fuel drops that remain near the nozzle and do not reach the region inside the diffusion flame, undergo partial oxidation and produce soot. This soot cannot be consumed by the diffusion flame any more and significantly increases the remaining mass of soot in the exhaust gases [161].

Figure 6.1 shows that the diffusion burning can be divided into two sub-phases. In the mixing-controlled phase 2, which has already been described, the burning rate is only limited by mixing of fuel fragments and air. The velocity of the chemical

reactions is much faster. In the subsequent phase 3 the final oxidation of the remaining unburned and partial oxidized fuel fragments as well as most of the soot particles takes place. However, due to the decrease of gas temperature during the expansion stroke and due to the strong decrease of oxygen, the chemical reactions become slower and are finally the limiting factor. Most of the diesel soot emissions are the result of quenching this final phase of oxidation. A sufficient reduction of soot is only achieved as long as the gas temperatures are not below 1600 K [161]. See section 3.6.2.6 titled oxidation of soot for more details.

6.2 Soot-NO_x Trade-off

According to the discussed mechanisms of soot and NO_x formation in previous sections, it is clear that the main problem of diesel engines in terms of emissions is: How to reduce both pollutants in the engine raw emissions? The so-called soot-NO_x trade-off which is schematically shown in Figure 6.3.

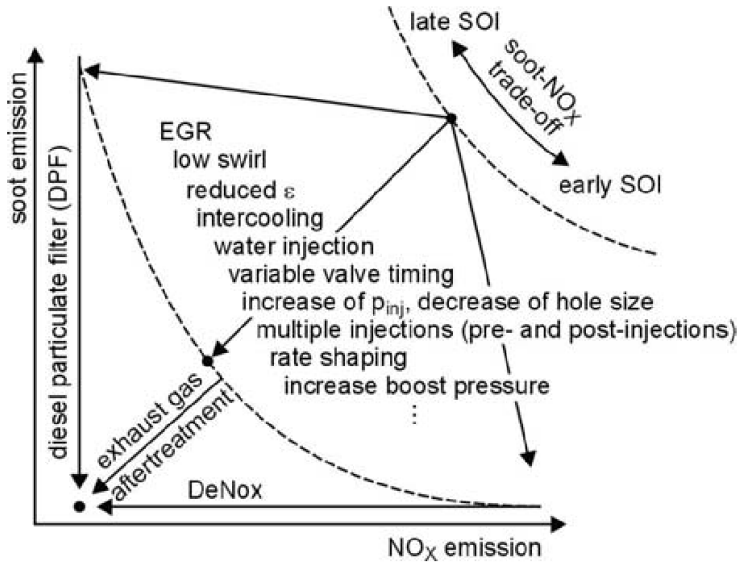

Figure 6.3 Soot-NO_x trade-off: measures for reduction of soot and NO_x in engine out raw emissions [161]

The problem is that both components show opposite behavior: conditions that reduce the formation of NO_x increase the production of soot, and vice versa. In order to reduce the NO_x formation, the combustion should be influenced in such a way that local temperatures above 2000–2200 K are avoided or only reached for very short times. A possible conventional measure is to start the injection at later crank angles in order to shift the main combustion phase into the expansion stroke. This results in

a significant reduction of maximum temperatures and NO_x formation. However, soot oxidation is less effective due to the lower temperatures, and fuel consumption increases due to a smaller thermal efficiency, caused by the late combustion. An early injection start results in an opposite effect: engine efficiency and NO_x production increase, while soot emissions are significantly reduced [161].

One of the most important influence factors is the fuel injection. The design of the injection nozzle as well as injection pressure, start, and duration of injection, shape of injection rate, etc. must be carefully adjusted to the boundary conditions like combustion camber geometry, air motion, and pressure inside the cylinder. The main concept which affects the soot or NO_x formation is the mixing process and the weight of premixed part of the combustion process. Hence the factors which affect mixing process also affect the emission behavior. For example, in the case of a strong contribution of air motion (swirl) to the mixture formation process, less nozzle holes and lower injection pressures are necessary than in the case of low-swirl combustion concepts. The generation of strong swirl increases the pressure losses in the intake system and tends to increases fuel consumption. Further on, ignition delay and premixed peak are usually increased. If too many nozzle holes are used, the burning spray plumes may be displaced by the air motion in a way that fuel is injected in the burnt gases of the neighbour plume. This strongly increases soot formation. Today, low-swirl combustion concepts are often used, and the energy for mixture formation is more or less solely provided by the spray. For this reason, injection pressures and hole numbers are increased, and wide piston bowls, which allow the necessary spray penetration in order to include the complete cylinder charge in the combustion process, are in use [161].

Further measures to reduce pollutants in, Heavy Duty Diesel Engine, HDDE, raw emissions are intercooling, cooled EGR and the early closing of the intake valves (Miller cycle) which usually requires variable valve timing [161].

An increase of charge pressure (reduction of soot due to increased amount of oxygen) combined with reduced compression ratios (prevention of increased peak temperatures and NO_x-formation) is also advantageous. However, highly efficient supercharging systems are necessary in order to provide the desired pressures at high mass flows.

In order to reduce both soot and NO_x emissions, a careful combination and adjustment of the different measures has to be applied in which some of them are the subject of this study.

6.3 Modulated Kinetics (MK) Spray Combustion

Modulated Kinetics, MK, combustion concept, proposed by Kimura et al., is essentially characterized as a low-temperature, premixed combustion system that is aimed at simultaneously to reduce raw NO_x and soot emissions in DI diesel engines [162, 163]. MK concept is based on low-temperature, premixed combustion regime realized in diesel engines in which those regimes were experimentally confirmed leading to lowering engine-out emissions [119]. At first, premixed combustion has been achieved by very early fuel injection in terms of the PREDIC (PREmixed lean DIesel Combustion) concept [164], however, mostly illustrating the problems in managing fuel/air mixing caused a high boiling point of conventional diesel oil. In order to reduce fuel impingement on the piston and cylinder walls, different injector configuration have been tested just confirming difficulties of effective control of ignition timing. However, MK combustion concept exploits fuel retarded injection to prolong the ignition delay over the injection duration and increases the fraction of premixed combustion regime. The basic concept of MK combustion, which is shaped according to the well known techniques for reducing major emissions NO_x and soot of DI diesel engines, is explained schematically in Figure 6.4.

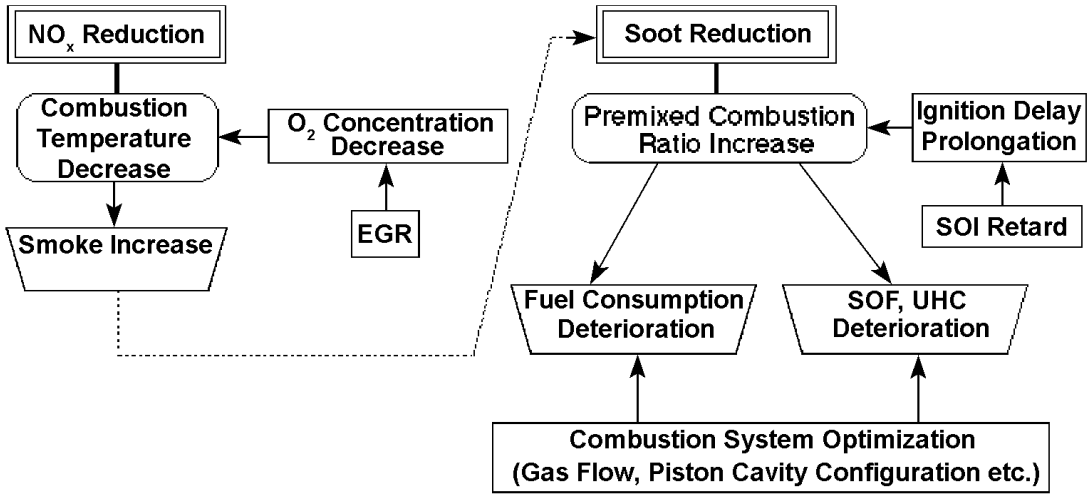

Figure 6.4 Schematic of MK combustion concept [162]

According to this schematic, MK combustion concept can be summarized on the following approaches:

1. Low-temperature combustion is accomplished in the MK combustion concept by applying heavy EGR to reduce oxygen concentration (shown in the "NO_x Reduction" path in Figure 6.4). However, this application results in a higher soot production.
2. Consisting wholly premixed combustion in order to reduce previously formed soot emissions because of the heavy EGR application in the NO_x reduction phase (shown in the "Soot Reduction" path in Figure 6.4). For premixed combustion, the fuel and oxygen must be thoroughly mixed prior to ignition which means that ignition delay must be longer than the injection duration (SOI Retard in Figure 6.4).
3. Additional measures such as toroidal combustion chamber shape for promoting dispersion of the injected fuel outside the piston cavity and high swirl ratio, SR, for suppressing the formation of HCs and Solueble Organic Fraction, SOF (see Combustion System Optimization in Figure 6.4).

Additionally, experimental results have further confirmed that this combustion system is effective in reducing cooling losses. It thus also incorporates a measure to counteract the deterioration of fuel consumption due to a decline in the degree of constant volume which is a side effect induced by retarding the fuel injection timing. So, considering the MK combustion concept, one can summarize its benefits below:

- reducing NO_x and soot emissions simultaneously
- keeping fuel efficiency in the same level whilst emission reduction measures
- reducing the rate of increase in cylinder pressure, which is thought to lead to a reduction of combustion noise

For the application detail of the concept, one can see the study of Kimura et al. [162]. They observed the combustion conditions on the basis of high-speed photographs to confirm that the MK concept works to promote low-temperature, premixed combustion in a DI diesel engine. In Figure 6.5, the photographs of MK combustion which are compared with those of the conventional DI combustion process, typified

by no EGR and a standard injection timing and SR are given [162]. The RoHR curves measured for each combustion process are also given in Figure 6.5.

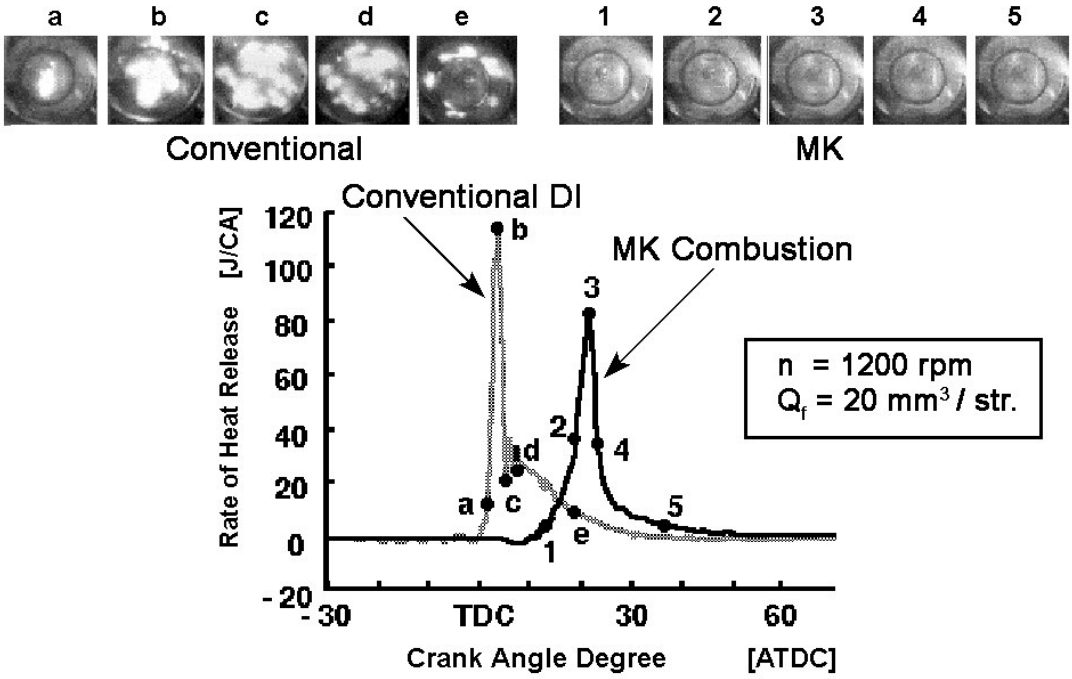

Figure 6.5 Comparison of RoHR and combustion photograph of MK and conventional diesel combustion processes by Kimura et al. [163]

The main specifications of the single-cylinder DI test engine used in the experiments are: Bore = 85 mm, Stroke = 86 mm, Displacement = 488 cm^3, SR = 3-5, CR = 18.00, injection system with high pressure VE pump and 5 x 0.22 mm injectors.

Looking at RoHR, it is seen that the onset of heat release with the MK concept was plainly later than for the conventional combustion process, owing to the large retardation of injection timing. Another characteristic of MK combustion is the low RoHR following the onset of heat release. This is attributed to the low rate of increase in cylinder pressure, which is thought to lead to a reduction of combustion noise. Although the initial heat release rate was low with the MK concept, combustion subsequently proceeded vigorously and the overall combustion period was virtually comparable to that of the conventional combustion process. Moreover, the general shape of the RoHR curve for the MK concept shows a single stage of entirely premixed combustion. This is in clear contrast to the two-stage profile observed for the conventional DI diesel spray combustion process, which is divided between an initial stage of premixed combustion and the main stage of diffusion combustion as shown in Figure 6.1 [162].

In the combustion photographs for the MK concept, virtually no clear sign of a brilliant flame is observed throughout the entire combustion period. By analogy with the high transparency of the flame, this is taken as proof not only of the weak luminous intensity of the flame but also of its low soot concentration on account of the low combustion temperature [162].

The effect of each combustion factor in the MK concept on exhaust emissions and thermal efficiency is shown individually in Figure 6.6.

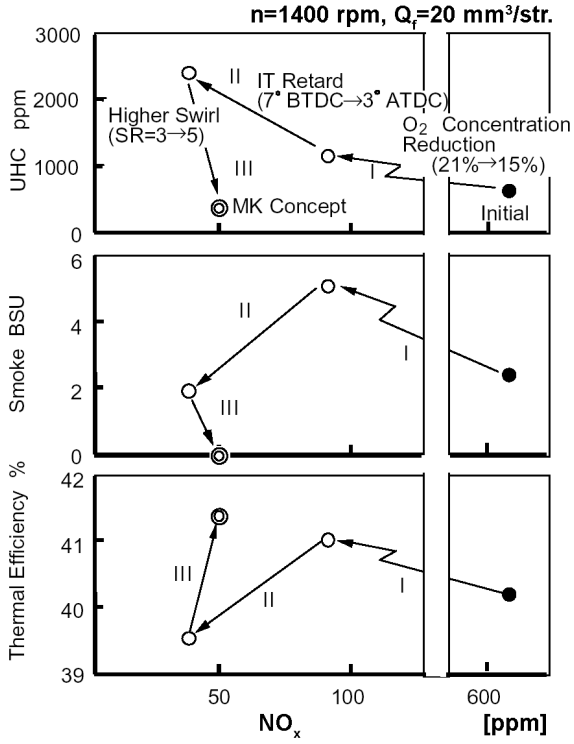

Figure 6.6 Effects of individual factors of MK combustion concept on emissions and thermal efficiency [163]

With a lower O_2 concentration, NO_x emissions were reduced by approximately 90%, and retarded injection timing reduced the smoke level markedly. It is seen that the higher SR played a part in reducing smoke and unburned HC emissions. While thermal efficiency was improved with lower O_2 concentration and deteriorated with retarded injection timing, it was improved over the normal level by higher SR [163].

MK combustion concept summarized above was named as first-generation MK combustion system and at first applied to low load and low speed engine operating conditions. Then, the question is: Is it possible to use MK combustion concept in high load and high speed engine operating conditions too? Appearance of first- and probable second-generation MK combustion concept is shown in Figure 6.7.

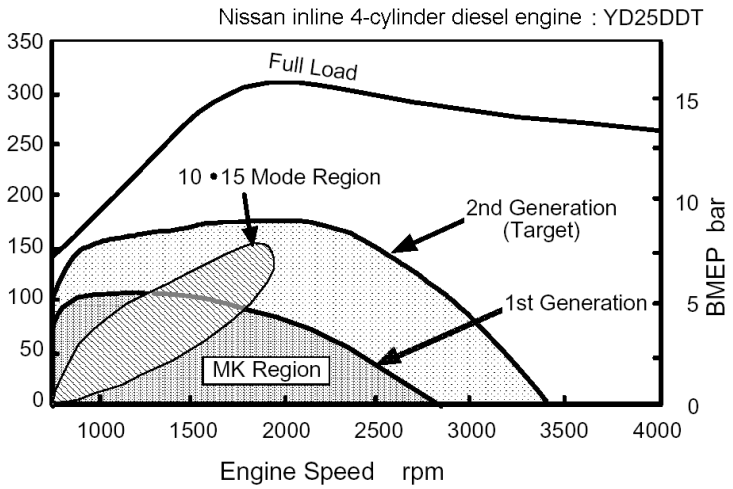

Figure 6.7 MK Combustion Region of First- and probable Second-generation target [163]

For the high load and high speed application there are two major problems which must be overcome, they are:

- Increased amount of fuel, because of the higher load, which must be injected into the combustion chamber prior to the auto-ignition. This results prolonged injection duration. On the contrary, shortened ignition delay because of the higher temperature of the EGR gas.
- Reduced available time, because of the increased engine speed, which will be used to prepare whole fuel/air mixture premixed.

These problems and solution approach are outlined in Figure 6.8.

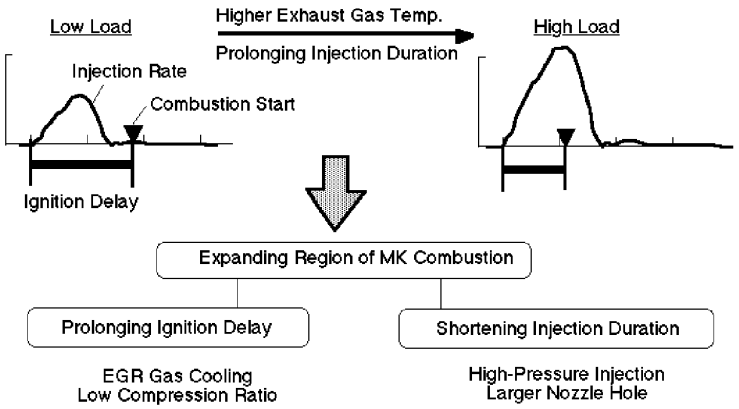

Figure 6.8 Expanding ways of MK Combustion concept [163]

Figure 6.8 summaries two possible ways to expand the MK Combustion region to the high-load range. One approach is to prolong the ignition delay and the other approach is to shorten the injection duration. The fundamental objective of prolonging the ignition delay is to lower the gas temperature of the combustion field

at TDC of the compression stroke. Specific ways of accomplishing that objective include cooling the EGR gas and lowering the compression ratio. On the other hand, the injection duration can be shortened with high pressure injection or a larger nozzle hole, among other approaches. Consequently, the effects of high-pressure injection, a reduced CR and EGR gas cooling were applied to expand the MK combustion region, and the combination of all three approaches resulted in an ignition delay that was longer than the injection duration. In order to avoid HC emission increase in cold conditions, a new piston with large cavity diameter was used [163].

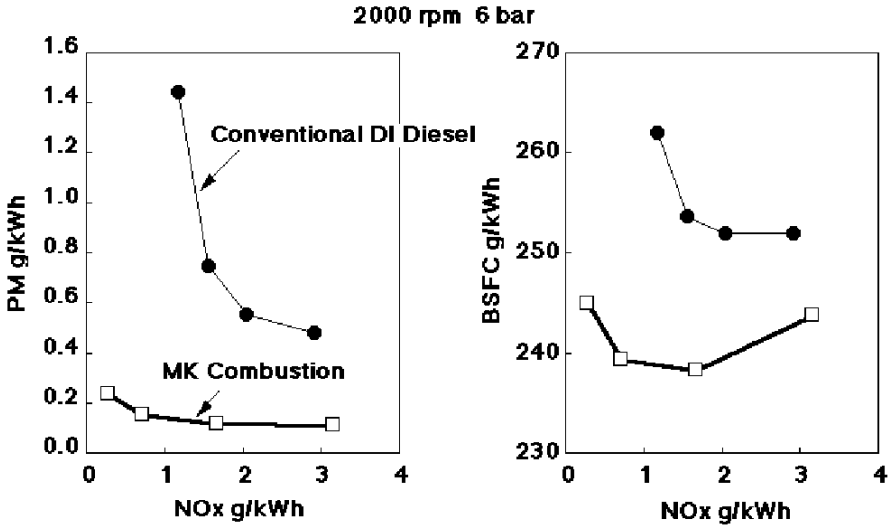

Figure 6.9 Comparison of emissions and BSFC in high load between Conventional and MK Combustion [163]

So it was proved that in the MK Combustion concept, combining a low compression ratio, high injection pressure and EGR gas cooling it is possible to achieve simultaneous reductions in the NO_x and soot emissions of a small DI diesel engine. The MK concept has been introduced in series of production engine, but its use is still limited to the low loads and speeds of engine operational conditions. On the other hand, the concept is especially attractive because conventional diesel and MK combustion regimes can be realized on the same engine [119].

7 DIESEL ENGINE APPLICATIONS

7.1 Volvo Direct Injection D12C Diesel Engine

The experiments were carried out at the division of the Applied Mechanics at Chalmers University of Technology. The research engine was a fully instrumented AVL single cylinder engine, based on the D12C version of the Volvo Heavy Duty DI Diesel engine (Figure 7.1) with the displacement volume of 2.02 l.

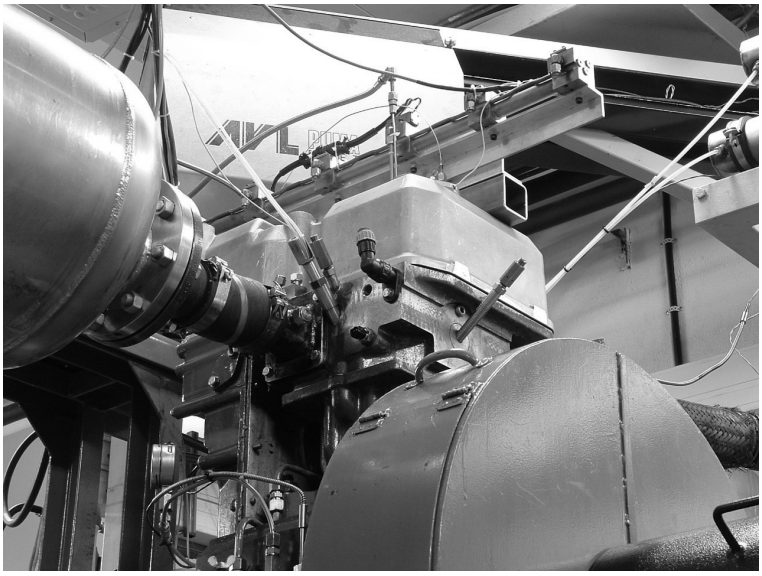

Figure 7.1 Single-cylinder Volvo D12C DI diesel research engine, the computer simulation has been applied to

Details of the injector specifications and combustion chamber dimensions are given in Table 7.1 and Figure 7.2.

Table 7.1 Volvo D12C engine specifications [165]

Based Engine Type	**Basic Unit: AVL 501, Single Cylinder Engine Diesel Engine**	
Cylinder Head	[-]	Volvo D12C, :4 valves, Low swirl
Bore	[mm]	131
Stroke	[mm]	151
Connecting Rod Length	[mm]	260
Displacement	[l]	2.02
Compression Ratio	[-]	18.0:1
Piston	[mm]	With omega shaped piston bowl, $\phi = 89$
Needle Lift Sensor	[-]	Inductive coil
Fuel Injection System	[-]	Delphi E3 Diesel Electronic Unit Injector
Spray Umbrella Angle	[°]	153
Nozzle (number x radius)	[mm]	6 x 0.237

Combustion chamber was omega shaped with a piston bowl with diameter of 89 mm and the engine "dead" volume (crevices, valve recessions, etc.) was estimated as 3% of the displacement volume (see Figure 7.2).

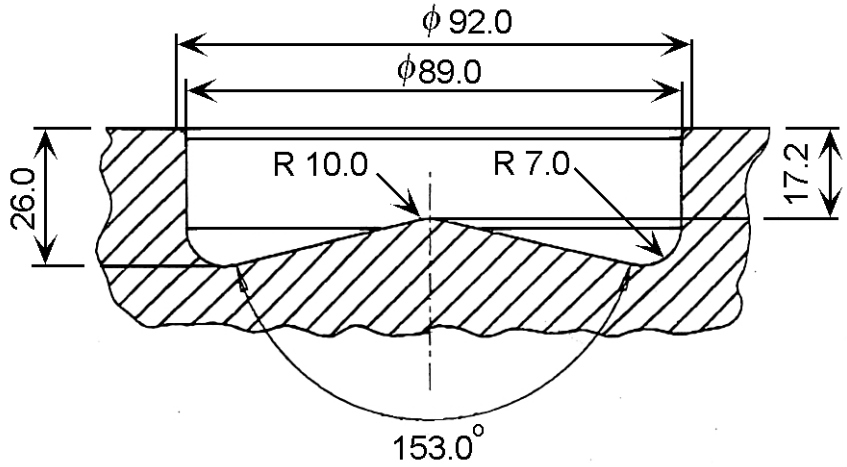

Figure 7.2 View of Volvo D12C piston bowl; units are in mm

For MK Combustion applications, especially at late injection cases, there is a danger of fuel spray contact to the piston bowl surface depending on the evaporation conditions and injection characteristics. Hence, it is better to use a piston with larger bowl and proper spray angle to avoid fuel spray impingement to the wall. The main characteristics of the bowl of the Volvo D12C piston are central, omega shaped and large enough reduce the possibility of fuel impingement to the wall (see Figure 7.2).

7.2 Experimental Setup

The engine was equipped with auxiliary systems for media conditioning such as intake air, fuel, oil, and water in order to supply stabilized conditions, see Figure 7.3. Measurements were taken when the engine reached stable conditions. Steady-state parameters such as emissions, intake charge air temperature, pressure, and back-pressure were sampled for 120 s with a frequency of 100 Hz and then averaged. Both cylinder and injection pressure were sampled at 0.1 °CA resolution. Soot was only measured once during each sampling period using an AVL 415 smoke meter and NO_x emissions using an Ecophysics CLD700EL device [165]. Intake air was fully dehydrated with the air conditioning system. Also the air intake pressure and temperature were controlled to avoid the variation of measurement values due to the atmospheric conditions.

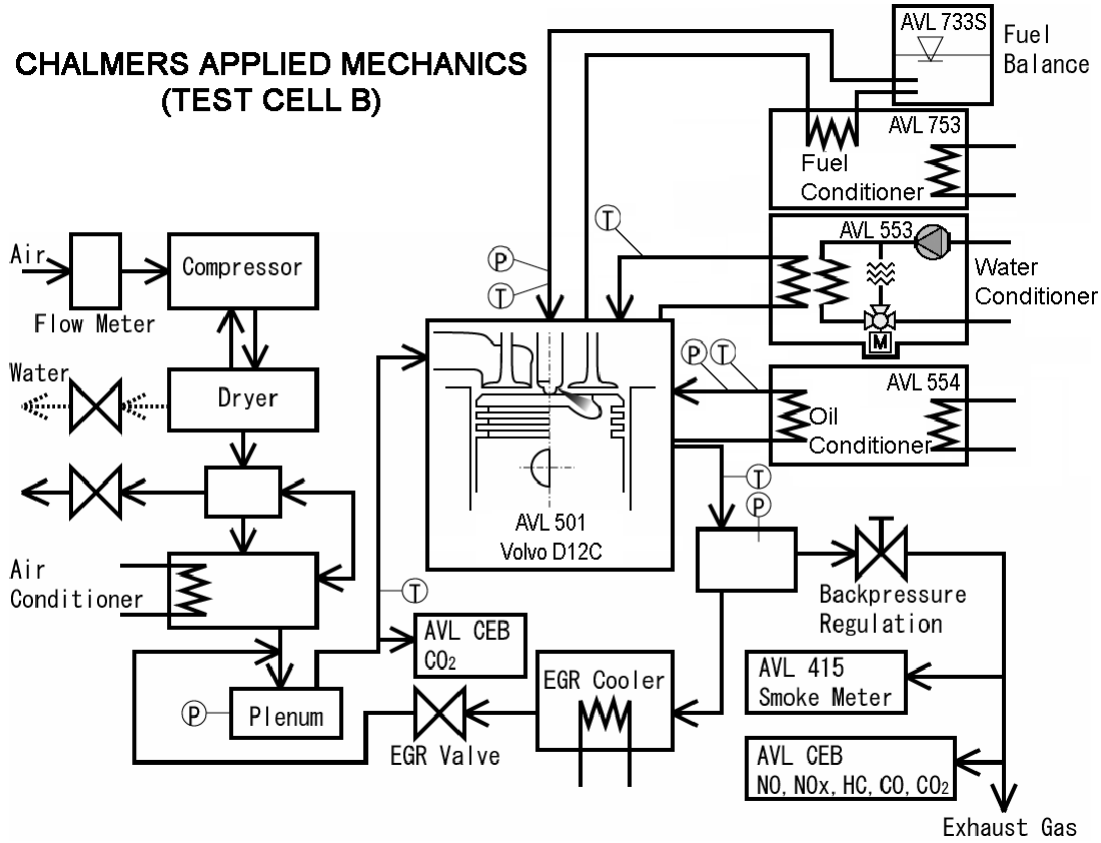

Figure 7.3 Schematic diagram of experimental setup (modified from [126])

The high precise fuel temperature control gives a constant pre-set fuel temperature at the engine and guarantees the high measurement accuracy of the whole test system. Fuel conditioning was made by AVL 753 conditioning system which can control the fuel temperature anywhere within the range of 10...80 °C and fuel consumption was measured by AVL Fuel Balance 733S. Engine water conditioning was made by AVL 553 Water Cooling/Conditioning Unit which enables high control dynamic based on its primary circuit control system using a three-way motored mixing valve and engine-inlet water temperature was controlled with ± 1 K accuracy. Back-pressure could be adjusted by a regulator in the exhaust pipe and EGR levels were varied by controlling this exhaust back pressure as illustrated in Figure 7.3. The EGR levels were calculated from the measured CO_2 levels in the exhaust and inlet systems. When the back pressure, EGR flow, was increased the amount of fresh air was reduced since the intake pressure was kept constant [166]. Also EGR gases were cooled in order to control intake-mixture temperature for EGR cases. Below, a typical measurement for testcell and engine parameters are shown in Figure 7.4 (SOI = -5 CAD ATDC). These measurements were repeated at least two times.

DATE	TIME					
11-Feb-00	15:10:39					
SPEED	P_BARO	T_EXH	TWI	WFLOW	FB_MASS	NOX
rpm	Bar	Cel	Cel	L/sec	g	ppm
1001	1.022	293.5	79.9	1.196	60.23	1097.75
TORQUE	P_AIR_IN	T_AIR_EN	TWO	OFLOW	T_FUEL_I	COL
Nm	mbar	Cel	Cel	L/sec	Cel	ppm
76.7	43	28.3	80.0	0.298	23.4	2.23
AIR_QUA	P_AIR_AB	T_AIR_SC	T_OIL_I	P_OIL	P_FUEL	HC_TAN
kg/h	mbar	Cel	Cel	Bar	Bar	ppm
72.87	1064.8	29.2	90.0	5.4	2.24	-0.8
BH	P_EXP	T_SET_SC	T_OIL_O	S415_FSN	S415_SC	NOX_PER
kg/h	mbar	Cel	Cel	SZ	mg/m3	%
1.81	40	30.7	89.8	0.0800	1.0000	0.06
FUELCOSP	P_EXH_AB	PHI	P_SET_EX	T_EGR	EGR	CO2_EGR
g/kWh	bar	%	mbar	Cel	%	%
224.92	1061.5	0.059	40	26	0	0.03
P	P_SET_SC	AIR_EXC	SPSOOT1	SPCO	SPHC	SPNOX
kW	mbar		g/kWh	g/kWh	g/kWh	g/kWh
8.04	50	2.766	0.0075	0.020	-0.004	13.797

Figure 7.4 Printout of a typical testcell measurement

7.3 Fuel Injection System

Fuel was supplied by the Delphi E3 Diesel Electronic Unit Injector (EUI) system [167]. An inductive coil used as a sensor to control the needle lift. The Delphi E3 EUI is an advanced diesel fuel injection system for heavy duty applications. It has two-solenoid valve technology; Spill Control Valve (SCV) and Needle Control Valve (NCV), which enables the system to generate higher pressures at lower engine speeds (see Figure 7.5). By using these two independent, fast response precision actuators, the system can change the injection pressure level (up to 2,500 bar) and adjust fuel delivery timing and duration on a per shot basis. This enables an ability to achieve full pressure control at low and high engine speeds [168].

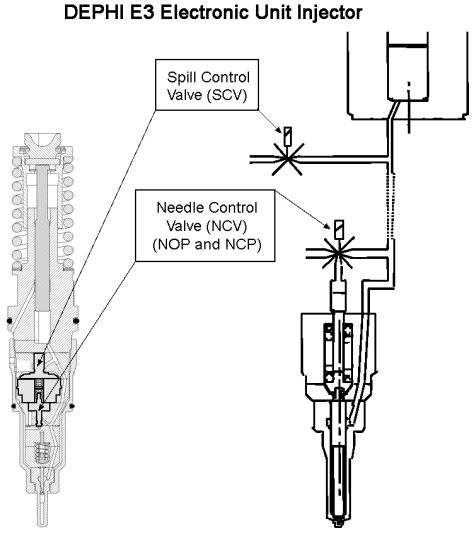

Figure 7.5 Schmatic of two-actuator Delphi E3 EUI (source from [167])

If the SCV valve is closed before the NCV valve is activated, then fuel pressure can be pumped up to a much higher level before the NCV is activated to allow the nozzle needle to open and by this way the pumped fuel pressure is applied at the back of the nozzle needle. This provides a means of substantially increasing the NOP and level of injection pressure during injection. If towards the end of injection the NCV valve is de-activated before the SCV is opened, then the needle can be closed with a greatly increased injection pressure and hence with a high NCP. These features provide the means of achieving a wide variety of injection characteristics with substantial and electronically programmable increases in the injection pressure and the capability for multiple injections. And the needle opening pressure, NOP, and needle closing pressure, NCP, can be adjusted to the desired values [165]. It gives pilot split- main- and post-injection along with a rising pressure characteristic.

7.4 Acquisition of Fast Signals

A sampling code named "Burst to fire" acquires high frequency signals related to key parameters including needle lift, in-cylinder pressure and injection pressure. These signals are further processed by the evaluation code, Dragon, a program that can analyze combustion and thermodynamic events using the measurements of in-cylinder pressure and other variables related to the fuel injection. The thermodynamic analysis gives a number of parameters that characterize the combustion processes, such as HR, ignition delay, injection duration and fractions of the premixed-diffusion combustion [165].

The most critical data acquisition is pressure measurement. Depending on the combustion characteristic, measured raw pressure data can be very unstable, see an example for SOI = -5 CA ATDC case in Figure 7.6, which shows a section of the pressure-volume, p-α, diagram around the peak pressure data. Hence, this kind of too wavy raw pressure data, sourced from the MK Combustion conditions, needs to be processed. This unstable behavior is mainly due to the diesel combustion and used injector characteristics which can affect the combustion and pressure curve. It is more evident in low load conditions (i.e., such 25%) which are also the subject of this MK Combustion study. In low load conditions, because the peak value of the pressure is relatively low, deviation of pressure from the mean value is more visible. For this reason, moving average of raw pressure data is applied in order to make

further processing task easier. In this averaging procedure, the most important criterion is to keep the CA position of the averaged pressure peak as close as possible to the CA position of the raw pressure peak. Because, even 1 °CA deviation from peak CA position on the in-cylinder pressure curve (p-α, diagram) causes ~ 5% error for the calculation of the effective work considering this pressure curve (effective work is the net area below the p-α diagram).

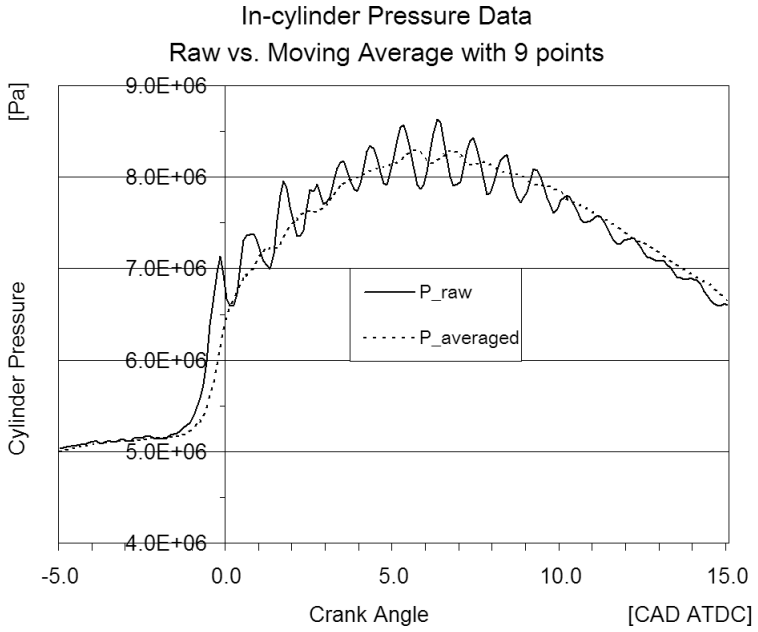

Figure 7.6 Raw and moving averaged in-cylinder pressure data

Considering two pressure curves, one can see that, with 9 points moving average, there is not noticable deviation of peak CA of the averaged pressure curve from the peak CA of the raw pressure curve. Only the start of pressure increase is slightly delayed (0.5-1.0 °CA) which is not crucial for simulations.

7.5 Analysis of MK Combustion with 3D-CFD and 0D Modeling

The MK Combustion concept optimization requires the integration of analysis of large-size chemical mechanisms with 3D-CFD models on a scale which is still far beyond the capabilities of practical simulations. EDC combustion model is the model which can facilitate the efforts making this integration a reality. Hence, realistic predictions of the MK diesel spray combustion were compared with the experimental data for the Volvo D12C engine operating in the MK regime [119].

The MK Combustion analysis was based on two phases: At first KIVA-3VR2 code was calibrated with the available experimental data of four cases; SOI = -5, 0, +5, +10 CAD ATDC. These experimental cases were EGR free. Also, parametric ϕ-T map technique was used for the evaluation of the main characteristics of combustion and emissions of these experimental cases. So, at the first phase: EGR-free experimental results, KIVA-3VR2 simulations and parametric ϕ-T map technique were in question. Then at the second phase, beyond these four experimental cases, six new simulation cases where SOI = -60, -40, -30, -20, -15, -10 CAD ATDC were added to search the possibilities for expanding the MK Combustion concept. As with the first phase, KIVA-3VR2 simulations and parametric ϕ-T map technique were used also in the second phase. These added cases include only simulations, but differently from first phase, calculated EGR cases were also considered in these simulations.

As it was given before in Figure 4.2, KIVA-3VR2 for 3D-CFD simulations and SENKIN for 0D simulations (parametric ϕ-T map) were integrated and used. There were two independent simulation routes in which KIVA-3VR2 simulation results were used by SENKIN simulations to produce parametric ϕ-T maps. Below, considering two iterations for EGR simulations, first outline of all the simulation cases for the MK Combustion analyses are summarized in Figure 7.7 as a plan.

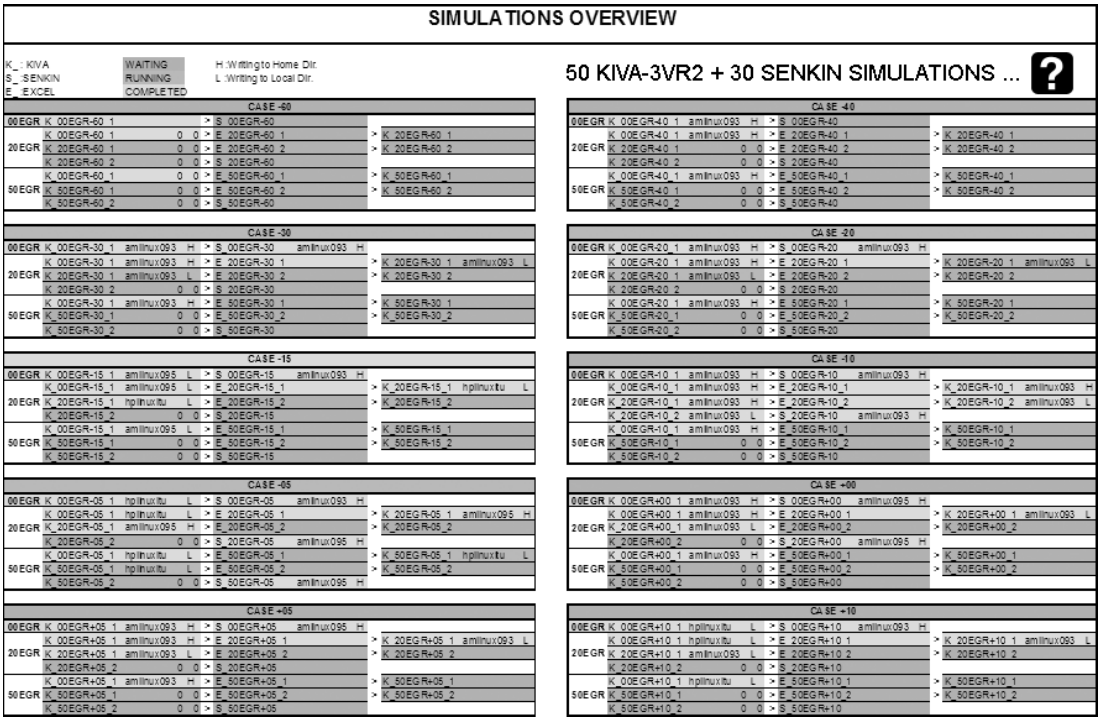

Figure 7.7 MK Combustion simulation plan with two iterations for EGR

In this plan, considering two iterations for KIVA-3VR2 EGR simulations, all possible KIVA-3VR2 and SENKIN simulations were shown. Because there is a connection between KIVA-3VR2 and SENKIN simulations it was important to arrange all the simulations properly. The situations of all ongoing simulations were classified as WAITING, RUNNING, COMPLETED; the name of the running processors and the place where simulation results were written were shown and followed. For each SOI case, considering two iterations for EGR, according to Figure 7.7:

- For 00% EGR case, 1 fresh KIVA-3VR2 and 1 SENKIN simulations
- For 20% EGR case, 2 KIVA-3VR2 iterations and 1 SENKIN simulations
- For 50% EGR case, 2 KIVA-3VR2 iterations and 1 SENKIN simulations,

hence, 5 KIVA-3VR2 and 3 SENKIN simulations would be necessary. Then, for all SOIs, 50 KIVA-3VR2 and 30 SENKIN simulations seemed to be necessary.

7.5.1 Experimental MK Combustion Cases

For the first phase analysis: the measured parameters for MK Combustion experimental cases are listed in Table 7.2. The SOI values were varied from -5, up to +10 CAD ATDC, and the injected fuel amount was kept constant [165].

Because it is not possible to measure average intake temperature exactly at the IVC point, a reasonable temperature calculation, which is checked by polytropic compression coefficient and measured characteristics listed above, is evaluated as a reference for simulation calculations. Hence, the “Calculated Temperature at IVC” in Table 7.2, was calculated according to the measured in-cylinder pressure corresponding engine stroke volume at IVC and measured air mass flow for all cases.

For MK Combustion analysis, at first, measured experimental values were given. In-cylinder pressure and calculated RoHRs from pressure curves were given in Figure 7.8 and Figure 7.9, respectively.

Table 7.2 Measured parameters for operating conditions: n = 1000 rpm and 25% load [38]

SOI [CAD ATDC]		**-5.0**	**0.0**	**5.0**	**10.0**
Engine Speed	[rpm]	1001	1001	1001	1001
Engine Torque	[Nm]	76.7	77.4	74.0	67.4
Effective Brake Power	[kW]	8.04	8.12	7.75	7.07
BSFC	[g/kWh]	224.73	224.50	230.65	254.51
Atmospheric Pressure	[bar]	1.022	1.022	1.022	1.022
Engine Intake Air Absolute Pressure	[mbar]	1064.8	1064.9	1063.0	1063.2
Engine Intake Air Temperature	[°C]	28.2	28.1	28.1	28.0
Engine Intake Air Mass Flow	[kg/h]	73.02	73.36	74.29	73.67
Fuel Temperature	[°C]	23.4	23.3	23.3	23.2
Fuel Pressure	[bar]	2.24	2.23	2.22	2.20
Measured Fuel Mass Flow	[kg/h]	1.81	1.82	1.79	1.80
Calculated Fuel Mass per Cycle	[mg/cycle]	60	61	60	60
Excess Air Ratio, λ	[-]	2.772	2.761	2.850	2.809
Measured Pressure at IVC	[bar]	1.4	1.3	1.3	1.3
Calculated Temperature at IVC	[K]	325	313	314	317
Engine Cooling Water Inlet Temperature	[°C]	79.91	80.00	80.03	79.95
Engine Cooling Water Outlet Temperature	[°C]	80.10	80.20	80.1	80.1
Cooling Water Flow Rate	[l/s]	1.196	1.195	1.195	1.196
Engine Oil Inlet Temperature	[°C]	90.00	90.00	90.00	90.0
Engine Oil Outlet Temperature	[°C]	89.83	89.78	89.73	89.8
Engine Oil Flow Rate	[l/s]	0.298	0.298	0.297	0.297
Engine Oil Pressure	[bar]	5.4	5.4	5.4	5.4
Engine Exhaust Absolute Pressure	[mbar]	1061.5	1062.5	1062.3	1061.2
Engine Exhaust Temperature	[°C]	294	303	307	303
EGR CO_2	[%]	0.03	0.03	0.03	0.03
EGR Ratio	[%]	0	0	0	0
EGR Temperature	[°C]	26	26	26	26
Specific Soot Emissions	[g/kWh]	0.0071	0.0056	0.0008	0.0003
Specific CO Emissions	[g/kWh]	0.021	0.021	0.023	0.025
Specific HC Emissions	[g/kWh]	-	-	-	-
Specific NO_x Emissions	[g/kWh]	12.003	9.618	8.641	12.464
NO Emissions	[ppm]	806	632	577	731
NO_x Emissions	[ppm]	1102	808	727	997

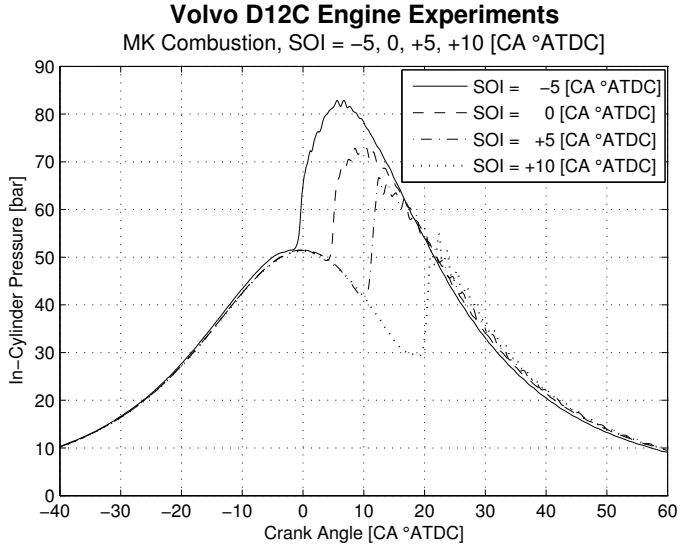

Figure 7.8 Measured In-cylinder pressure for MK Combustion

Maximum In-cylinder pressure decreased with retarded injection (see Figure 7.8). This is because the fuel amount was constant and for the late injections, combined effects of combustion chamber volume increase and the ignition delay resulted a decreasing pressure trend.

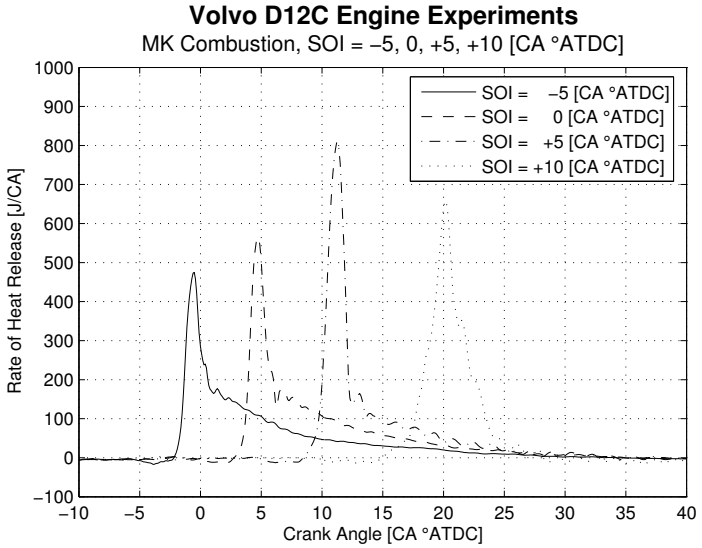

Figure 7.9 Measured RoHR for MK Combustion

On the other hand, for the late injections, ignition delay increases and ignition could occur after the premixed mixture, hence, combustion shifted to the more-premixed HCCI-like mode, except the last case, SOI = 10 CA °ATDC. At the last case, lower combustion efficiency and increased volume decreased the RoHR (see Figure 7.9). Main engine working parameters are given in below.

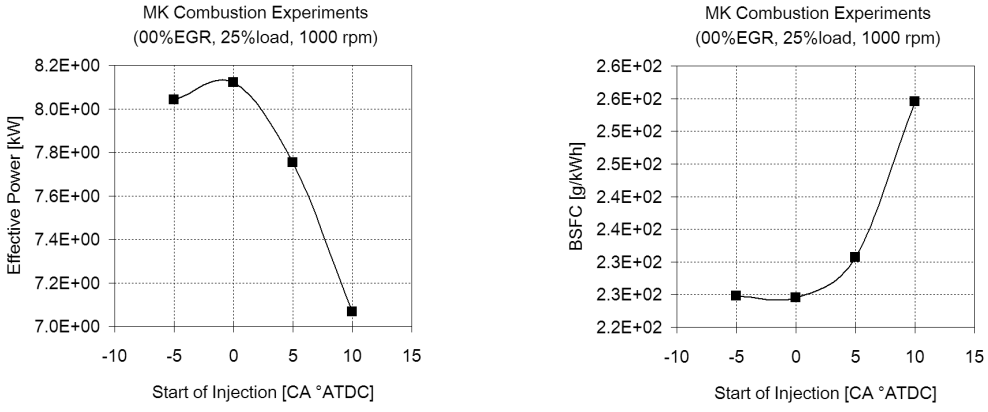

(a) (b)

Figure 7.10 Measured parameters for MK Combustion: a) Power and b) BSFC

As fuel amount and engine speed are constant for all cases (constant load operation), measured engine power is nearly constant for all cases, except SOI = +10 ATDC (Figure 7.10a) which results in a relatively low combustion efficiency which can be seen from high BSFC (Figure 7.10b) and CO emission (Figure 7.12b) values. The increase of BSFC in Figure 7.10b is the result of the decrease in power for the same case.

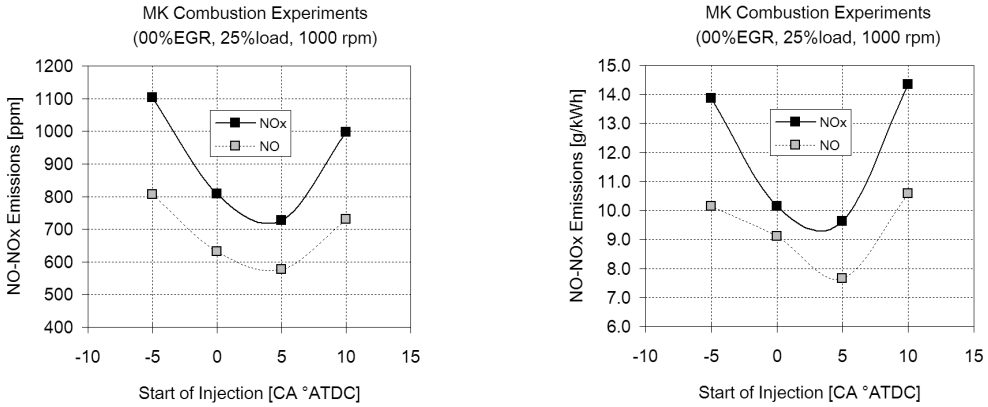

(a) (b)

Figure 7.11 Measured NO and NO_x emissions for MK Combustion: a) Volumetric (ppm) and b) Specific (g/kWh) values

In Figure 7.11 measured NO and NO_x emissions are given. Depending on the combustion characteristics (influence of premixed and diffusion parts) NO_x emissions were changed. At first sight, SOI = -5 and +10 cases seemed to be premixed-like combustion because of the higher NO_x emissions. Here, from the behaviour of NOx emissions one can expect that, SOI = 0 and +5 cases have more diffusion like combustion characteristics which result lower peak combustion temperatures. This is why NO_x emissions are lower for these two cases.

Specific soot and CO emissions are also given in Figure 7.12 below. Here, it seems unexpected behaviour between the trends of the measured soot emissions in Figure 7.12a and NO_x emissions in Figure 7.11b for SOI change from -5 to 0 CAD ATDC cases. While opposite trends between those two cases (NO_x-soot dilemma) was expected, they had same trend. This will be analysed in more detailed in the related forthcoming section.

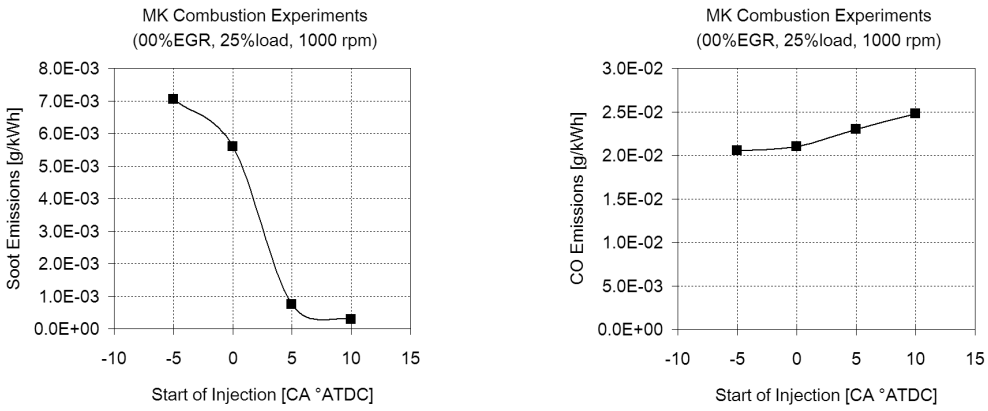

(a) (b)

Figure 7.12 Measured specific emissions for MK Combustion: a) Soot and b) CO

7.5.2 3D-CFD Numerical Modeling (KIVA-3VR2)

Mean features and characteristics (in-cylinder pressure, RoHR) of MK combustion under conditions of delayed injection engine spray auto-ignition has much in common with HCCI process are predicted in accordance with data obtained in the engine experiments [119]. The in-cylinder temperature and RoHR have been calculated beginning from the Intake Valve Closing, IVC, of the engine by using measured pressure vs. CAD distribution. The pressure and temperature corresponding to IVC = -121 CAD ATDC were taken as initial conditions in the engine modeling [38].

The changed parameter between experimental cases was SOI. For this reason numerical modeling was started with the appropriate injection parameters and then calibrated according to the experimental data.

7.5.2.1 Fuel Injection Parameters

One can see measured needle lift and calculated injection velocity profile of the MK Combustion experimental cases of Volvo D12C engine in Figure 7.13. These injection profiles were used to create the necessary tabular data for the simulations. This tabular data was entered in the input file, itape5, of the KIVA-3VR2 code as tables (numvel). Then, the code calculates a fixed time increment between the velocity entries by using the injection duration, cadinj, and the number of numvel table entries. So, using this fixed time increment it creates a velocity injection table, velinj, ensuring that injected fuel mass will be equal to the given actual total fuel

mass. These resulting velocities (velinj table) are the fuel parcel velocities in each of the three component directions and they are written to an output file (otape12).

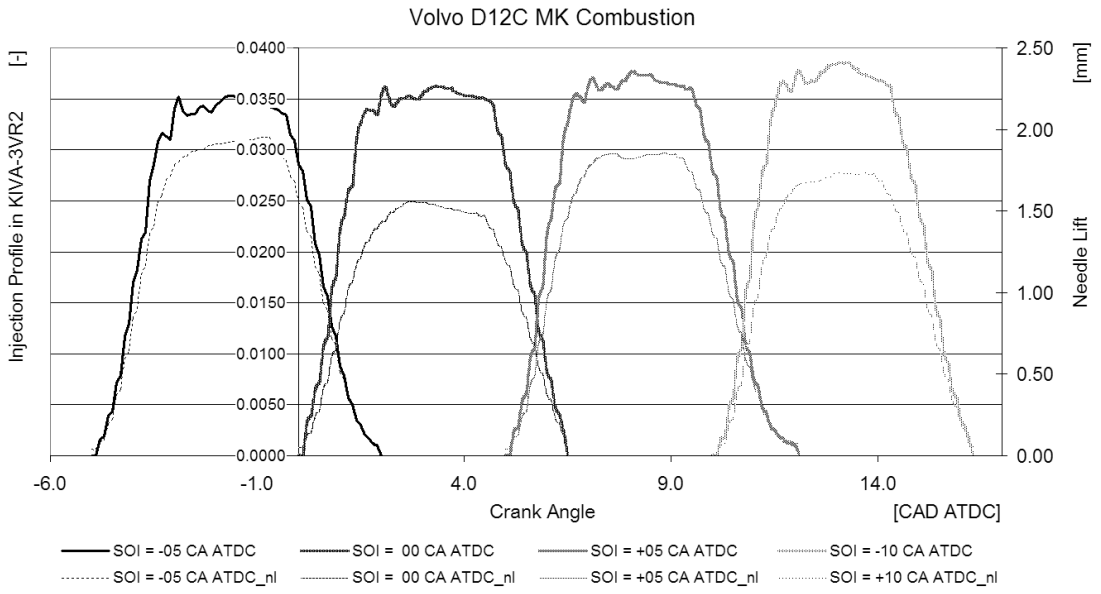

Figure 7.13 Measured needle lift (dotted line) and injection profile (continues line) used in KIVA-3VR2 for MK Combustion simulation cases

Main injection parameters of the KIVA-3VR2 simulations were given in Table 7.3 which was taken from itape5 file of the KIVA-3VR2 simulations. Spray inclination angle and cone angle are adjusted according to the experimental values. A proper SMR value was selected. There were small variations for the simulation parameters in Table 7.3 because of the stability of the code. For example, although fuel amount was same for all cases, one can see small variations in the simulations mostly due to obtain a stable simulation condition which the code will not crash. Spray angle, SMR, fuel amount, the shape of the injection profile can cause severe problems in the simulations, hence, sometimes small chages were made to overcome this deficiencies.

Table 7.3 Main injection parameters of MK Combustion simulations

SOI [CAD ATDC]		**-5.0**	**0.0**	**5.0**	**10.0**
Injection Mode	[-]	Vel. Table	Vel. Table	Vel. Table	Vel. Table
Injected Mass	[mg]	60.8	63.9	64.8	62.3
Injection Pressure	[bar]	~ 700	~ 700	~ 700	~ 700
Injection Duration	[CA]	7.0	6.5	7.1	6.3
Injection Velocity	[m/s]	300-500	300-500	300-500	300-500
Initial Droplet Temperature	[K]	350	350	350	350
Sauter Mean Radius, SMR	[m]	1.17E-04	1.12E-04	1.17E-04	1.13E-04
Spray Inclination Angle	[°]	153.0	153.0	153.0	145.0
Spray Cone Angle	[°]	12.5	13.5	12.5	13.0

7.5.2.2 Example Calibration Case of the KIVA-3VR2

These modeling results which are shown above were obtained with fine tuning of the code, e.g., related subroutines. Subgrid scale length scale (sgsl), initial turbulence kinetic energy density (tkei), activation energy and rate of the reactions (here, a global reaction: $C_7H_{16} + O_2 = HCO + H_2O$), turbulence/chemistry interaction (PaSR) are among the examples of the possible parameters which can be tuned. Below it is given an example about how to tune the code to get similar results with the experiments for case SOI = +10 CAD ATDC. Table 7.4 gives the tuned parameters.

Table 7.4 Tuning example for the code

SOI [CAD ATDC]		**1st trial**	**2nd trial**
sgsl (itape5)	[-]	0.5	0.5
tkei (itape5)	[(cm/s)**2]	0.2	0.3
E(J) (chem.dat) $C_7H_{16} + O_2 = HCO + H_2O$	[J/mol]	28000	28500
capa_mix (chemcell.f)	[-]	0.01	0.01

For this particular example, there were differences between calculated values (calc.) of start of pressure and RoHR increase with experiment results (exp.). As it can be seen in Figure 7.14, it was aimed to delay start of combustion to obtain better agreement with the experiments.

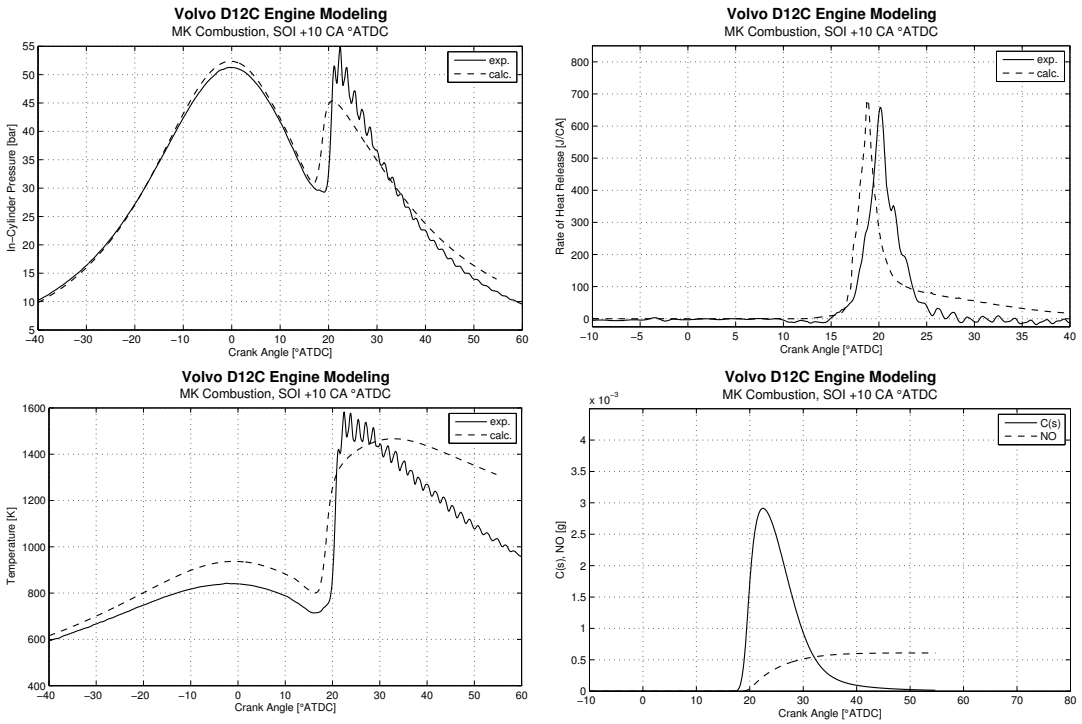

Figure 7.14 Tuning example: SOI = 10 CAD ATDC, 1st trial: There are discrepancies between start of pressure and RoHR increases.

The parameters were changed as shown in Table 7.4. This moved the starting place of pressure and RoHR increase.At the first trial, the peak pressure CA was 20.9 CAD ATDC with 45.3 bar (see Figure 7.14) and at the second trial the peak pressure CA became 22.3 CAD ATDC with 44.8 bar (see Figure 7.15). Also at the first case, the peak RoHR CA was 18.9 CAD ATDC with 676 J/CA bar (see Figure 7.14) and at the second trial the peak RoHR CA became 20.2 CAD ATDC with 722 J/CA (see Figure 7.15).

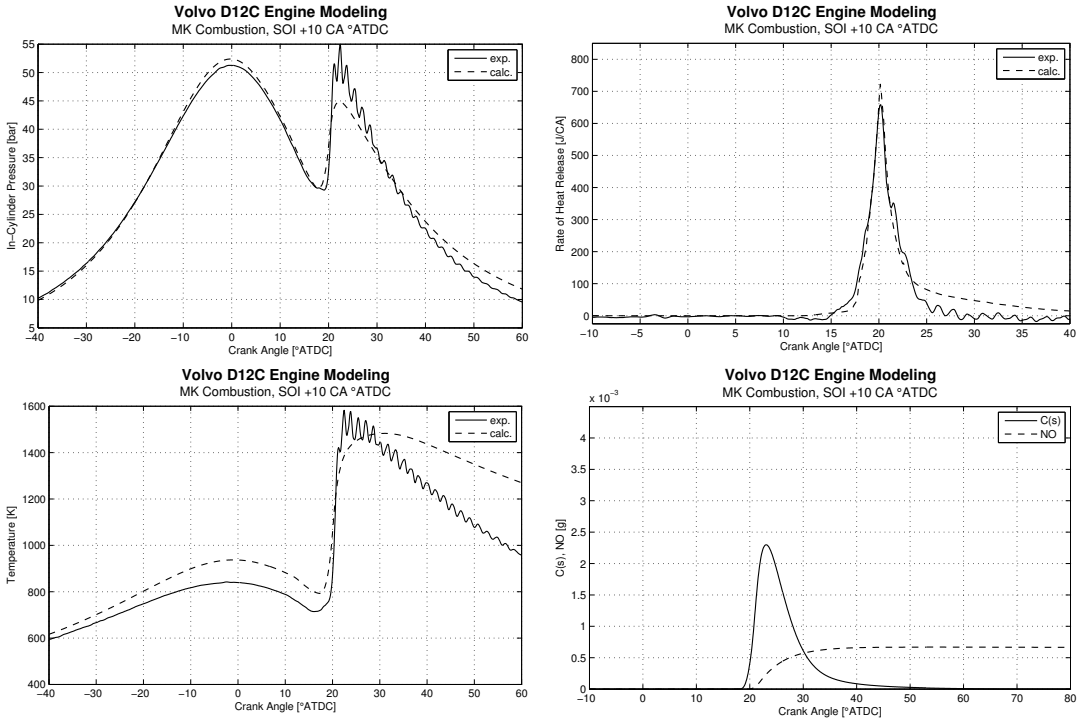

Figure 7.15 Modeling, SOI = 10 CAD ATDC, 2nd trial: Better agreement with the experiments

Although there is no significant difference for the average in-cylinder temperature, soot formation was decreased for the 2nd trial. It is probably due to premixed combustion characteristics of this case. Because the injection is too late and all combustion takes place in premixed mode.

7.5.2.3 Modeling Results and Comparison with Experiments

At first, it was proved that MK combustion regimes were predicted in an agreement with the experimental data. The comparisons were carried out in terms of in-cylinder pressure and RoHR, vs. CAD for SOI = -5, 0, 5 and 10 CAD ATDC. The predicted trends clearly indicate that the combustion mode shifts from conventional diesel-like to the HCCI, Homogeneous Charge Compression Ignition, mode following from

early to late injection cases. The predicted pressure and RoHR are compared with the experimental data and the results are presented in Figure 7.16 and Figure 7.17.

Here, the calculated RoHR values correspond to the integrated HR of all chemical reactions; the integrated RoHR was compared with the diesel oil lower heating value (42.5 MJ/kg) to evaluate the combustion efficiency. The same value for diesel oil surrogate represented by a blend of n-heptane and toluene was found ~ 45 MJ/kg. This accuracy is supposed to be sufficient to evaluate the combustion completeness [38].

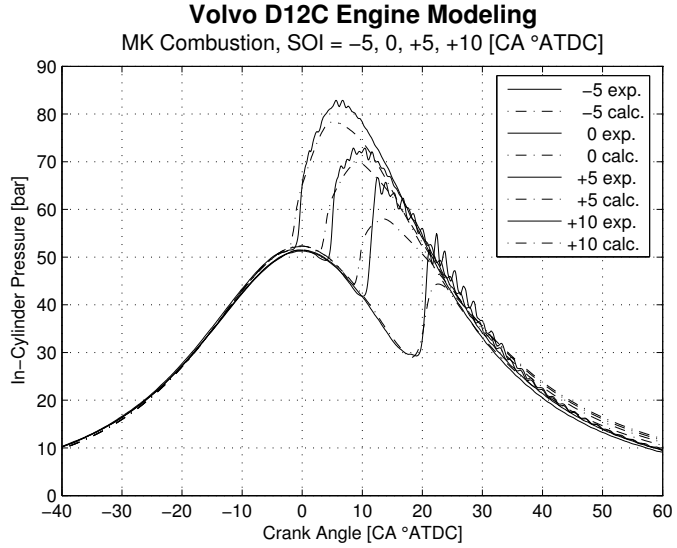

Figure 7.16 Comparison of predicted and measured in-cylinder pressure for SOIs = -5, 0, +5, +10 CAD

It can be seen that calculated in-cylinder pressures (see Figure 7.16) and RoHR distributions (see Figure 7.17) are in good agreement with experiments. For all cases calculated maximum pressure was slightly lower than the experiments. The difference between calculated and experimental peak pressures increases for the late injection cases. Actually, this proves the difficulties of premixed combustion simulation where chemistry is more dominant than the physical processes; hence, detailed reaction mechanisms are needed. For this reason at late injection cases, the role of reaction mechanism in the calculations increased and it became relatively harder to simulate these HCCI-like modes. Except SOI = 5 CA ATDC case, start of combustion is quite well reproduced. RoHR calculations illustrate the transition from the conventional diesel combustion to the premixed combustion mode (see Figure 7.17).

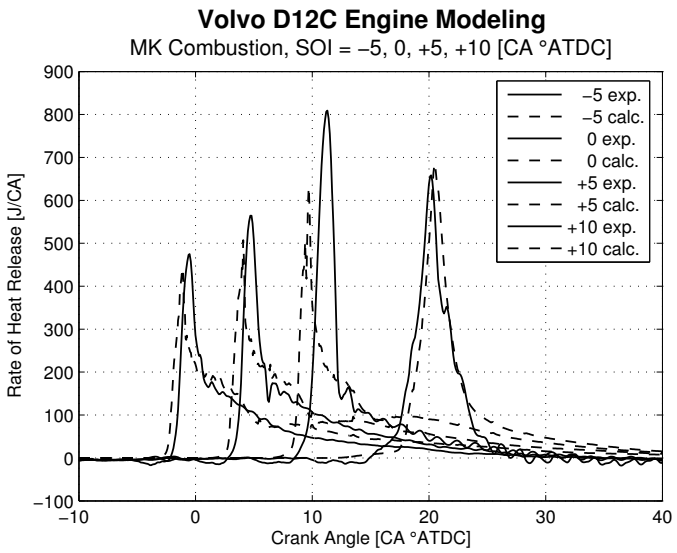

Figure 7.17 Comparison of predicted and measured RoHR for SOIs = -5, 0, +5, +10 CAD

From experimental observations [169], it follows that the RoHR in the course of conventional diesel spray combustion development has two distinct phases. The first one is characterized by a high RoHR (rapid pressure growth), while the second phase is more gradual (see Figure 6.1). The first stage is called premixed combustion and is the result of combined effects of auto-ignition and flame propagation. The second stage is referred to as the mixing controlled, since it develops after the fuel spray is fully surrounded by the flame and combustion is the diffusion controlled process. In these MK Combustion cases this conventional RoHR character was not occurred (see Figure 7.17). If fuel injection takes place after the TDC such as SOI = +5, +10 CAD ATDC cases of MK Combustion, the auto-ignition starts after a period of "cold" flow development under conditions of dropping pressure and temperature. As observed such an ignition can occur at several regions simultaneously and then rapidly spreads over the all chamber volume similar to the HCCI.

Below, a perspective view from KIVA-3VR2 simulation of SOI = -5 CA ATDC case is given in Figure 7.18 for CA = 5 ATDC. This moment is close to the peak value of the soot formation.

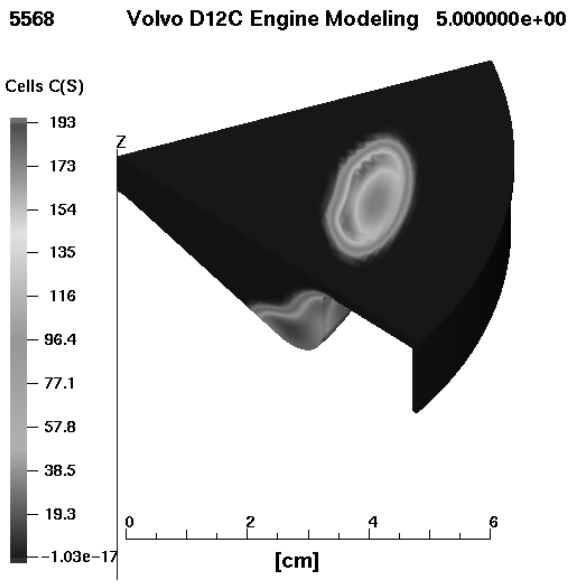

Figure 7.18 Soot distribution of KIVA-3VR2 simulation for SOI = -5 CAD ATDC

And for the same case above, NO distribution is given in Figure 7.19.

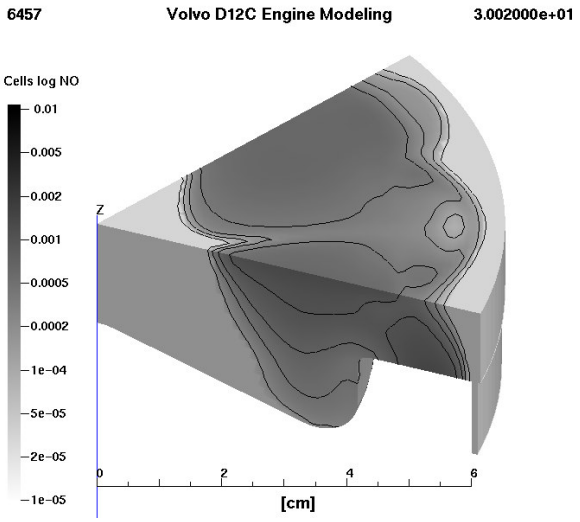

Figure 7.19 NO distribution of KIVA-3VR2 simulation for SOI = -5 CAD ATDC

Different from soot formation, the peak NO formation results in the late stages of combustion, because of the slow rate of the NO reactions. Figure 7.19 shows NO distribution for CA = 30 ATDC which is close to the maximum NO value of the cycle. After this stage, NO formation slows down and saturates because in the expansion stroke in-cylinder temperature decreases. In other words NO formation frezees. Cutplane views of the same simulation give detailed spatial distribution of soot and NO emissions (see Figure 7.20).

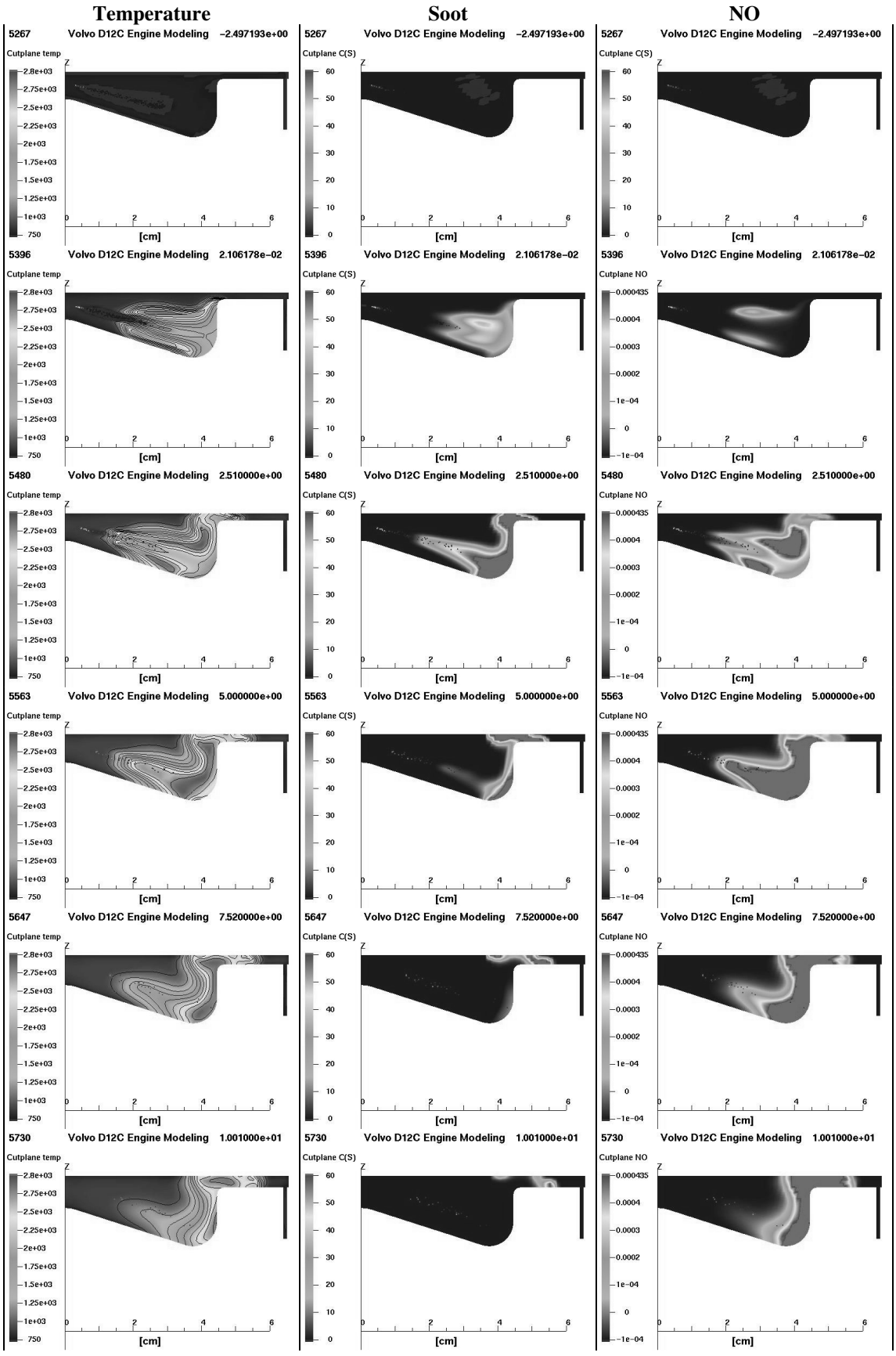

Figure 7.20 MK Combustion modeling : Variation of in-cylinder temperature and soot and NO emissions for SOI = -5 CA ATDC

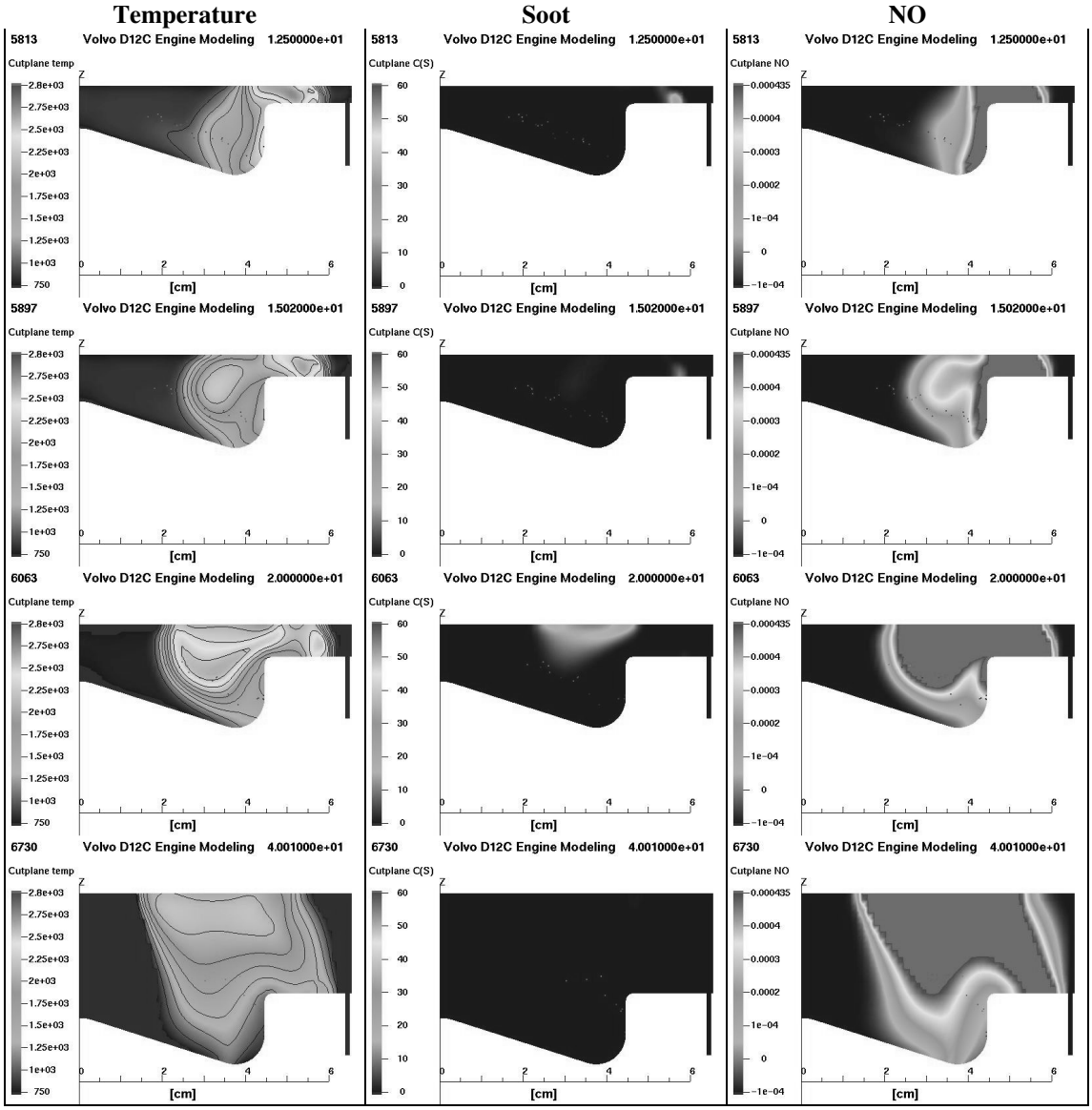

Figure 7.20 MK Combustion modeling: Variation of in-cylinder temperature and soot and NO emissions for SOI = -5 CA ATDC continued

To facilitate the analyse, temperature, soot and NO emission variations were given side by side in Figure 7.20 in three columns respectively. SOI = -5 CA ATDC and ignition occurs about -2 CA ATDC as can be seen from temperature column above. Simulation results approves the exected emission behavior, in which, while in low temperature regions soot emissions were dominant, in high temperature regions NO emissions was high. Also maximum soot formation occurs between 5-20 CAD ATDC then oxidation consumes the formed soot. NO formation starts from TDC and continues to the latest figure (40 CAD ATDC). Actually most of the NO formation was completed at 30 CAD ATDC and there was not any significant NO increase after then. Other slice views for SOI = -5, +5 were given in Figure 7.21.

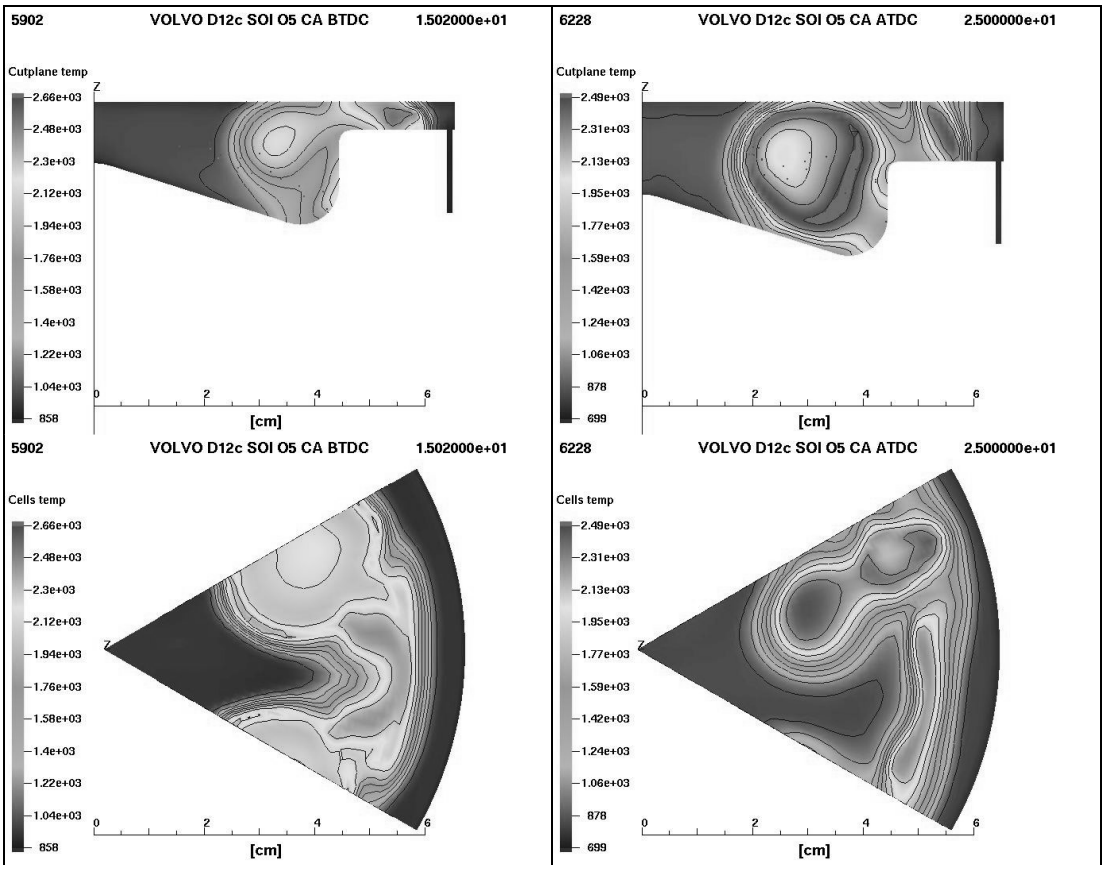

(a) (b)

Figure 7.21 MK Combustion modeling: In-cylinder temperature slice and top view for SOI = a) -5 and b) +5 CA ATDC cases

In Figure 7.21 in-cylinder temperature was shown 20 CAD after SOI for both cases. Resulted maximum temperatures are quite similiar for both cases. Also in the top views it is possible to see spray-spray interaction. For SOI = -5 CAD ATDC, spray-spray interaction was stronger. And spray penetration is slightly different between two cases. For the late injection case, SOI = +5 CA ATDC, it is evident that, high temperature region is more close to the piston bowl. Also, evaporation is not enough for the late injection case. One can see more droplets in the slice view of SOI = +5 CA ATDC (Figure 7.21b) than the early injection case, SOI = -5 CA ATDC (Figure 7.21a)

Change of NO and soot emissions for all cases in the combustion chamber per cycle were given in Figure 7.22. In Figure 7.22, soot formation is only drastically changed for the very late injection case, SOI = 10 CAD ATDC. Maximum soot formation was observed at SOI = 0 CA ATDC. Because of the premixed characteristics of late injection (SOI = 10 CA ATDC) although soot formation were suppressed, NO formation was increased.

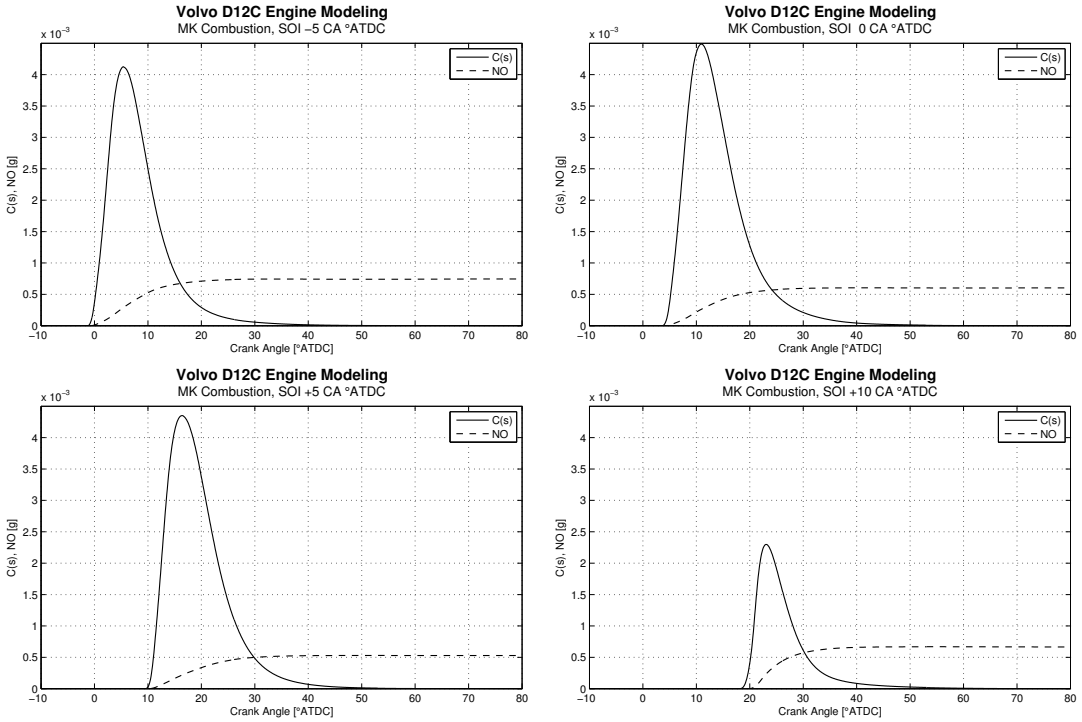

Figure 7.22 MK Combustion modeling: Soot and NO emission variation per cycle

In Figure 7.23 variation of average in-cylinder temperature was given. For all cases, calculated average in-cylinder temperatures were higher than the experiments. This is probably due to heat loses calculation deficiency of the code or wrong estimation of the initial mixture composition. Although these MK Combustion cases are EGR free, in fact, there is some residual gas in the initial mixture.

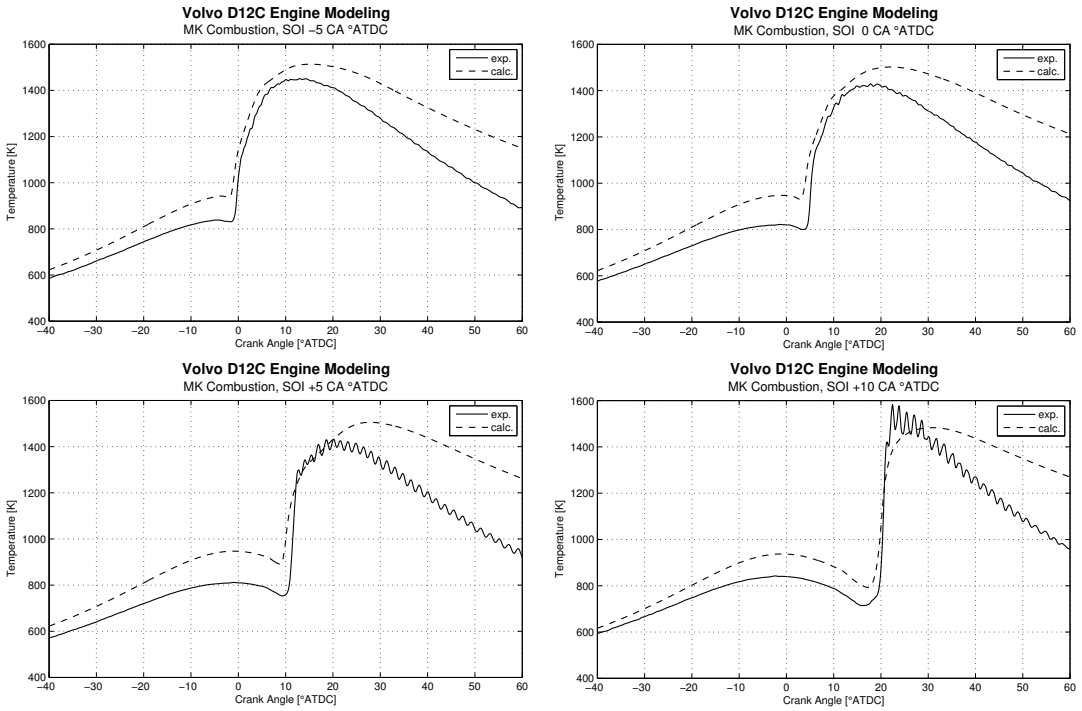

Figure 7.23 MK Combustion modeling: Average in-cylinder temperature variation

But in this study, these residual gas was not accounted and this may cause these differences for the temperature. On the other hand, the temperature tendencies represent the SOI behaviour as expected. And for SOI = 10 CA ATDC, the steep pressure rise is clearly visible which proves that this case was most close to the fully premixed combustion.

The comparisons of predicted and measured NO_x, soot (C(s)) and CO levels are presented in Figure 7.24 and Figure 7.25, respectively, to illustrate an accuracy of the emission formation calculations. Predicted emissions were calculated at IVC point. From data in Figure 7.24 and Figure 7.25b, it follows that the tendencies of NO_x and CO formation are correctly reproduced.

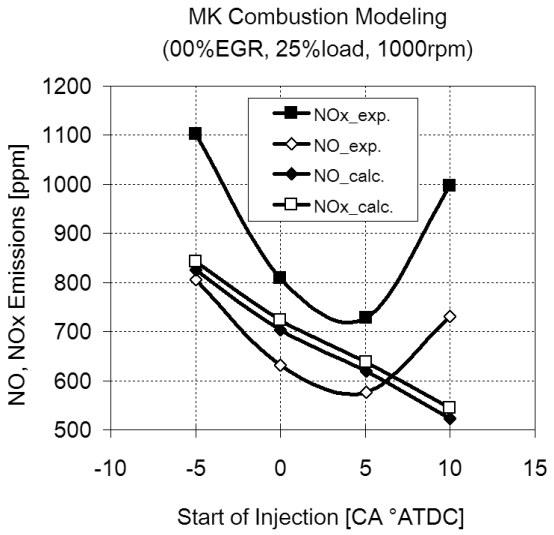

Figure 7.24 Measured and calculated NO and NO_x emissions

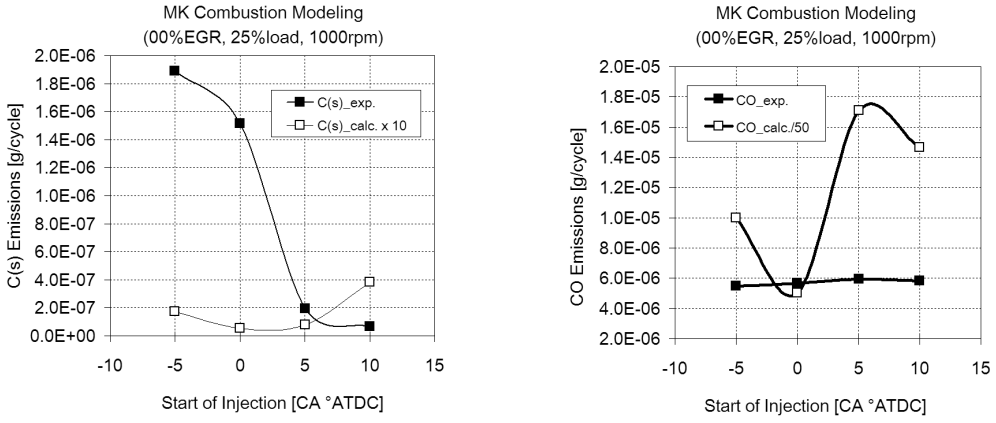

(a) (b)

Figure 7.25 Measured and calculated emissions: a) C(s) and b) CO

The discrepancies between predictions and measurements (especially soot emissions, see Figure 7.25a) can be explained that accurate modeling based on the detailed chemistry requires a proper balance between NO_x formation, soot oxidation producing CO and CO oxidation into CO_2. It will be the matter of a future work. To characterize the problem, let us note that while NO_x formation paths at low temperatures are as follows:

$$NO + HO_2 \longrightarrow NO_2 + OH \tag{3.98}$$

$$N_2O + O \longrightarrow NO + NO \tag{7.1}$$

$$N_2O + OH \longrightarrow N_2 + HO_2 \tag{7.2}$$

for high temperatures a conventional Zel'dovich mechanism is valid [38].

7.5.3 0D Numerical Modeling (Parametric Map Technique)

The MK Combustion modeling with parametric ϕ-T map technique illustrate that the MK combustion in terms of emissions formation and combustion efficiency is well characterized by the approach. Details of this map technique were given before. It can be illustrated that for the MK Combustion case, combustion trajectories are crossing the regions of emission formations only during a small fraction of the engine operation cycle. The high combustion efficiency can be concluded by inspecting the CO and HC maps. The optimized (high efficiency, low emissions), Premixed Charged Compression Ignition, PCCI, combustion regime similar to that described in [122] was confirmed.

The examples of the parametric maps constructed for MK Combustion EGR-free cases are presented in Figure 7.26 for SOI = 0 CA ATDC case. Soot-NO, C_2H_2 and CO species are shown in the figure. When a cluster of cells intersect these peninsulas of emissions (NO_x or soot) formation, see Figure 7.26, it characterizes their formation process. These three species are important and can represent basic diesel combustion characteristics, e.g, beside Soot-NO, acetylene, C_2H_2 for the formation of soot precursors, CO for the products of non-complete combustion are selected. One of the main advantages of this developed parametric map analysis is that it is possible to obtain the maps of different chemical species of interest.

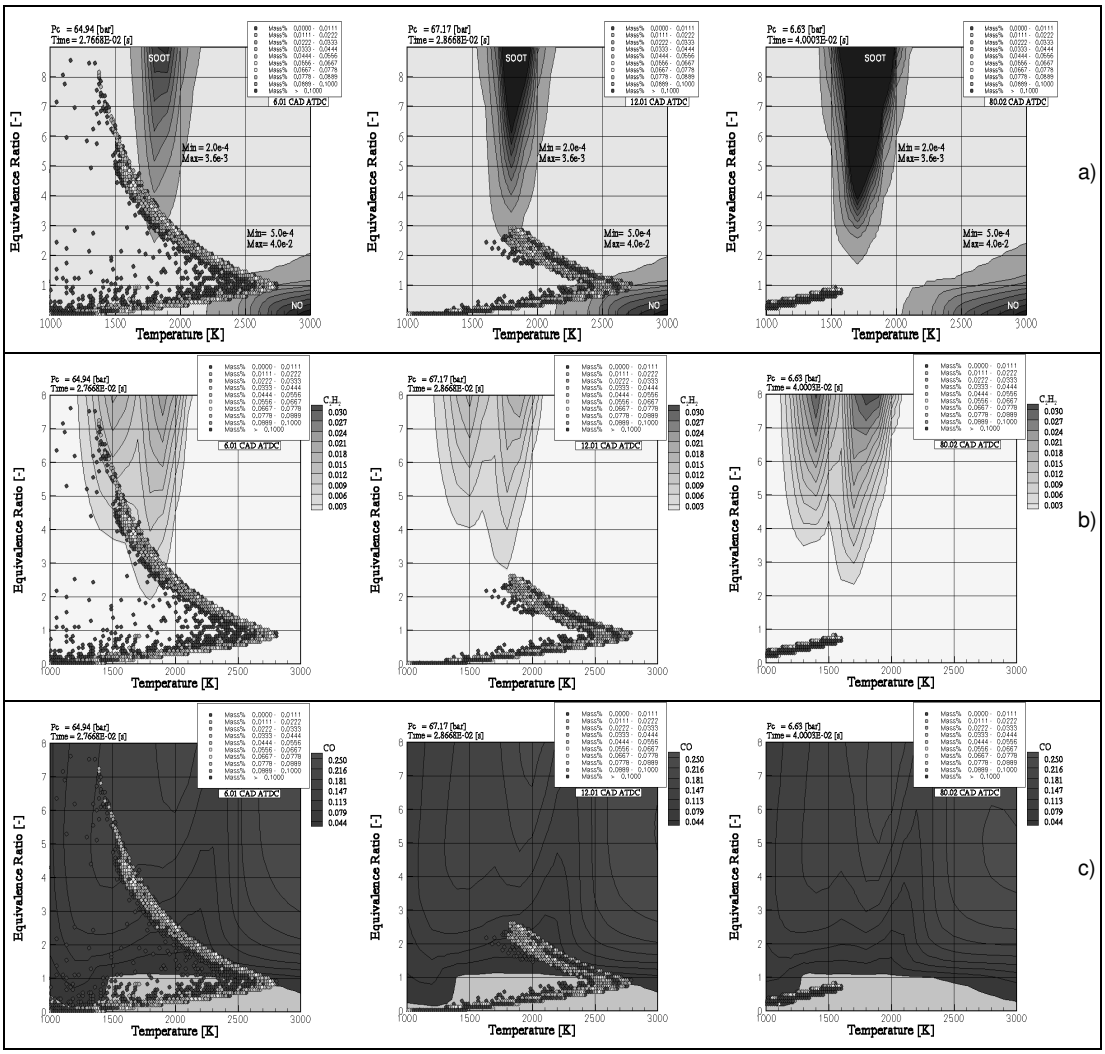

Figure 7.26 Emission formation and combustion efficiency analysis for 00% EGR load case by using a) Soot-NO, b) Acetylene and c) CO ϕ-T parametric maps, SOI = 0 CAD ATDC, in–cylinder cell conditions correspond to 6.01, 12.01 and 80.02 CAD ATDC, respectively

7.6 Extended MK Combustion Analysis and Effect of EGR Loads

As it is summarized previously in Figure 7.7, there are lots of possible simulation cases for the extended MK Combustion analysis, including EGR. Extension of the MK Combustion analysis was based on only simulations. It is accepted that previously simulated four experimental cases are reference for the KIVA-3VR2 and SENKIN simulations. At first, all cases where SOI = -60, -40, -30, -20, -15, -10, -05, 00, +5, +10 were considered. For the simulations earlier than -5 CA ATDC, injection parameters were taken same as the -5 CA ATDC case. And it was not aimed to tune the code for those earlier injections. Below in Figure 7.27, first simulation results are given for very early injection, SOI = -60 and -40 CA ATDC cases.

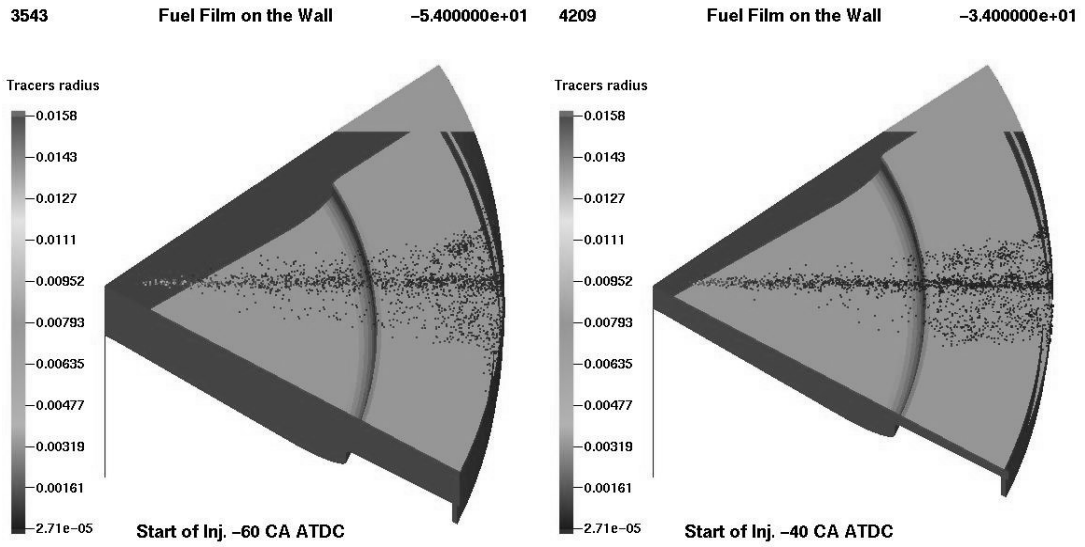

(a) (b)

Figure 7.27 Very early injection cases, SOI = a) -60 and b) -40 CAD ATDC

As it can be seen above, for the very early injection cases, there was no proper evaporation and mixture formation. Fuel spray wholly hitted the wall and even there was no combustion for SOI = -60 CAD ATDC. For that reason these two cases were eliminated from extended analysis cases.

7.6.1 EGR Iterarion Number

One of the most important questions is "How much iteration is sufficient for EGR calculations?" Answer of this question would define also the number of simulations which were necessary for the extended MK Combustion analysis (see Figure 7.28). Remember that at initial plan in Figure 7.7 for each case two EGR iterations were considered. Hence, before starting to all simulations, a detailed study was made to decide if two iterations are really necessary or what can be the minimum EGR iteration number for a particular case. By this way it is possible to rearrange, probably reduce, the number of simulation points.

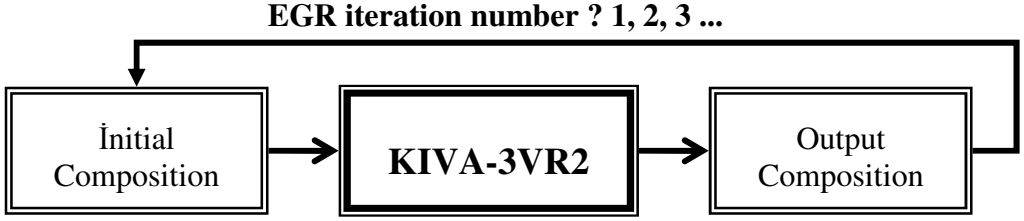

Figure 7.28 EGR iteration: Output composition takes place input compostion

Below in Figure 7.29, for a selected case, SOI = -10 ATDC, two iteration results were compared.

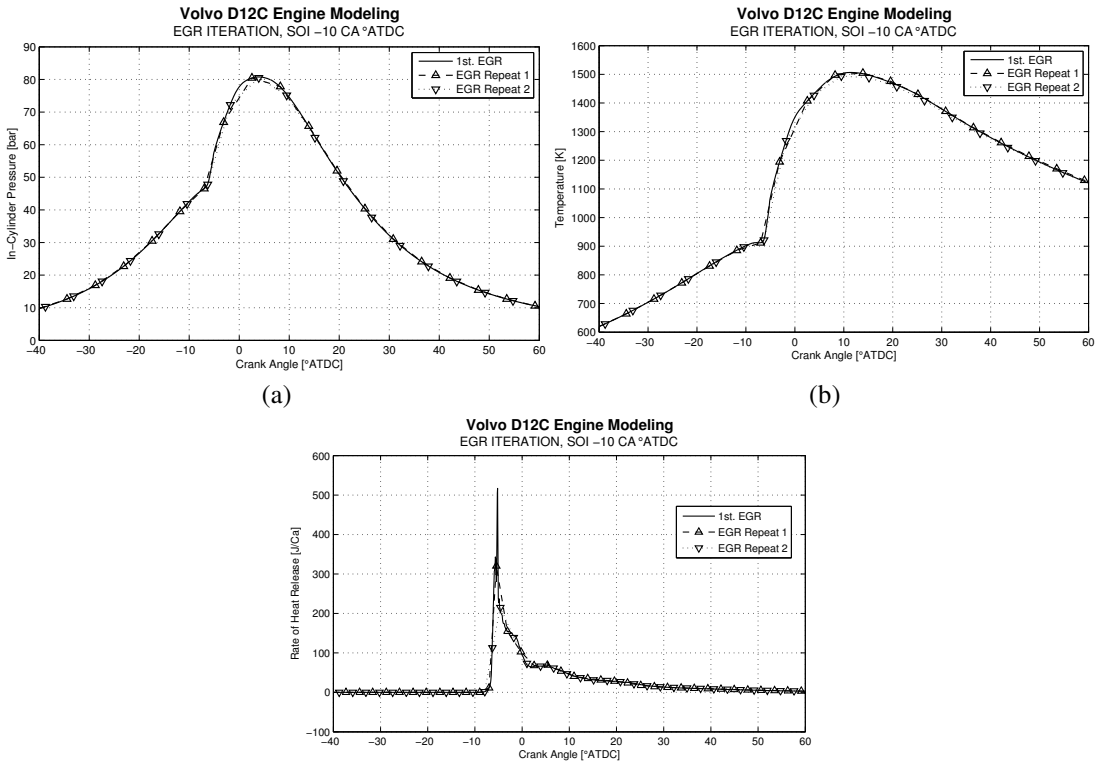

Figure 7.29 Effect of EGR iterations for a) In-cylinder pressure, b) Average temperature and c) RoHR

There is no considerable difference between two or one EGR iteration considering in-cylinder pressure, temperature and RoHR (Figure 7.29). Also for emission values, the situation is same. There is only a slight decrease for the NO emissions with the second iteration (see Figure 7.30). In general, one iteration is acceptable.

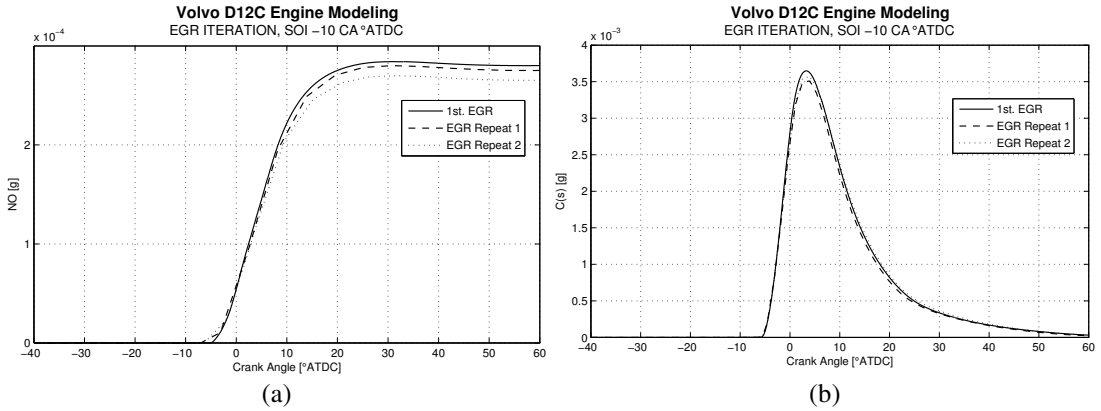

Figure 7.30 Effect of EGR iterations for a) NO b) Soot emissions

Hence, the simulation plan was modified from Figure 7.7 to the Table 7.5 by excluding SOI = -60 and -40 cases and considering one EGR iteration. So, total simulation cases were reduced to 24 KIVA-3VR2 and 24 SENKIN simulations.

Table 7.5 Extended MK Combustion analysis simulation cases

SOI	-30	-20	-15	-10	-5	+0	+5	+10
00% EGR	KIVA-3V	KIVA-3V	KIVA-3V	KIVA-3V	KIVA-3V	KIVA-3V	KIVA-3V	KIVA-3V
	SENKIN	SENKIN	SENKIN	SENKIN	SENKIN	SENKIN	SENKIN	SENKIN
20% EGR	KIVA-3V	KIVA-3V	KIVA-3V	KIVA-3V	KIVA-3V	KIVA-3V	KIVA-3V	KIVA-3V
	SENKIN	SENKIN	SENKIN	SENKIN	SENKIN	SENKIN	SENKIN	SENKIN
50% EGR	KIVA-3V	KIVA-3V	KIVA-3V	KIVA-3V	KIVA-3V	KIVA-3V	KIVA-3V	KIVA-3V
	SENKIN	SENKIN	SENKIN	SENKIN	SENKIN	SENKIN	SENKIN	SENKIN

7.6.2 Extended Analysis with 3D-CFD Numerical Modeling (KIVA-3VR2)

To optimize the engine combustion process, the studied SOI range was extended by those early injection cases given in Table 7.5. The in-cylinder pressures calculations for EGR-free cases are summarized in Figure 7.31.

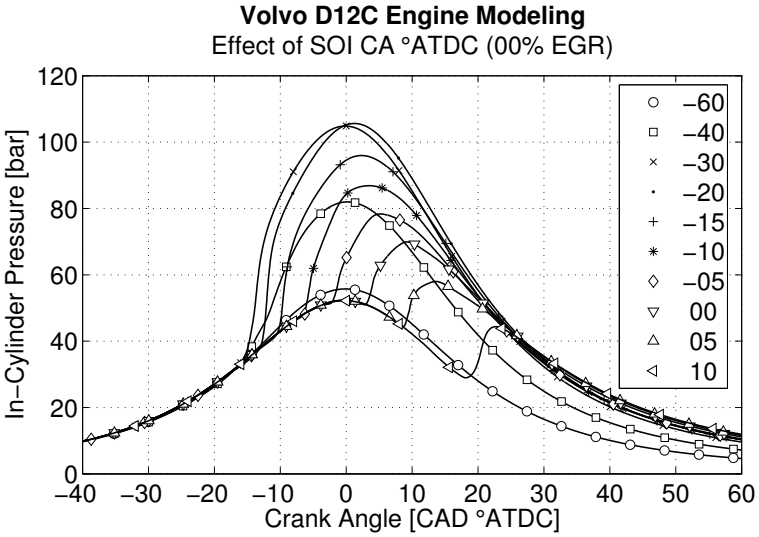

Figure 7.31 Comparison of predicted in-cylinder pressure for 00% EGR

At first, one can see from the pressure curve of SOI = -60 CAD ATDC case that there was no combustion. Also for SOI = -40 CAD ATDC, although the mixture could be ignited, the intense of combustion was very poor. The reason of these combustion problems were explained before with the observed fuel film on the walls resulting very bad mixture formations (Figure 7.27). Hence, these two cases SOI = -60 and -40 were eliminated hereafter.

Also Figure 7.32 and Figure 7.33 show in-cylinder pressures for 20% and 50% EGR cases. Maximum pressure values decrease with the increasing amount of EGR.And for all cases, EGR-free and with EGR, maximum pressures were obtained at SOI = -30 and -20 conditions.

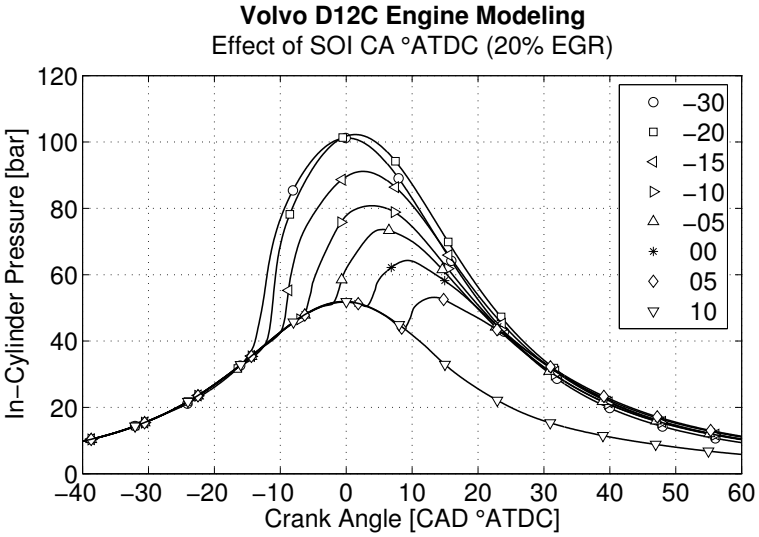

Figure 7.32 Comparison of predicted in-cylinder pressure for 20% EGR

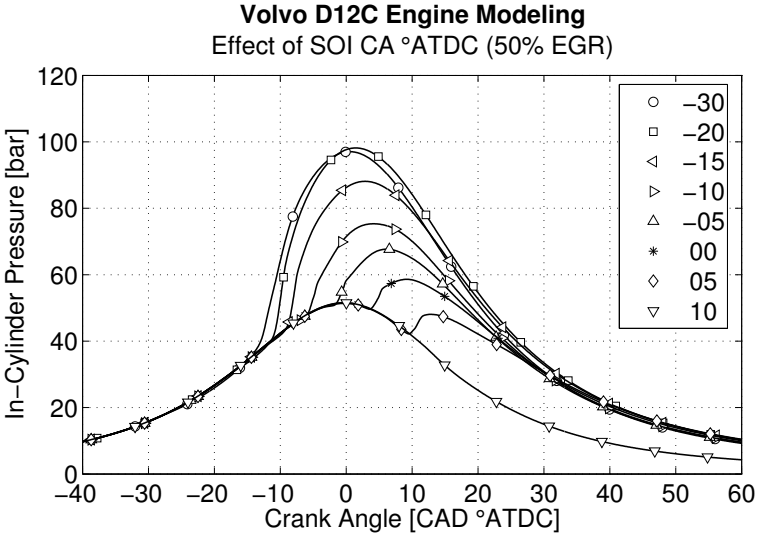

Figure 7.33 Comparison of predicted in-cylinder pressure for 50% EGR

For the very late injection case, SOI = 10 CAD ATDC, combustion could occur at only EGR-free case. With EGR applications it was seen that the mixture could not be ignited (see Figure 7.32 and Figure 7.33). This is probably due to the reduced temperature of the mixture at the end of the compression stroke because of the increased specific heat value of the mixure with EGR gases (see Figure 7.34). So the end-compression temperatures were not high enough to ignite the mixture for SOI = 10 CAD ATDC in EGR cases. Note that there was not any experimental data for this

case and it is not possible to judge exactly for this misfire. Another possibility for the reason of this lack of ignition may be the lack of the used reaction mechanism. Because it is hard to model the LTC conditions especially with EGR although detailed reaction mechanism was considered. A final note on pressure curves is that, for SOI = -30, -20, -15 the combustion characteristics seem to be similar to the HCCI combustion. The pressure rise is much sharper at these SOI cases.

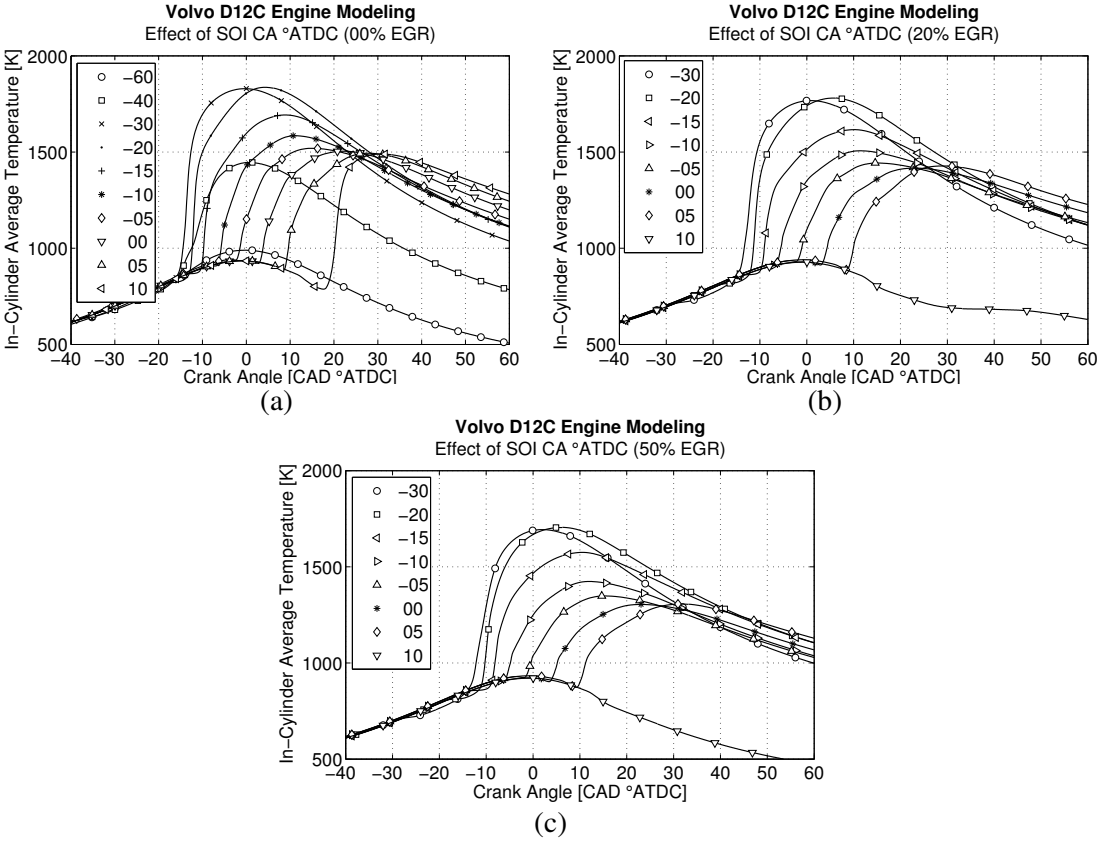

Figure 7.34 Effect of EGR on average in-cylinder temperature. Predicted average in-cylinder temperatures for a) EGR-free, b) 20 % EGR and c) 50 % EGR cases

In Figure 7.35 RoHR calculations are given for all 00% EGR cases. RoHR distributions show that early injections, e.g., SOIs = -30, -20, -15 can cause the rapid energy release rates with maxima to be higher than those for the later injections. Hence, the premixed combustion mode is more visible for these early injection cases. Also for the late injection cases, combustion mode tends to premixed mode again which can be seen with the increasing trend of RoHR distributions. But, different from early injection cases, because injections occur at the expansion stroke in decreasing pressure and temperature conditions, it results reduced RoHR peaks in comparison with the early injection cases.

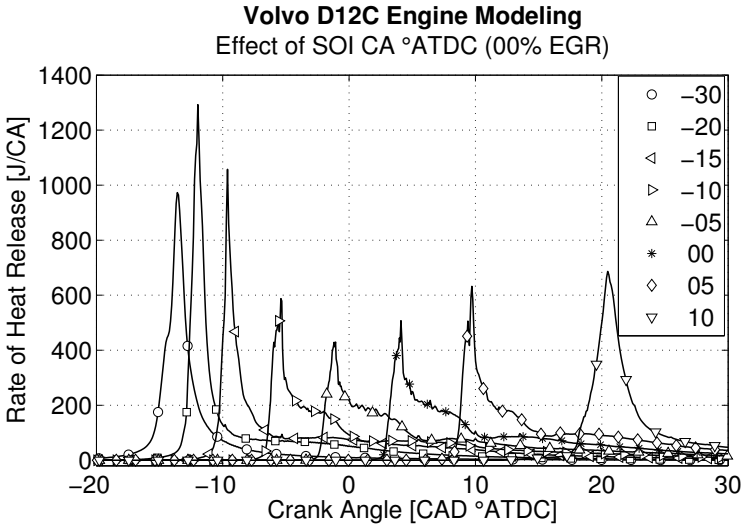

Figure 7.35 Comparison of predicted RoHR for 00% EGR

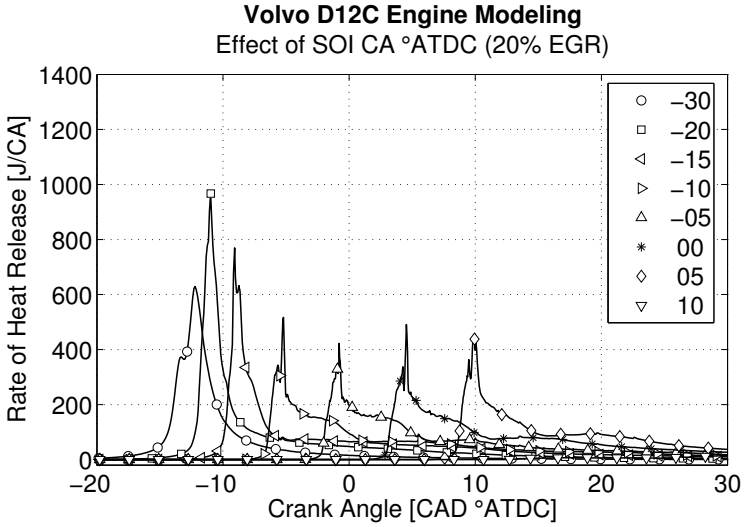

Figure 7.36 Comparison of predicted RoHR for 20% EGR

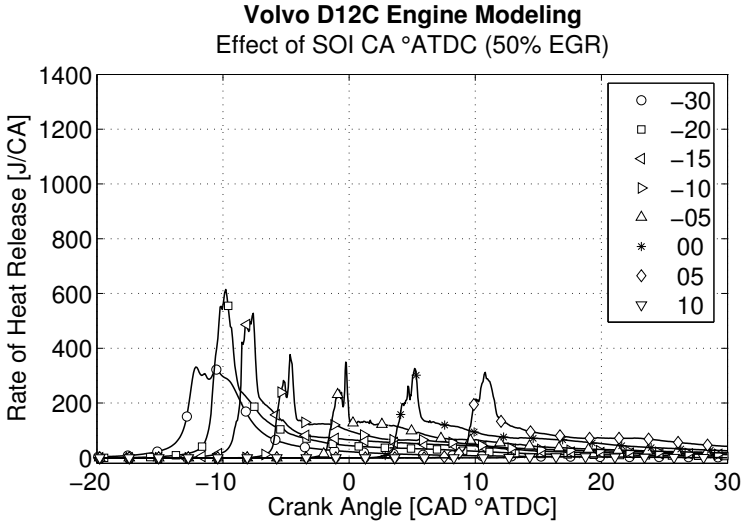

Figure 7.37 Comparison of predicted RoHR for 50% EGR

For 20% EGR load the RoHR peaks were reduced as expected (Figure 7.36). This reduction is even better pronounced for higher EGR loads such as 50 % EGR (Figure 7.37). Also note that, for 20 % EGR load condition, the increasing trend of RoHR distributions for the late injections was disappeared and even at 50% EGR load, the maximums of RoHR distributions were decreased.

Soot formation tendencies vs. SOIs for 00%, 20% and 50% EGR load mixtures are presented in Figure 7.38, Figure 7.39 and Figure 7.40, respectively. Since the engine experiments correspond to the 25% low load, predicted and measured soot levels at EVO were also low.

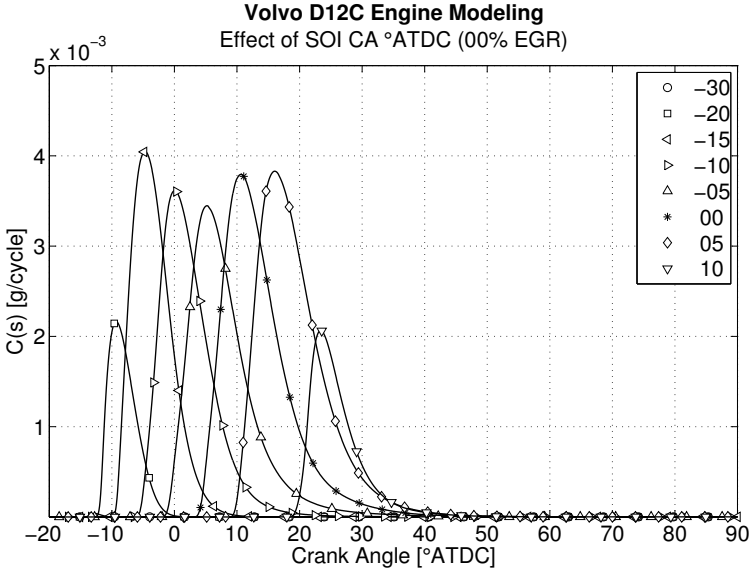

Figure 7.38 Comparison of predicted soot emissions for 00% EGR

The maximum soot values could be used in the evaluations to characterize the soot formation process. But for the exhaust soot emissions, maximum soot values are not a measure. Although maximum soot formation values are higher for early injection cases, in contrary, resulted end soot emissions are lower for these cases because of soot oxidation process. Figure 7.38 shows that for early injection cases, soot oxidation was completed earlier. For late injection cases (see Figure 7.39 and Figure 7.40), although soot formation is not so high such as early injection cases, soot oxidation is delayed and relatively higher amount of soot emissions are predicted at EVO.

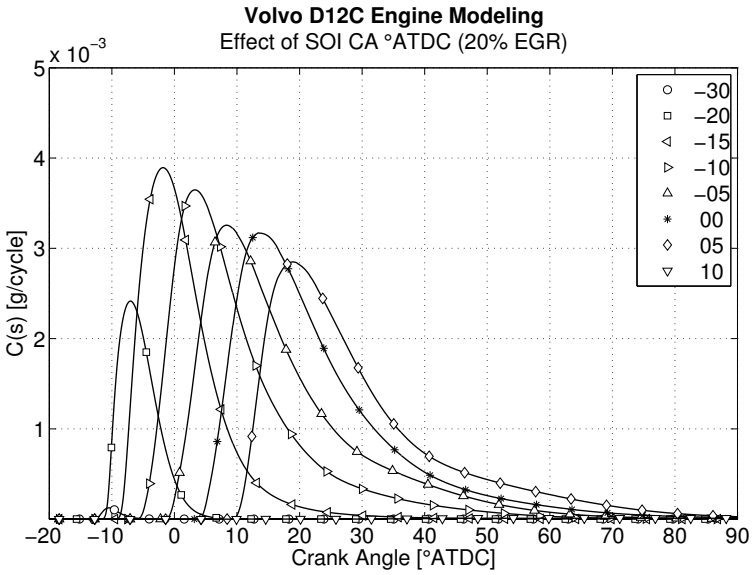

Figure 7.39 Comparison of predicted soot emissions for 20% EGR

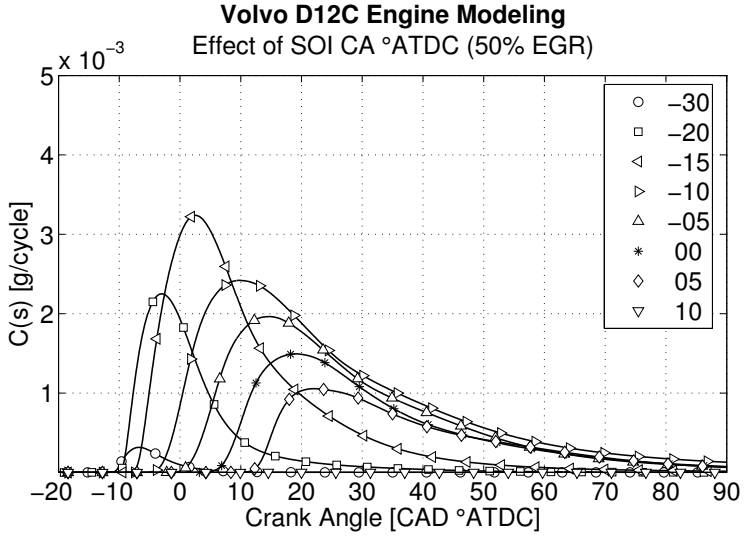

Figure 7.40 Comparison of predicted soot emissions for 50% EGR

The most noticeable effect of EGR was seen on NO emissions. In general, for early injections, because of the premixed combustion characteristics, NO emissions are higher (Figure 7.41). With 20% EGR load, nearly four times reduction was achieved in NO emissions (Figure 7.42) and 50% EGR load drastically suppresses NO formation (Figure 7.43).

Decreasing trend of NO emissions with the late injection only change for SOI = 10 CAD ATDC. Because of the very late injection, combustion mode is similar to the early injection cases and wholly premixed combustion increases NO emissions according to the previous case, SOI = +5 CAD ATDC.

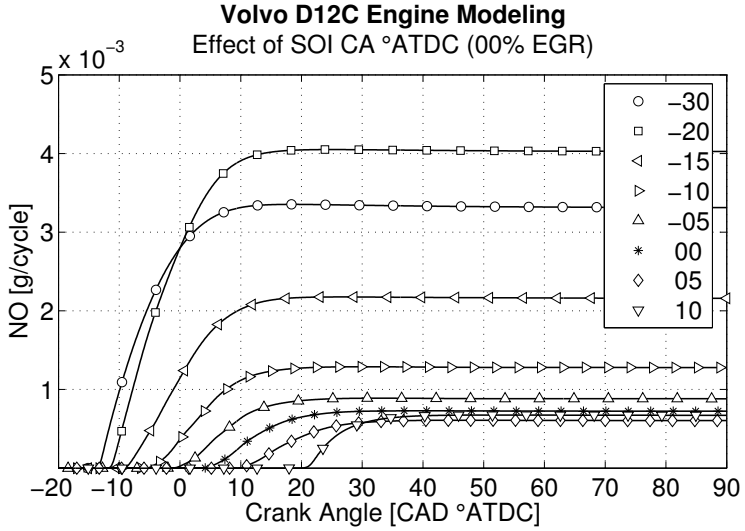

Figure 7.41 Comparison of predicted NO emissions for 00% EGR

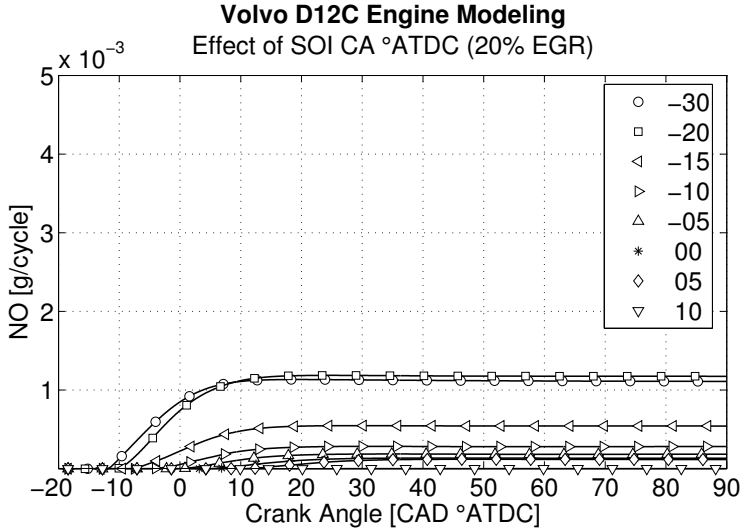

Figure 7.42 Comparison of predicted NO emissions for 20% EGR

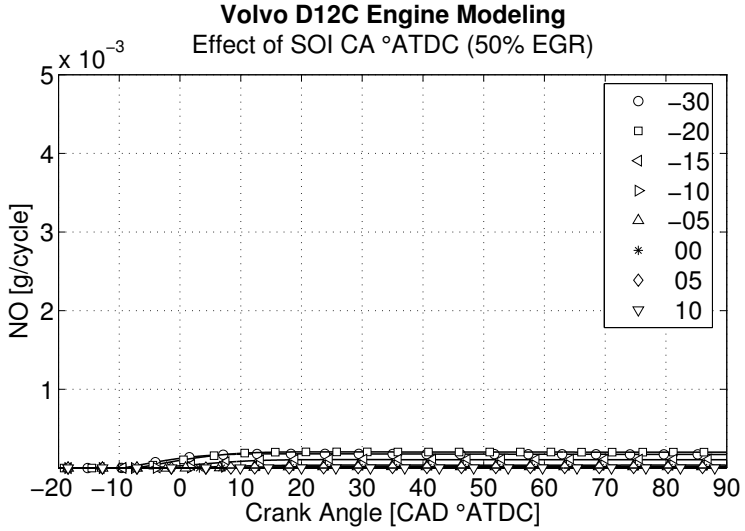

Figure 7.43 Comparison of predicted NO emissions for 50% EGR

Figure 7.44 shows KIVA-3VR2 NO_x emission simulation results. High EGR load and too late injection can lead to the misfire as it can be seen also in Figure 7.44 and Figure 7.45 for SOI = 10 CAD ATDC regimes (50% EGR load). In order to reduce the CO amount formed keeping low NO_x, concentration, different strategies were tested. One of them is to use earlier fuel injection as it was studied in [124].

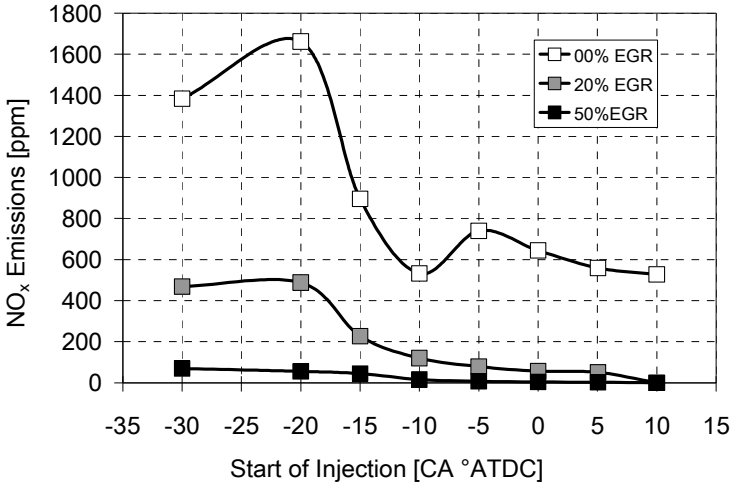

Figure 7.44 Overview of the simulated NO_x emissions for 00%, 20% and 50% EGR cases

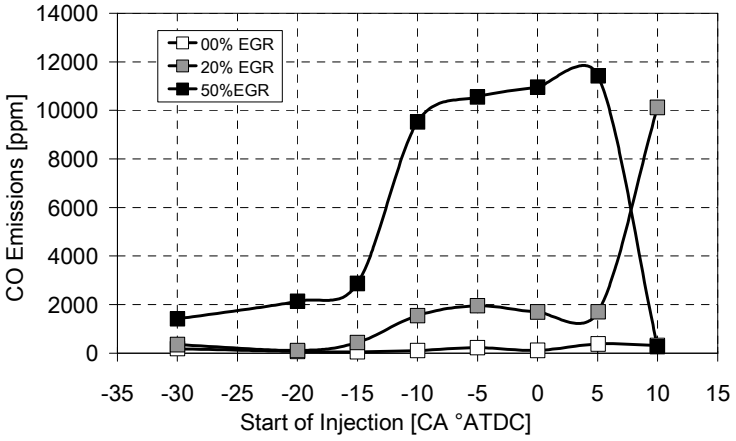

Figure 7.45 Overview of the simulated CO emissions for 00%, 20% and 50% EGR cases

Figure 7.46 shows the simulated soot emissions for all cases. For very early or late injections with the increased amont of EGR, it is possible to keep both soot and CO emissions lower. This behavior is similar to the premixed combustion together with high EGR in MK Combustion concept which was experimentally studied by Kimura et al [162 and 163].

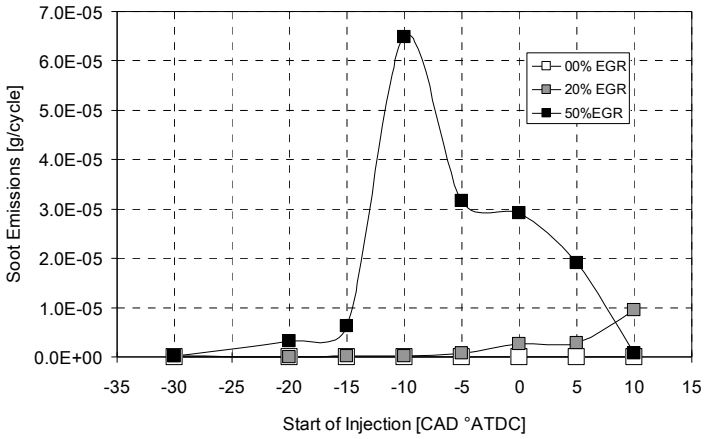

Figure 7.46 Overview of the simulated soot emissions for 00%, 20% and 50% EGR cases

7.6.3 Extended Analysis with 0D Numerical Modeling (Parametric Map Technique)

The simulated case in Figure 7.47 is 20% EGR case of the experimental results which were simulated before and was given in Figure 7.26. One can see differences between those two cases. For 00% EGR case, cell clusters representing combustion process intersect NO formation peninsula and can reach even up to ~ 2700 K temperature. Here in Figure 7.45 clusters intersect with emission formation peninsulas in different regions depending on the EGR load. For example, clusters which intersect with NO formation peninsula can reach lower, i.e., ~ 2400 K temperatures. So, from the ϕ-T map analysis, in the presence of the 20% EGR load, one can anticipate reduced amount of NO_x formed due to the reduced mixture temperature. Contrary, the amount of CO and soot formed will be increased for 20% EGR case as it can be seen in Figure 7.47.

These foresights are in a good agreement with direct engine modeling results for NO_x and CO concentrations presented in KIVA-3VR2 simulation results (see Figure 7.44 and Figure 7.45). This effect becomes more visible for higher EGR loads.

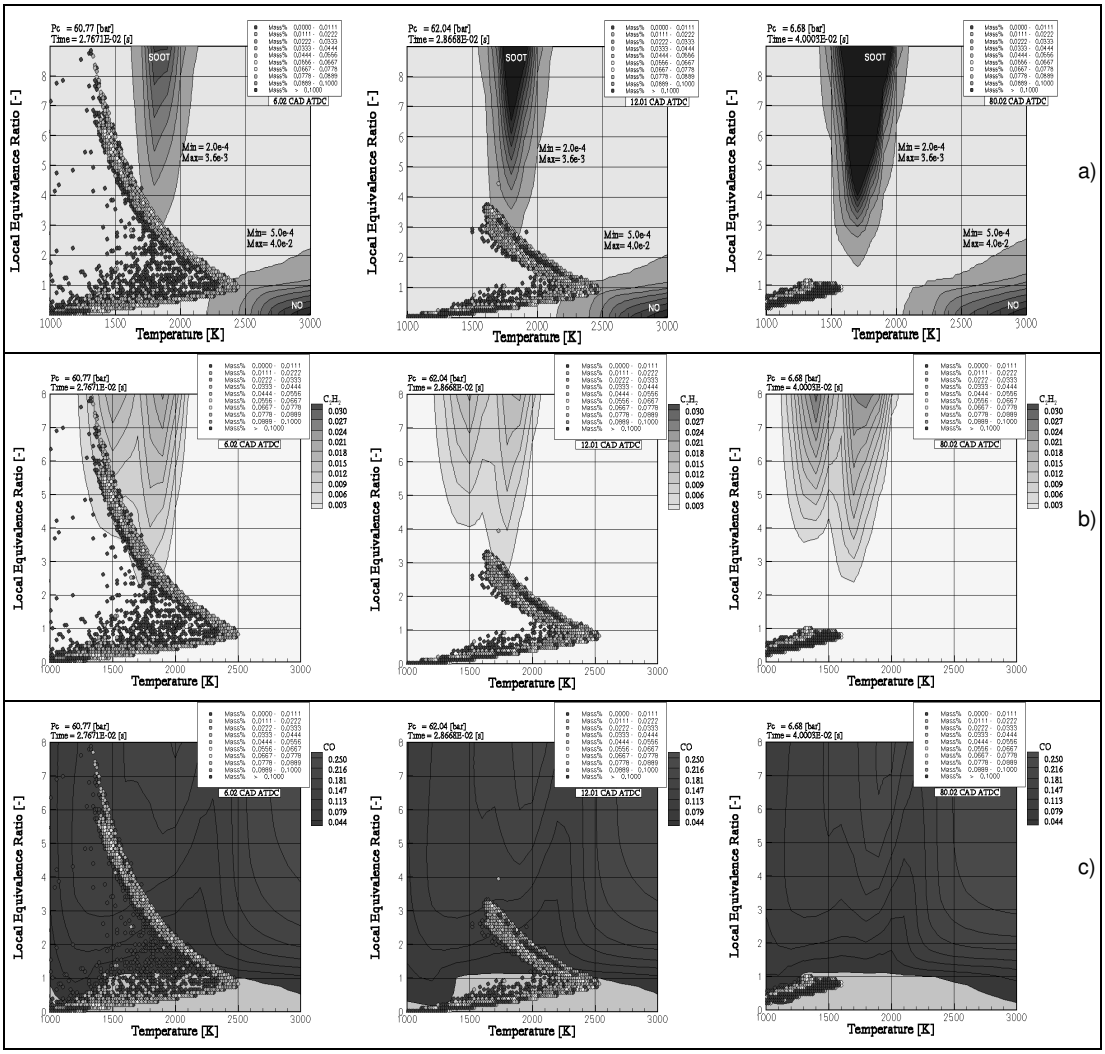

Figure 7.47 Emission formation and combustion efficiency analysis for 20% EGR load case by using a) Soot-NO, b) Acetylene and c) CO ϕ-T parametric maps, SOI = 0 CAD ATDC, in–cylinder cell conditions correspond to 6.01, 12.01 and 80.02 CAD ATDC, respectively

The parametric ϕ-T maps for the early injection case (SOI = -10 CAD ATDC) for EGR-free and 20% EGR load mixtures are presented in Figure 7.48 and Figure 7.49. From the soot-NO maps in Figure 7.48 one can expect the higher NO_x production than for retarded injections such as SOI = 0 CAD ATDC (see Figure 7.26). Contrary, CO levels are expected to be lower, as it can be also seen in Figure 7.45. To reduce the amount of NO_x, the usual remedy of EGR can be used without a substantial penalty in the CO and soot levels that can be concluded from comparing plots in Figure 7.48 and Figure 7.49.

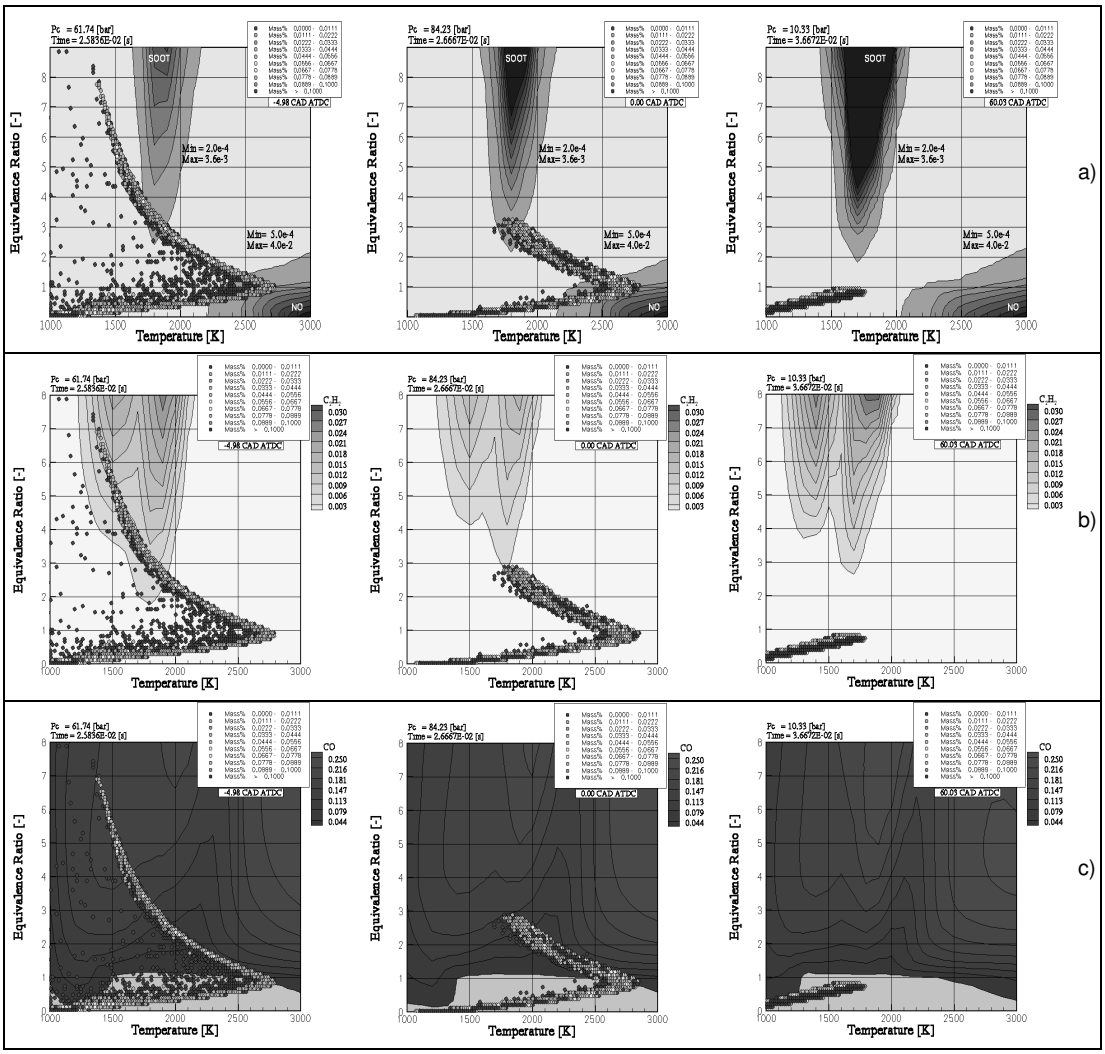

Figure 7.48 Emission formation and combustion efficiency analysis for 00% EGR load case by using a) Soot-NO, b) Acetylene and c) CO ϕ-T parametric maps, SOI = -10 CAD ATDC, in–cylinder cell conditions correspond to -4.98, 0.00 and 60.03 CAD ATDC

Also one can see the difference in, soot precursor, C_2H_2 formation between Figure 7.48 and Figure 7.49. C_2H_2 distributions are in agreement with the soot formation tendencies in the Soot-NO maps for the same figures. For boot soot and C_2H_2 species, the cell clusters intersect with the soot and C_2H_2 islands in Figure 7.48 and Figure 7.49. For 20% EGR case, increased amount of soot were simulated both in soot and C_2H_2 maps.

CO emissions are also increased with the EGR. This can be seen also in CO maps. Close to the end of combustion, CO islands were more intersected by the cell clusters in the 20 % EGR case (see Figure 7.49).

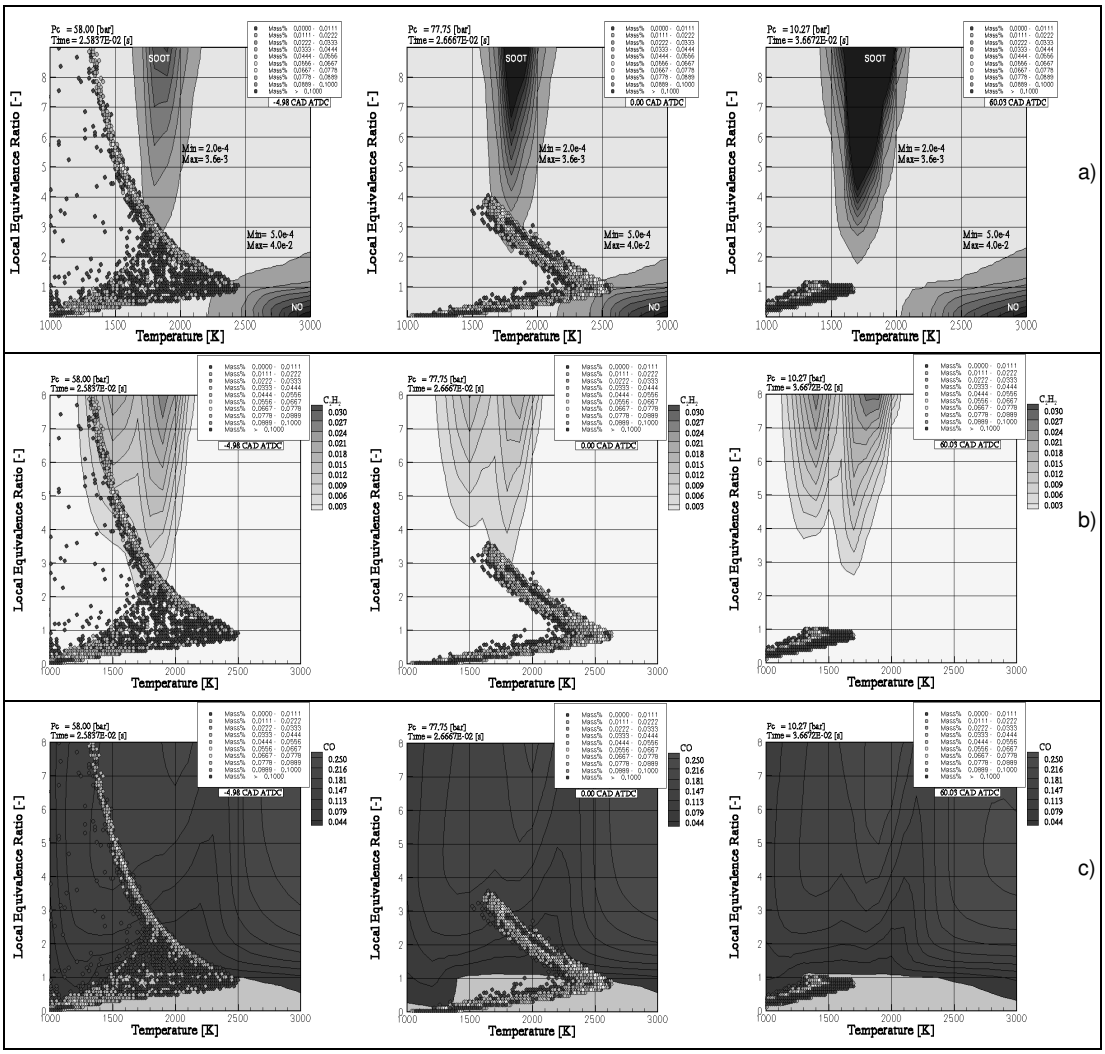

Figure 7.49 Emission formation and combustion efficiency analysis for 20% EGR load case by using a) Soot-NO, b) Acetylene and c) CO ϕ-T parametric maps, SOI = -10 CAD ATDC, in–cylinder cell conditions correspond to -4.98, 0.00 and 60.03 CAD ATDC

7.7 Analysis of Low Temperature (LT) Combustion

For low temperature combustion, different engine speed and EGR conditions were modeled. The engine is the same Volvo D12C engine. Differently from MK Combustion conditions, injection pressures and engine speed is higher and CR is lower for LT combustion cases. Main operating characteristics are given in Table 7.6. Here, experimental results for EGR cases are also available and it gives the opportunity to compare simulated EGR results with experiments also. The same reaction mechanism was used in LT Combustion simulations. The most critical part of LT Combustion modeling is determination of initial mixture composition. To define the EGR load, mainly measured species CO_2 were used and other EGR species were assumed according to literature [7].

Table 7.6 Low Temperature Combustion Experimental Cases

		EGR-free	30% EGR load
Engine speed	[rpm]	1500	1500
Engine load	[%]	25	25
Engine torque	[Nm]	71.4	74.78
Engine power	[kW]	11.22	11.74
Compression ratio	[-]	14.0	14.0
SOI	[CAD ATDC]	-9.0	-9.0
Injected mass	[mg]	63.12	63.07
Injection pressure	[bar]	1750	1750
Measured intake pressure	[mbar]	1500	1300

Simulated in-cylinder pressures are given in Figure 7.50 both for EGR-free and 30% EGR load conditions.

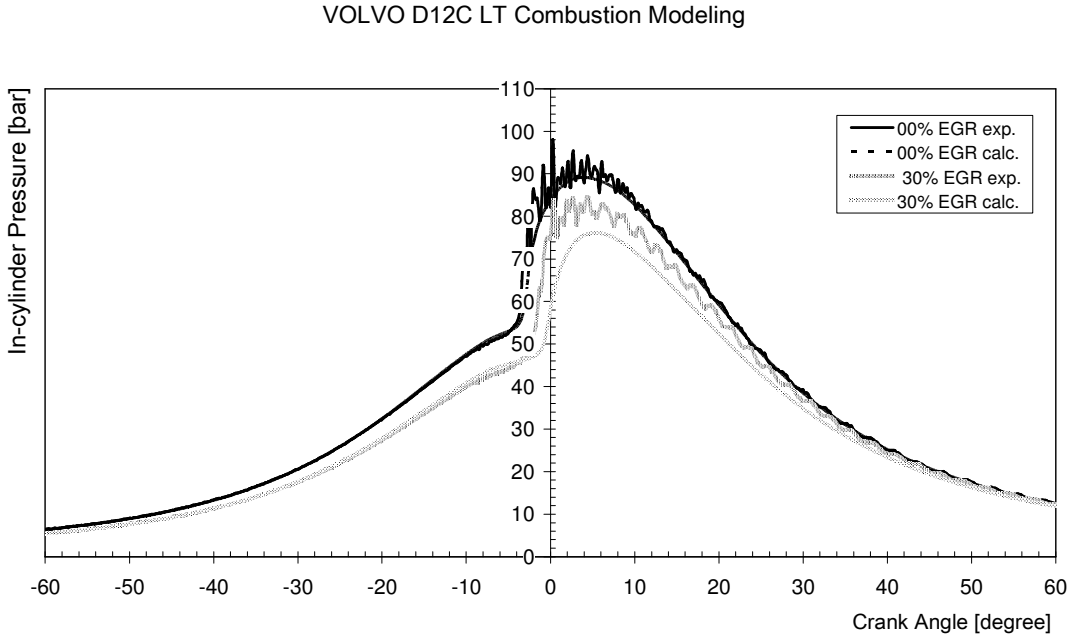

Figure 7.50 In-cylinder pressure distribution for LT Combustion modeling

Although for EGR-free case in-cylinder pressure distribution is predicted very well, for EGR cases there is slight decrease in the simulation pressure. Both compression and combustion pressures are predicted lower than the experiments. This can be because of the initial mixture gas composition or mass. Initial mixture mass was checked with the experimental results and, charge of the KIVA-3VR2 calculations are tuned considering the measured air mass flow, pressure and temperatures. Namely it is not possible to determine the average in-cylinder temperature at the IVC moment exactly because only intake pressure was measured and average temperature was calculated according to this measured pressure. Hence, using this measured pressure and calculated intake temperature, a certain calculated initial charge mass

was obtained. Then this initial mass was checked with the measured real air and fuel mass flow in the experiments. Nevertheless, there is still difference between experimental and calculated in-cylinder pressure curves.

RoHR variations are given in Figure 7.51 for the same EGR-free and 30% EGR cases.

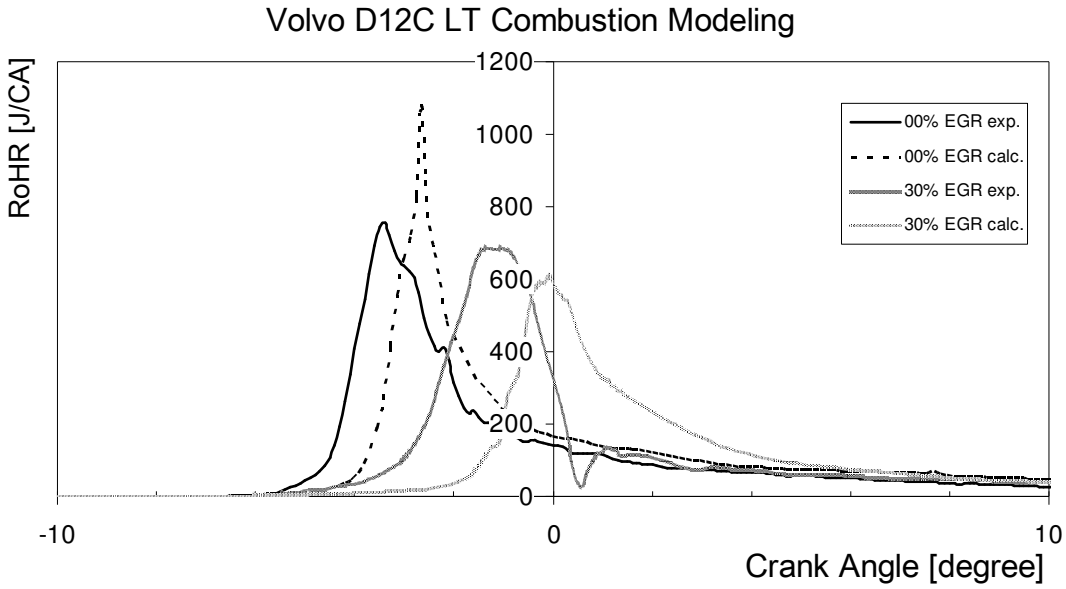

Figure 7.51 RoHR distribution for LT Combustion modeling

Above, for EGR-free and 30% EGR cases, there is a delay between experimental and predicted RoHR curves mostly due to the lower pressure and in-cylinder temperature values of the simulations. For EGR-free case, both peak values and corresponding CA values of RoHR are different. At 30% EGR case, although maximum values of the experimental and predicted RoHR curves are similar, there is still a delay for the calculated RoHR curves.

Also parametric ϕ-T map analysis result are shown for both 00% EGR and 30% EGR cases in Figure 7.52 and Figure 7.53. While from Figure 7.52, 00% EGR case, at CA = -2.5 CAD ATDC NO formation is visible, for the same case with 30% EGR there are no clusters from KIVA-3VR2 simulations which correspond to the temperature and ER area. This is probably because of the EGR; hence, the cell temperatures were below 1000 K which makes them invisible for these maps (see Figure 7.53). In order to better analyse this LT Combustion regimes, it is necessary to use temperature range lower than 1000 K in ϕ-T dynamic map technique.

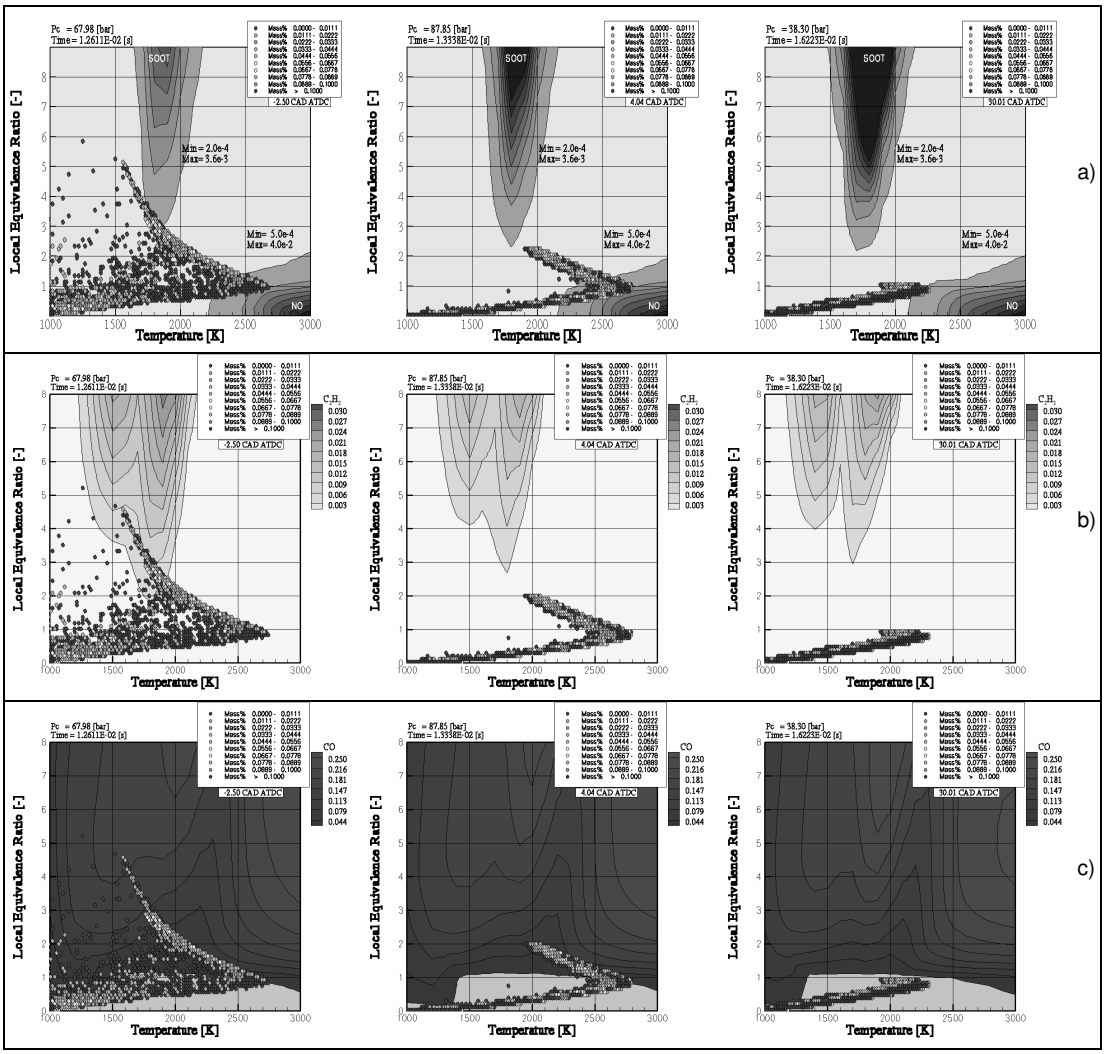

Figure 7.52 Emission formation and combustion efficiency analysis for LT Combustion, 00% EGR load case by using a) Soot-NO, b) Acetylene and c) CO ϕ-T parametric maps, SOI = -9 CAD ATDC, in–cylinder cell conditions correspond to -2.50, 4.04 and 34.01 CAD ATDC

30% EGR also increased soot tendency as can be seen from C_2H_2 and soot maps of the Figure 7.52 and Figure 7.53 especially for CA = 4.04 CAD ATDC. Also for EGR-free case, one can see from CO maps that the cell clusters don't intersect with CO emission formation area for 34.01 CAD ATDC (see Figure 7.52). For the same CA, with 30% EGR load, cell clusters intersect with CO emission formation area (see Figure 7.53).

These examples indicate that one can use this dynamic parametric ϕ-T map technique to identify emission formation regions in accordance with ER and temperature values and can suggest combustion concepts with proper paths to avoid emission formation. This evaluation method does not give quantitative results yet. It can be improved also to get quantitative results.

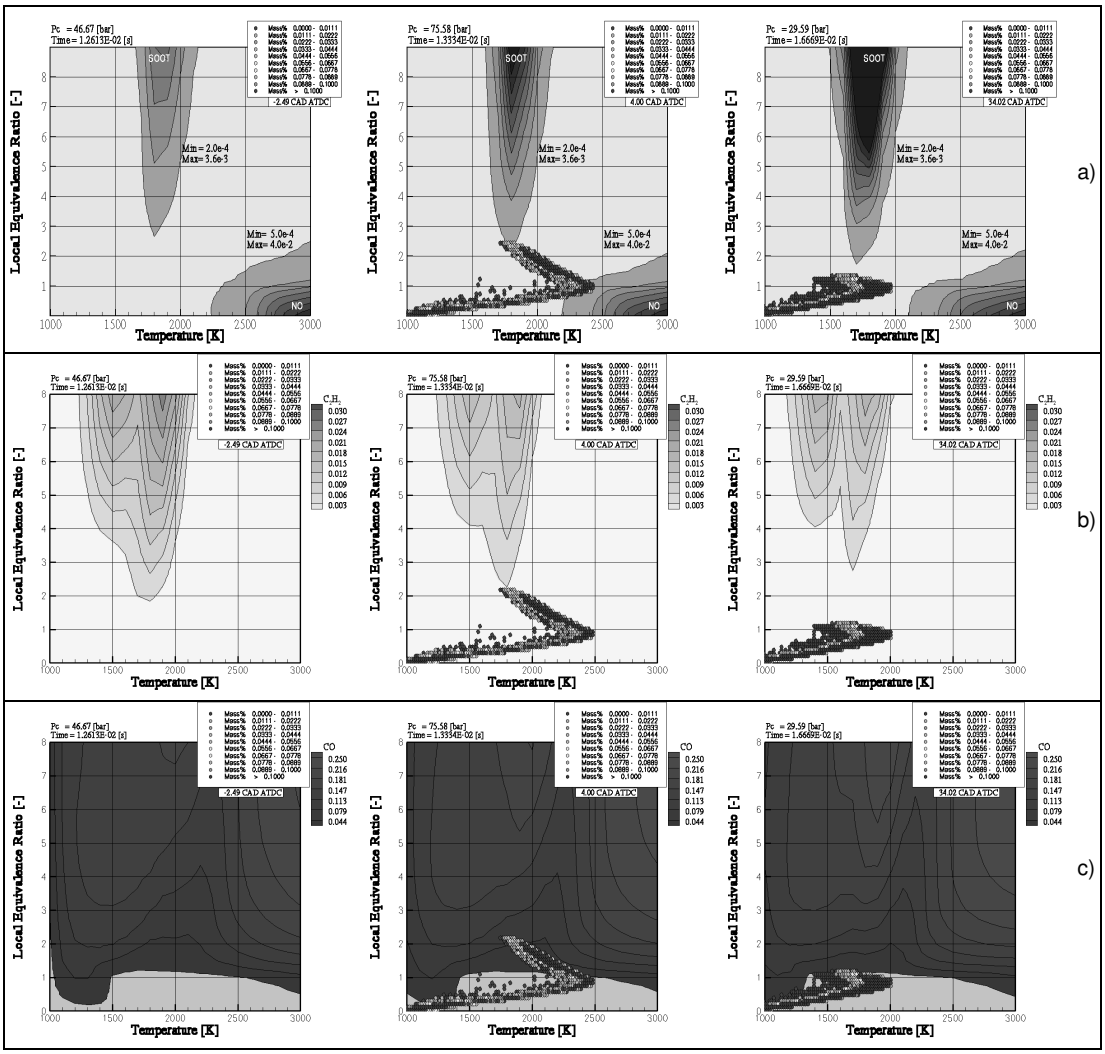

Figure 7.53 Emission formation and combustion efficiency analysis for LT Combustion, 30% EGR load case by using a) Soot-NO, b) Acetylene and c) CO ϕ-T parametric maps, SOI = -9 CAD ATDC, in–cylinder cell conditions correspond to -2.50, 4.00 and 34.02 CAD ATDC

Another advantage of this dynamic parametric ϕ-T map technique is simplification of the 3D simulation results on to 2D graphical representation. So, it becomes easier to judge about emission formation tendency of the whole combustion at any certain moment (specific CA), because all combustion chamber mass were classified and plotted over emission formation backgrounds according to predefined ER and temperature range values. Also, this map analysis enables to use simpler reaction mechanism with 3D CFD codes to get temperature and ER distribution and then by using detailed reaction mechanism in the parametric map technique it becomes possible to make further analyse of the 3D simulation results. Hence, it can be possible to eliminate use of time consuming detailed reaction mechanism in 3D simulations. This can be achieved if this map technique is further developed.

CONCLUSIONS

The study is planned for MK Combustion and LT Combustion analysis. Both combustion regimes include EGR-free and with EGR cases. These analyses were made by 3D KIVA-3VR2 code and 0D SENKIN code which enables a new technique, dynamic ϕ-T parametric map analysis. A detailed chemical mechanism was validated and used with both 3D and 0D simulations.

Set of spray combustion models developed at Combustion Division was applied to simulate combustion and emission formation in the VOLVO D12C diesel engine for EGR-free and different EGR load cases using KIVA-3VR2 code.

Experimental data was available for MK Combustion cases and LT Combustion cases. At first, the code was validated with the available experimental data of MK Combustion cases (reference cases) and then it has been used in the simulations.

The predicted and measured in-cylinder pressures and RoHR were found in a good agreement for MK Combustion cases and EGR-free LT Combustion cases. When EGR cases are considered in LT Combustion, pressure and RoHR curves are not well enough. Hence, the effect of high EGR load on the pressure and temperature distribution still requires explanation. We can only suggest that the observed affects are due to the complex initial mixture composition at high EGR loads. For LT Combustion regime, further study will be useful to find the reason of the differences of the simulation results from the experiments.

Different combustion modes characterized by different SOIs from early to retarded injections are analyzed including PCCI and MK combustion regimes. To summarize simulation quality we would like to outline that conventional diesel combustion better repreoduced than combustion for the retarded injection cases.

Different combustion modes for different EGR loads were analyzed. To prevent high CO and soot levels in the presence of EGR gases for retarded injections, the option of the earlier injection combined with the moderate EGR load is proved to be

advantageous for low emission complete combustion engine operation. This combustion mode can be referred to the PCCI combustion regime.

Soot-NO_x and CO formation tendencies were predicted in a reasonable agreement with experiments. Although tendency of the calculated emissions is in a good agreement with the experiments, a quantitative improvement of emission predictions is required. We found that selection of the proper proportions between soot oxidation, CO oxidation and NO_x formation rates is an important factor for accurate emission prediciton. This is because all these processes require same oxidizing species. If soot formation/oxidation rates are too high – a considerable amount of CO and not enough NO_x is formed.

In this study, the concept of the dynamic ϕ-T parametric map analysis has been extended and applied to the combustion and emission formation processes to analyze different compression ignition combustion modes in internal combustion engines. The maps constructed are time transient because the map parameters, such as pressures and elapsed times are corresponding to the values provided by the 3D engine modeling. The application of map analysis to these cases revealed the effect of EGR gases.

Emission formation and combustion efficiency can be predicted with the usage of parametric dynamic map analysis. The consistency of the map analysis technique is mature enough to use it as a common tool for analyzing combustion and emission formation processes. Hence, this dynamic parametric ϕ-T map technique should be a standard evaluation technique for the 3D engine combustion simulations.

One of the most advantegous improvement subject for this map analysis is to use simpler reaction mechanism with 3D CFD codes only to get temperature and ER distribution and then by using detailed reaction mechanism in the parametric map technique it is possible to make further analyse of the 3D simulation results. Hence, there will be no need to use detailed reaction mechanism in 3D simulations. This can be achieved if this map technique is further developed.

Further combustion cases, especially for LT Combustion modes, need to be simulated and validated with the available experimental data to investigate the EGR effect and to clarify the reason of insufficient predictions for LT Combustion cases with EGR.

REFERENCES

[1] **Warnatz, J., Maas, U. and Dibble, R.W.,** 1996. Combustion: Physical and Chemical Fundamentals, Modeling and Simulation, Experiments, Pollutant Formation, Springer-Verlag Berlin Heidelberg New York, Germany.

[2] **Lenz, H.P. and Cozzarini, C.,** 1999. Emission and Air Quality 1st Ed., SAE International.

[3] **Mondt, J.R.,** 2001. Cleaner Cars: The History of Emission Control Since the 1960s, SAE International.

[4] **Schaefer, F. and Basshuysen, R.V.,** 1996. Reduced Emissions and Fuel Consumption in Automobile Engines, Springer-Verlag New York, LLC.

[5] **BP,** 2006. BP Statistical Review of World Energy—June 2006, p.l.c., 1 St James's Square, London SW1Y 4PD, UK.

[6] **Kutlar, O.A., Arslan, H. and Calik, A.T.,** 2005. Methods to Improve Efficiency of Four Stroke Spark Ignition Engines at Part Load, *Energy Conversion and Management*, **46**, 3202-3220.

[7] **Heywood, J. B.,** 1988. Internal Combustion Engine Fundamentals, McGraw-Hill Series in Mechanical Engineering, Singapore.

[8] **Merker, G. P., Schwarz, C., Stiesch, G. and Otto, F.,** 2006. Simulating Combustion: Simulation of combustion and pollutant formation for engine development, Springer-Verlag Berlin Heidelberg, Germany.

[9] **Mehdiyev, R.I., Ergeneman, A. M., Arslan, H., Kutlar, O. A. and Çalık, A. T.,** 2003. Application of MR-Process in Diesel Engines (In Turkish), *1th Ege Energy Symposium and Exhibition*, Pamukkale University, Denizli, May 22-24.

[10] **Keating, E.L.,** 1993. Applied Combustion, Marcel Dekker, Inc. USA.

[11] **Dagaut, P.,** 2002. On the kinetics of hydrocarbons oxidation from natural gas to kerosene and diesel fuel, *Physical Chemistry Chemical Physic*, **4**, 2079-2094.

[12] **Cathonnet, M.,** 2003. Advances and challenges in the chemical kinetics of combustion, *Proceedings of the European Combustion Meeting 2003*, Paper 2, Orléans, France, October 25 – 28.

[13] **Glassman, I.,** 1996. Combustion-Third Edition, Academic Press Inc., USA.

[14] http://en.wikipedia.org/wiki/Alkanes, 2007.

[15] **Safgonul, B., Ergeneman, A. M., Arslan, H. and Sorusbay, C.,** 1995. Internal Combustion Engines (In Turkish), Birsen Yayinevi, Turkey.

[16] http://en.wikipedia.org/wiki/Alkene, 2007.

[17] http://en.wikipedia.org/wiki/Alkyne, 2007.

[18] http://en.wikipedia.org/wiki/Cycloalkanes, 2007.

[19] http://en.wikipedia.org/wiki/Polycyclic_aromatic_hydrocarbon, 2007.

[20] http://www.eia.doe.gov/cneaf/alternate/page/glossary.html, 2007.

[21] **ASTM D 613-05,** 2007. Standard Test Method for Cetane Number of Diesel Fuel Oil, *ASTM International*.

[22] **Andersson, J. D., Wedekind, B. G. A., Hall, D., Stradling, R. and Wilson, G.,** 2001. DETR/SMMT/CONCAWE Particulate Research Programme: Light Duty Results, *SAE Technical Papers*, **2001-01-3577**.

[23] **Linnaila, R.,** 2005. Status of Neste Oil's biobased NExBTL diesel production for 2007, *Automotive Biofuels International Conference*, Stockholm, Sweden, May 18-20.

[24] **Kalghatgi, G.T., Risberg, P. and Ångstrom, H.E.,** 2006. Advantages of fuels with high resistance to auto-ignition in late-injection, low-temperature, compression ignition combustion, *SAE Technical Papers*, **2006-01-3385**.

[25] **Kutlar, O. A., Arslan, H. and Calik, A. T.,** 1999. Studies Made on Otto Engine to Reduce Fuel Consumption in Partial Load Conditions Until Now: Variable Valve Timing and Lift, Variable Compression Ratio (In Turkish), *Union of Chambers of Turkish Engineers and Architects-Chamber of Mechanical Engineers Press*, **Vol. 477**, December.

[26] **Kutlar, O. A., Arslan, H. and Calik, A. T.,** 2001. A Review of Some Methods to Decrease the Fuel Consumption at Part Load of Four Stroke Spark Ignition Engine, *MOTAUTO 2001*, Varna, Bulgaria, December 17-19.

[27] **Mehdiyev, R.I., Kutlar, O. A., Arslan, H. and Calik, A. T.,** 2001. Two-Stage Combustion in a Stratified Charge Spark Ignition Engine for Reduced Emissions and Improved Fuel Ecenomy, *MOTAUTO 2001*, Varna, Bulgaria, December 17-19.

[28] **Kutlar, O. A., Arslan, H. and Calik, A. T.,** 2000. A Method to Decrease Fuel Consumption at Part Load Conditions in SI Engine: Lean Burn Stratified Charged Engine (In Turkish), *Union of Chambers of Turkish Engineers and Architects-Chamber of Mechanical Engineers Press*, **Vol. 483**, April.

[29] **Mehdiyev, R.I., Kutlar, O. A., Arslan, H. and Calik, A. T.,** 2002. An Ecological and Efficient Combustion Method for Engine Fuels (In Turkish), *IV. National Clean Energy Symposium*, İstanbul, Turkey, October.

[30] **Kutlar, O.A., Arslan, H. and Calik, A.T.,** 2007. Skip cycle system for spark ignition engines: An experimental investigation of a new type working strategy, *Energy Conversion and Management*, **48**, 370-379.

[31] **Kalghatgi, G.T., Risberg, P. and Ångstrom, H.E.,** 2003. A method of defining ignition quality of fuels in HCCI engines, *SAE Technical Papers*, **2003-01-1826**.

[32] **Risberg, P., Kalghatgi, G.T., Ångstrom, H.E. and Wåhlin, F.,** 2003. Auto-ignition quality of Gasloline-like fuels in HCCI engines, *SAE Technical Papers*, **2003-01-3215**.

[33] **Risberg, P., Kalghatgi, G.T., Ångstrom, H.E. and Wåhlin, F.,** 2005. Auto-ignition quality of Diesel-like fuels in HCCI engines, *SAE Technical Papers*, **2005-01-2127**.

[34] **Kalghatgi, G.T., Risberg, P. and Ångstrom, H.E.,** 2007. Partially pre-mixed auto-ignition of gasoline to attain low smoke and low NO_x at high load in a compression ignition engine and comparison with a diesel fuel, *SAE Technical Papers*, **2007-01-0006**.

[35] **Kalghatgi, G.T.,** 2007. Autoignition and Knock in Engines, *Seminar*, ITU Mechanical Engineering Faculty, Gümüşsuyu, İstanbul, Turkey, May 10.

[36] **Kalghatgi, G.T.,** 2007. Is Gasoline the Best Fuel for Advanced Engines? Fuel Effects in "Premixed-enough" CI Engines, *Seminar*, ITU Mechanical Engineering Faculty Automotive Engineering Laboratories, Maslak, İstanbul, Turkey, May 11.

[37] **Flynn, P.F., Durrett, R.P., Hunter, G.L., zur Loye, A.O., Akinyemi, O.C., Dec, J.E. and Westbrook, C.K.,** 1999. Diesel combustion: An integrated view combining laser diagnostics, chemical kinetics, and empirical validation, *SAE Technical Papers*, **1999-01-0509**.

[38] **Golovitchev, V.I., Calik, A.T. and Montorsi, L.,** 2007. Analysis of Combustion Regimes in Compression Ignited Engines Using Parametric φ-T Dynamic Maps, *SAE Technical Papers*, **2007-7260**.

[39] **Corcione, F.E., Costa, M., Allocca, L. and Golovitchev, V.I.,** 2004. Study of Multiple Injections and Auto-Ignition of Diesel Sprays in a Constant Volume Vessel, *COMODIA 2004 The Sixth International Symposium on Diagnostics and Modeling of Combustion in Internal Combustion Engines*, Yokohama, Japan, August 2–5.

[40] **Golovitchev, V.I., Atarashiya, K., Tanaka, L., and Yamada, S.,** 2003. Towards Universal EDC-Based Combustion Model for Compression Ignited Engine Simulations, *SAE Technical Papers*, **2003-01-1849**.

[41] **Amsden, A.A.,** 1997. KIVA-3V: A Block-structured KIVA Program for Engines with Vertical or Canted Valves, *Technical Report*, Los Alamos National Laboratory, **LA-13313-MS**.

[42] **Häggström, A.,** 2004. Modelling and Simulation of Diesel Sprays: Lagrangian Multicomponent Fuel Treatment, *Licentiate Thesis,* Department of Thermo and Fluid Dynamics, Chalmers University of Technology, Göteborg.

[43] **Ely, J.F. and Huber, M.L.,** 1992. NIST Thermophysical Properties of Hydrocarbon Mixtures Database (SUPERTRAPP) Version 3.1 Users' Guide.

[44] **Gauthier, B.M., Davidson, D.F. and Hanson, R.K.,** 2004. Shock Tube Determination Of Ignition Delay Times In Full-Blend and Surrogate Fuel Mixtures, *Combustion and Flame*, **139**, Issue 4, pp. 300-311.

[45] **Panchenkov, G.M. and Lebedev, V.P.,** 1976. Chemical Kinetics and Catalysis, Mir Publishers Moscow, Printed in the Union of Soviet Socialist Republics.

[46] http://en.wikipedia.org/wiki/Reaction_order, 2007.

[47] Jr. **Gardiner, W.C.** (Editor), 1984. Combustion Chemistry, Springer-Verlag New York Inc., Printed in the United States of America.

[48] http://en.wikipedia.org/wiki/Arrhenius_law, 2007.

[49] http://en.wikipedia.org/wiki/Steric_factor, 2007.

[50] **Matyushov, D.,** 2002. Lecture Notes CHM 341: Elementary Physical Chemistry Chapters 25-27: The rates of chemical reactions and Transition state theory, Physical Chemistry Department of Chemistry and Biochemistry, Arizona State University, Tepme, Arizona, USA.

[51] www.rpi.edu/dept/chem-eng/Biotech-Environ/Projects00/enzkin/transition.htm

[52] **Ogink, R.,** 2004. Computer Modeling of HCCI Combustion, *PhD Thesis,* Division of Thermo and Fluid Dynamics, Chalmers University of Technology, Göteborg, Sweden.

[53] http://en.wikipedia.org/wiki/Reaction_mechanism, 2007.

[54] **Westbrook, C.K.,** 2006. Modeling Strategies for Advanced Automotive Engine and Fuels Research, *Biennial CHEMKIN™ in Combustion Workshop Immediately prior to the start of 31st International Symposium on Combusstion*, Heidelberg, Germany, August 6.

[55] **Westbrook, C.K., Mizobuchi, Y., Poinsot, T.J., Smith, P.J. and Warnatz, J.,** 2004. Computational Combustion, *30th International Symposium on Combustion*, Chicago, IL, United States, July 25-30.

[56] **Curtiss, C.F. and Hirschfelder, J.O.,** 1952. Integration of stiff equations, *Proc. Nat. Acad. Sci.*, **38**, pp. 235–243.

[57] **Turanyi, T. and Toth, J.,** 1992. Comments to an Article of Frank-Kamenetskii on The Quasi-Steady-State Approximation, *Acta Chimica Hungarica-Models in Chemistry*, **129(6)**, pp. 903-914.

[58] **Tomlin, A.S., Pilling, M.J., Turanyi, T., Merkin, J.H. and Brindley, J.,** 1992. Mechanism Reduction for the Oscillatory Oxidation of Hydrogen: Sensitivity and Quasi-Steady-State Analyses, *Combustion and Flame*, **91**, pp. 107-130.

[59] **Warnatz, J.,** 1981. Concentration-, pressure-, and temperature dependence of the flame velocity in the hydrogen-oxygen-nitrogen mixtures, *Combustion Science and Technology*, **26**, pp. 203-213.

[60] **Ogink, R. and Golovitchev, V.I.,** 2001. Gasoline HCCI Modeling: Computer Program Combining Detailed Chemistry and Gas Exchange Processes, *SAE Technical Papers*, **2001-01-3614**.

[61] **Nordin, P.A.N.,** 2001. Complex Chemistry Modeling of Diesel Spray Combustion, *PhD Thesis,* Department of Thermo and Fluid Dynamics, Chalmers University of Technology, Göteborg, Sweden.

[62] **Kee, R.J., Miller, J.A. and Jefferson, T.H.,** 1980. CHEMKIN: A General-Purpose Problem-Independent Transportable FORTRAN Chemical Kinetics Code Package, *Technical Report*, **SAND80-8003**, *Sandia National Laboratories*.

[63] **Gustavsson, J. and Golovitchev, V.I.,** 2003. Spray Combustion Simulation Based on Detailed Chemistry Approach for Diesel Fuel Surrogate Model, *SAE Technical Papers*, **2003-01-1848**.

[64] http://www.ca.sandia.gov/chemkin/index.html, 2007.

[65] **Kee, R.J., Rupley, F.M., Miller, J.A., Coltrin, M.E., Grcar, J.F., Meeks, E., Moffat, H.K., Lutz, A.E., Dixon-Lewis, G., Smooke, M.D., Warnatz, J., Evans, G.H., Larson, R.S., Mitchell, R.E., Petzold, L.R., Reynolds, W.C., Caracotsios, M., Stewart, W.E., Glarborg, P., Wang, C. and Adigun, O.,** 2000. CHEMKIN Collection Release 3.6, *Reaction Design Inc.*, San Diego, CA, USA, September.

[66] **Lutz, A., Kee, R. and Miller, J.,** 1994. SENKIN: A Fortran Program for Predicting Homogeneous Gas Phase Chemical Kinetics with Sensivity Analysis, *Technical Report Reprinted*, **SAND87-8248**, Sandia National Laboratories.

[67] **Caracotsios, M. and Stewart, W.E.,** 1985. Sensitivity Analysis of Initial Value Problems with Mixed ODEs and Algebraic Equations, *Computers and Chemical Engineering*, **9**, pp. 359-365.

[68] **Petzold, L.R.,** 1982. A Description of DASSL, *Technical Report*, **SAND82-8637**, *Sandia National Laboratories*.

[69] **Hindmarsh, A.C.,** 1980. Lsode and Lsodi, Two New Initial Value Ordinary Differential Equation Solvers, *ACM-SIGNUM Newsletter*, **15**, No. 4, pp. 10–11.

[70] **Reynolds, W.C.,** 1986. The Element Potential Method for Chemical Equilibrium Analysis: Implementation in the Interactive Program STANJAN Version 3, Technical Report (unnumbered), Department of Mechanical Engineering of Standford University.

[71] **Glarborg, P., Kee, R.J., Grcar, J.F. and Miller, J.A.,** 1986. PSR: A FORTRAN Program for Modeling Well-Stirred Reactors, *Technical Report*, **SAND86-8209**, Sandia National Laboratories.

[72] **Edman, J.,** 2005. Modeling Diesel Spray Combustion Using a Detailed Chemistry Approach, *PhD Thesis*, Division of Thermo and Fluid Dynamics, Chalmers University of Technology, Göteborg, Sweden.

[73] **Nordin, N. and Golovitchev, V.I.,** 1999. 3-D KIVA Simulation Using New Detailed Chemistry Diesel Spray Combustion Model, *Combustion Modeling in I.C.E. Workshop*, Cassino, Italy, December 14-15.

[74] **Golovitchev, V.I. and Chomiak, J.,** 2000. Comprehensive Chemical Mechanism of Soot Formation for Diesel Spray Combustion Modeling, *XXII Event of the Italian Section of the Combustion Institute*, Lacco Ameno, Ischia, May 22-25.

[75] **Golovitchev, V.I. and Chomiak, J.,** 2000. Simple Detailed Chemistry Approach for Turbulent Spray Combustion Modeling, *28th (International) Symposium on Combustion*, The Combustion Institute, Pittsburgh, Edinburgh, Scotland, July 30-August 4.

[76] **Golovitchev, V.I., Nordin, N., Jarnicki, R. and Chomiak, J.,** 2000. 3-D Diesel Spray Simulations Using a New Detailed Chemistry Turbulent Combustion Model, *SAE Technical Papers*, **2000-01-1891**.

[77] **Tao, F., Golovitchev, V.I. and Chomiak, J.,** 2000. Self-Ignition and Early Combustion Process of n-Heptane Sprays Under Diluted Air Conditions: Numerical Studies Based on Detailed Chemistry, *SAE Technical Papers*, **2000-01-2931**.

[78] **Golovitchev, V.I. and Nordin, N.,** 2001. Detailed Chemistry Spray Combustion Model for the KIVA Code, *The 11th International Multidimensional Engine Modeling User's Group Meeting at the SAE Congress*, Detroit, MI, USA, March 4.

[79] **Rente, T., Golovitchev, V.I. and Denbratt, I.,** 2001. Numerical Study of n-Heptain Diesel Spray Auto-ignition at Different Level of Pre-ignition Turbulence, *The Fifth International Symposium on Diagnostics and Modeling of Combustion in Internal Combustion Engines COMODIA 2001*, Nagoya, Japan, July 1-4.

[80] **Bergman, M. and Golovitchev, V.I.,** 2005. Chemical Mechanisms for Modelling HCCI with Gasoline and Diesel Oil Surrogates, *Engine Combustion Processes Current Problems and Modern Techniques (VII. Congress)*, Munich, Germany, March 15-16.

[81] **Davidson, D.F., Gauthier, B.M. and Hanson, R.K.,** 2005. Shock tube ignition measurements of iso-octane/air and toluene/air at high pressures, *Proceedings of the Combustion Institute*, **30**, Issue 1, pp. 1175-1182.

[82] **Fredriksson, J.L., Bergman, M., Golovitchev, V.I. and Denbratt, I.G.,** 2006. Modeling the Effect of Injection Schedule Change on Free Piston Engine, *SAE Technical Papers*, **2006-01-0449**.

[83] **Curran, H.J., Gaffuri, P., Pitz, W.J. and Westbrook, C.K.,** 1998. A Comprehensive Modeling Study of n-Heptane Oxidation, *Combustion and Flame*, **114**, Issues 1-2, pp. 149 -177.

[84] Howard, J.B., 2001. http://web.mit.edu/anish/www/MITcomb.html, 2007.

[85] **Campbell, A.S.,** 1979. Thermodynamic Analysis of Combustion Engines, John Wiley & Sons Inc., New York, USA.

[86] http://en.wikipedia.org/wiki/Adiabatic_flame_temperature, 2007.

[87] **Davis, S.G and Law, C. K.,** 1998. Laminar Flame Speed and Oxidation Kinetics of iso-Octane/Air and n-Heptane/Air Flames, *Twenty-Seventh Symposium (International) on Combustion*, The Combustion Institute, Pittsburgh, PA, pp. 521-528.

[88] http://en.wikipedia.org/wiki/Nitrogen_oxide#NOx, 2007.

[89] **Mehdiyev, R.I., Ismailov, A., Ergeneman, A.M., Calik, A.T., San, D., Yildirim, M.,** 2002. Methods of NO_x Emissions Calculation and Decreasing in Diesel Engines (In Turkish), *Automotive Technologies Congress 2002*, Bursa, Turkey, June 24-26.

[90] **Zeldovich, Y.B.,** 1946. The oxidation of nitrogen in combustion and explosions. , *Acta Physiochimica*, **21**, 577-628, USSR.

[91] **Lavoie, G.A., Heywood, J.B. and Keck, J.C.,** 1970. Experimental and Theoretical Study of Nitric Oxide Formation in Internal Combustion Engines, *Combustion Science and Technology*, **1**, Issue 4, pp 313-326, February.

[92] **Baulch, D.L., Cobos, C.J., Cox, A.M., Frank, P., Haymann, G., Just, T., Kerr, J.A., Murrels, T., Pilling, M.J., Twe, J., Walker, R.W. and Warnatz, J.,** 1991. Compilation of Rate Data for Combustion Modeling Supplement, *I. J. Phys. Chem. Ref. Data*, **22**, pp. 847.

[93] **Smith, G.P., Golden, D.M., Frenklach, M., Moriarty, N.W., Eiteneer, B., Goldenberg, M., Bowman, C.T., Hanson, R.K., Song, S., Gardiner, W.C., Lissianski, Jr., V.V. and Qin, Z.,** 2000. GRI-MECH 3.0, *http://www.me.berkeley.edu/gri_mech/*.

[94] **Pattas, K., Häfner, G.,** 1973. Stickoxidbildung bei der Ottomotorischen Verbrennung, *MTZ Motortechnische Zeitschrift*, **34**, Heft 12.

[95] **Baulch, D.L., Drysdale, D.D., Horne, D.G., and Lloyd, A.C.,** 1969. High Temperature Reaction Rate Data, *Report No.4*, University of Leeds.

[96] **Marteney, P.J.,** 1970. *Combust. Sci. Technol Technol.*,**1**,pp.461.

[97] **Weaving, J.H.,** 1990. Internal Combustion Engineering: Science&Technology, *London: Elsevier Applied Science*.

[98] **Fenimore, C.P.,** 1979. Studies of Fuel-Nitrogen in Rich-Flame Gases. *17th (International) Symposium on Combustion*. The Combustion Institute, pp. 661-669, Pittsburgh.

[99] **Wolfrum, J.,** 1972. Bildung von Stickstoffoxiden bei der Verbrennung. *Chemie-. Ing.-Techn.*, **44**, pp. 656–659.

[100] **Golovitchev, V.I., Montorsi, L., Denbratt, I., Corcione, F. and Coppola, S.,** 2007. Numerical Evaluation of Direct Injection of Urea as NO_x Reduction Method for Heavy Duty Diesel Engines, *SAE Technical Papers*, **2007-01-0909**.

[101] **Rota, R., Antos, D., Zanoelo, É. F. and Morbidelli, M.,** 2002. Experimental and Modeling Analysis of the NO_xOUT Process, *Chemical Engineering Science J.*, **57**, pp 27-38.

[102] **Mehdiyev, R. and Wolanski, P.,** 2000. Bi-Modal Combustion Chamber for a Stratified Charge Engine, *SAE Technical Papers*, **2000-01-0196**.

[103] **Mehdiyev, R.,** 1997. Internal Combustion Engine with Stratified Charge, *Archivum Combustionis*, **17**, Nr 1-4, pp. 47-56.

[104] **Mehdiyev, R.I., Sorusbay, C., Kutlar, O.A., Arslan, H. and Calik, A.T.,** 2001. Two-stage combustion in a Stratified Charge Spark Ignition Engine for Reduced Emissions and Improved Fuel Economy, International Scientific-Technical Conference on Internal Combustion Engines, *Automobile Techniques and Transport MOTAUTO'01*, **1**, pp. 63-66, Varna, Bulgaria, October 17-19.

[105] **Tao, F.,** 2003. Numerical Modeling of Soot and NO_x Formation in Non-stationary Diesel Flames with Complex Chemistry, *PhD Thesis*, Division of Thermo and Fluid Dynamics, Chalmers University of Technology, Göteborg, Sweden.

[106] **Palmer H.B. and Cullis C.F.,** 1965. The Formation of Carbon From Gases In: Walker Jr. P.L. (Ed.), *Chemistry and Physics of Carbon*, **1**, pp. 205, M.Decker Inc, New York.

[107] **Bockhorn, H. (Editor),** 1994. Soot Formation in Combustion: Mechanisms and Models, *Springer-Verlag*, Berlin.

[108] **Harris, S.J., Weiner, A.M. and Ashcraft, C.C.,** 1986. Soot particle inception kinetics in a premixed ethylene flame, *Combustion and Flame*, **64**, Issue 1, pp. 65-81.

[109] **Mauss, F., Schäfer, T. and Bockhorn, H.,** 1994 Inception and growth of soot particles in dependence on the surrounding gas phase, *Combustion and Flame*, **99**, Issues 3-4, pp. 697-705.

[110] **Homann, K.H.,** 1967. Carbon formation in premixed flames, Combustion and Flame, **11**, Issue 4, pp. 265-287.

[111] **Golovitchev, V.I., Tao, F. and Chomiak, J.,** 1999. Numerical Evaluation of Soot Formation Control At Diesel-Like Conditions By Reducing Fuel Injection Timing, *SAE Technical Papers*, **1999-01-3552**.

[112] **Frenklach, M.,** 2002. Reaction mechanism of soot formation in flames, *Physical Chemistry Chemical Physics (PCCP)*, **4**, pp. 2028-2037.

[113] **Golovitchev, V.I.,** 2006. http://www.tfd.chalmers.se/~valeri/MECH.html

[114] **Frenklach, M. and Wang, H.,** 1994. Detailed Mechanism and Modeling of Soot Particle Formation In: Bockhorn, H. (Editor) Soot Formation in Combustion, *Springer-Verlag*, pp. 165-192, Berlin.

[115] **Warnatz, J., Maas, U. and Dibble, R. W.,** 1997. Verbrennung, 2. Auflage, Springer-Verlag, Berlin, Heidelberg.

[116] **Golovitchev, V.I. and Chomiak, J.,** 2000. Comprehensive Chemical Mechanism of Soot Formation and Oxidation for Diesel Spray Combustion Modeling, *Open Meeting on Combustion of the Italian Section of the Combustion Institute*, Lacco Ameno, Ischia, Italy, May 22-25.

[117] **Wang, H. and Frenklach, M.,** 1997. A Detailed Kinetic Modeling Study of Aromatics Formation in Laminar Premixed Acetylene and Ethylene Flames, *Combustion and Flame*, **110**, 173-221.

[118] **Bradley, D., Dixon-Lewis, G., Habik, S.E. and Mushi, E.M.J.,** 1984. The Oxidation Of Graphite Powder In Flame Reaction Zones, Twentieth Symposium (International) on Combustion, The Combustion Institute, pp. 931-940.

[119] **Golovitchev, V.I., Rente, T. and Calik, A.T.,** 2005. Computational and Experimental Study of MK Diesel Spray Combustion, *Engine Combustion Processes Current Problems and Modern Techniques (VII. Congress)*, Munich, Germany, March 15-16.

[120] **Stiesch, G.,** 2003. Modeling Engine Spray and Combustion Processes, *Springer-Verlag*, Berlin Heidelberg New York, Germany.

[121] **Kamimoto, T. and Bae, M.H.,** 1988. High Combustion Temperature for the Reduction of Particulate in Diesel Engines, *SAE Technical Paper*, **880423**.

[122] **Akihama, K., Takatori, Y., Inagaki, K., Sasaki, S. and Anthony, M.D.,** 2001. Mechanism of the Smokeless Rich Diesel Combustion by Reducing Temperature, *SAE Technical Papers*, **2001-01-0655**.

[123] **Kook, S., Bae, C., Miles, P.C., Choi, D. and Pickett, L.M.,** 2005. The Influence of Charge Dilution and Injection Timing on Low-Temperature Diesel Combustion and Emissions, *SAE Technical Papers*, **2005-01-3837**.

[124] **Shimo, D., Kataoka, M., Sagane, Y., Fujimoto, H. and Terazawa, Y.,** 2006. EM Reduction by a Large Amount of EGR and Excessive Cooled Intake Gas in Diesel Engines, *FISITA Paper*, **F2006P372**.

[125] **Kim, S., Wakisaka, T. and Aoyagi, Y.,** 2005. Numerical Study of the Effects of Boost Pressure and EGR Ratio on the Combustion Process and Exhaust Emissions in a Diesel Engine, *JSAE Paper*, **20056064**.

[126] **Kusaka, J. Montorsi, L., Golovitchev, V.I. and Denbratt, I.,** 2006. Numerical Simulation of Combustion in a Heavy Duty Diesel Engine, FISITA Paper, **F2006P398**.

[127] **Bergman, M. and Golovitchev, V.I.,** 2007. Application of Transient Temperature vs. Equivalence Ratio Emission Maps to Engine Simulations, *SAE Technical Papers*, **2007-01-1086**.

[128] **Golovitchev, V.I., Montorsi, L. and Denbratt, I.,** 2006., Towards a New Type of Hybrid Engine: The Two-Stroke Free-Piston Compression Ignited Engine, FISITA Paper, **F2006P421**.

[129] **Montorsi, L., Rinaldini, C.A., Golovitchev, V.I. and Rosetti, A.,** 2006. CFD Combustion and Emission Formation Modeling for a HSDI Diesel Engine Using Detailed Chemistry, Proceedings of ICEF2006, **ICEF2006-1506**, *ASME Internal Combustion Engine Division 2006 Fall Technical Conference*, Sacramento, California, USA, November 5-8.

[130] **Salsing H., Rinaldini, C.A., Golovitchev, V.I. and Denbratt, I.,** 2006. Performance and Emissions of a DME Diesel Engine Equipped with a Fuel Specific Common Rail System, *Proceedings. JSAE Annual Congress*, S0434A, **54-06**, pp. 13-18, Japan

[131] **Calik, A.T. and Golovitchev, V.I.** 2007, CERC Project: Injection Strategies, *Reference Group Meeting*, Applied Mechanics Division of Chalmers University of Technology, January 17, Gothenburg, Sweden

[132] **Gordon, S. and McBride, B.J.**, 1994. Computer Program for Calculating of Complex Chemical Equilibrium Compositions and Applications I. Analysis, *NASA Reference Publication*, **1311**.

[133] **Mueller, J.C.,** 2005. The Quantification of Mixture Stoichiometry when Fuel Molecules Contain Oxidizer Elements or Oxidizer Molecules Contain Fuel Elements, *SAE Technical Papers*, **2005-01-3705**.

[134] **Mattavi, J.N. and Amann, C.A.,** 1980. Combustion Modeling in Reciprocating Engines, General Motors Research Laboratories, Plenum Press, New York-London, pp. 5.

[135] **Amsden, A.A.,** 1999. KIVA-3V, Release 2, Improvements to KIVA-3V, *Technical Report*, Los Alamos National Laboratory, **LA-13608-MS**.

[136] **Amsden, A.A., Ramshaw, J.D., O'Rourke, P.J. and Dukowicz, J.K.,** 1985. KIVA: A Computer Program for Two- And Three-Dimensional Fluid Flows With Chemical Reactions And Fuel Sprays, *Technical Report*, Los Alamos National Laboratory, **LA-10245-MS**.

[137] **Amsden, A.A., O'Rourke, P.J. and Butler, T.D.,** 1989. KIVA-II: A Computer Program for Chemically Reactive Flows with Sprays, *Technical Report*, Los Alamos National Laboratory, **LA-11560-MS**.

[138] **Amsden, A.A.,** 1993. KIVA-3: A KIVA Program with Block-Structured Mesh for Complex Geometries, *Technical Report*, Los Alamos National Laboratory, **LA-12503-MS**.

[139] **Amsden, D.C. and Amsden, A.A.,** 1993. The KIVA Story: A Paradigm of Technology Transfer, *IEEE Transactions on Professional Communication*, **36**, No: 4, December.

[140] **Golovitchev, V.I. and Jarnicki, R.,** 2002. Numerical Modeling of High Temperature Air "Flameless" Combustion, *Proceeding of the 6th European Conference INFUB*, Lisbon, Portugal.

[141] **Daubert, T. and Danner, R.,** (1989-1994). Physical and Thermodynamic Properties of Pure Chemicals: Data Compilations, **Chap. 1-5**, Taylor & Fransis.

[142] **Taskiran, O.O,** 2004. Multidimensional Modeling of Marine Diesel Engine Using Detailed Chemistry and Turbulent Diesel Spray Combustion Model (In Turkish), *MSc Thesis,* Automotive Program of Mechanical Engineering Division of ITU Institute of Science and Technology, Istanbul, Turkey.

[143] http://www.ansys.com, 2007.

[144] **Ortega, F.A.,** 2007. GMV General Mesh Viewer, Los Alamos National Laboratory, **LA-UR-95-2986**, http://www-xdiv.lanl.gov/XCM/gmv.

[145] **Imren, A., Sorusbay, C., Ergeneman, A.M., San, D. and Gurarslan, E.,** 2005. Multidimensional Modeling of Combustion and Emissions in Diesel Engines, *CAPAC2005 1st International Conference on Air Pollution and Combustion*, ODTU, Ankara, Turkey.

[146] **Edman, J. and Golovitchev, V.I.,** 2005. Modeling of Spray-Spray Interactions in DI Diesel Engines, *ECCOMAS Thematic Conference on Computational Combustion*, Lisbon, Portugal, June 21-24.

[147] **Dec, J.E., et al.,** 1997. A Conceptual Model of DI Diesel Combustion Based on Laser-Sheet Imaging, *SAE Technical Papers*, **970873**.

[148] **Tao, F., Golovitchev, V.I. and Chomiak, J.,** 2001. Application of Complex Chemistry to Investigate the Combustion Zone Structure of DI Diesel Sprays under Engine-like Conditions, *The Fifth International Symposium on Diagnostics and Modeling of Combustion in Internal Combustion Engines COMODIA 2001*, Nagoya, Japan, July 1-4.

[149] **Chomiak, J. and Karlsson, A.,** 1996. Flame Liftoff in Diesel Sprays, *26th Symposium (International) on Combustion*, Proceedings of Combustion Institute, **2**, pp. 2557-2564.

[150] **Golovitchev, V.I. and Chomiak, J.,** 2001. Structure of Combustion Zone and Soot Formation in Lifted DI Diesel Spray Flames, *The 24th Event of the Italian Section of the Combustion Institute Combustion and Environment*, S. Marghareta Ligure, Italy, September 16-19.

[151] **Tao, F. and Chomiak, J.,** 2002. Numerical Investigation of Reaction Zone Structure and Flame Liftoff of DI Diesel Sprays with Complex Chemistry, *SAE Technical Papers*, **2002-01-1114**.

[152] **Ganippa, L.C.**, 2003. Atomisation and Combustion Studies of Diesel Sprays, *PhD Thesis,* Department of Thermo and Fluid Dynamics, Chalmers University of Technology, Göteborg, Sweden.

[153] **Beale, J.C. and Reitz, R.D.**, 1999. Modeling Spray Atomization with the Kelvin-Helmholtz/Rayleigh-Taylor Hybrid Model, *Atomization and Sprays*, **9**, pp. 623-650.

[154] **Golovitchev, V.I., Nordin, N., Tao, F., Edman, J., Montorsi, L., Kusaka, J., Häggström, A., and Bergman, M.,** 2005. Tools for Solving Spray Combustion Problems in Simulations of New Compression Ignited Engines, *ICE2005 7th International Conference on Engines for Automobile*, Capri, Italy, September 11-16.

[155] **Gustavsson, J. and Golovitchev,V.I.,** 2004. 3D Simulations of Multiple Injections in DI Diesel Engine, **Paper A8-1**, *Proceedings of COMODIA 2004*, Yokohama, p.167, August 2-5.

[156] **Karlsson, J.A.J.**, 1995. Modeling Auto-Ignition, Flame Propagation and Combustion in Non-Stationary Turbulent Sprays, *PhD Thesis,* Department of Thermo and Fluid Dynamics, Chalmers University of Technology, Göteborg, Sweden.

[157] **Villermaux, J. and Devillon, J.C.,** 1972. Représentation de la coalescence et de la redispersion des domaines de ségrégation dans un fluide par un modèle d'interaction phénoménoloqique, *Proceedings of the 2nd Int. Symposium on Chemical Reaction Engineering*, pp. 1-13.

[158] **Magnussen, B.F. and Hjertager, B.H.,** 1976. On the Numerical Modeling of Turbulent Combustion with Special Emphasis on Soot Formation and Combustion, *Sixteenth Symposium (International) on Combustion*, Pittsburgh: The Combustion Institute, pp. 719-729.

[159] **Fredriksson, J.,** 2006. Modeling of a Free Piston Energy Converter, *PhD Thesis*, Division of Thermo and Fluid Dynamics, Chalmers University of Technology, Göteborg, Sweden.

[160] **Golovitchev, V.I.,** 2003. Analysis of Assumptions Underlying EDC based Approach for Detailed Chemistry CFD Modeling, *European Combustion Meeting ECM2003*, Orléans, France,October 25 – 28.

[161] **Baumgarten C.,** 2006. Mixture Formation in Internal Combustion Engines, Springer-Verlag Berlin Heidelberg, Germany, pp. 226-230.

[162] **Kimura, S., Aoki, O., Muranaka, Y. and Emomoto, Y.,** 1999. New Combustion Concept for Ultra-Clean and High Efficiency Small Diesel Engines, *SAE Technical Papers*, **1999-01-3681**.

[163] **Kimura, S., Aoki, O. and Aiyoshizawa, E.,** 2001. Ultra-Clean Combustion Technology Combining a Low-Temperature and Premixed Combustion Concept for Meeting Future Emission Standards, *SAE Technical Papers*, **2001-01-0200**.

[164] **Nishijima, Y., Asaumi, Y. and Aoyagi, Y.,** 2001. Premixed Lean Diesel Combustion (PREDIC) using Impingement Spray System, *SAE Technical Papers*, **2001-01-1892**.

[165] **Husberg, T., Gjirja, S. and Denbratt, I.G.,** 2004. Visualization of Egr Influence on Diesel Combustion With Long Ignition Delay in a Heavy-Duty Engine, *SAE Technical Papers*, **2004-01-2947**.

[166] **Greeves, G., Tullis, S. and Barker, B.,** 2003. Advanced Two-Actuator EUI and Emission Reduction for Heavy-Duty Diesel Engines, *SAE Technical Papers*, **2003-01-0698**.

[167] http://delphi.com/manufacturers/auto/powertrain/diesel/inject/, 2007.

[168] **Rente, T.,** 2004. Injection Strategies for Heavy Duty DI Diesel Engines, *PhD Thesis*, Department of Thermo and Fluid Dynamics, Chalmers University of Technology, Göteborg, Sweden.

[169] **Edwards, C.F., Siebers, D.L. and Hoskin, D.H.,** 1992. A Study of the Autoignition Process of a Diesel Spray via High Speed Visualization, *SAE Technical Papers*, **920108**.

ANNEX I

Diesel Surrogate Oil Reaction Mechanism

		k = A T**b exp(-E/RT)		
	REACTIONS	**A**	**b**	**E**
1.	1.5C14H28+0.5O2=>C7H8+2.C7H16+H2O	5.00E+10	0.0	10500.0
2.	A2R5=>12C(S)+4H2	5.00E+03	0.0	4000.0
3.	C6H2=>6C(S)+H2	2.00E+04	0.0	4000.0
4.	C7H8=C6H5+CH3	1.40E+16	0.0	99800.0
5.	C7H8+O2=C7H7+HO2	3.00E+14	0.0	42992.0
6.	C7H8+OH=C7H7+H2O	1.48E+13	0.0	2583.0
7.	C7H8+O=C7H7+OH	7.00E+11	0.0	0.0
8.	C7H8+H=C7H7+H2	1.20E+14	0.0	8235.0
9.	C7H8+H=C6H6+CH3	1.20E+12	0.0	5148.0
10.	C7H8+CH3=C7H7+CH4	3.16E+11	0.0	9500.0
11.	C7H8+C2H3=C7H7+C2H4	1.20E+08	0.0	8000.0
12.	C7H7+O=C6H5CHO+H	1.58E+13	0.0	0.0
13.	C7H7+O=C6H5+CH2O	1.00E+13	0.0	0.0
14.	C7H7+HO2=C6H5CHO+H+OH	2.60E+13	0.0	0.0
15.	C7H7+HO2=C6H5CHO+H2O	7.50E+12	0.0	0.0
16.	C7H7+HO2=C6H5+CH2O+OH	6.00E+12	0.0	0.0
17.	C7H7+OH=C7H8O	1.00E+13	0.0	0.0
18.	C7H7+H=C7H8	1.40E+14	0.0	0.0
19.	C7H7+C3H3=C7H8+C3H2	5.00E+12	0.0	0.0
20.	C7H8O+OH=C6H5CHO+H2O+H	8.43E+12	0.0	2583.0
21.	C7H8O+O2=C6H5CHO+H+HO2	1.00E+14	0.0	41400.0
22.	C7H8O+H=C6H5CHO+H2+H	8.00E+13	0.0	8250.0
23.	C7H8O+H=C7H8+OH	2.21E+13	0.0	7910.0
24.	C7H8O+H=C6H5OH+CH3	1.20E+13	0.0	5148.0
25.	C7H8O+C7H7=C6H5CHO+C7H8+H	2.11E+11	0.0	9500.0
26.	C6H5CHO+O2=C6H5CO+HO2	1.02E+13	0.0	38950.0
27.	C6H5CHO+OH=C6H5CO+H2O	1.71E+09	1.2	-447.0
28.	C6H5CHO+H=C6H5CO+H2	5.00E+13	0.0	4928.0
29.	C6H5CHO+O=C6H5CO+OH	9.04E+12	0.0	3080.0
30.	C6H5CHO+C7H7=C6H5CO+C7H8	3.77E+03	2.8	5773.0
31.	C6H5CO=C6H5+CO	3.98E+14	0.0	29400.0
32.	C6H5+CH3=C7H7+H	5.70E-02	5.0	15700.0
33.	C6H5+O2=CH2CO+CH2CO+C2H	7.80E+16	-1.8	0.0
34.	C4H3+O2=HCCO+CH2CO	1.00E+12	0.0	0.0
35.	C6H5+HO2=C6H5O+OH	5.00E+13	0.0	1000.0

		k = A T**b exp(-E/RT)		
	REACTIONS	**A**	**b**	**E**
36.	C6H5+O2=C6H5O+O	2.60E+13	0.0	6120.0
37.	C6H5+OH=C6H5O+H	5.00E+13	0.0	0.0
38.	C6H5OH+H=C6H5O+H2	1.15E+14	0.0	12400.0
39.	C6H5OH+O=C6H5O+OH	2.81E+13	0.0	7352.0
40.	C6H5OH+HO2=C6H5O+H2O2	3.00E+13	0.0	15000.0
41.	C6H5OH+C2H3=C2H4+C6H5O	6.00E+12	0.0	0.0
42.	C6H5OH+OH=C6H5O+H2O	2.95E+06	2.0	-1312.0
43.	C7H7+C6H5OH=C7H8+C6H5O	1.05E+12	0.0	9500.0
44.	C3H3+C3H3=C6H6	2.00E+12	0.0	0.0
45.	C4H5+C2H2=C6H6+H	1.60E+16	-1.3	5400.0
46.	C4H5+C2H3=C6H6+H2	1.84E+13	0.0	7070.0
47.	C7H8+C6H5=C7H7+C6H6	2.10E+12	0.0	4400.0
48.	C6H5CHO+H=C6H6+HCO	1.20E+13	0.0	5148.0
49.	C6H5CHO+C6H5=C6H5CO+C6H6	7.01E+11	0.0	4400.0
50.	C6H5+H=C6H6	2.20E+14	0.0	0.0
51.	C6H6+O2=C6H5+HO2	6.30E+13	0.0	60000.0
52.	C6H6+OH=C6H5+H2O	1.60E+08	1.4	1450.0
53.	C6H6+O=C6H5O+H	2.20E+13	0.0	4668.0
54.	C6H6+O=C6H5OH	1.00E+13	0.0	4530.0
55.	C7H16+C7H7=C7H8+C7H15-1	5.00E+12	0.0	0.0
56.	C7H16+C7H7=C7H8+C7H15-2	5.00E+12	0.0	0.0
57.	C7H16+O2=C7H15-1+HO2	4.50E+13	0.0	48810.0
58.	C7H16+O2=C7H15-2+HO2	3.00E+14	0.0	47380.0
59.	C7H16+H=C7H15-1+H2	5.60E+07	2.0	7667.0
60.	C7H16+H=C7H15-2+H2	4.38E+07	2.0	4750.0
61.	C7H16+OH=C7H15-1+H2O	8.61E+09	1.1	1815.0
62.	C7H16+OH=C7H15-2+H2O	6.80E+09	1.3	690.5
63.	C7H16+HO2=C7H15-1+H2O2	8.00E+12	0.0	19300.0
64.	C7H16+HO2=C7H15-2+H2O2	1.60E+13	0.0	16950.0
65.	C7H16=C4H9+C3H7	3.40E+16	0.0	80710.0
66.	C7H15-1+O2=C7H15O2	2.00E+12	0.0	0.0
67.	C7H15-2+O2=C7H15O2	2.50E+12	0.0	0.0
68.	C7H15O2=C7H14O2H	5.00E+11	0.0	20380.0
69.	C7H14O2H+O2=C7H14O4H	2.00E+11	0.0	0.0
70.	C7H14O4H=C7KET21+OH	2.96E+13	0.0	26700.0
71.	C7KET21=C5H11CO+CH2O+OH	1.05E+16	0.0	44200.0
72.	C5H11CHO+O2=C5H11CO+HO2	2.00E+13	0.5	42200.0
73.	C5H11CHO+OH=C5H11CO+H2O	1.00E+13	0.0	0.0
74.	C5H11CHO+H=C5H11CO+H2	4.00E+13	0.0	4200.0
75.	C5H11CHO+O=C5H11CO+OH	5.00E+12	0.0	1790.0
76.	C5H11CHO+HO2=C5H11CO+H2O2	2.80E+12	0.0	13600.0
77.	C5H11CHO+CH3=C5H11CO+CH4	1.70E+12	0.0	8440.0
78.	C5H11CO=C5H11+CO	1.00E+11	0.0	9600.0
79.	C5H11=C2H5+C3H6	3.20E+13	0.0	28300.0

		k = A T**b exp(-E/RT)		
	REACTIONS	**A**	**b**	**E**
80.	C7H15-1=C2H4+C5H11	2.50E+13	0.0	28810.0
81.	C7H15-2=CH3+C6H12	3.00E+13	0.0	29800.0
82.	C6H12=C3H7+C3H5	1.00E+16	0.0	68000.0
83.	C6H12=C3H6+C3H6	1.00E+16	0.0	68000.0
84.	C7H15-2=C4H9+C3H6	1.50E+13	0.0	28600.0
85.	C7H15-1=C7H15-2	2.00E+11	0.0	18050.0
86.	C4H9=C3H6+CH3	2.23E+17	-1.4	30830.0
87.	C4H9=C2H5+C2H4	2.50E+13	0.0	28810.0
88.	C3H7=C2H4+CH3	9.60E+13	0.0	30950.0
89.	C3H7=C3H6+H	1.25E+14	0.0	36900.0
90.	C3H7+CH3=C2H5+C2H5	1.90E+13	-0.3	0.0
91.	C3H7+O2=C3H6+HO2	1.00E+12	0.0	4980.0
92.	C3H7+H=CH3+C2H5	4.06E+06	2.2	890.0
93.	C3H6=C2H3+CH3	6.25E+15	0.0	85500.0
94.	C3H6+H=C3H5+H2	5.00E+12	0.0	1500.0
95.	C3H6+CH3=C3H5+CH4	9.00E+12	0.0	8480.0
96.	C3H6+O2=C3H5+HO2	4.00E+12	0.0	39900.0
97.	C3H5+HO2=C2H3+CH2O+OH	1.00E+12	0.0	0.0
98.	C3H5+H=C3H4+H2	1.00E+13	0.0	0.0
99.	C3H5+O2=CH3+CH2O+CO	4.00E+12	0.0	0.0
100.	C3H4+OH=C2H3+CH2O	1.00E+12	0.0	0.0
101.	C3H4+OH=C2H4+HCO	1.00E+12	0.0	0.0
102.	C3H4+O2=C3H3+HO2	4.00E+13	0.0	39160.0
103.	CH3O+CO=CH3+CO2	1.57E+14	0.0	11800.0
104.	CH3O+H=CH2O+H2	2.00E+13	0.0	0.0
105.	CH3O+H=CH3+OH	1.00E+14	0.0	0.0
106.	CH3O+OH=CH2O+H2O	5.00E+12	0.0	0.0
107.	CH3O+O=CH2O+OH	1.00E+13	0.0	0.0
108.	CH3O+O2=CH2O+HO2	4.28E-13	7.6	-3530.0
109.	CH3O=CH2O+H	3.00E+12	0.0	27420.0
110.	CO+O+M=CO2+M H2/2.0/ O2/6.0/ H2O/6.0/ CH4/2.0/ CO/1.5/... ...CO2/3.5/ C2H6/3.0/ N2/0.7/	4.17E+14	0.0	3000.0
111.	CO+OH=CO2+H	3.51E+07	1.2	70.0
112.	CO+O2=CO2+O	1.60E+13	0.0	47800.0
113.	CO+HO2=CO2+OH	1.50E+14	0.0	23600.0
114.	H2+O2=OH+OH	1.70E+13	0.0	47780.0
115.	H2+OH=H2O+H	1.17E+09	1.3	3626.0
116.	O+OH=O2+H	4.00E+14	-0.5	0.0
117.	O+H2=OH+H	5.06E+04	2.7	6290.0
118.	O+OH+M=HO2+M H2/2.0/ O2/6.0/ H2O/6.0/ N2/0.7/	1.00E+16	0.0	0.0
119.	H+O2+M=HO2+M H2/2.0/ O2/0.0/ H2O/3.0/ CO/0.8/... ...CO2/1.5/ C2H6/1.5/ N2/ 0.0/ AR/0.0/	2.80E+18	-0.9	0.0

		k = A T**b exp(-E/RT)		
	REACTIONS	**A**	**b**	**E**
120.	H+O2+N2=HO2+N2	2.60E+19	-1.2	0.0
121.	H+O2+O2=HO2+O2	2.08E+19	-1.2	0.0
122.	H+O2+AR=HO2+AR	7.00E+17	-0.8	0.0
123.	OH+HO2=H2O+O2	2.89E+13	0.0	-500.0
124.	H+HO2=OH+OH	1.70E+14	0.0	874.0
125.	O+HO2=O2+OH	1.40E+13	0.0	1073.0
126.	OH+OH=O+H2O	6.00E+08	1.3	0.0
127.	H+H+M=H2+M	1.00E+18	-1.0	0.0
	H2/0.0/ H2O/0.0/ CO2/0.0/ N2/0.7/			
128.	H+H+H2=H2+H2	9.20E+16	-0.6	0.0
129.	H+H+H2O=H2+H2O	6.00E+19	-1.3	0.0
130.	H+H+CO2=H2+CO2	5.49E+20	-2.0	0.0
131.	H+OH+M=H2O+M	1.60E+22	-2.0	0.0
	H2/2.0/ O2/6.0/ H2O/6.0/ N2/0.7/			
132.	H+O+M=OH+M	6.20E+16	-0.6	0.0
	H2/2.0/ O2/6.0/ H2O/6.0/ N2/0.7/			
133.	O+O+M=O2+M	1.89E+13	0.0	-1788.0
	H2/2.0/ O2/6.0/ H2O/6.0/ N2/0.7/			
134.	HO2+H=H2+O2	4.28E+13	0.0	1411.0
135.	HO2+HO2=H2O2+O2	2.20E+14	0.0	12000.0
136.	H2O2+M=OH+OH+M	5.30E+16	0.0	45500.0
	H2/2.5 / H2O/12.0/ CO/1.9/ CO2/3.8/ N2/0.7/			
137.	H2O2+OH=H2O+HO2	1.00E+13	0.0	1800.0
138.	H2O2+H=H2O+OH	1.00E+13	0.0	3590.0
139.	H2O2+H=HO2+H2	1.70E+12	0.0	3755.0
140.	H2O2+O=H2O+O2	8.40E+11	0.0	4260.0
141.	H2O2+O=OH+HO2	2.00E+13	0.0	5900.0
142.	HO2+H2=H2O+OH	6.50E+12	0.0	18800.0
143.	CH2O+O=HCO+OH	3.80E+13	0.0	3540.0
144.	CH2O+H=HCO+H2	2.30E+10	1.1	3270.0
145.	CH2O+OH=HCO+H2O	3.34E+10	1.2	-447.0
146.	CH2O+O2=HCO+HO2	1.00E+14	0.0	39000.0
147.	CH2O+HO2=HCO+H2O2	3.00E+12	0.0	8000.0
148.	CH2O+CH3=HCO+CH4	5.54E+03	2.8	5860.0
149.	CH2O+M=HCO+H+M	3.30E+16	0.0	81000.0
	H2/2.0/ O2/6.0/ H2O/6.0/ N2/0.7/			
150.	HCO+HCO=CH2O+CO	3.01E+13	0.0	0.0
151.	HCO+OH=H2O+CO	1.00E+14	0.0	0.0
152.	HCO+H=H2+CO	1.19E+13	0.3	0.0
153.	HCO+O=OH+CO	3.00E+13	0.0	0.0
154.	HCO+O=H+CO2	3.00E+13	0.0	0.0
155.	HCO+O2=HO2+CO	3.30E+13	-0.4	0.0
156.	HCO+M=H+CO+M	1.87E+17	-1.0	17000.0
	H2/2.0/ O2/6.0/ H2O/6.0/ N2/0.7/			

		k = A T**b exp(-E/RT)		
	REACTIONS	**A**	**b**	**E**
157.	HCO+HO2=CO2+OH+H	3.00E+13	0.0	0.0
158.	CH4+O2=CH3+HO2	7.90E+13	0.0	56000.0
159.	CH4+H=CH3+H2	6.60E+08	1.6	10840.0
160.	CH4+OH=CH3+H2O	1.60E+06	2.1	2460.0
161.	CH4+O=CH3+OH	1.02E+09	1.5	8604.0
162.	CH4+HO2=CH3+H2O2	1.00E+13	0.0	18700.0
163.	CH4+CH2=CH3+CH3	4.00E+12	0.0	-570.0
164.	CH3+HCO=CH4+CO	1.20E+14	0.0	0.0
165.	CH3+HCO=CH2O+CH2	3.00E+13	0.0	0.0
166.	CH3+H=CH4	1.90E+36	-7.0	9050.0
167.	CH3+H=CH2+H2	9.00E+13	0.0	15100.0
168.	CH3+CH3O=CH4+CH2O	4.30E+14	0.0	0.0
169.	CH3+CH3=C2H6	2.12E+16	-1.0	620.0
170.	CH3+CH3=C2H5+H	4.99E+12	0.1	10600.0
171.	CH3+O=CH2O+H	8.00E+13	0.0	0.0
172.	CH3+OH=CH2+H2O	7.50E+06	2.0	5000.0
173.	CH3+OH=CH2O+H2	4.00E+12	0.0	0.0
174.	CH3+CH2=C2H4+H	3.00E+13	0.0	-570.0
175.	CH3+HO2=CH3O+OH	5.00E+13	0.0	0.0
176.	CH3+O2=CH3O+O	4.67E+13	0.0	30000.0
177.	CH3+O2=CH2O+OH	1.00E+11	0.0	9000.0
178.	CH3+C2H4=CH4+C2H3	6.62E+00	3.7	9482.0
179.	CH3+CH3=C2H4+H2	1.00E+15	0.0	31000.0
180.	CH2+OH=CH2O+H	2.50E+13	0.0	0.0
181.	CH2+O2=HCO+OH	4.30E+10	0.0	-500.0
182.	CH2+O2=CO2+H2	6.90E+11	0.0	500.0
183.	CH2+O2=CO+H2O	2.00E+10	0.0	-1000.0
184.	CH2+O2=CH2O+O	5.00E+13	0.0	9000.0
185.	CH2+O2=CO2+H+H	1.60E+12	0.0	1000.0
186.	CH2+O2=CO+OH+H	8.60E+10	0.0	-500.0
187.	CH2+CH2=C2H2+H2	1.20E+13	0.0	800.0
188.	CH2+CH2=C2H2+H+H	1.20E+14	0.0	800.0
189.	CH2+CO2=CH2O+CO	1.00E+11	0.0	1000.0
190.	C2H4+H=C2H3+H2	1.10E+14	0.0	8500.0
191.	C2H4+O=CH3+HCO	1.60E+09	1.2	746.0
192.	C2H4+O=CH2O+CH2	3.00E+04	1.9	180.0
193.	C2H4+O=C2H3+OH	1.51E+07	1.9	3790.0
194.	C2H4+OH=CH2O+CH3	6.00E+13	0.0	960.0
195.	C2H4+HO2=C2H3+H2O2	7.10E+11	0.0	17110.0
196.	C2H4+OH=C2H3+H2O	6.02E+13	0.0	5955.0
197.	C2H4+M=C2H2+H2+M H2/2.0/ O2/6.0/ H2O/6.0/ N2/0.7/	1.50E+15	0.0	55800.0
198.	C2H4+M=C2H3+H+M H2/2.0/ O2/6.0/ H2O/6.0/ N2/0.7/	2.60E+17	0.0	96570.0

		k = A T**b exp(-E/RT)		
	REACTIONS	**A**	**b**	**E**
199.	C2H4+H=C2H5	2.60E+43	-9.2	52580.0
200.	C2H6+O2=C2H5+HO2	1.00E+13	0.0	48960.0
201.	C2H5+O2=C2H4+HO2	2.00E+10	0.0	-2200.0
202.	C2H4+O2=C2H3+HO2	4.20E+14	0.0	57590.0
203.	C2H4+C2H4=C2H5+C2H3	5.00E+14	0.0	64700.0
204.	C2H5+HO2=C2H4+H2O2	3.00E+11	0.0	0.0
205.	C2H2+O2=HCO+HCO	4.00E+12	0.0	28000.0
206.	C2H2+O=CH2+CO	1.02E+07	2.0	1900.0
207.	C2H3+H=C2H2+H2	4.00E+13	0.0	0.0
208.	C2H3+O2=CH2O+HCO	4.00E+12	0.0	-250.0
209.	C2H3+O2=C2H2+HO2	1.00E+12	0.0	10000.0
210.	C2H3+OH=C2H2+H2O	3.00E+13	0.0	0.0
211.	C2H3+CH2=C2H2+CH3	3.00E+13	0.0	0.0
212.	C2H3+HCO=C2H4+CO	6.03E+13	0.0	0.0
213.	C2H3+C2H3=C2H2+C2H4	1.45E+13	0.0	0.0
214.	C2H3+O=C2H2+OH	1.00E+13	0.0	0.0
215.	C2H2+OH=CH3+CO	4.83E-04	4.0	-2000.0
216.	C2H2+CH2=C3H3+H	1.20E+13	0.0	6620.0
217.	C3H3+OH=C3H2+H2O	1.00E+13	0.0	0.0
218.	C3H3+O=CH2O+C2H	1.00E+13	0.0	0.0
219.	C2H3=C2H2+H	4.60E+40	-8.8	46200.0
220.	C2H2=C2H+H	2.37E+32	-5.3	130688.0
221.	C2H+O2=HCO+CO	5.00E+13	0.0	1500.0
222.	C2H+H2=H+C2H2	4.90E+05	2.5	560.0
223.	C2H2+O=C2H+OH	4.60E+19	-1.4	28950.0
224.	C2H2+OH=C2H+H2O	3.37E+07	2.0	14000.0
225.	C2H2+C2H=C4H2+H	9.60E+13	0.0	0.0
226.	C4H+H2=H+C4H2	4.90E+05	2.5	560.0
227.	C4H2+OH=C4H+H2O	3.37E+07	2.0	14000.0
228.	C4H2+O=C3H2+CO	2.70E+13	0.0	1720.0
229.	C3H2+O=C2H2+CO	5.80E+13	0.0	0.0
230.	C3H2+OH=HCO+C2H2	5.80E+13	0.0	0.0
231.	C3H2+CH2=C4H3+H	3.00E+13	0.0	0.0
232.	C3H2+C3H2=C6H2+H2	2.00E+13	0.0	85000.0
233.	C4H+C2H2=C6H2+H	9.60E+13	0.0	0.0
234.	C4H2+C2H=C6H2+H	9.60E+13	0.0	0.0
235.	C6H+H(+M)=C6H2(+M)	1.00E+17	-1.0	0.0
	low pressure limit	3.75E+33	-4.8	1900.0
	TROE centering /0.6/132.0/1.32E+03/5.57E+03/			
	H2/2.0/ H2O/6.0/ CH4/2.0/ CO/1.5/ CO2/2.0/ C2H6/3.0/ AR/ 0.7/			
236.	C6H+H2=H+C6H2	4.90E+05	2.5	560.0
237.	C6H2+C2H=C4H+C4H2	1.00E+13	0.0	0.0
238.	C6H2+OH=C6H+H2O	3.37E+07	2.0	14000.0
239.	C3H3+C3H3=C6H5+H	2.00E+12	0.0	0.0

		k = A T**b exp(-E/RT)		
	REACTIONS	**A**	**b**	**E**
240.	C3H2+HCCO=C4H3+CO	1.00E+13	0.0	0.0
241.	C2H2+OH=CH2CO+H	2.18E-04	4.5	-1000.0
242.	CH2CO+H=HCCO+H2	5.00E+13	0.0	8000.0
243.	CH2CO+H=CH3+CO	1.13E+13	0.0	3428.0
244.	CH2CO+O=HCCO+OH	1.00E+13	0.0	8000.0
245.	C2H2+C2H2=C4H2+H2	1.00E+17	0.0	81000.0
246.	C2H2+C2H=C4H3	4.50E+37	-7.7	7100.0
247.	C2H3+C2H2=C4H5	8.10E+37	-8.1	13400.0
248.	C4H5+C3H4=C7H8+H	2.00E+11	0.0	3600.0
249.	C4H5+O2=C2H4+CO+HCO	4.16E+10	0.0	2500.0
250.	C4H3+M=C4H2+H+M	1.00E+14	0.0	30000.0
251.	C4H3+H=C2H2+C2H2	6.30E+25	-3.3	10014.0
252.	C4H3+H=C4H2+H2	1.50E+13	0.0	0.0
253.	C4H3+OH=C4H2+H2O	5.00E+12	0.0	0.0
254.	C2H+OH=H+HCCO	2.00E+13	0.0	0.0
255.	C2H2+O=HCCO+H	1.02E+07	2.0	1900.0
256.	HCCO+O2=OH+CO+CO	1.46E+12	0.0	2500.0
257.	HCCO+CH2=C2H3+CO	3.00E+13	0.0	0.0
258.	C2H+C2H=C4H2	1.80E+13	0.0	0.0
259.	C3H4+O=HCCO+CH3	6.30E+12	0.0	2010.0
260.	HCCO+HCCO=C2H2+CO+CO	1.00E+13	0.0	0.0
261.	CH2CO+O=CH2+CO2	1.75E+12	0.0	1350.0
262.	CH2CO+O2=CH2O+CO2	2.00E+13	0.0	61500.0
263.	CH2CO+OH=HCCO+H2O	7.50E+12	0.0	2000.0
264.	CH2CO+M=CH2+CO+M H2/2.0/ O2/6.0/ H2O/6.0/ N2/0.7/	2.00E+16	0.0	60000.0
265.	C2H3+O=CH2CO+H	3.00E+13	0.0	0.0
266.	C3H3+O2=CH2CO+HCO	3.00E+10	0.0	2878.0
267.	C3H4+O=CH2CO+CH2	2.00E+07	1.8	1000.0
268.	C6H5+O2=C6H4O2+H	3.00E+13	0.0	8980.0
269.	C6H4O2+O=>2CO+C2H2+CH2CO	3.00E+13	0.0	5000.0
270.	C6H5O+O=C6H4O2+H	5.00E+13	0.0	0.0
271.	C6H5O+HO2=C6H4O2+H2O	1.00E+13	0.0	0.0
272.	C4H3+C2H2=C6H5	2.80E+03	2.9	1400.0
273.	C3H3+C3H3=A1	2.00E+10	0.0	0.0
274.	C4H3+C2H2=A1-	1.90E+63	-15.2	30600.0
275.	C4H5+C2H2=A1+H	1.60E+18	-1.9	7400.0
276.	C6H5=A1-	3.50E+46	-10.4	33600.0
277.	C6H5+C2H=A1C2H	2.54E+17	-1.5	1541.0
278.	A1+H=A1-+H2	2.59E+14	0.0	16000.0
279.	A1+OH=A1-+H2O	1.06E+08	1.4	1450.0
280.	A1-+H=A1	1.00E+14	0.0	0.0
281.	C4H3+C4H2=A1C2H-	1.90E+63	-15.2	30600.0
282.	A1+C2H=A1C2H+H	5.00E+13	0.0	0.0

		k = A T**b exp(-E/RT)		
	REACTIONS	**A**	**b**	**E**
283.	A1-+C2H2=A1C2H2	7.90E+29	-5.2	13700.0
284.	A1-+C2H2=A1C2H+H	2.50E+29	-4.4	26400.0
285.	A1C2H+H=A1C2H2	1.60E+32	-5.7	11090.0
286.	A1C2H+H=A1C2H-+H2	2.50E+14	0.0	16000.0
287.	A1C2H+OH=A1C2H-+H2O	1.60E+08	1.4	1450.0
288.	A1C2H-+H+M=A1C2H+M H2/2.0/ O2/6.0/ H2O/6.0/ N2/0.7/	1.00E+14	0.0	0.0
289.	A1-+C2H3=A1C2H2+H	9.40E+00	4.1	23234.0
290.	A1-+C4H2=A2-1	5.10E+48	-10.5	28000.0
291.	A1-+C6H2=A2R5-	5.10E+48	-10.5	28000.0
292.	A1C2H2+H=A1C2H+H2	1.50E+13	0.0	0.0
293.	A1C2H2+OH=A1C2H+H2O	2.50E+12	0.0	0.0
294.	A1C2H-+C2H2=A2-1	5.10E+48	-10.5	28000.0
295.	A1C2H-+C2H2=A1C2H)2+H	2.10E+10	0.8	13700.0
296.	A1C2H)2+H=A2-1	1.50E+51	-10.8	25500.0
297.	A1C2H+C2H=A1C2H)2+H	5.00E+13	0.0	0.0
298.	A1C2H2+C2H2=A2+H	1.60E+18	-1.9	7400.0
299.	A2+H=A2-1+H2	2.50E+14	0.0	16000.0
300.	A2+OH=A2-1+H2O	1.60E+08	1.4	1450.0
301.	A2-1+O2=A1C2H+HCO+CO	2.10E+12	0.0	7470.0
302.	A2-1+C2H2=A2R5+H	1.10E+07	1.7	3900.0
303.	A2R5+O=A2-1+HCCO	2.20E+13	0.0	4530.0
304.	A2R5-+O2=A2-1+CO+CO	2.10E+12	0.0	7470.0
305.	A2R5+H=A2R5-+H2	2.50E+14	0.0	16000.0
306.	A2R5+OH=A2R5-+H2O	1.60E+08	1.4	1450.0
307.	A2R5-+H=A2R5	1.00E+14	0.0	0.0
308.	A1C2H+OH=A1-+CH2CO	2.18E-04	4.5	-1000.0
309.	A1C2H)2+OH=A1C2H-+CH2CO	2.18E-04	4.5	-1000.0
310.	A2+OH=A1C2H+CH2CO+H	1.30E+13	0.0	10600.0
311.	A2+O=CH2CO+A1C2H	2.20E+13	0.0	4530.0
312.	A2R5+OH=A2-1+CH2CO	1.30E+13	0.0	10600.0
313.	C(S)+O2=>O+CO	1.00E+11	0.0	12800.0
314.	C(S)+H2O=>CO+H2	3.00E+11	0.0	42800.0
315.	C(S)+OH=>CO+H	1.00E+11	0.0	36800.0
316.	C(S)+OH+OH=>CO2+H2	2.00E+12	0.0	36800.0
317.	C(S)+OH+O=>CO2+H	2.00E+12	0.0	36800.0
318.	C(S)+NO2=>CO+NO	1.00E+11	0.0	12800.0
319.	N+NO=N2+O	3.50E+13	0.0	330.0
320.	N+O2=NO+O	2.65E+12	0.0	6400.0
321.	N+OH=NO+H	7.33E+13	0.0	1120.0
322.	N+CO2=NO+CO	1.90E+11	0.0	3400.0
323.	NO+NO=N2+O2	3.00E+11	0.0	65000.0
324.	N2O+O=N2+O2	1.40E+12	0.0	10810.0
325.	N2O+O=NO+NO	2.90E+13	0.0	23150.0

		k = A T**b exp(−E/RT)		
	REACTIONS	**A**	**b**	**E**
326.	N2O+H=N2+OH	4.40E+14	0.0	18880.0
327.	N2O+OH=N2+HO2	2.00E+12	0.0	21060.0
328.	N2O+M=N2+O+M	1.30E+11	0.0	59620.0
	H2/2.0/ O2/6.0/ H2O/6.0/ N2/0.7/			
329.	NO+HO2=NO2+OH	2.11E+12	0.0	−480.0
330.	NO+O+M=NO2+M	1.06E+20	−1.4	0.0
	H2/2.0/ H2O/6.0/ CH4/2.0/ CO/1.5/ CO2/2.0/ C2H6/3.0/ N2/0.7/			
331.	NO2+O=NO+O2	3.90E+12	0.0	−240.0
332.	NO2+H=NO+OH	1.32E+14	0.0	360.0

CURRICULUM VITAE

Alper Tolga ÇALIK was born in Trabzon, Turkey in 2 May 1974. He graduated at Mechanical Engineering Faculty of İstanbul Technical University in 1996 and he was employed as Research&Teaching assistant in Automotive Division of Mechanical Engineering Faculty of ITU since 1997.

He obtained his M.Sc. degree in 1998. His master thesis was entitled "Data acquisition and analysis from research engine". In his master study, he worked on the documentation of the data acquisition and control of the single-cylinder experimental research engine.

Mainly, he was experienced on experimental studies on internal combustion engines, data acquisition and measurement on internal combustion engines, emission, power, fuel consumption measurements on internal combustion engines for research and type approval tests, thermodynamic calculations of engine characteristics and engine media conditioning systems. He had knowledge about main aspects of engine test room design and studied in the design of engine media conditioning systems such as cooling water temperature, engine oil temperature and pressure, fuel temperature conditioning. Also he worked in a cooling system project for conditioned water supply to the engine brakes and hydropuls of the Automotive Laboratory of Mechanical Engineering Faculty.

He worked also as laboratory assistant for the control of the execution of Internal Combustion Engines Laboratory Work of Experimental Methods in Mechanical Engineering Course.

Alper Tolga ÇALIK has basic knowledge on Basic and Fortran Programming Languages and familiar with MATLAB, LINUX and Microsoft WINDOWS operating systems and goon in MS Office tools.

He was a member of Society of Automotive Engineers since 2001.